Title: Shifting the limits in wheat research and breeding using a fully annotated reference genome

Authors: International Wheat Genome Sequencing Consortium (IWGSC)* †.

Affiliations:

*Correspondence to: rudi.appels@unimelb.edu.au (Rudi Appels), eversole@eversoleassociates.com (Kellye Eversole), and stein@ipk-gatersleben.de (Nils Stein).

† All authors with their affiliations appear in the acknowledgements at the end of this paper.

Abstract (100 – 125 words): An annotated reference sequence representing the hexaploid bread wheat genome in 21 pseudomolecules has been analyzed to identify the distribution and genomic context of coding and non-coding elements across the A, B and D sub-genomes. With an estimated coverage of 94% of the genome and containing 107,891 high confidence gene models, this assembly enabled the discovery of tissue and developmental stage related co-expression networks using a transcriptome atlas representing all stages of wheat development. Dynamics of complex gene families involved in environmental adaptation and end-use quality were revealed at sub-genome resolution and contextualized to known agronomic single gene or quantitative trait loci. This community resource establishes the foundation for accelerating wheat research and application through improved understanding of wheat biology and genomics-assisted breeding.

One Sentence Summary (keep under 125 characters): The 21 annotated chromosomes of bread wheat provide a foundation for accelerated innovation in wheat research and breeding.

Main Text: Wheat (*Triticum aestivum* L.), the most widely-cultivated crop on earth, contributes about a fifth of total calories consumed by humans and provides more protein than any other food

source (*1*). Thus, wheat yields and production impact the global economy and failed harvests result in malnutrition and can lead to social unrest as evidenced by the 2007-2008 crisis when average wheat prices doubled rapidly because of major drought-related crop losses around the world (*2*). Breeders strive to develop improved varieties by fine-tuning genetically complex yield and end-use quality parameters while maintaining yield stability and regional adaptation to specific biotic and abiotic stresses (*3*). These efforts are limited, however, by insufficient knowledge and understanding of the molecular basis of key agronomic traits. To meet the demands of human population growth, there is an urgent need for wheat research and breeding to accelerate genetic gain while increasing wheat yield and protecting quality traits. In other plant and animal species, access to a fully annotated and ordered genome sequence, including regulatory sequences and genome diversity information, has promoted the development of systematic and more time-efficient approaches for the selection and understanding of important traits (*4*). Wheat has lagged behind primarily due to the challenges of assembling a genome that is large (1C=16 Gb) (*5*), hexaploid and complex with over 85% repetitive DNA.

To provide a foundation for improvement through molecular breeding, the International Wheat Genome Sequencing Consortium (IWGSC) established a road map in 2006 to deliver a high-quality reference genome sequence of the bread wheat cultivar ‘Chinese Spring’ (CS). In 2014, a chromosome survey sequence (CSS) intermediate product assigned 124,201 gene loci across the 21 chromosomes (*6*) and revealed the evolutionary dynamics of the wheat genome through gene loss, gain, and duplication. The lack of global sequence contiguity and incomplete coverage (only 10 Gb were assembled), however, did not provide the wider regulatory genomic context of genes. Subsequently, whole genome assemblies improved contiguity (*7*-*9*) but none

provided full annotation, resolved the intergenic space, or, more importantly for applications in breeding and gene cloning, presented the genome in the correct physical order.

Here, the IWGSC reports an ordered and annotated assembly (IWGSC RefSeq v1.0) of the 21 chromosomes of the allohexaploid wheat cultivar CS, integrated with extensive genetic and genomic resources. The completeness and accuracy of IWGSC RefSeq v1.0 provided novel insights into global genome composition and enabled the construction of complex gene co-expression networks to identify central regulators in critical pathways such as flowering time control. The ability to resolve the inherent complexity of gene families related to important agronomic traits demonstrated the impact of IWGSC RefSeq v1.0 on dissecting quantitative traits genetically and implementing modern breeding strategies including genome editing for future wheat improvement.

Chromosome-scale assembly of the wheat genome

Pseudomolecule sequences representing the 21 chromosomes of the bread wheat genome were assembled by integrating a draft whole genome *de novo* assembly (WGA), built from Illumina short read sequences using NRGene deNovoMagic2 (Table 1, Fig. 1A, Table S1, S2) with additional layers of genetic, physical, and sequence data (Table S3-S8, Fig. S1, S2). In the resulting 14.5 Gb genome assembly, contigs and scaffolds with N50s of 52 kb and 7 Mb, respectively, were linked into superscaffolds (N50 = 22.8 Mb), with 97% (14.1 Gb) assigned and ordered along the 21 chromosomes and almost all of the assigned sequences also oriented (13.8 Gb, 98%). Unanchored scaffolds comprising 481 Mb (2.8% of the assembly length) formed the ‘unassigned chromosome’ (ChrUn) bin. The quality and contiguity of the IWGSC RefSeq v1.0 genome assembly was assessed through alignments with three independent datasets: (i) radiation hybrid maps for the A, B, and D sub-genomes showed high collinearity to the pseudomolecules

(average Spearman's ρ: 0.98); (ii) the genetic positions of 7,832 and 4,745 genotyping-by-sequencing (GBS) derived genetic markers in 88 double haploid and 993 recombinant inbred lines, respectively, showed a high correlation to their positions in the pseudomolecules (Spearman's r: 0.986 and 0.987, respectively); and (iii) 1.24 million pairs of neighbor insertion site based polymorphism markers (ISBPs) (*10*) of which 97% were collinear and mapped in a similar size range (difference <2 kb) between the de novo WGA and the available BAC-based sequence assemblies. Finally, IWGSC RefSeq v1.0 was assessed using independent data derived from coding and non-coding sequences revealing that 99% and 98% of the previously known coding exons (*6*) and TE-derived (ISBP) markers (Table S9), respectively, were present in the assembly. The approximate 1 Gb size difference between IWGSC RefSeq v1.0 and the new genome size estimates of 15.4-15.8 Gb (Material and Methods) can be accounted for by collapsed or unassembled sequences of highly-repeated clusters, such as ribosomal RNA coding regions and telomeric sequences.

A key feature distinguishing the IWGSC RefSeq v1.0 from previous draft wheat assemblies (*6-9*) is the long-range organization with 90% of the genome represented in super-scaffolds larger than 4.1 Mb and with each chromosome represented on average by only 76 super-scaffolds (Table 1). The largest super-scaffold spanned 166 Mb, i.e. half the rice (*Oryza sativa* L.) genome, and larger than the *Arabidopsis thaliana* L. genome (*11, 12*). Moreover, the 21 pseudomolecules now provide unique positions for large numbers of molecular markers widely used in wheat research and breeding (504 SSRs, 3,025 DArTs, 6,689 ESTs, 205,807 SNPs, 4,512,979 ISBPs) (Table S9), thus providing a direct link between the genome sequence and genetic loci / genes underlying traits of agronomic importance.

The composition of the wheat genome

Analyses of the components of the genome sequence revealed the distribution of key elements and enabled detailed comparisons of the homeologous A, B and D sub-genomes. Accounting for 85% of the genome with a relatively equal distribution across the three sub-genomes (Table 2), 3,968,974 copies of transposable elements (TEs) belonging to 505 families were annotated. Large numbers (112,744) of full length long terminal-repeat retrotransposons (fl-LTRs) were identified that have been previously notoriously difficult to define from short read sequence assemblies (Fig. S3). Although the TE content has been extensively rearranged through rounds of deletions / amplifications since the divergence of the A, B and D sub-genomes about 5 million years ago, the TE families that shaped the Triticeae genomes have been maintained in similar proportions: 76% of the 165 TE families present in a cumulative length greater than 1Mb contributed similar proportions (<2-fold change between sub-genomes) and only 11 families, accounting for 2% of total TEs, showed a higher than 3-fold change between 2 sub-genomes (*13*). TE abundance accounts, in part, for the size differences between sub-genomes, e.g. 64% of the 1.2 Gb size difference between the B and D sub-genomes can be attributed to lower gypsy retrotransposon content. Significant differences in the low-copy DNA content (primarily unclassified sequences) (e.g. 97 Mb of the 245 Mb size difference between A and B genomes) were also observed (Fig. S4). As reported previously (*14*), no evidence was found for a major burst of transposition after polyploidization. The independent evolution in the diploid lineages was reflected in differences in the specific composition of A, B and D at the sub-family (variants) level as evidenced by sub-genome specific over-representation of individual transposon domain signatures (Fig. 1B). A more detailed analysis of the TE content and its impact on the evolution of the wheat genome is presented in a companion manuscript (*13*).

In addition to TEs, annotation of the intergenic space included non-coding RNAs. The analysis of miRNA and tRNA content identified eight new miRNA families with an excess of lysine tRNAs (Fig. S5, S6, Table S10). Around 8,000 NUPTs (nuclear inserted plastid DNA segment) and 11,000 NUMTs (nuclear inserted mitochondrial DNA segments) representing respectively 5 and 17 Mb were also revealed by comparing the genome assembly with complete plastid and mitochondrial genomes assembled from the IWGSC RefSeqv1.0 raw read data (Material and Methods).

Precise positions for the centromeres were defined by integrating Hi-C, CSS data (*6*) and published chromatin immuno-precipitation sequencing (ChIP-seq) data for CENH3, a centromere-specific histone H3 variant (*15*). Clear ChIP-Seq peaks were evident in all chromosomes and coincided with the centromere-specific repeat families (Fig. 1C, Fig. S7, Table S11). CENH3 targets were also found in unassigned sequence scaffolds (ChrUn) indicating that centromeres of several chromosomes are not yet completely resolved. Based on these data, a conservative estimate for the minimal average size of a wheat centromere is 4.9Mb (6.7Mb, if including ChrUn, Table S11) contrasting with ~1.8 Mb in maize (*16*, *17*) and 0.4-0.8 Mb in rice (*18*).

Gene models were predicted using two independent pipelines previously utilized for wheat genome annotation and then consolidated to produce the RefSeq Annotation v1.0 (Fig. S8). Subsequently, a set of manually-curated gene models was integrated to build RefSeq Annotation v1.1 (Fig. S9, Table S12-S17). In total, 107,891 high confidence (HC) protein coding loci were identified, with relatively equal distribution across the A, B and D sub-genomes (35,345, 35,643, and 34,212, respectively; Fig. 2A, Fig. S10, Table S18). In addition, 161,537 other protein coding

loci were classified as low confidence (LC) genes representing partially supported gene models, gene fragments, and orphans (Table S18). A predicted function was assigned to 82.1% (90,919) of HC genes in RefSeq Annotation v1.0 (Table S19, S20) and evidence for transcription was found for 85% (94,114), compared to 49% of the LC genes (*19*). Within the pseudogene category, 25,419 (8%) of 303,818 candidates matched LC gene models. The D sub-genome contained significantly fewer pseudogenes than the A and B sub-genomes (81,905 versus 99,754 and 109,097, respectively; P <2.2e-16), consistent with the more ancient allo-tetraploidization between A and B (Table S21, S22, Fig. S10). In ChrUn, 2,691 HC and 675 LC gene models were identified.

The quality of the RefSeq Annotation v1.1 gene set was benchmarked against BUSCO v3 (*20*) representing 1,440 Embryophyta near-universal single-copy orthologs and previously published annotated wheat gene sets (Fig. 2B, Fig. S11). 99% (1436) of the BUSCO v3 genes were represented in at least one complete copy in RefSeq Annotation v1.1 and 90% (1292) in three complete copies, a major improvement over the 25% (353) and 70% (1,014) identified in the previous IWGSC (*6*) and TGACv1 (*8*) gene sets, respectively (Fig. 2B). Improved contiguity of sequences in the immediate vicinity of genes was also found: 61% of the HC and LC genes were flanked by at least 10 kb of sequence without Ns, in contrast to 37% and only 5% of TGACv1 and IWGSC CSS gene models, respectively (Fig. S12).

To further characterize the gene-space, a phylogenomic approach was applied to identify gene homeologs and paralogs between and within the wheat sub-genomes, in addition to orthologs in other plant genomes (Table S23, Fig. S13-S15). Analysis of a subset of 181,036 genes (“filtered gene set”, see Material and Methods, Table 3) comprising 103,757 HC and 77,279 LC genes,

identified 39,238 homeologous groups, i.e. clades of A, B and D sub-genome orthologs deduced from gene trees, containing a total of 113,653 genes (63% of the filtered set). Gene losses / retention and gene gains (gene duplications) were determined for all homeologous loci of IWGSC RefSeq v1.0 (Table 3) assuming the presence of a single gene copy at every homeologous locus (referred to as a "triad"). The percentage of genes in homeologous groups for all configurations (ratios) is highly similar, hence balanced, across the three sub-genomes: 63% (A), 61% (B), and 66% (D). The slightly higher percentage of homeologs on the D sub-genome, together with the lower number of pseudogenes (Table S22) is consistent with its more recent hybridization with the A / B genome progenitor. Although the majority of genes are present in homeologous groups, only 18,595 (47%) of the groups contained triads with one single gene copy per sub-genome (1:1:1 configuration). 5,673 (15%) groups of homeologous genes exhibited at least one sub-genome inparalog, i.e. a gene copy resulting from a tandem or segmental / trans-duplication (1:1:N configuration). The three genomes exhibited similar levels of loss of individual homeologs, affecting 10.7% (0:1:1), 10.3% (1:0:1), and 9.5% (1:1:0) of the homeologous groups in the A, B and D sub-genomes, respectively (Table 3, Table S24, S25).

Among the 67,383 (37%) genes of the filtered set not present in homeologous groups, 31,140 genes also had no orthologs in species included in the comparisons outside of bread wheat and comprised, mainly, gene fragments, non-protein-coding loci with open reading frames or other gene calling artifacts. The remaining 36,243 genes had homologs outside of bread wheat and appeared to be sub-genome specific (Table 3). Two of the genes in this category were *granule bound starch synthase*, *GBSS*, on chromosome 4A (1:0:0, a gene that is a key determinant of udon noodle quality) and *ZIP4* within the *Ph1* (*Pairing homeologous 1*) locus on chromosome 5B [0:1:0, a locus critical for the diploid meiotic behavior of the wheat homeologous chromosomes

(*21*)]. The phylogenomic analysis indicated the *GBSS* on 4A is a divergent translocated homeolog originally located on chromosome 7B (Fig. S16); whereas, *ZIP4* is a trans-duplication of a chromosome 3B locus (Table S26). Both genes confer important properties on wheat and illustrate the diversity in origin and function of gene models that are not in a 1:1:1 configuration.

No evidence was found for sub-genome dominance, as suggested for maize and other grasses (*22-24*) as well as for wheat (*25*). Rather, our analysis supported a scenario of gradual gene loss and gene movement among the sub-genomes that may have occurred either in the diploid progenitor species, the tetraploid ancestor or following the final hexaploidization event in modern bread wheat (Table 3, Table S24, S25).

The bread wheat genome contains 29,737 HC genes (27%) in tandem duplication, which is up to 10% higher than found for other monocotyledonous species (Table S27). Tandemly repeated genes are most prevalent in the B genome (29%), contributing to its higher gene content and larger number of 1:N:1 homeologous groups (Table 3). The postulated hybrid origin of the D sub-genome as a result of inter-specific crossing with AB genome progenitors 1-2 My after they diverged (*26*), is mirrored by the synonymous substitution rates of homeologous gene pairs (Fig. S17). Homeologous groups with gene duplicates in at least one sub-genome (1:1:N, 1:N:1, N:1:1) showed elevated evolutionary rates (for the sub-genome carrying the duplicate) compared to strict 1:1:1 or 1:1 groups (Fig. S18-S22). Homeologs with recent duplicates also showed higher levels of expression divergence (Fig. S23), consistent with gene / genome duplications acting as a driver of functional innovation (*27*, *28*).

Analysis of synteny between the seven triplets of homeologous chromosomes showed high levels of conservation. There was no evidence for any major rearrangements since the A, B and D sub-genomes diverged ~5 Mya (Fig. 1D), although collinearity between homeologs was disturbed by

inversions occurring on average every 74.8 Mb involving blocks of ten genes or more (mean gene number 48.2 with a mean size of 10.5 Mb) (Fig. 1D, Table S28). Macro-synteny was conserved across centromeric (C) regions, but collinearity (micro-synteny) broke down specifically in these recombination-free, gene-poor regions, for all seven sets of homeologous chromosomes (Fig. 1D, Fig. S24-S26, Table S29). Among the 113,653 homeologous genes, 80% (90,232) were found organized in macro-synteny, i.e. still present at their ancestral position (Table S24). At the micro-synteny scale, 72% (82,308) of the homeologs were organized in collinear blocks i.e. intervals with a highly-conserved gene order (Fig. 1D). A higher proportion of syntenic genes was found in the interstitial regions [short arm, R2a (*14*), 46% and long arm, R2b (*14*), 61%] compared to the distal telomeric [short arm, R1 (*14*), 39% and long arm, R3 (*14*), 51%] and centromere regions [C (*14*), 29%], respectively, and the interstitial compartments harbored larger syntenic blocks (Fig. S27, Fig. S28). The higher proportions of duplicated genes in distal-terminal regions (34% and 27% versus 13-15% in the other regions; Fig. S29) exerted a strong influence on the decay of syntenic block size and contributed to the higher sequence variability in these regions. Overall, distal chromosomal regions are the preferential targets of meiotic recombination and the fastest evolving compartments. As such, they represent the genomic environment for creating sequence, hence, allelic diversity, providing the basis for adaptability to changing environments.

Atlas of transcription reveals trait associated gene co-regulation networks

The gene annotation coupled with identification of homeologs and paralogs in IWGSC RefSeq v1.0 provided a unique resource to study gene expression in genome-wide and sub-genome contexts. A total of 850 RNA-Seq samples derived from 32 tissues at different growth stages and/or challenged by different stress treatments were mapped to RefSeq Annotation v1.0

(Database S1, Fig. 3A, Table S30, S31, S32). Expression was observed for 94,114 (84.9%) HC genes (Fig. S30) and for 77,920 (49.1%) LC genes, the latter showing lower expression breadth and level [median 6 tissues; average 2.9 transcripts per million (tpm)] than the HC genes (median 20 tissues; average 8.2 tpm) (Fig. S31). This correlated with the higher average methylation status of LC genes (Fig. S32, S33). A principal component analysis (PCA) identified tissue (Fig. 3B), rather than growth stage or stress (Fig. S34), as the main factor driving differentiated expression between samples, consistent with studies in other organisms (*29*-*32*), with 31.0 % of genes expressed in over 90% of tissues (average 16.9 tpm, ≥ 30 tissues), and 21.5% of genes expressed in 10% or fewer tissues (average 0.22 tpm; ≤ 3 tissues; Fig. S31).

8,231 HC genes showed tissue-exclusive expression (Fig. S35), with reproductive tissues (microspores, anther and stigma/ovary) accounting for around half of these, as observed in rice (*33*). The tissue-exclusive genes were enriched for response to extra-cellular stimuli and reproductive processes (Database S2). In contrast, 23,146 HC genes expressed across all 32 tissues were enriched for biological processes associated with house-keeping functions such as protein translation and protein metabolic processes. Tissue specific genes were shorter (1,147 ± 8 bp), had fewer exons (2.76 ± 0.3), and were expressed at lower levels (3.4 ± 0.1 tpm) compared to ubiquitous genes (1,429 ± 7 bp; 7.87 ± 0.4 exons, 17.9 ± 0.4 tpm) (Fig. S35).

Genes located in distal regions R1 and R3 (Fig. S25, Table S29) showed significantly lower expression breadth than those in the proximal regions (15.7 and 20.7 tissues, respectively) (Fig. 3C; Fig. S36). This correlated with enrichment of Gene Ontology (GO) slim terms such as ‘cell cycle’, ‘translation’, and ‘photosynthesis’ for genes in the proximal regions, whereas, genes enriched for ‘response to stress’ and ‘external stimuli’ were found in the highly recombinant distal R1 and R3 regions (Database S3, Fig. S36, Table S33). The expression breadth pattern was

also correlated with the distribution of the repressive H3K27me3 (R= -0.76, P < 2.2E-16) and with the active H3K36me3 and H3K9ac (R= 0.9 and 0.83, respectively, P < 2.2E-16) histone marks (Fig. S37).

Global patterns of co-expression (*34*) were determined using a weighted gene co-expression network analysis (WGCNA) on 94,114 expressed HC genes. 58% of these genes (54,401) could be assigned to 38 modules (Fig. 3D, Database S4) and, consistent with the PCA, tissues were the major driver of module identity (Fig. 3D, Fig. S38 – S40). The analysis focused initially on the 9,009 triads (syntenic and non-syntenic) with a 1:1:1 A:B:D relationship and for which all homeologs were assigned to a module. 16.4% of the triads had at least one homeolog in a divergent module with the B homeolog most likely to be divergent (37.4% B divergent vs 31.7% A divergent and 30.9% D divergent triads, χ^2 P = 0.007). However, the expression profiles of the majority (83.6%) of triads were relatively consistent with all homeologs in the same (57.6%) or a closely related module (26.0%). The proportion of homeologs found within the same module was higher than expected, pointing to a highly-conserved expression pattern of homeologs across the 850 RNA-Seq samples (Fig. 3E, Table S34). Triads with at least one gene in a non-syntenic position had more divergent expression patterns compared to syntenic triads (21.2% vs 16.2%, χ2 P <0.001) and fewer triads with all homeologs in the same module (48.7%) compared to syntenic triads (58.0%, χ2 P= 0.009). Similar patterns were observed in the 1,933 duplets having a 1:1 relationship between only two homeologs (Table S34). These results were consistent with syntenic homeologs showing similar expression patterns while more dramatic changes in chromosome context associate with divergent expression and possible sub- or neo-functionalization. These trends were also found across diverse tissue-specific networks (*19*).

To explore the potential of the WGCNA network for identifying novel pathways in wheat, a search was undertaken for modules containing known regulators of wheat flowering time [eg. *PPD1*, (*35*); *FT* (*18*); Fig. 3F]. Genes belonging to this pathway were grouped into specific modules. The upstream genes (*PHYB, PHYC, PPD1, ELF3, VRN2*) were present mainly in modules 1 and 5 and were most highly correlated with expression in leaf/shoot tissues (0.68 and 0.67 respectively, Padj<E-108). In contrast, the integrating gene *FT* and downstream genes *VRN1*, *FUL2* and *FUL3* were found in modules 8 and 11, most highly correlated with expression in spikes (0.69 and 0.65 respectively, Padj<E-101, Table S35). The MADS_II TF family generally associated with the above pathways, was examined more closely with a focus on the gene tree OG0000041 containing 54 of the 118 MADS_II genes in wheat. 24 MADS_II genes from modules 8 and 11 were identified within this gene tree, clustering into two main clades along with Arabidopsis and rice orthologs associated with floral patterning (Fig. S41; Database S5). Within these clades, other MADS_II genes were found that were not in modules 8 or 11 (Fig. 3G), indicating a different pattern of co-expression. None of the 24 MADS_II genes had a simple 1:1 ortholog in Arabidopsis, suggesting that some wheat orthologs function in flowering (those within modules 8 and 11), whereas others could have developed different functions, despite being phylogenetically closely related. Thus, these data provide a new framework to identify and prioritize the most likely functional orthologs of known model system genes within polyploid wheat, to characterize them functionally (*36*) and to dissect genetic factors controlling important agronomic traits (*37, 38*). A more detailed analysis of tissue-specific and stress-related networks is presented elsewhere (*19*) and provides a framework for defining quantitative variation and interactions between homeologs for many agronomic traits (*39*).

Gene family expansion / contraction with relevance to wheat traits

Gene duplication and gene family expansion are important mechanisms of evolution and environmental adaptation, as well as major contributors to phenotypic diversity (*40, 41*). In a phylogenomic comparative analysis, wheat gene family size and wheat-specific gene family expansion / contraction were benchmarked against nine other grass genomes, including five closely related diploid Triticeae species (Table S23, Fig. S13-15, S42). A total of 30,597 gene families (groups of orthologous genes traced to a last common ancestor in the evolutionary hierarchy of the compared taxa) were defined with 26,080 families containing gene members from at least one of the three wheat sub-genomes (Tables S36-S38). Among the 8,592 expanded wheat gene families (33% of all families), 6,216 were expanded in all three A, B and D sub-genomes (24%; either shared with the wild ancestor or specific to bread wheat, Fig. 4A). Another 1,109 were expanded in only one of the wheat sub-genomes and 2,102 gene families were also expanded in either the A or the D genome lineages (i.e. *T. urartu* or *A. tauschii*) (Fig. 4A, Table S36, Fig. S43). Overall, only 78 gene families were contracted in wheat. Gene Ontology (GO; ontology of biomedical terms for the areas 'cellular component', 'biological process', 'molecular function'), Plant Ontology (PO; ontology terms describing anatomical structures and growth and developmental stages across Viridiplantae) and Plant Trait Ontology (TO; ontology of controlled vocabulary to describe phenotypic traits and QTLs that were physically mapped to a gene in flowering plant species) analysis identified 1,169 distinct GO/PO/TO terms (15% of all assigned terms) enriched in genes belonging to expanded wheat gene families (Fig. 4B, Fig. S44, S45). 'A sub-genome' or 'A-lineage' expanded gene families showed a bias for terms associated with seed formation [overrepresentation of the TO term "plant embryo morphology" (TO:0000064) and several seed, endosperm, and embryo-developmental GO terms] (Fig. S46). Similarly, 'B sub-genome' expanded gene families were significantly enriched for TO terms related to plant

vegetative growth and development (Database S6, Fig. S47). Gene families that were expanded in all wheat sub-genomes were enriched for 14 TO terms associated with yield-affecting morphological traits and five terms associated with fertility and abiotic stress tolerance (Fig. 4B), which was also mirrored by enrichment for GO and PO terms associated with adaptation to abiotic stress ('salt stress', 'cold stress') and grain yield and quality ('seed maturation', 'dormancy' and 'germination'). The relationship between the patterns of enriched TO/PO/GO terms for expanded wheat gene families and key characteristics of wheat performance (Fig. S45-S51) provides a novel resource (Database S6) to explore future QTL mapping and candidate gene identification for breeding.

Many gene families with high relevance to wheat breeding and improvement were among the expanded group and their genomic distribution was analyzed in greater detail (Fig. 4C, Fig. S52-S54). Disease resistance related NLR (nucleotide-binding site leucine-rich repeat)-like loci and WAK (wall-associated receptor)-like genes were clustered in high numbers at the distal (R1 and R3) regions of all chromosome arms, with NLRs often co-localizing with known disease resistance loci (Fig. 4C). The Restorer of Fertility-Like (RFL) sub-clade of P class PPR proteins, potentially of interest for hybrid wheat production, comprised 207 genes, nearly three-fold more per haploid sub-genome than in any other plant genome analyzed to date (*42*, *43*). They localized mainly as clusters of genes in regions on the group 1, 2, and 6 chromosomes, which are known to carry fertility restoration QTLs in wheat (Fig. 4C, Fig. S54). Among the dehydrin gene family, implicated with drought tolerance in plants, 25 genes that formed well defined clusters on chromosomes 6A, 6B and 6D (Fig. S53, S55) showed early increased expression under severe drought stress (*44*). As the structural variation in the *CBF* genes of wheat is known to be associated with winter survival (*45*), the array of CBF paralogs at the Fr-2 locus (Fig. S56)

revealed by IWGSC RefSeqv1.0 provides a basis for targeted allele mining for novel CBF haplotypes from highly frost tolerant wheat genetic resources. Lastly, high levels of expansion and variation in members of grain prolamin gene families (Fig. S52, Table S37) that can either be related to the response to heat stress or whose protein epitopes are associated with levels of coeliac disease and food allergies (*46*), provide candidates for future selection in breeding programs. From these few examples, it is evident that significant flexibility in gene copy numbers within the wheat genome has contributed to the adaptability of wheat to produce high quality grain under diverse climates and environments (*47*). Knowledge of the complex picture of the genome-wide distribution of gene families (Fig. 4C), that needs to be considered for selection in breeding programs in the context of distribution of recombination and allelic diversity (*48*) can now be applied in wheat improvement strategies. This is especially true if 'must-have traits' that are allocated in chromosomal compartments with highly contrasting characteristics, are fixed in repulsion, or are found only in incompatible genepools of the respective breeding germplasm.

Rapid trait improvement using physically resolved markers and genome editing

The selection and modification of genetic variation underlying agronomic traits in breeding programs is often complicated if phenotypic selection depends on the expression of multiple loci with quantitative effects that can be strongly influenced by the environment. This dilemma can be overcome if DNA markers in strong linkage disequilibrium with the phenotype are identified through forward genetic approaches, or if the underlying genes can be targeted through genome editing. The potential for IWGSC RefSeq v1.0, together with the detailed genome annotation, to accelerate the identification of potential candidate genes underlying important agronomic traits was exemplified for two targets. A forward genetics approach was used to fully resolve a QTL

for stem solidness (*SSt1*) conferring resistance to drought stress and to insect damage (*49*) that was disrupted in previous wheat assemblies by a lack of scaffold ordering and annotation, partial assembly, and/or incomplete gene models (Fig. S57, Table S39, S40). In IWGSC RefSeq v1.0, *SSt1* contains 160 HC genes (Table S41), of which 26 were differentially expressed (adj p <0.01) between wheat lines with contrasting phenotypes. One of the differentially expressed genes, *TraesCS3B01G608800* was present as a single copy in RefSeq v1.0, but showed copy number variation (CNV) associated with stem-solidness in a diverse panel of hexaploid cultivars (Fig. 5A, Fig. S58, Table S42). Using IWGSC RefSeq v1.0, we developed a diagnostic SNP marker physically linked to the CNV that has been deployed to select for stem-solidness in wheat breeding programs (Fig. 5B).

Knowledge from model species can also be used to annotate genes and provide a route to trait enhancement through reverse genetics. The approach here targeted flowering time which is important for crop adaptation to diverse environments and is well-studied in model plants. Six wheat homologues of the *Flowering Locus C* (*FLC*) gene have been identified as having a role in the vernalization response, a critical process regulating flowering time (*50*). IWGSC RefSeqv1.0 was used to refine the annotation of these six sequences to identify four HC genes and then to design guide RNAs to specifically target by CRISPR/Cas9-based gene editing one of these genes, *TaAGL33*, on all sub-genomes [*TraesCS3A01G435000 (A), TraesCS3B01G470000* (B), and *TraesCS3D01G428000* (D)] (Fig. 5C). The three homeologs were sequenced to describe eight gene edits in five independent events. Editing was obtained at the targeted gene and led to truncated proteins after the MADS box through small deletions/insertions (Fig. 5D). Expression of all homeologs was high prior to vernalization, dropped during vernalization, and remained low post-vernalization, implying a role for this gene in flowering control. This expression pattern was

not affected by the genome edits (data not shown). Plants with the two D-genome editing events flowered 2-3 days earlier than controls (Fig. 5E). Further refinement of the editing approach will help to fully understand the significance of the *TaAGL33* gene for vernalization in monocots. These results exemplify how the IWGSC RefSeqv1.0 could accelerate the development of diagnostic markers and the design of targets for genome editing for traits relevant to breeding.

Conclusions

IWGSC RefSeq v1.0 is a resource that has a potential for disruptive innovation in wheat improvement. By necessity, breeders work with the genome at the whole chromosome level, as each new cross involves the modification of genome-wide gene networks that control the expression of complex traits such as yield. With the annotated and ordered reference genome sequence in place, researchers and breeders can now easily access sequence level information to define changes in the genomes of lines in their programs. While several hundred wheat QTLs have been published, only a small number of genes have been cloned and functionally characterized. IWGSC RefSeq v1.0 underpins immediate application by providing access to regulatory regions and it will serve as the backbone to anchor all known QTLs to one common annotated reference. Combining this knowledge with the distribution of meiotic recombination frequency, and genomic diversity (*48*) will enable breeders to tackle more efficiently the challenges imposed by the need to balance the parallel selection processes for adaptation to biotic and abiotic stress, end-use quality, and yield improvement. Strategies can now be defined more precisely to bring desirable alleles into coupling phase, especially in less recombinant regions of the wheat genome. Here the full potential of the newly available genome information may be realised by the implementation of DNA marker platforms and targeted breeding technologies, including genome editing (*51*).

Methods Summary

Whole genome sequencing of cultivar 'Chinese Spring' by short read sequencing-by-synthesis provided the data for de novo genome assembly and scaffolding using the software package DenovoMAGIC2^{TM}. The assembly was super-scaffolded and anchored into 21 pseudomolecules using high density genetic (POPSEQ) and physical (Hi-C and 21 chromosome-specific physical maps) mapping information and by integrating additional genomic resources. Validation of the assembly used independent genetic (de novo GBS maps) and physical mapping evidences (Radiation hybrid maps, BioNano 'optical maps' for group 7 homeologous chromosomes). The genome assembly was annotated for genes, repetitive DNA, and other genomic features and in-depth comparative analyses were carried out to analyze the distribution of genes, recombination, position and size of centromeres and the expansion/contraction of wheat gene families. An atlas of wheat gene transcription was built from an extensive panel of 850 independent transcriptome datasets which was then used to study gene co-expression networks. Furthermore, the assembly was used for the dissection of an important stem solidness QTL and to design targets for genome

editing of genes implied in flowering time control in wheat. Detailed methodological procedures are described in the supplementary materials.

References and Notes:

1. Food and Agriculture Organization of the United Nations, FAOSTAT Statistics Database, 78, http://www.fao.org/faostat/en/#data/FBS, http://www.fao.org/faostat/en/#data/QC (2017).

2. B. Shiferaw *et al.*, Crops that feed the world 10. Past successes and future challenges to the role played by wheat in global food security. *Food Security* **5**, 291-317 (2013).

3. G. N. Atlin, J. E. Cairns, B. Das, Rapid breeding and varietal replacement are critical to adaptation of cropping systems in the developing world to climate change. *Global Food Security* **12**, 31-37 (2017).

4. J. M. Hickey, T. Chiurugwi, I. Mackay, W. Powell, C. B. P. W. P. Implementing Genomic Selection in, Genomic prediction unifies animal and plant breeding programs to form platforms for biological discovery. *Nat Genet* **49**, 1297-1303 (2017).

5. K. Arumuganathan, E. D. Earle, Nuclear DNA content of some important plant species. *Plant Molecular Biology Reporter* **9**, 208-218 (1991).

6. The International Wheat Genome Sequencing Consortium, A chromosome-based draft sequence of the hexaploid bread wheat (*Triticum aestivum*) genome. *Science* **345**, (2014).

7. J. A. Chapman *et al.*, A whole-genome shotgun approach for assembling and anchoring the hexaploid bread wheat genome. *Genome Biology* **16**, 26 (2015).

8. B. J. Clavijo *et al.*, An improved assembly and annotation of the allohexaploid wheat genome identifies complete families of agronomic genes and provides genomic evidence for chromosomal translocations. *Genome Research* **27**, 885-896 (2017).

9. A. V. Zimin *et al.*, The first near-complete assembly of the hexaploid bread wheat genome, Triticum aestivum. *GigaScience* **6**, 1-7 (2017).

10. E. Paux *et al.*, Insertion site-based polymorphism markers open new perspectives for genome saturation and marker-assisted selection in wheat. *Plant Biotechnology Journal* **8**, 196-210 (2010).

11. The Arabidopsis Genome Initiative, Analysis of the genome sequence of the flowering plant Arabidopsis thaliana. *Nature* **408**, 796-815 (2000).

12. International Rice Genome Sequencing Project, The map-based sequence of the rice genome. *Nature* **436**, 793-800 (2005).

13. T. Wicker *et al.*, Impact of transposable elements on genome structure and evolution in wheat. *Science* **submitted as companion paper**, (2018).

14. F. Choulet *et al.*, Structural and functional partitioning of bread wheat chromosome 3B. *Science* **345**, (2014).

15. X. Guo *et al.*, De Novo Centromere Formation and Centromeric Sequence Expansion in Wheat and its Wide Hybrids. *PLOS Genetics* **12**, e1005997 (2016).

16. K. Wang, Y. Wu, W. Zhang, R. K. Dawe, J. Jiang, Maize centromeres expand and adopt a uniform size in the genetic background of oat. *Genome Research* **24**, 107-116 (2014).

17. Y. Jiao *et al.*, Improved maize reference genome with single-molecule technologies. *Nature* **advance online publication**, (2017).

18. L. Yan *et al.*, The wheat and barley vernalization gene *VRN3* is an orthologue of *FT*. *Proceedings of the National Academy of Sciences* **103**, 19581-19586 (2006).

19. R. Ramirez-Gonzalez *et al.*, The transcriptional landscape of hexaploid wheat across tissues and cultivars. *Science* **submitted as companion paper**, (2018).

20. F. A. Simão, R. M. Waterhouse, P. Ioannidis, E. V. Kriventseva, E. M. Zdobnov, BUSCO: assessing genome assembly and annotation completeness with single-copy orthologs. *Bioinformatics* **31**, 3210-3212 (2015).

21. M.-D. Rey *et al.*, Exploiting the ZIP4 homologue within the wheat *Ph1* locus has identified two lines exhibiting homoeologous crossover in wheat-wild relative hybrids. *Molecular Breeding* **37**, 95 (2017).

22. M. R. Woodhouse *et al.*, Following tetraploidy in maize, a short deletion mechanism removed genes preferentially from one of the two homeologs. *PLOS Biology* **8**, e1000409 (2010).

23. J. C. Schnable, M. Freeling, E. Lyons, Genome-wide analysis of syntenic gene deletion in the grasses. *Genome Biology and Evolution* **4**, 265-277 (2012).

24. J. Schnable, X. Wang, J. Pires, M. Freeling, Escape from preferential retention following repeated whole genome duplications in plants. *Frontiers in Plant Science* **3**, (2012).

25. C. Pont, J. Salse, Wheat paleohistory created asymmetrical genomic evolution. *Current Opinion in Plant Biology* **36**, 29-37 (2017).

26. T. Marcussen *et al.*, Ancient hybridizations among the ancestral genomes of bread wheat. *Science* **345**, (2014).

27. Y. Van de Peer, S. Maere, A. Meyer, The evolutionary significance of ancient genome duplications. *Nature Reviews Genetics* **10**, 725 (2009).

28. P. S. Soltis, D. E. Soltis, Ancient WGD events as drivers of key innovations in angiosperms. *Current Opinion in Plant Biology* **30**, 159-165 (2016).

29. M. Melé *et al.*, The human transcriptome across tissues and individuals. *Science* **348**, 660-665 (2015).

30. S. C. Stelpflug *et al.*, An expanded maize gene expression atlas based on RNA sequencing and its use to explore root development. *The Plant Genome* **9**, (2016).

31. F. He *et al.*, Large-scale atlas of microarray data reveals the distinct expression landscape of different tissues in Arabidopsis. *The Plant Journal* **86**, 472-480 (2016).

32. X. Wang *et al.*, Comparative genomic analysis of C4 photosynthetic pathway evolution in grasses. *Genome Biology* **10**, R68 (2009).

33. L. Xia *et al.*, Rice Expression Database (RED): An integrated RNA-Seq-derived gene expression database for rice. *Journal of Genetics and Genomics* **44**, 235-241 (2017).

34. R. J. Schaefer, J.-M. Michno, C. L. Myers, Unraveling gene function in agricultural species using gene co-expression networks. *Biochimica et Biophysica Acta (BBA) - Gene Regulatory Mechanisms* **1860**, 53-63 (2017).

35. J. Beales, A. Turner, S. Griffiths, J. Snape, D. Laurie, A pseudo-response regulator is misexpressed in the photoperiod insensitive *Ppd-D1a* mutant of wheat (*Triticum aestivum* L.). *Theoretical and Applied Genetics* **115**, 721-733 (2007).

36. K. V. Krasileva *et al.*, Uncovering hidden variation in polyploid wheat. *Proceedings of the National Academy of Sciences* **114**, E913-E921 (2017).

37. Y. Wang *et al.*, Transcriptome Association Identifies Regulators of Wheat Spike Architecture. *Plant Physiology* **175**, 746-757 (2017).

38. M. Pfeifer *et al.*, Genome interplay in the grain transcriptome of hexaploid bread wheat. *Science* **345**, (2014).

39. P. Borrill, N. Adamski, C. Uauy, Genomics as the key to unlocking the polyploid potential of wheat. *New Phytologist* **208**, 1008-1022 (2015).

40. F. A. Kondrashov, Gene duplication as a mechanism of genomic adaptation to a changing environment. *Proceedings of the Royal Society B: Biological Sciences* **279**, 5048-5057 (2012).

41. P. Schiffer, J. Gravemeyer, M. Rauscher, T. Wiehe, Ultra large gene families: a matter of adaptation or genomic parasites? *Life* **6**, 32 (2016).

42. T. Sykes *et al.*, In-silico identification of candidate genes for fertility restoration in cytoplasmic male sterile perennial ryegrass (Lolium perenne L.). *Genome Biology and Evolution*, (2016).

43. J. Melonek, J. D. Stone, I. Small, Evolutionary plasticity of restorer-of-fertility-like proteins in rice. *Scientific Reports* **6**, 35152 (2016).

44. S. Gálvez *et al.*, The genomic architecture of field drought responses for wheat. *Science* **submitted as companion paper**, (2018).

45. T. Würschum, C. F. H. Longin, V. Hahn, M. R. Tucker, W. L. Leiser, Copy number variations of CBF genes at the Fr-A2 locus are essential components of winter hardiness in wheat. *The Plant Journal* **89**, 764-773 (2017).

46. A. Juhász *et al.*, Wheat proteins as a source of food intolerance: Genome mapping and influence of environment. *Science Advances* **submitted as companion paper**, (2018).

47. M. Feldman, A. A. Levy, in *Alien Introgression in Wheat: Cytogenetics, Molecular Biology, and Genomics*, M. Molnár-Láng, C. Ceoloni, J. Doležel, Eds. (Springer International Publishing, Cham, 2015), pp. 21-76.

48. C. Pont *et al.*, Tracing the ancestry of modern cultivated bread wheats. *Science* **submitted as companion paper**, (2018).

49. K. T. Nilsen *et al.*, High density mapping and haplotype analysis of the major stem-solidness locus SSt1 in durum and common wheat. *PLOS ONE* **12**, e0175285 (2017).

50. N. Sharma *et al.*, A flowering locus C homolog is a vernalization-regulated repressor in *Brachypodium* and is cold regulated in wheat. *Plant Physiology* **173**, 1301-1315 (2017).

51. H. Puchta, Applying CRISPR/Cas for genome engineering in plants: the best is yet to come. *Current Opinion in Plant Biology* **36**, 1-8 (2017).

52. H.-Q. Ling *et al.*, Draft genome of the wheat A-genome progenitor Triticum urartu. *Nature* **496**, 87 (2013).

53. J. Jia *et al.*, Aegilops tauschii draft genome sequence reveals a gene repertoire for wheat adaptation. *Nature* **496**, 91-95 (2013).

54. Y. Ishida, M. Tsunashima, Y. Hiei, T. Komari, in *Agrobacterium Protocols: Volume 1*, K. Wang, Ed. (Springer New York, New York, NY, 2015), pp. 189-198.

55. M. Alaux *et al.*, Linking the International Wheat Genome Sequencing Consortium bread wheat reference genome sequence to wheat genetic and phenomic data. *Genome Biology* **submitted as companion paper**, (2018).

56. R. Avni *et al.*, Wild emmer genome architecture and diversity elucidate wheat evolution and domestication. *Science* **357**, 93-97 (2017).

57. F. Choulet *et al.*, Megabase Level Sequencing Reveals Contrasted Organization and Evolution Patterns of the Wheat Gene and Transposable Element Spaces. *The Plant Cell* **22**, 1686-1701 (2010).

58. G. Keeble-Gagnère *et al.*, Optical and physical mapping with local finishing enables megabase-scale resolution of agronomically important regions on wheat chromosome 7A. *Genome Biology* **submitted as companion paper**, (2018).

59. R. Kalhor, H. Tjong, N. Jayathilaka, F. Alber, L. Chen, Genome architectures revealed by tethered chromosome conformation capture and population-based modeling. *Nat Biotech* **30**, 90-98 (2012).

60. E. Lieberman-Aiden *et al.*, Comprehensive Mapping of Long-Range Interactions Reveals Folding Principles of the Human Genome. *Science* **326**, 289-293 (2009).

61. S. Beier *et al.*, Construction of a map-based reference genome sequence for barley, Hordeum vulgare L. *Scientific Data* **4**, 170044 (2017).

62. J. Šafář *et al.*, Dissecting large and complex genomes: flow sorting and BAC cloning of individual chromosomes from bread wheat. *The Plant Journal* **39**, 960-968 (2004).

63. J. Šafář *et al.*, Development of chromosome-specific BAC resources for genomics of bread wheat. *Cytogenetic and Genome Research* **129**, 211-223 (2010).

64. M.-C. Luo *et al.*, High-throughput fingerprinting of bacterial artificial chromosomes using the snapshot labeling kit and sizing of restriction fragments by capillary electrophoresis. *Genomics* **82**, 378 (2003).

65. J. van Oeveren *et al.*, Sequence-based physical mapping of complex genomes by whole genome profiling. *Genome Research* **21**, 618-625 (2011).

66. C. Soderlund, S. Humphray, I. Dunham, L. French, Contigs built with fingerprints, markers, and FPC V4.7. *Genome Res* **11**, 934 - 941 (2000).

67. Z. Frenkel, E. Paux, D. Mester, C. Feuillet, A. Korol, LTC: a novel algorithm to improve the efficiency of contig assembly for physical mapping in complex genomes. *BMC Bioinformatics* **11**, 584 (2010).

68. H. Staňková *et al.*, BioNano genome mapping of individual chromosomes supports physical mapping and sequence assembly in complex plant genomes. *Plant Biotechnology Journal* **14**, 1523-1531 (2016).

69. N. Poursarebani *et al.*, Whole-genome profiling and shotgun sequencing delivers an anchored, gene-decorated, physical map assembly of bread wheat chromosome 6A. *The Plant Journal* **79**, 334-347 (2014).

70. F. Kobayashi *et al.*, A high-resolution physical map integrating an anchored chromosome with the BAC physical maps of wheat chromosome 6B. *BMC Genomics* **16**, 595 (2015).

71. M. Kubaláková, J. Vrána, J. Číhalíková, H. Šimková, J. Doležel, Flow karyotyping and chromosome sorting in bread wheat (*Triticum aestivum* L.). *Theoretical and Applied Genetics* **104**, 1362-1372 (2002).

72. V. K. Tiwari *et al.*, A whole-genome, radiation hybrid mapping resource of hexaploid wheat. *The Plant Journal* **86**, 195-207 (2016).

73. H. Rimbert *et al.*, High throughput SNP discovery and genotyping in hexaploid wheat. *PLOS ONE* **in press**, (2017).

74. S. de Givry, M. Bouchez, P. Chabrier, D. Milan, T. Schiex, Carhta Gene: multipopulation integrated genetic and radiation hybrid mapping. *Bioinformatics* **21**, 1703-1704 (2005).

75. M. E. Sorrells *et al.*, Reconstruction of the Synthetic W7984 × Opata M85 wheat reference population. *Genome* **54**, 875-882 (2011).

76. J. A. Poland, P. J. Brown, M. E. Sorrells, J.-L. Jannink, Development of high-density genetic maps for barley and wheat using a novel two-enzyme genotyping-by-sequencing approach. *PLoS ONE* **7**, e32253 (2012).

77. Y. Wu, P. R. Bhat, T. J. Close, S. Lonardi, Efficient and accurate construction of genetic linkage maps from the minimum spanning tree of a graph. *PLoS Genet* **4**, e1000212 (2008).

78. J. Doležel, M. Kubaláková, E. Paux, J. Bartoš, C. Feuillet, Chromosome-based genomics in the cereals. *Chromosome Research* **15**, 51-66 (2007).

79. A. A. Myburg *et al.*, The genome of *Eucalyptus grandis*. *Nature* **510**, 356 (2014).

80. H. Li, R. Durbin, Fast and accurate short read alignment with Burrows–Wheeler transform. *Bioinformatics* **25**, 1754-1760 (2010).

81. H. Li *et al.*, The Sequence Alignment/Map format and SAMtools. *Bioinformatics* **25**, 2078-2079 (2009).

82. R. Whitford *et al.*, Hybrid breeding in wheat: technologies to improve hybrid wheat seed production. *Journal of Experimental Botany* **64**, 5411-5428 (2013).

83. J. N. Burton *et al.*, Chromosome-scale scaffolding of de novo genome assemblies based on chromatin interactions. *Nature Biotechnology* **31**, 1119 (2013).

84. A. R. Quinlan, I. M. Hall, BEDTools: a flexible suite of utilities for comparing genomic features. *Bioinformatics* **26**, 841-842 (2010).

85. J. Daron *et al.*, Organization and evolution of transposable elements along the bread wheat chromosome 3B. *Genome Biology* **15**, 546 (2014).

86. S. Kurtz *et al.*, Versatile and open software for comparing large genomes. *Genome Biology* **5**, R12 (2004).

87. M. Martin, Cutadapt removes adapter sequences from high-throughput sequencing reads. *EMBnet.journal* **17**, 10-12 (2011).

88. P. Leroy *et al.*, TriAnnot: A Versatile and High Performance Pipeline for the Automated Annotation of Plant Genomes. *Frontiers in Plant Science* **3**, 5 (2012).

89. A. F. Smit, Identification of a new, abundant superfamily of mammalian LTR-transposons. *Nucleic Acids Research* **21**, 1863-1872 (1993).

90. S. F. Altschul *et al.*, Gapped BLAST and PSI-BLAST: a new generation of protein database search programs. *Nucl. Acids Res.* **25**, 3389-3402 (1997).

91. L. Pingault *et al.*, Deep transcriptome sequencing provides new insights into the structural and functional organization of the wheat genome. *Genome Biology* **16**, 29 (2015).

92. L. Dong *et al.*, Single-molecule real-time transcript sequencing facilitates common wheat genome annotation and grain transcriptome research. *BMC Genomics* **16**, 1039 (2015).

93. The International Barley Genome Sequencing Consortium (IBSC) *et al.*, A physical, genetical and functional sequence assembly of the barley genome. *Nature (London)* **491**, 711-716 (2012).

94. G. S. C. Slater, E. Birney, Automated generation of heuristics for biological sequence comparison. *BMC Bioinformatics* **6**, 31 (2005).

95. M. Stanke, S. Waack, Gene prediction with a hidden Markov model and a new intron submodel. *Bioinformatics* **2**, 215-225 (2003).

96. N. Amano, T. Tanaka, H. Numa, H. Sakai, T. Itoh, Efficient plant gene identification based on interspecies mapping of full-length cDNAs. *DNA Research* **17**, 271-279 (2010).

97. T. D. Wu, C. K. Watanabe, GMAP: a genomic mapping and alignment program for mRNA and EST sequences. *Bioinformatics* **21**, 1859-1875 (2005).

98. C. Trapnell *et al.*, Transcript assembly and quantification by RNA-Seq reveals unannotated transcripts and isoform switching during cell differentiation. *Nature Biotechnology* **28**, 511 (2010).

99. D. Kim, B. Langmead, S. L. Salzberg, HISAT: a fast spliced aligner with low memory requirements. *Nature Methods* **12**, 357 (2015).

100. D. W. Barnett, E. K. Garrison, A. R. Quinlan, M. P. Strömberg, G. T. Marth, BamTools: a C++ API and toolkit for analyzing and managing BAM files. *Bioinformatics* **27**, 1691-1692 (2011).

101. M. Pertea *et al.*, StringTie enables improved reconstruction of a transcriptome from RNA-seq reads. *Nature Biotechnology* **33**, 290 (2015).

102. The UniProt Consortium, UniProt: the universal protein knowledgebase. *Nucleic Acids Research* **45**, D158-D169 (2017).

103. G. Gremme, V. Brendel, M. E. Sparks, S. Kurtz, Engineering a software tool for gene structure prediction in higher organisms. *Information and Software Technology* **47**, 965-978 (2005).

104. J. Keilwagen *et al.*, Using intron position conservation for homology-based gene prediction. *Nucleic Acids Research* **44**, e89-e89 (2016).

105. K. Mochida, T. Yoshida, T. Sakurai, Y. Ogihara, K. Shinozaki, TriFLDB: a database of clustered full-length coding sequences from Triticeae with applications to comparative grass genomics. *Plant Physiology* **150**, 1135-1146 (2009).

106. S. Ghosh, C.-K. K. Chan, in *Plant Bioinformatics: Methods and Protocols*, D. Edwards, Ed. (Springer New York, New York, NY, 2016), pp. 339-361.

107. S. R. Eddy, Accelerated Profile HMM Searches. *PLOS Computational Biology* **7**, e1002195 (2011).

108. L. Venturini, S. Caim, G. Kaithakottil, D. L. Mapleson, D. Swarbreck, Leveraging multiple transcriptome assembly methods for improved gene structure annotation. *bioRxiv* **doi.org/10.1101/216994**, (2017).

109. D. Mapleson, L. Venturini, G. Kaithakottil, D. Swarbreck, Efficient and accurate detection of splice junctions from RNAseq with Portcullis. *bioRxiv* **doi.org/10.1101/217620**, (2017).

110. A. Kozomara, S. Griffiths-Jones, miRBase: integrating microRNA annotation and deep-sequencing data. *Nucleic Acids Research* **39**, D152-D157 (2011).

111. S. J. Lucas, H. Budak, Sorting the wheat from the chaff: identifying miRNAs in genomic survey sequences of *Triticum aestivum c*hromosome 1AL. *PLOS ONE* **7**, e40859 (2012).

112. N. R. Markham, M. Zuker, in *Bioinformatics: Structure, Function and Applications*, J. M. Keith, Ed. (Humana Press, Totowa, NJ, 2008), pp. 3-31.

113. H. B. Cagirici, S. Biyiklioglu, H. Budak, Assembly and annotation of transcriptome provided evidence of miRNA mobility between wheat and wheat stem sawfly. *Frontiers in Plant Science* **8**, 1653 (2017).

114. B. A. Akpinar, M. Kantar, H. Budak, Root precursors of microRNAs in wild emmer and modern wheats show major differences in response to drought stress. *Functional & Integrative Genomics* **15**, 587-598 (2015).

115. T. M. Lowe, S. R. Eddy, tRNAscan-SE: a program for improved detection of transfer RNA genes in genomic sequence. *Nucleic Acids Research* **25**, 955-964 (1997).

116. The Gene Ontology Consortium, Expansion of the Gene Ontology knowledgebase and resources. *Nucleic Acids Research* **45**, D331-D338 (2017).

117. L. Cooper *et al.*, The Plant Ontology as a tool for comparative plant anatomy and genomic analyses. *Plant and Cell Physiology* **54**, e1-e1 (2013).

118. E. Arnaud *et al.*, Towards a reference Plant Trait Ontology for modeling knowledge of plant traits and phenotypes. *DOI:10.13140/2.1.2550.3525*, (2012).

119. P. Borrill, R. Ramirez-Gonzalez, C. Uauy, expVIP: a customizable RNA-seq data analysis and visualization platform. *Plant Physiology* **170**, 2172-2186 (2016).

120. N. L. Bray, H. Pimentel, P. Melsted, L. Pachter, Near-optimal probabilistic RNA-seq quantification. *Nat Biotech* **34**, 525-527 (2016).

121. P. Langfelder, S. Horvath, WGCNA: an R package for weighted correlation network analysis. *BMC Bioinformatics* **9**, 559 (2008).

122. M. I. Love, W. Huber, S. Anders, Moderated estimation of fold change and dispersion for RNA-seq data with DESeq2. *Genome Biology* **15**, 550 (2014).

123. Y. Benjamini, D. Yekutieli, The Control of the false discovery rate in multiple testing under dependency. *The Annals of Statistics* **29**, 1165-1188 (2001).

124. F. Krueger, S. R. Andrews, Bismark: a flexible aligner and methylation caller for Bisulfite-Seq applications. *Bioinformatics* **27**, 1571-1572 (2011).

125. A. Veluchamy *et al.*, *LHP1* regulates H3K27me3 spreading and shapes the three-dimensional conformation of the Arabidopsis genome. *PLOS ONE* **11**, e0158936 (2016).

126. A. M. Bolger, M. Lohse, B. Usadel, Trimmomatic: a flexible trimmer for Illumina sequence data. *Bioinformatics* **30**, 2114-2120 (2014).

127. B. Langmead, S. L. Salzberg, Fast gapped-read alignment with Bowtie 2. *Nature Methods* **9**, 357 (2012).

128. A. D. Zimmer *et al.*, Reannotation and extended community resources for the genome of the non-seed plant *Physcomitrella patens* provide insights into the evolution of plant gene structures and functions. *BMC Genomics* **14**, 498 (2013).

129. J. S. Bernardes, F. R. J. Vieira, G. Zaverucha, A. Carbone, A multi-objective optimization approach accurately resolves protein domain architectures. *Bioinformatics* **32**, 345-353 (2016).

130. D. M. Emms, S. Kelly, OrthoFinder: solving fundamental biases in whole genome comparisons dramatically improves orthogroup inference accuracy. *Genome Biology* **16**, 157 (2015).

131. J. Huerta-Cepas, H. Dopazo, J. Dopazo, T. Gabaldón, The human phylome. *Genome Biology* **8**, R109 (2007).

132. J. Huerta-Cepas, F. Serra, P. Bork, ETE 3: reconstruction, analysis, and visualization of phylogenomic data. *Molecular Biology and Evolution* **33**, 1635-1638 (2016).

133. S. Mirarab, T. Warnow, ASTRAL-II: coalescent-based species tree estimation with many hundreds of taxa and thousands of genes. *Bioinformatics* **31**, i44-i52 (2015).

134. D. Lang *et al.*, Genome-wide phylogenetic comparative analysis of plant transcriptional regulation: a timeline of loss, gain, expansion, and correlation with complexity. *Genome Biology and Evolution* **2**, 488-503 (2010).

135. J. T. Garland, A. W. Dickerman, C. M. Janis, J. A. Jones, Phylogenetic analysis of covariance by computer simulation. *Systematic Biology* **42**, 265-292 (1993).

136. S. Grossmann, S. Bauer, P. N. Robinson, M. Vingron, Improved detection of overrepresentation of Gene-Ontology annotations with parent–child analysis. *Bioinformatics* **23**, 3024-3031 (2007).

137. S. Aibar, C. Fontanillo, C. Droste, J. De Las Rivas, Functional Gene Networks: R/Bioc package to generate and analyse gene networks derived from functional enrichment and clustering. *Bioinformatics* **31**, 1686-1688 (2015).

138. G. Su, A. Kuchinsky, J. H. Morris, D. J. States, F. Meng, GLay: community structure analysis of biological networks. *Bioinformatics* **26**, 3135-3137 (2010).

139. N.-p. D. Nguyen, S. Mirarab, K. Kumar, T. Warnow, Ultra-large alignments using phylogeny-aware profiles. *Genome Biology* **16**, 124 (2015).

140. M. N. Price, P. S. Dehal, A. P. Arkin, FastTree 2 – approximately maximum-likelihood trees for large alignments. *PLOS ONE* **5**, e9490 (2010).

141. I. Letunic, P. Bork, Interactive tree of life (iTOL) v3: an online tool for the display and annotation of phylogenetic and other trees. *Nucleic Acids Research* **44**, W242-W245 (2016).

142. N. M. Glover, H. Redestig, C. Dessimoz, Homoeologs: what are they and how do we infer them? *Trends in Plant Science* **21**, 609-621 (2016).

143. Y. Wang *et al.*, MCScanX: a toolkit for detection and evolutionary analysis of gene synteny and collinearity. *Nucleic Acids Research* **40**, e49-e49 (2012).

144. M. Mascher *et al.*, A chromosome conformation capture ordered sequence of the barley genome. *Nature* **544**, 427-433 (2017).

145. L. Al Ait, Z. Yamak, B. Morgenstern, DIALIGN at GOBICS—multiple sequence alignment using various sources of external information. *Nucleic Acids Research* **41**, W3-W7 (2013).

146. D. Wang, Y. Zhang, Z. Zhang, J. Zhu, J. Yu, KaKs_Calculator 2.0: A toolkit incorporating gamma-series methods and sliding window strategies. *Genomics, Proteomics & Bioinformatics* **8**, 77-80 (2010).

147. J. C. Zadoks, T. T. Chang, C. F. Konzak, A decimal code for the growth stages of cereals. *Weed Research (Oxford)* **14**, 415-421 (1974).

148. A. Dobin *et al.*, STAR: ultrafast universal RNA-seq aligner. *Bioinformatics* **29**, 15-21 (2013).

149. M. Pertea, D. Kim, G. M. Pertea, J. T. Leek, S. L. Salzberg, Transcript-level expression analysis of RNA-seq experiments with HISAT, StringTie and Ballgown. *Nat. Protocols* **11**, 1650-1667 (2016).

150. K. J. Livak, T. D. Schmittgen, Analysis of relative gene expression data using real-time quantitative PCR and the $2^{-\Delta\Delta CT}$ method. *Methods* **25**, 402-408 (2001).

151. A. H. Paterson *et al.*, The *Sorghum bicolor* genome and the diversification of grasses. *Nature* **457**, 551 (2009).

152. P. S. Schnable *et al.*, The B73 Maize genome: complexity, diversity, and dynamics. *Science* **326**, 1112-1115 (2009).

153. E. Bauer *et al.*, Towards a whole-genome sequence for rye (*Secale cereale* L.). *The Plant Journal* **89**, 853-869 (2017).

154. M. J. Sanderson, Estimating absolute rates of molecular evolution and divergence times: a penalized likelihood approach. *Molecular Biology and Evolution* **19**, 101-109 (2002).

155. P.-A. Christin *et al.*, Molecular dating, evolutionary rates, and the age of the grasses. *Systematic Biology* **63**, 153-165 (2014).

156. M. Krzywinski *et al.*, Circos: an information aesthetic for comparative genomics. *Genome Res* **19**, 1639 - 1645 (2009).

157. C. E. Niederhuth *et al.*, Widespread natural variation of DNA methylation within angiosperms. *Genome Biology* **17**, 194 (2016).

158. Y. Benjamini, Y. Hochberg, Controlling the false discovery rate: a practical and powerful approach to multiple testing. *Journal of the Royal Statistical Society. Series B (Methodological)* **57**, 289-300 (1995).

159. G. Yu *et al.*, GOSemSim: an R package for measuring semantic similarity among GO terms and gene products. *Bioinformatics* **26**, 976-978 (2010).

160. S. Fischer *et al.*, in *Current Protocols in Bioinformatics*. (John Wiley & Sons, Inc., 2002).

161. S. Cheng *et al.*, Redefining the structural motifs that determine RNA binding and RNA editing by pentatricopeptide repeat proteins in land plants. *The Plant Journal* **85**, 532-547 (2016).

162. Z. Li *et al.*, SSR analysis and identification of fertility restorer genes *Rf1* and *Rf4* of *Triticum timopheevii* cytoplasmic male sterility (T-CMS) in wheat (*Triticum aestivum* L.). *Journal of Agricultural Biotechnology* **22**, 1114-1122 (2014).

163. M. Geyer, T. Albrecht, L. Hartl, V. Mohler, Exploring the genetics of fertility restoration controlled by *Rf1* in common wheat (*Triticum aestivum* L.) using high-density linkage maps. *Molecular Genetics and Genomics* **293**, 451-462 (2017).

164. P. Sinha, S. M. S. Tomar, Vinod, V. K. Singh, H. S. Balyan, Genetic analysis and molecular mapping of a new fertility restorer gene *Rf8* for *Triticum timopheevi* cytoplasm in wheat (*Triticum aestivum* L.) using SSR markers. *Genetica* **141**, 431-441 (2013).

165. J. Breen *et al.*, A physical map of the short arm of wheat chromosome 1A. *PLOS ONE* **8**, e80272 (2013).

166. S. J. Lucas *et al.*, Physical mapping integrated with syntenic analysis to characterize the gene space of the long arm of wheat chromosome 1A. *PLOS ONE* **8**, e59542 (2013).

167. D. Raats *et al.*, The physical map of wheat chromosome 1BS provides insights into its gene space organization and evolution. *Genome Biology* **14**, R138 (2013).

168. R. Philippe *et al.*, A high density physical map of chromosome 1BL supports evolutionary studies, map-based cloning and sequencing in wheat. *Genome Biology* **14**, R64 (2013).

169. E. Paux *et al.*, A physical map of the 1-Gigabase bread wheat chromosome 3B. *Science* **322**, 101-104 (2008).

170. K. Holušová *et al.*, Physical map of the short arm of bread wheat chromosome 3D. *The Plant Genome* **10**, (2017).

171. O. Shorinola *et al.*, Association mapping and haplotype analysis of the pre-harvest sprouting resistance locus *Phs-A1* reveals a causal role of *TaMKK3-A* in global germplasm. *bioRxiv*, 10.1101/131201 (2017).

172. D. Barabaschi *et al.*, Physical mapping of bread wheat chromosome 5A: an integrated approach. *The Plant Genome* **8**, (2015).

173. E. A. Salina *et al.*, Features of the organization of bread wheat chromosome 5BS based on physical mapping. *BMC Genomics* **in press**, (2018).

174. B. A. Akpinar *et al.*, The physical map of wheat chromosome 5DS revealed gene duplications and small rearrangements. *BMC Genomics* **16**, 453 (2015).

175. T. Belova *et al.*, Utilization of deletion bins to anchor and order sequences along the wheat 7B chromosome. *Theoretical and Applied Genetics* **127**, 2029-2040 (2014).

176. Z. Tulpová *et al.*, Integrated physical map of bread wheat chromosome arm 7DS to facilitate gene cloning and comparative studies. *New Biotechnology*, **10.1016/j.nbt.2018.03.003**, (2018).

177. F.-H. Lu *et al.*, Independent assessment and improvement of wheat genome assemblies using Fosill jumping libraries. *bioRxiv*, 10.1101/219352 (2017).

178. M. A. Nesterov *et al.*, Identification of microsatellite loci based on BAC sequencing data and their physical mapping into the soft wheat 5B chromosome. *Russian Journal of Genetics: Applied Research* **6**, 825-837 (2016).

179. E. M. Sergeeva *et al.*, Fine organization of genomic regions tagged to the 5S rDNA locus of the bread wheat 5B chromosome. *BMC Plant Biology* **17**, 183 (2017).

180. M.-C. Luo *et al.*, A 4-gigabase physical map unlocks the structure and evolution of the complex genome of *Aegilops tauschii*, the wheat D-genome progenitor. *Proceedings of the National Academy of Sciences* **110**, 7940-7945 (2013).

181. X. Zeng *et al.*, The draft genome of Tibetan hulless barley reveals adaptive patterns to the high stressful Tibetan Plateau. *Proceedings of the National Academy of Sciences* **112**, 1095-1100 (2015).

182. Y. Kawahara *et al.*, Improvement of the *Oryza sativa* Nipponbare reference genome using next generation sequence and optical map data. *Rice* **6**, 4 (2013).

Acknowledgments: The IWGSC would like to thank the following individuals: Michael Burrell and Chris Bridson (Norwich Biosciences Institute) for computational support of RNA-Seq data; Idun Christie (Graminor AS) and Heidi Rudi (Norwegian University of Life Sciences) for assistance with chromosome 7B; Robert P. Davey (Earlham Institute) for assistance with RNA-Seq data; Jasline Deek (Tel Aviv University) for growing the source plants and DNA extraction used for whole genome sequencing; Zdeňka Dubská, Eva Jahnová, Marie Seifertová, Romana Šperková, Radka Tušková, and Jitka Weiserová (Institute of Experimental Botany, Olomouc) for assistance with flow cytometric chromosome sorting, BAC library construction, and estimation of genome size; Sophie Durand, Véronique Jamilloux, Mathilde Lainé, and Célia Michotey (URGI, INRA) for assistance with and access to the IWGSC sequence repository; Anne Fiebig of the Leibniz Institute of Plant Genetics and Crop Plant Research (IPK) for submitting the Hi-C data; Tobin Florio for the design of the wheat schematic for the expression atlas and Sst Figure (www.flozbox.com/Science_Illustrated); Chithra Karunakaran and Toby Bond of the Canadian Light Source for performing CT imaging; Jun Kawai, Naoto Kondo Hiromi Sano, Naoko Suzuki, Michihira Tagami, Hiroshi Tarui of RIKEN and Hiroko Fujisawa, Yuichi Katayose, Kanako

Kurita, Satomi Mori, Yoshiyuki Mukai, and Harumi Sasaki of the Institute of Crop Science, NARO, and Takashi Matsumoto of Tokyo University of Agriculture for assistance with deep sequencing of chromosome 6B; Patricia Lenoble and Céline Orvain of Genoscope for assistance in the sequencing of chromosome 1B; Adam J. Lukaszewski (University of California, Riverside), Bernd Friebe and Jon Raupp (Kansas State University) for providing seeds of wheat telosomic lines for chromosome sorting; Csaba Maulis (https://polytypo.design, https://propepper.net) for design and graphics of the prolamin super-family chromosome map; Marie Seifertová and Helena Tvardíková of the Institute of Experimental Botany for assistance with BAC DNA extraction and sequencing for chromosomes 3DS, 4A, and 7DS; and Ian Willick and Karen Tanino of the University of Saskatchewan for their assistance in sample preparation and the use of lab facilities.

Funding: The authors would like to thank the following for their financial support of research that enabled the completion of the IWGSC RefSeq v1.0 Project: Agence Nationale pour la Recherche (ANR), ANR-11-BSV5-0015- Ploid-Ploid Wheat- Unravelling bases of polyploidy success in wheat and ANR-16-TERC-0026-01- 3DWHEAT; Agriculture and Agri-Food Canada National Wheat Improvement Program and the AgriFlex Program; Alberta Wheat Development Commission through the Canadian Applied Tricticum Genomics (CTAG2); Australian Government, Department of Industry, Innovation, Climate Change, Science, Research and Tertiary Education: Australia China Science and Research Fund Group Mission (Funding Agreement ACSRF00542); Bayer CropScience; Biotechnology and Biological Sciences Research Council (BBSRC) 20:20 Wheat® (project number BB/J00426X/1), Institute Strategic Programme grant [BB/J004669/1], Designing Future Wheat (DFW) Institute Strategic Programme (BB/P016855/1), the Wheat Genomics for Sustainable Agriculture (BB/J003557/1), and the Anniversary Future Leader Fellowship (BB/M014045/1); Canada First Research Excellence Fund through the Designing Crops for Global Food Security initiative at the University of Saskatchewan; Council for Agricultural Research and Economics, Italy, through CREA-Interomics; Department of Biotechnology, Ministry of Science and Technology, Govt. of India File No. F. No.BT/IWGSC/03/TF/2008; DFG (SFB924) for support of KFXM; European Commission through the *TriticeaeGenome* (FP7-212019); France Génomique (ANR-10-INBS-09,) Genome Canada through the CTAG2 project; Genome Prairie through the CTAG2 project; German Academic Exchange Service (DAAD) PPP Australien 1j16; German Federal Ministry of Food and Agriculture grant 2819103915 WHEATSEQ"; German Ministry of Education and Research grant 031A536 “de.NBI”; Global Institute for Food Security Genomics and Bioinformatics fund; Gordon and Betty Moore Foundation Grant GBMF4725 to Two Blades Foundation; Grain Research Development Corporation (GRDC) Australia; Graminor AS NFR project 199387 - Expanding the technology base for Norwegian wheat breeding; Sequencing wheat chromosome 7B; illumina; INRA - French National Institute for Agricultural Research; International Wheat Genome Sequencing Consortium and its sponsors; Israel Science Foundation grants 999/12, 1137/17, and 1824/12; Junta de Andalucía, Spain, project P12-AGR-0482; MINECO (Spanish Ministry of Economy, Industry and Competitiveness) project BIO2011-15237-E; Ministry of Agriculture, Forestry and Fisheries of Japan through Genomics for Agricultural Innovation, KGS-1003 and through Genomics-based Technology for Agricultural Improvement, NGB-1003; Ministry of Education and Science of Russian Federation project RFMEFI60414X0106 and project RFMEFI60414 X0107; Ministry of Education, Youth and Sport of the Czech Republic Award no. LO1204 (National Program of Sustainability I); Nisshin

Flour Milling Inc.; National Research Council of Canada Wheat Flagship program; Norwegian University of Life Sciences (NMBU) NFR project 199387 - Expanding the technology base for Norwegian wheat breeding - Sequencing wheat chromosome 7B; National Science Foundation, United States, Award (FAIN) 1339389, GPF-PG: Genome Structure and Diversity of Wheat and Its Wild Relatives, Award DBI-0701916, and Award IIP-1338897; Russian Science Foundation project 14-14-00161; Saskatchewan Ministry of Agriculture through the CTAG2 project; Saskatchewan Wheat Development Commission through the CTAG2 project; The Czech Science Foundation Award no. 521/06/1723 (Construction of BAC library and physical mapping of the wheat chromosome 3D), Award no. 521-08-1629 (Construction of BAC DNA libraries specific for chromosome 4AL, and positional cloning of gene for adult plant resistance to powdery mildew in wheat), Award no. P501/10/1740 (Physical map of the wheat chromosome 4AL and positional cloning of a gene for yield), Award no. P501/12/2554 (Physical map of wheat chromosome arm 7DS and its use to clone a Russian wheat aphid resistance gene), Award no. P501/12/G090 (Evolution and Function of Complex Plant Genomes), Award no. 14-07164S (Cloning and molecular characterization of wheat QPm-tut-4A gene conferring seedling and adult plant race nonspecific powdery mildew resistance), and Award no. 13-08786S (Chromosome arm 3DS of bread wheat: its sequence and function in allopolyploid genome); The Research Council of Norway (NFR) project 199387 - Expanding the technology base for Norwegian wheat breeding; Sequencing wheat chromosome 7B; United States Department of Agriculture NIFA 2008-35300-04588, the University of Zurich; Western Grains Research Foundation through the CTAG2 project; Western Grains Research Foundation National Wheat Improvement Program; and the Winifred-Asbjornson Plant Science Endowment Fund. The research leading to these results also has received funding from the French Government managed by the Research National Agency (ANR) under the Investment for the Future programme (BreedWheat project ANR-10-BTBR-03), from FranceAgriMer (2011-0971 and 2013-0544), French Funds to support Plant Breeding (FSOV) and from INRA. Axiom genotyping was conducted on the genotyping platform GENTYANE at INRA Clermont-Ferrand (gentyane.clermont.inra.fr). This research was supported in part by the NBI Computing infrastructure for Science (CiS) group through the HPC cluster.

Author contributions: The International Wheat Genome Sequencing Consortium (IWGSC). Authorship of this paper should be cited as "International Wheat Genome Sequencing Consortium" (IWGSC, 2018). Participants are arranged by working group and contributions with leaders/co-leaders and major contributors listed alphabetically first and then other contributors follow alphabetically. Corresponding authors (*), major contributors (†) and working group leader(s) or co-leaders (‡) are indicated.

IWGSC RefSeq Principal Investigators: Rudi Appels[1,36*‡] (rudi.appels@unimelb.edu.au), Kellye Eversole[2,3*‡] (eversole@eversoleassociates.com), Catherine Feuillet[17] (feuillet@bayer.com), Beat Keller[41] (bkeller@botinst.uzh.ch), Jane Rogers[6‡] (janerogersh@gmail.com), and Nils Stein[4,5*‡].

IWGSC Whole Genome Assembly Principal Investigators: Curtis J. Pozniak[11‡] (curtis.pozniak@usask.ca), Nils Stein[4,5*‡] (stein@ipk-gatersleben.de), Frédéric Choulet[7] (frederic.choulet@inra.fr), Assaf Distelfeld[25] (adistel@tauex.tau.ac.il), Kellye Eversole[2,3*] (eversole@eversoleassociates.com), Jesse Poland[28] (jpoland@ksu.edu), Jane Rogers[6]

(janerogersh@gmail.com), Gil Ronen[12] (gil@nrgene.com), and Andrew G. Sharpe[43] **(**andrew.sharpe@gifs.ca**).**

Whole Genome Sequencing and Assembly: Curtis Pozniak[11‡] (curtis.pozniak@usask.ca), Gil Ronen[12‡] (gil@nrgene.com), Nils Stein[4,5*‡] (stein@ipk-gatersleben.de), Omer Barad[12†] (omerb@nrgene.com), Kobi Baruch[12†] (kobi@nrgene.com), Frédéric Choulet[7†] (frederic.choulet@inra.fr), Gabriel Keeble-Gagnère[1†] (gabriel.keeble-gagnere@ecodev.vic.gov.au), Martin Mascher[4,67†] (mascher@ipk-gatersleben.de), Andrew G. Sharpe[43†] (andrew.sharpe@gifs.ca), Gil Ben-Zvi[12†] (bzgil@nrgene.com), and Ambre-Aurore Josselin[7] (ambre-aurore.josselin@inra.fr),

Hi-C Data Based Scaffolding: Nils Stein[4,5*‡] (stein@ipk-gatersleben.de), Martin Mascher[4,67‡] (mascher@ipk-gatersleben.de), and Axel Himmelbach[4] (himmelba@ipk-gatersleben.de).

Whole Genome Assembly QC & Analyses: Frédéric Choulet[7‡] (frederic.choulet@inra.fr), Gabriel Keeble-Gagnère[‡] (gabriel.keeble-gagnere@ecodev.vic.gov.au), Martin Mascher[4,67‡](mascher@ipk-gatersleben.de), Jane Rogers[6‡] (janerogersh@gmail.com), François Balfourier[7] (francois.balfourier@inra.fr), Juan Gutierrez-Gonzalez[30] (jgutierr@umn.edu), Matthew Hayden[1] (matthew.hayden@ecodev.vic.gov.au), Ambre-Aurore Josselin[7] (ambre-aurore.josselin@inra.fr), ChuShin Koh[43] (kevin.koh@gifs.ca), Gary Muehlbauer[30] (muehl003@umn.edu), Raj K Pasam[1] (raj.pasam@ecodev.vic.gov.au), Etienne Paux[7] (etienne.paux@inra.fr), Curtis J. Pozniak[11] (curtis.pozniak@usask.ca), Philippe Rigault[39] (prigault@gydle.com), Andrew G. Sharpe[43] **(**andrew.sharpe@gifs.ca**),** Josquin Tibbits[1] (josquin.tibbits@ecodev.vic.gov.au), and Vijay Tiwari[54] (vktiwari@umd.edu).

Pseudomolecule Assembly: Frédéric Choulet[7‡] (frederic.choulet@inra.fr), Gabriel Keeble-Gagnère[1‡] (gabriel.keeble-gagnere@ecodev.vic.gov.au), Martin Mascher[4,67‡] (mascher@ipk-gatersleben.de), Ambre-Aurore Josselin[7] (ambre-aurore.josselin@inra.fr), and Jane Rogers[6] (janerogersh@gmail.com).

RefSeq Genome Structure and Gene Analyses: Manuel Spannagl[9‡] (manuel.spannagl@helmholtz-muenchen.de), Frédéric Choulet[7‡] (frederic.choulet@inra.fr), Daniel Lang[9†] (daniel.lang@helmholtz-muenchen.de), Heidrun Gundlach[9] (h.gundlach@helmholtz-muenchen.de), Georg Haberer[9] (g.haberer@helmholtz-muenchen.de), Gabriel Keeble-Gagnère[1] (gabriel.keeble-gagnere@ecodev.vic.gov.au), Klaus F.X. Mayer[9,44] (k.mayer@helmholtz-muenchen.de), Danara Ormanbekova[9,48] (danara.ormanbekova2@unibo.it), Etienne Paux[7] (etienne.paux@inra.fr), Verena Prade[9] (verena.prade@helmholtz-muenchen.de), Hana Šimková[8] (simkovah@ueb.cas.cz), and Thomas Wicker[41] (wicker@botinst.uzh.ch).

Automated Annotation: Frédéric Choulet[7‡] (frederic.choulet@inra.fr), Manuel Spannagl[9‡] (manuel.spannagl@helmholtz-muenchen.de), David Swarbreck[50‡] (david.swarbreck@earlham.ac.uk), Hélène Rimbert[7†] (helene.rimbert@inra.fr), Marius Felder[9] (marius.felder@helmholtz-muenchen.de), Nicolas Guilhot[7] (nicolas.guilhot@inra.fr), Heidrun Gundlach[9] (h.gundlach@helmholtz-muenchen.de), Georg Haberer[9] (g.haberer@helmholtz-muenchen.de), Gemy Kaithakottil[50] (Gemy.Kaithakottil@earlham.ac.uk), Jens Keilwagen[40] (jens.keilwagen@julius-kuehn.de), Daniel Lang[9] (daniel.lang@helmholtz-muenchen.de), Philippe Leroy[7] (philippe.leroy.2@inra.fr), Thomas Lux[9] (thomas.lux@helmholtz-muenchen.de),

Klaus F.X. Mayer[9,44] (k.mayer@helmholtz-muenchen.de), Sven Twardziok[9] (sven.twardziok@posteo.de), and Luca Venturini[50] (Luca.Venturini@earlham.ac.uk).

Manual Gene Curation: Rudi Appels[1,36‡*] (rudi.appels@unimelb.edu.au), Hélène Rimbert[7†] (helene.rimbert@inra.fr), Frédéric Choulet[7] (frederic.choulet@inra.fr), Angéla Juhász[36,37] (A.Juhasz@murdoch.edu.au), and Gabriel Keeble-Gagnère[1] (gabriel.keeble-gagnere@ecodev.vic.gov.au).

Sub-Genome Comparative Analyses: Frédéric Choulet[7‡] (frederic.choulet@inra.fr), Manuel Spannagl[9‡] (manuel.spannagl@helmholtz-muenchen.de), Daniel Lang[9†] (daniel.lang@helmholtz-muenchen.de), Michael Abrouk[8,19] (abrouk@ueb.cas.cz), Georg Haberer[9] (g.haberer@helmholtz-muenchen.de), Gabriel Keeble-Gagnère[1] (gabriel.keeble-gagnere@ecodev.vic.gov.au), Klaus F.X. Mayer[9,44] (k.mayer@helmholtz-muenchen.de), and Thomas Wicker[41] (wicker@botinst.uzh.ch).

Transposable Elements: Frédéric Choulet[7‡] (frederic.choulet@inra.fr), Thomas Wicker[41†](wicker@botinst.uzh.ch), Heidrun Gundlach[9†] (h.gundlach@helmholtz-muenchen.de), Daniel Lang[9] (daniel.lang@helmholtz-muenchen.de), and Manuel Spannagl[9] (manuel.spannagl@helmholtz-muenchen.de).

Phylogenomic Analyses: Daniel Lang[9‡] (daniel.lang@helmholtz-muenchen.de) Manuel Spannagl[9‡] (manuel.spannagl@helmholtz-muenchen.de), Rudi Appels[1,36*] (rudi.appels@unimelb.edu.au), and Iris Fischer[9] (iris.fischer@helmholtz-muenchen.de).

Transcriptome Analyses & RNASeq Data: Cristobal Uauy[10‡] (cristobal.uauy@jic.ac.uk), Philippa Borrill[10†] (Philippa.Borrill@jic.ac.uk), Ricardo H. Ramirez-Gonzalez[10†] (Ricardo.Ramirez-Gonzalez@jic.ac.uk), Rudi Appels[1,36*] (rudi.appels@unimelb.edu.au), Dominique Arnaud[63] (dominiquearnaud.fr@gmail.com), Smahane Chalabi[63] (smahane.chalabi@gmail.com), Boulos Chalhoub[62,63] (boulos.chalhoub@yahoo.com), Frédéric Choulet[7] (frederic.choulet@inra.fr), Aron Cory[11] (aron.cory@usask.ca), Raju Datla[22] (raju.datla@nrc-cnrc.gc.ca), Mark W. Davey[18] (mark.davey@bayer.com), Matthew Hayden[1] (matthew.hayden@ecodev.vic.gov.au), John Jacobs[18] (j.jacobs@bayer.com), Daniel Lang[9] (daniel.lang@helmholtz-muenchen.de), Stephen J. Robinson[52] (steve.robinson@agr.gc.ca), Manuel Spannagl[9] (manuel.spannagl@helmholtz-muenchen.de), Burkhard Steuernagel[10] (burkhard.steuernagel@jic.ac.uk), Josquin Tibbits[1] (josquin.tibbits@ecodev.vic.gov.au), Vijay Tiwari[54] (vktiwari@umd.edu), Fred van Ex[18] (frederic.vanex@bayer.com), and Brande B. H. Wulff[10] (brande.wulff@jic.ac.uk).

Whole Genome Methylome: Curtis J. Pozniak[11‡] (curtis.pozniak@usask.ca), Stephen J. Robinson[52‡] (steve.robinson@agr.gc.ca), Andrew G. Sharpe[43‡] (andrew.sharpe@gifs.ca), and Aron Cory[11] (aron.cory@usask.ca).

Histone Mark Analyses: Moussa Benhamed[15‡] (moussa.benhamed@u-psud.fr), Etienne Paux[7‡] (etienne.paux@inra.fr), Abdelhafid Bendahmane[15] (abdel.bendahmane@u-psud.fr), Lorenzo Concia[15] (lorenzo.concia@u-psud.fr), and David Latrasse[15] (david.latrasse@u-psud.fr).

BAC Chromosome MTP IWGSC-Bayer Whole Genome Profiling(WGP™) Tags: Jane Rogers[6‡] (janerogersh@gmail.com), John Jacobs[18‡] (j.jacobs@bayer.com), Michael Alaux[13] (michael.alaux@inra.fr), Rudi Appels[1,36*] (rudi.appels@unimelb.edu.au), Jan Bartoš[8] (bartos@ueb.cas.cz), Arnaud Bellec[20] (arnaud.bellec@inra.fr), Hélène Berges[20] (helene.berges@inra.fr), Jaroslav Doležel[8] (dolezel@ueb.cas.cz), Catherine Feuillet[17] (feuillet@bayer.com), Zeev Frenkel[26] (zvfrenkel@gmail.com), Bikram Gill[28] (bsgill@ksu.edu), Abraham Korol[26] (korol@research.haifa.ac.il), Thomas Letellier[13] (thomas.letellier@inra.fr), Odd-Arne Olsen[56] (odd-arne.olsen@nmbu.no), Hana Šimková[8] (simkovah@ueb.cas.cz), Kuldeep Singh[65] (kuldeep35@pau.edu), Miroslav Valárik[8](valarik@ueb.cas.cz), Edwin van der Vossen[64] (edwin.van-der-vossen@keygene.com), Sonia Vautrin[20] (sonia.vautrin@inra.fr), and Song Weining[66] (sweining2002@yahoo.com).

Chromosome LTC Mapping & Physical Mapping Quality Control: Abraham Korol[26‡] (korol@research.haifa.ac.il), Zeev Frenkel[26†] (zvfrenkel@gmail.com), Tzion Fahima[26†] (fahima@research.haifa.ac.il), Vladimir Glikson[29] (lvglikson@gmail.com), Dina Raats[50] (dina.raats@earlham.ac.uk), and Jane Rogers[6] (janerogersh@gmail.com).

RH Mapping: Vijay Tiwari[54‡] (vktiwari@umd.edu), Bikram Gill[28] (bsgill@ksu.edu), Etienne Paux[7] (etienne.paux@inra.fr), and Jesse Poland[28] (jpoland@ksu.edu).

Optical Mapping: Jaroslav Doležel[8‡] (dolezel@ueb.cas.cz), Jarmila Číhalíková[8] (cihalikovaj@seznam.cz), Hana Šimková[8] (simkovah@ueb.cas.cz), Helena Toegelová[8] (toegelova@ueb.cas.cz), and Jan Vrána[8] (vrana@ueb.cas.cz).

Recombination Analyses: Pierre Sourdille[‡7] (pierre.sourdille@inra.fr) and Benoit Darrier[7] (benoit.darrier@inra.fr).

Gene Family Analyses: Rudi Appels[1,36*‡] (rudi.appels@unimelb.edu.au), Manuel Spannagl[9‡] (manuel.spannagl@helmholtz-muenchen.de), Daniel Lang[9†] (daniel.lang@helmholtz-muenchen.de), Iris Fischer[9] (iris.fischer@helmholtz-muenchen.de), Danara Ormanbekova[9,48] (danara.ormanbekova2@unibo.it), and Verena Prade[9] (verena.prade@helmholtz-muenchen.de).

CBF gene family: Delfina Barabaschi[16‡] (delfina.barabaschi@crea.gov.it) and Luigi Cattivelli[16] (luigi.cattivelli@crea.gov.it).

Dehydrin gene family: Pilar Hernandez[33‡] (phernandez@ias.csic.es), Sergio Galvez[27‡] (galvez@uma.es), and Hikmet Budak[14] (hikmet.budak@montana.edu).

NLR gene family: Burkhard Steuernagel[10‡] (burkhard.steuernagel@jic.ac.uk), Jonathan D. G. Jones[35] (jonathan.jones@sainsbury-laboratory.ac.uk), Kamil Witek[35] (kamil.witek@sainsbury-laboratory.ac.uk), Brande B. H. Wulff[10] (brande.wulff@jic.ac.uk), and Guotai Yu[10], (guotai.yu@jic.ac.uk).

PPR gene family: Ian Small[45‡] (ian.small@uwa.edu.au), Joanna Melonek[45†] (joanna.melonek@uwa.edu.au), and Ruonan Zhou[4], (zhou@ipk-gatersleben.de).

Prolamin gene family: Angéla Juhász[36,37‡] (A.Juhasz@murdoch.edu.au), Tatiana Belova[56†] (tatiana.belova@nmbu.no), Rudi Appels[1,36*] (rudi.appels@unimelb.edu.au), and Odd-Arne Olsen[56] (odd-arne.olsen@nmbu.no).

WAK gene family: Kostya Kanyuka[38‡] (kostya.kanyuka@rothamsted.ac.uk), Robert King[42†] (robert.king@rothamsted.ac.uk)

Stem Solidness (Sst1) QTL Team: Kirby Nilsen[11‡] (kirby.nilsen@usask.ca), Sean Walkowiak[11‡] (sean.walkowiak@usask.ca), Curtis J. Pozniak[11‡] (curtis.pozniak@usask.ca), Richard Cuthbert[21] (richard.cuthbert@agr.gc.ca), Raju Datla[22] (raju.datla@nrc-cnrc.gc.ca), Ron Knox[21] (ron.knox@agr.gc.ca), Krysta Wiebe[11] (k.wiebe@usask.ca), and Daoquan Xiang[22] (daoquan.xiang@nrc-cnrc.gc.ca).

Flowering Locus C (FLC) Gene Team: Antje Rohde[72‡] (antje.rohde@bayer.com) and Timothy Golds[18‡] (timothy.golds@bayer.com)

Genome Size Analysis: Jaroslav Doležel[8‡] (dolezel@ueb.cas.cz), Jana Čížková[8] (cizkova@ueb.cas.cz), and Josquin Tibbits[1] (josquin.tibbits@ecodev.vic.gov.au).

MicroRNA and tRNA annotation: Hikmet Budak[14‡] (hikmet.budak@montana.edu), Bala Ani Akpinar[14] (aniakpinar@gmail.com), and Sezgi Biyiklioglu[14] (sezgi.biyiklioglu@montana.edu).

Genetic Maps and Mapping: Gary Muehlbauer[30‡] (muehl003@umn.edu), Jesse Poland[28‡] (jpoland@ksu.edu), Liangliang Gao[28] (lianggao@ksu.edu), Juan Gutierrez-Gonzalez[30] (jgutierr@umn.edu), and Amidou N'Daiye[11](amidou.ndaiye@usask.ca).

BAC libraries and Chromosome Sorting: Jaroslav Doležel[8‡] (dolezel@ueb.cas.cz), Hana Šimková[8†] (simkovah@ueb.cas.cz), Jarmila Číhalíková[8] (cihalikovaj@seznam.cz), Marie Kubaláková[8] (kubalakovam@seznam.cz), Jan Šafář[8] (safar@ueb.cas.cz), and Jan Vrána[8] (vrana@ueb.cas.cz).

BAC Pooling, BAC library Repository, and Access: Hélène Berges[20‡] (helene.berges@inra.fr), Arnaud Bellec[20] (arnaud.bellec@inra.fr), and Sonia Vautrin[20] (sonia.vautrin@inra.fr).

IWGSC Sequence & Data Repository and Access: Michael Alaux[13‡] (michael.alaux@inra.fr), Françoise Alfama[13] (francoise.alfama-depauw@inra.fr), Anne-Françoise Adam-Blondon[13] (anne-francoise.adam-blondon@inra.fr), Raphael Flores[13] (raphael.flores@inra.fr), Claire Guerche[13] (claire.guerche@inra.fr), Thomas Letellier[13] (thomas.letellier@inra.fr), Mikaël Loaec[13] (mikael.loaec@inra.fr), and Hadi Quesneville[13] (hadi.quesneville@inra.fr).

Physical Maps and BAC-based Sequences:

1A BAC Sequencing & Assembly: Curtis J. Pozniak[11‡] (curtis.pozniak@usask.ca), Andrew G. Sharpe[22,43‡] **(**andrew.sharpe@gifs.ca**),** Sean Walkowiak[‡11] (sean.walkowiak@usask.ca), Hikmet Budak[14] (hikmet.budak@montana.edu), Janet Condie[22] (Janet.Condie@nrc-cnrc.gc.ca), Jennifer Ens[11] (jennifer.ens@usask.ca), ChuShin Koh[43] (kevin.koh@gifs.ca), Ron Maclachlan[11]

(ron.maclachlan@usask.ca), Yifang Tan[22] (yifang.tan@nrc-cnrc.gc.ca), and Thomas Wicker[41] (wicker@botinst.uzh.ch).

1B BAC Sequencing & Assembly: Frédéric Choulet[7‡] (frederic.choulet@inra.fr), Etienne Paux[7‡] (etienne.paux@inra.fr), Adriana Alberti[61] (aalberti@genoscope.cns.fr), Jean-Marc Aury[61] (jmaury@genoscope.cns.fr), François Balfourier[7] (francois.balfourier@inra.fr), Valérie Barbe[61] (vbarbe@genoscope.cns.fr), Arnaud Couloux[61] (acouloux@genoscope.cns.fr), Corinne Cruaud[61] (cruaud@genoscope.cns.fr), Karine Labadie[61] (klabadie@genoscope.cns.fr), Sophie Mangenot[61] (mangenot@genoscope.cns.fr), and Patrick Wincker[61,68,69] (pwincker@genoscope.cns.fr).

1D, 4D, 6D Physical Mapping: Bikram Gill[28‡] (bsgill@ksu.edu), Gaganpreet Kaur[28] (gaganchahal@gmail.com), Mingcheng Luo[34] (mcluo@ucdavis.edu), and Sunish Sehgal[53] (sunish.sehgal@sdstate.edu).

2AL Physical Mapping: Kuldeep Singh[65‡] (kuldeep35@pau.edu), Parveen Chhuneja[65] (pchhuneja@pau.edu), Om Prakash Gupta[65] (opgupta@pau.edu), Suruchi Jindal[65] (suruchi-coasab@pau.edu), Parampreet Kaur[65] (parampreet.pau@gmail.com), Palvi Malik[65] (palvimalik@pau.edu), Priti Sharma[65] (pritisharma@pau.edu), and Bharat Yadav[65] (bharat_yadav@pau.edu).

2AS Physical Mapping: Nagendra K. Singh[70‡] (nksingh4@gmail.com), Jitendra P. Khurana[71‡] (khuranaj@genomeindia.org), Chanderkant Chaudhary[71] (ckryptone@gmail.com), Paramjit Khurana[71] (param@genomeindia.org), Vinod Kumar[70] (kumar.vinod81@gmail.com), Ajay Mahato[70] (ajaybioinfo@gmail.com), Saloni Mathur[71] (saloni@genomeindia.org), Amitha Sevanthi[70] (amithamithra.nrcpb@gmail.com), Naveen Sharma[71] (naveenlalosharma@gmail.com), and Ram Sewak Tomar[70] (rsstomar@rediffmail.com).

2B, 2D, 4B, 5BL, & 5DL IWGSC-Bayer Whole Genome Profiling(WGP™) Physical Maps: Jane Rogers[6‡] (janerogersh@gmail.com), John Jacobs[18‡] (j.jacobs@bayer.com), Michael Alaux[13] (michael.alaux@inra.fr), Arnaud Bellec[20] (arnaud.bellec@inra.fr), Hélène Berges[20] (helene.berges@inra.fr), Jaroslav Doležel[8] (dolezel@ueb.cas.cz), Catherine Feuillet[17] (feuillet@bayer.com), Zeev Frenkel[26] (zvfrenkel@gmail.com), Bikram Gill[28] (bsgill@ksu.edu), Abraham Korol[26] (korol@research.haifa.ac.il), Edwin van der Vossen[64] (edwin.van-der-vossen@keygene.com), and Sonia Vautrin[20] (sonia.vautrin@inra.fr).

3AL Physical Mapping: Bikram Gill[28‡] (bsgill@ksu.edu), Gaganpreet Kaur[28] (gaganchahal@gmail.com), Mingcheng Luo[34] (mcluo@ucdavis.edu), and Sunish Sehgal[53] (sunish.sehgal@sdstate.edu).

3DS Physical Mapping & BAC Sequencing & Assembly: Jan Bartoš[8‡] (bartos@ueb.cas.cz), Kateřina Holušová[8] (holusovak@ueb.cas.cz), and Ondřej Plíhal[49] (ondrej.plihal@upol.cz).

3DL BAC Sequencing & Assembly: Matthew D. Clark[50,73] (matt.clark@nhm.ac.uk), Darren Heavens[50] (Darren.Heavens@earlham.ac.uk), George Kettleborough[50] (kettleg@gmail.com), and Jon Wright[50] (Jon.Wright@earlham.ac.uk).

4A Physical Mapping, BAC Sequencing, Assembly, & Annotation: Miroslav Valárik[8‡] (valarik@ueb.cas.cz), Michael Abrouk[8,19] (abrouk@ueb.cas.cz), Barbora Balcárková[8] (balcarkova.bara@seznam.cz), Kateřina Holušová[8] (holusovak@ueb.cas.cz), Yuqin Hu (yqhu@ucdavis.edu), and Mingcheng Luo[34] (mcluo@ucdavis.edu).

5BS BAC Sequencing, & Assembly: Elena Salina[47‡] **(**salina@bionet.nsc.ru**),** Nikolai Ravin[23,51‡] (nravin@biengi.ac.ru), Konstantin Skryabin[23,51‡] (skryabin@biengi.ac.ru), Alexey Beletsky[23] (mortu@yandex.ru), Vitaly Kadnikov[23] (vkadnikov@bk.ru), Andrey Mardanov[23] (mardanov@biengi.ac.ru), Michail Nesterov[47] (mikkanestor@bionet.nsc.ru), Andrey Rakitin[23] (rakitin@biengi.ac.ru), and Ekaterina Sergeeva[47] (sergeeva@bionet.nsc.ru).

6B BAC Sequencing & Assembly: Hirokazu Handa[31‡] (hirokazu@affrc.go.jp), Hiroyuki Kanamori[31] (kanamo@affrc.go.jp), Satoshi Katagiri[31] (skatagiri@affrc.go.jp), Fuminori Kobayashi[31] (kobafumi@affrc.go.jp), Shuhei Nasuda[46] (nasushu@kais.kyoto-u.ac.jp), Tsuyoshi Tanaka[31] (tstanaka@affrc.go.jp), and Jianzhong Wu[31] (jzwu@affrc.go.jp).

7A Physical Mapping & BAC Sequencing: Rudi Appels[1,36*‡] (rudi.appels@unimelb.edu.au), Matthew Hayden[1] (matthew.hayden@ecodev.vic.gov.au), Gabriel Keeble-Gagnère[1] (gabriel.keeble-gagnere@ecodev.vic.gov.au), Philippe Rigault[39] (prigault@gydle.com), and Josquin Tibbits[1] (josquin.tibbits@ecodev.vic.gov.au).

7B Physical Mapping, BAC Sequencing, & Assembly: Odd-Arne Olsen[56‡] (odd-arne.olsen@nmbu.no), Tatiana Belova[56†] (tatiana.belova@nmbu.no), Federica Cattonaro[58] (cattonaro@igatechnology.com), Min Jiumeng[60] (minjm@bgi.com), Karl Kugler[9] (Kg.kugler@gmail.com), Klaus F.X. Mayer[9,44] (k.mayer@helmholtz-muenchen.de), Matthias Pfeifer[9] (matthiaspfeifer@gmx.net), Simen Sandve[57] (simen.sandve@nmbu.no), Xu Xun[59] (xuxun@genomics.cn), and Bujie Zhan[56†] (bujie.zhan@gmail.com).

7DS BAC Sequencing & Assembly: Hana Šimková[8‡] (simkovah@ueb.cas.cz), Michael Abrouk[8,19] (abrouk@ueb.cas.cz), Jacqueline Batley[24] (jacqueline.batley@uwa.edu.au), Philipp E. Bayer[24] (philipp.bayer@uwa.edu.au), David Edwards[24] (Dave.Edwards@uwa.edu.au), Satomi Hayashi[32] (satomi.hayashi@qut.edu.au), Helena Toegelová[8] (toegelova@ueb.cas.cz), Zuzana Tulpová[8] (tulpova@ueb.cas.cz), and Paul Visendi[55] (P.Muhindira@greenwich.ac.uk),

7DL Physical Mapping & BAC Sequencing: Song Weining[66‡] (sweining2002@yahoo.com), Licao Cui[66] (juelianjunjie@foxmail.com), Xianghong Du[66] (xianghongdu@nwsuaf.edu.cn), Kewei Feng[66] (fkwyc@hotmail.com), Xiaojun Nie[66] ours2011@163.com), Wei Tong[66] (tongw@nwsuaf.edu.cn), and Le Wang[66] (lerwang@ucdavis.edu).

Figures: Philippa Borrill[10] (Philippa.Borrill@jic.ac.uk), Heidrun Gundlach[9] (h.gundlach@helmholtz-muenchen.de), Sergio Galvez[27] (galvez@uma.es), Gemy Kaithakottil[50] (Gemy.Kaithakottil@earlham.ac.uk), Daniel Lang[9] (daniel.lang@helmholtz-muenchen.de), Thomas Lux[9] (thomas.lux@helmholtz-muenchen.de), Martin Mascher[4,67] (mascher@ipk-gatersleben.de), Danara Ormanbekova[9,48] (danara.ormanbekova2@unibo.it), Verena Prade[9] (verena.prade@helmholtz-muenchen.de), Ricardo H. Ramirez-Gonzalez[10] (Ricardo.Ramirez-Gonzalez@jic.ac.uk), Manuel Spannagl[9] (manuel.spannagl@helmholtz-muenchen.de), Nils

Stein[4,5]* (stein@ipk-gatersleben.de) Cristobal Uauy[10] (cristobal.uauy@jic.ac.uk), and Luca Venturini[50] (Luca.Venturini@earlham.ac.uk).

Manuscript Writing Team: Nils Stein[4,5]*‡ (stein@ipk-gatersleben.de), Rudi Appels[1,36]*‡ (rudi.appels@unimelb.edu.au), Kellye Eversole[2,3]* (eversole@eversoleassociates.com), Jane Rogers[6†] (janerogersh@gmail.com), Philippa Borrill[10] (Philippa.Borrill@jic.ac.uk), Luigi Cattivelli[16] (luigi.cattivelli@crea.gov.it), Frédéric Choulet[7] (frederic.choulet@inra.fr), Pilar Hernandez[33] (phernandez@ias.csic.es), Kostya Kanyuka[38] (kostya.kanyuka@rothamsted.ac.uk), Daniel Lang[9] (daniel.lang@helmholtz-muenchen.de), Martin Mascher[4,67] (mascher@ipk-gatersleben.de), Kirby Nilsen[11] (kirby.nilsen@usask.ca), Etienne Paux[7] (etienne.paux@inra.fr), Curtis J. Pozniak[11] (curtis.pozniak@usask.ca), Ricardo H. Ramirez-Gonzalez[10] (Ricardo.Ramirez-Gonzalez@jic.ac.uk), Hana Šimková[8] (simkovah@ueb.cas.cz), Ian Small[45](ian.small@uwa.edu.au), Manuel Spannagl[9] (manuel.spannagl@helmholtz-muenchen.de), David Swarbreck[50], (david.swarbreck@earlham.ac.uk), and Cristobal Uauy[10] (cristobal.uauy@jic.ac.uk).

[1]AgriBio, Centre for AgriBioscience, Department of Economic Development, Jobs, Transport and Resources, 5 Ring Rd, La Trobe University, Bundoora, Victoria 3083 Australia.

[2]International Wheat Genome Sequencing Consortium (IWGSC), 5207 Wyoming Road, Bethesda, Maryland, 20816, United States.

[3]Eversole Associates, 5207 Wyoming Road, Bethesda, Maryland, 20816, United States.

[4]Leibniz Institute of Plant Genetics and Crop Plant Research (IPK), Genebank, Corrensstr. 3, 06466 Stadt Seeland, Germany.

[5]The University of Western Australia (UWA), School of Agriculture and Environment, 35 Stirling Highway, Crawley WA 6009, Australia.

[6]International Wheat Genome Sequencing Consortium (IWGSC), 18 High Street, Little Eversden, Cambridge CB23 1HE, United Kingdom.

[7]GDEC (Genetics, Diversity and Ecophysiology of Cereals), INRA, Université Clermont Auvergne (UCA), 5 chemin de Beaulieu, 63039 Clermont-Ferrand, France.

[8]Institute of Experimental Botany, Centre of the Region Haná for Biotechnological and Agricultural Research, Šlechtitelů 31, CZ-78371, Olomouc, Czech Republic.

[9]Helmholtz Center Munich, Plant Genome and Systems Biology (PGSB), Ingolstaedter Landstr. 1 85764 Neuherberg, Germany.

[10]John Innes Centre, Crop Genetics, Norwich Research Park, Norwich NR4 7UH, United Kingdom.

[11]University of Saskatchewan, Crop Development Centre, Agriculture Building, 51 Campus Drive, Saskatoon SK, S7N 5A8, Canada.

[12]NRGene Ltd., 5 Golda Meir St., Ness Ziona 7403648, Israel.

[13]URGI, INRA, Université Paris-Saclay, 78026 Versailles, France.

[14]Montana State University, Plant Sciences and Plant Pathology, Cereal Genomics Lab, 412 Leon Johnson Hall, Bozeman, MT 59717, USA.

[15]Institute of Plant Sciences - Paris-Saclay, Biology Department, Bâtiment 630, rue de Noetzlin, Plateau du Moulon, CS80004, 91192 - Gif-sur-Yvette Cedex, France.

[16]Council for Agricultural Research and Economics (CREA), Research Centre for Genomics & Bioinformatics, via S. Protaso, 302, I -29017 Fiorenzuola d'Arda, Italy.

[17]Bayer CropScience, Crop Science Division, Research & Development, Innovation Centre, 3500 Paramount Parkway, Morrisville, NC 27560, United States.

[18]Bayer CropScience, Trait Research, Innovation Center, Technologiepark 38, 9052, Gent, Belgium.

[19]King Abdullah University of Science and Technology, Biological and Environmental Science & Engineering Division, Thuwal, 23955-6900, Kingdom of Saudi Arabia.

[20]INRA, CNRGV, Chemin de Borde Rouge CS 52627 31326 Castanet Tolosan cedex, France.

[21]Agriculture and Agri-Food Canada, Swift Current Research and Development Centre, Box 1030, Swift Current, SK S9H 3X2, Canada.

[22]National Research Council Canada, Aquatic and Crop Resource Development, 110 Gymnasium Place, Saskatoon SK S7N 0W9, Canada.

[23]Research Center of Biotechnology of the Russian Academy of Sciences, Institute of Bioengineering, Leninsky Ave. 33, bld 2, Moscow 119071, Russia.
[24]University of Western Australia, School of Biological Sciences and Institute of Agriculture, University of Western Australia, Perth, 6009 Australia.

[25]School of Plant Sciences and Food Security, Tel Aviv University, Ramat Aviv 69978, Israel.

[26]University of Haifa, Institute of Evolution and the Department of Evolutionary and Environmental Biology, 199 Abba-Hushi Avenue,Mount Carmel, Haifa 3498838, Israel.

[27]Universidad de Málaga, Lenguajes y Ciencias de la Computación, Campus de Teatinos, 29071 Málaga, Spain.

[28]Kansas State University, Plant Pathology, Throckmorton Hall, Kansas State University, Manhattan KS, 66506, United States.

[29]Multi-QTL Ltd., University of Haifa, Haifa, Israel.

[30]University of Minnesota, Department of Agronomy and Plant Genetics, 411 Borlaug Hall, St. Paul, MN 55108.

[31]Institute of Crop Science, NARO (former NIAS), 2-1-2 Kannondai, Tsukuba, Ibaraki 305-8518, Japan.

[32]Queensland University of Technology, Earth, Environmental and Biological Sciences, Brisbane, Queensland, Australia.

[33]Instituto de Agricultura Sostenible (IAS-CSIC), Consejo Superior de Investigaciones Científicas, Alameda del Obispo s/n, 14004 Córdoba, Spain.

[34]University of California, Davis, Department of Plant Sciences, One Shield Avenue, Davis, CA 95617, United States.

[35]The Sainsbury Laboratory, Norwich Research Park, NR4 7UH, Norwich, United Kingdom.

[36]Murdoch University, Australia China Centre for Wheat Improvement, School of Veterinary and Life Sciences, 90 South Street, Murdoch WA 6150, Australia.

[37]Agricultural Institute, MTA Centre for Agricultural Research, Applied Genomics Department, 2 Brunszvik Street, Martonvásár H 2462, Hungary.

[38]Rothamsted Research, Biointeractions and Crop Protection, West Common, Harpenden, AL5 2JQ, United Kingdom.

[39]GYDLE, Suite 220, 1135 Grande Allée, Ouest, Suite 220, Québec, QC G1S 1E7, Canada.

[40]Julius Kühn-Institut, Institute for Biosafety in Plant Biotechnology, Erwin-Baur-Str. 27 06484 Quedlinburg, Germany.

[41]University of Zurich, Department of Plant and Microbial Biology, Zollikerstrasse 107, 8008 Zurich, Switzerland.

[42]Rothamsted Research, Computational and Analytical Sciences, West Common, Harpenden, AL5 2JQ, United Kingdom.

[43]University of Saskatchewan, Global Institute for Food Security, 110 Gymnasium Place Saskatoon SK S7N 4J8, Canada.

[44]Technical University of Munich, School of Life Sciences, Weihenstephan, Germany.

[45]The University of Western Australia, School of Molecular Sciences, ARC Centre of Excellence in Plant Energy Biology, 35 Stirling Highway, Crawley WA 6009, Australia.

[46]Kyoto University, Graduate School of Agriculture, Kitashirakawaoiwake-cho, Sakyo-ku, Kyoto 606-8502, Japan.

[47]The Federal Research Center Institute of Cytology and Genetics, SB RAS, pr. Lavrentyeva 10, Novosibirsk 630090, Russia.

[48]University of Bologna, Department of Agricultural Sciences,Viale Fanin, 44 40127 Bologna, Italy.

[49]Palacký University, Centre of the Region Haná for Biotechnological and Agricultural Research, Department of Molecular Biology, Šlechtitelů 27, CZ-78371 Olomouc, Czech Republic.

[50]Earlham Institute, Core Bioinformatics, Norwich, NR4 7UZ, United Kingdom.

[51]Moscow State University, Faculty of Biology, Leninskie Gory, 1, Moscow, 119991, Russia.

[52]Agriculture and Agri-Food Canada, Saskatoon Research and Development Centre, 107 Science Place, Saskatoon, SK, S7N 0X2, Canada.

[53]South Dakota State University, Agronomy Horticulture and Plant Science, 2108 Jackrabbit Dr, Brookings, SD 57006, United States.

[54]University of Maryland, Plant Science and Landscape Architecture, 4291 Fieldhouse Road, 2102 Plant Sciences Building College Park, MD 20742, United States.

[55]University of Greenwich, Natural Resources Institute, Central Avenue, Chatham, Kent ME4 4TB, United Kingdom.

[56]Norwegian University of Life Sciences, Faculty of Bioscience, Department of Plant Science, Arboretveien 6, 1433 Ås, Norway.

[57]Norwegian University of Life Sciences, Faculty of Bioscience, Department of Animal and Aquacultural Sciences, Arboretveien 6, 1433 Ås, Norway.

[58]Instituto di Genomica Applicata, Via J. Linussio 51, Udine, 33100, Italy.

[59]BGI-Shenzhen, BGI Genomics, Yantian, Shenzhen, Guangdong, China.

[60]BGI-Shenzhen, BGI Genomics, Building No.7, BGI Park, No.21 Hongan 3rd Street, Yantian District, Shenzhen, China.

[61]CEA - Institut de Biologie François-Jacob, Genoscope, 2 Rue Gaston Cremieux 91057 Evry Cedex, France.

[62]Monsanto SAS, 28000 Boissay, France.

[63] Institut National de la Recherche Agronomique (INRA), 2 rue Gaston Crémieux, 9057 Evry, France.

[64]Keygene, N.V., Agro business Park 90, 6708 PW Wageningen, The Netherlands.

[65]Punjab Agricultural University, Ludhiana, School of Agricultural Biotechnology, ICAR-National Bureau of Plant Genetic Resources, Dev Prakash Shastri Marg, New Delhi 110012, India.

[66]Northwest A&F University, State Key Laboratory of Crop Stress Biology in Arid Areas, College of Agronomy, Northwest A&F University, Yangling 712101, Shaanxi, China.

[67]German Centre for Integrative Biodiversity Research (iDiv) Halle-Jena-Leipzig, Deutscher Platz 5e, 04103 Leipzig, Germany.

[68]CNRS, UMR 8030, CP5706, Evry, France.

[69]Université d'Evry, UMR 8030, CP5706, Evry, France.

[70]ICAR-National Research Centre on Plant Biotechnology, LBS Building, Pusa Campus, New Delhi 110012, India.

[71]University of Delhi South Campus, Interdisciplinary Center for Plant Genomics & Department of Plant Molecular Biology, Benito Juarez Road, New Delhi-110021, India.

[72]Bayer CropScience, Breeding & Trait Development, Technologiepark 38, 9052, Gent, Belgium.

[73]Department of Lifesciences, Natural History Museum, Cromwell Road, London SW7 5BD, U.K.

Competing interests: Authors declare no competing interests.

Data and materials availability: The IWGSC RefSeq v1.0 assembly and annotation data, physical maps for all chromosomes/chromosome arms, as well as all data related to this study are available in the IWGSC Data Repository hosted at URGI: https://wheat-urgi.versailles.inra.fr/Seq-Repository. The BAC libraries for all chromosomes/chromosomes arms are available at the CNRGV-INRA: https://cnrgv.toulouse.inra.fr/en/Library/Wheat. The raw sequencing data is in the Sequence Read Archive under accession number SRP114784. Further details on data accessibility are outlined in the supplementary Materials and Methods. Accession numbers for raw sequence datasets submitted to public databases are listed in the Supplementary Materials section.

Supplementary Materials:

Materials and Methods

Figures S1-S58

Tables S1-S42

External Databases S1-S6

References (55-182)

Figure captions

Fig. 1. Structural, functional, and conserved synteny landscape of the 21 wheat chromosomes. (A) Circular diagram visualizing genomic features of wheat. The tracks towards the center of the circle display: a - chromosome name and size (100 Mb tick size, light grey bar = short arm, dark grey= long arm of the chromosome); b - dimension of chromosomal segments R1, R2a, C, R2b, R3 ((*14*)Table S29); c - Kmer 20 frequencies distribution; d - LTR-retrotransposons density; e - pseudogenes density (0 to 130 genes per Mb); f - density of high confidence gene models (HC; 0 to 32 genes per Mb); g - density of recombination rate; h- SNP density (*48*). Connecting lines in the center of the diagram highlight homeologous relationships of chromosomes (blue lines) and translocated regions (green lines). (B) Distribution of PFAM domain PF08284 'retroviral aspartyl protease' signatures across the different wheat chromosomes. (C) Positioning of the centromere in the 2D pseudomolecule. Upper panel: Density of CENH3 ChIP-seq data along wheat chromosome. Lower panel: Distribution and proportion of the total pseudomolecule sequence composed of TE of the Cereba/Quinta families. The bar below the lower panel indicates pseudomolecule scaffolds assigned to the short (black) or long (blue) arm based on CSS data (*6*) mapping. (D) Dot pot visualization of collinearity between homeologous chromosomes 3A and 3B in relation to distribution of gene density and recombination frequency (left and lower panel

boxes: blue and purple lines, respectively). Chromosomal zones R1, R2a, C, R2b, R3 colored as per in Fig. 1A.

Fig. 2. Evaluation of automated gene annotation. (A) Selected gene prediction statistics of IWGSC RefSeq annotation version 1.1 including number and sub-genome distribution of high confidence (HC) and low confidence (LC) genes as well as pseudogenes. (B) BUSCO v3 gene model evaluation comparing IWGSC RefSeq annotation v1.1 to earlier published bread wheat whole genome annotations as well as to annotations of related grass reference genome sequences. BUSCO provides a measure for the recall of highly conserved gene models.

Fig. 3. Wheat atlas of transcription. (A) Schematic illustration of a mature wheat plant and high-level tissue definitions ‘roots’, ‘leaves’, ‘spike’ and ‘grain’ used in the further analysis. (B) Principal component analysis plots for similarity of overall transcription with samples coloured according to their high-level tissue of origin (as introduced in A). (C) Chromosomal distribution of the average expression breadth [number of tissues in which genes are expressed (total number of tissues, n=32)]. The average (dark orange line) is calculated based on a scaled position of each gene within the corresponding genomic compartment (blue, aqua and white background) across the 21 chromosomes (orange lines). (D) Heatmap illustrating the expression of a representative gene (eigengene) for the 38 co-expression modules defined by WGCNA. Modules are represented as columns, with the dendrogram illustrating eigengene relatedness. Each row represents one sample; coloured bars to the left indicate the high-level tissue of origin. DESeq2 normalised expression levels are shown. Modules 1 and 5 (pale green boxes) were most correlated with high-level ‘leaf tissue’ whereas modules 8 and 11 (dark green boxes) were most correlated with ‘spike’. (E) Bar plot of module assignment (same, near or distant) of

homeologous triads and duplets in WGCNA network. (F) Simplified flowering pathway in polyploid wheat. Genes are coloured according to their assignment to 'leaf' (pale green) or 'spike' (dark green) correlated modules. (G) Excerpt from phylogenetic tree for MADS transcription factors including known Arabidopsis flowering regulators *SEP1*, *SEP2* and *SEP4* (black) (for the full phylogenetic tree see Fig. S38). Green branches represent wheat orthologs of modules 8 and 11, whereas purple branches are wheat orthologs assigned to other modules (0 and 2). Grey branches indicate non-wheat genes.

Fig. 4. Gene families of wheat. (A) Heatmap of expanded and contracted gene families. Columns correspond to the individual gene families. Rows in the upper panel illustrate the sets of gene family expansions (++; red) and contractions (–; blue) found for the wheat A lineage (*T. urartu* and A sub-genome), the D lineage (*A. tauschii* and D sub-genome), the A, B or D sub-genomes or bread wheat (expanded/contracted in all sub-genomes). In the latter four categories, expansions/contractions do not imply bread-wheat specific gene copy number variations. Similar dynamics might have remained unobserved in *T. urartu* or *A. tauschii* due to the inherent limitations of the used draft genome assemblies (*52*, *53*). Rows in the lower panel heatmap (color scheme on z-score scale) indicate the fold expansion and contraction of gene families for the taxa / species included in the analysis [*Oryza sativa* (Osat), *Sorghum bicolor* (Sbic), *Zea mays* (Zmay), *Brachypodium distachyon* (Bdis), *Hordeum vulgare* (Hvul1/2), *Secale cereale* (Scer), *Aegilops tauschii* (Aetau), *Triticum urartu* (Tura), wheat A (TraesA), B (TraesB) and D (TraesD) sub-genomes]. (B) All enriched Plant Trait Ontology (TO) terms for the gene families depicted in (A). Over-represented TO terms were found for expanded families in bread wheat (all sub-genomes; red), the B sub-genome (green) and the A lineage (*T. urartu* and A sub-genome; blue) only, respectively. The x-axis represents the percentage of genes annotated with the respective

TO term that were contained in the gene set in question. The size of the bubbles corresponds to the p-value (-log10) significance of expansion. (C) Genomic distribution of gene families associated with adaptation to biotic (light/dark blue) or abiotic stress (light/dark pink), RNA metabolism in organelles and male fertility (orange) or end-use quality (light/medium/dark green). Known positions of agronomically important genes / loci are indicated by red arrows / arrowheads to the left of the chromosome bars. Recombination rates are displayed as heat maps in the chromosome bars (light green = 7.2 cM/Mb to black = 0 cM/Mb).

Fig. 5. IWGSC RefSeq v1.0 guided dissection of *SSt1* and *TaAGL33*. (A) The Lillian/Vesper population genetic map was anchored to IWGSC RefSeq v1.0 (left) and differentially expressed genes were identified between solid and hollow-stemmed lines of hexaploid- (bread) and tetraploid (durum) wheat (right). (B) Cross-sectioned stems of 'Lillian' (solid) and 'Vesper' (hollow) are shown as a phenotypic reference (top). Increased copy number of *TraesCS3B01G608800* (annotated as a DOF transcription factor) is associated with stem phenotypic variation (bottom). (C) A high-throughput SNP marker tightly linked to *TraesCS3B01G608800* reliably discriminates solid from hollow-stemmed wheat lines. (D) Schematic of the three TaAGL33 proteins, showing the typical MADS, I, K and C domains. Triangles indicate the position of the 5 introns that occur in all three homeologs. Bars indicate the position of sgRNAs designed for exons 2 and 3. Three T-DNA vectors each containing the *bar* selectable marker gene, CRISPR nuclease and one of three sgRNA sequences were used for *Agrobacterium*-mediated wheat transformation, essentially as described earlier (*54*). Transgenic plants were obtained with edits at the targeted positions in all TaGL33 homeologs. The putatively resulting protein sequence is displayed starting close to the edits with wild-type amino acids in black font and amino acids resulting from the induced frame shifts in red font. * indicates

premature termination codons. (E) Mean days to flowering (after 8 weeks of vernalization) for progeny of four homozygous edited plants (light grey bars) and the respective homozygous wild-type segregants (dark grey bars). Numbers in brackets refer to the number of edited and wild-type plants examined, respectively. Error bars display SEM. Growth conditions were as described by Sharma et al. (*50*).

Table 1. Assembly statistics of IWGSC Refseq v1.0.

Assembly size	14.5 Gb
Number of scaffolds	138,665
Size of assembly in scaffolds >= 100Kb	14.2 Gb
Number of scaffolds >= 100Kb	4,443
N50 contig length	51.8 Kb
Contig L50	81,427
N90 contig length	11.7 Kb
Contig L90	294,934
Largest contig	580.5 Kb
Ns in contigs	0
N50 scaffold length	7.0 Mb
Scaffold L50	571
N90 scaffold length	1.2 Mb
Scaffold L90	2,390
Largest scaffold	45.8 Mb
Ns in scaffolds	261.9 Mb
Gaps filled with BAC sequences	183 (1.7 Mb)
Average size of inserted BAC sequence	9.5 Kb
N50 super-scaffold length	22.8 Mb
Super-scaffold L50	166
N90 super-scaffold length	4.1 Mb
Super-scaffold L90	718
Largest super-scaffold	165.9 Mb
Sequence assigned to chromosomes	14.1 Gb (96.8%)
Sequence >=100Kb assigned to chromosomes	14.1 Gb (99.1%)
Number of super-scaffolds on chromosomes	1,601
Number of oriented super-scaffolds	1,243
Length of oriented sequence	13.8 Gb (95%)
Length of oriented sequence >= 100Kb	13.8 Gb (97.3%)
Smallest number of super-scaffolds per sub-genome chromosome	35 (7A) / 68 (2B) / 36 (1D)
Highest number of super-scaffolds per sub-genome chromosome	111 (4A) / 176 (3B) / 90 (3D)
Average number of super-scaffolds per chromosome	76

Table 2. Relative proportions of the major elements of the wheat genome. Proportions of TEs are given as the percentage of sequences assigned to each superfamily relative to genome size.

			AA	BB	DD	AABBDD
Assembled sequence assigned to chromosomes (Gb)			4.935	5.180	3.951	14.066
Size of TE-related sequences (Gb)			4.240	4.388	3.285	11.913
%TEs			85.9%	84.7%	83.1%	84.7%
Class 1	LTR-retrotransposons					
		Gypsy (RLG)	50.8%	46.8%	41.4%	46.7%
		Copia (RLC)	17.4%	16.2%	16.3%	16.7%
		Unclassified LTR-RT (RLX)	2.6%	3.5%	3.7%	3.2%
	Non-LTR-retrotransposons					
		LINE (RIX)	0.81%	0.96%	0.93%	0.90%
		SINE (SIX)	0.01%	0.01%	0.01%	0.01%
Class 2	DNA transposons					
		CACTA (DTC)	12.8%	15.5%	19.0%	15.5%
		Mutator (DTM)	0.30%	0.38%	0.48%	0.38%
		Unclassified with TIRs	0.21%	0.20%	0.22%	0.21%
		Harbinger (DTH)	0.15%	0.16%	0.18%	0.16%
		Mariner (DTT)	0.14%	0.16%	0.17%	0.16%
		Unclassified class#2	0.05%	0.08%	0.05%	0.06%
		hAT (DTA)	0.01%	0.01%	0.01%	0.01%
	Helitrons	(DHH)	0.0046%	0.0044%	0.0036%	0.0042%
Unclassified repeats			0.55%	0.85%	0.63%	0.68%
Coding DNA			0.89%	0.89%	1.11%	0.95%
Un-annotated DNA			13.2%	14.4%	15.7%	14.4%
(pre)-miRNAs			0.039%	0.057%	0.046%	0.047%
tRNAs			0.0056%	0.0050%	0.0068%	0.0057%

Table 3. Groups of homeologous genes in wheat. Homeologous genes are "sub-genome orthologs" and were inferred by species tree reconciliation in the respective gene family. Numbers include both HC and LC genes filtered for TEs ("filtered gene set"). Conserved sub-genome-specific (orphan) genes are found only in one sub-genome but have homologs in other plant genomes used in this study. This includes orphan outparalogs resulting from ancestral duplication events and conserved only in one of the sub-genomes. Non-conserved orphans are either singletons or duplicated in the respective sub-genome, but do neither have obvious homologs in the other sub-genomes or the other plant genomes studied. Microsynteny is defined as the conservation and collinearity of local gene ordering between orthologous chromosomal regions. Macrosynteny is defined as the conservation of chromosomal location and identity of genetic markers like homeologs, but may include the occurrence of local inversions, insertions or deletions. Additional data are presented in Table S24.

homeologous group (A:B:D)	# in wheat genome	% of groups	# genes in A	# genes in B	# genes in D	# total genes
1:1:1	21,603	55.1%	21,603	21,603	21,603	64,809
1:1:N	644	1.6%	644	644	1,482	2,770
1:N:1	998	2.5%	998	2,396	998	4,392
N:1:1	761	1.9%	1,752	761	761	3,274
1:1:0	3,708	9.5%	3,708	3,708	0	7,416
1:0:1	4,057	10.3%	4,057	0	4,057	8,114
0:1:1	4,197	10.7%	0	4,197	4,197	8,394
other ratios	3,270	8.3%	4,999	5,371	4,114	14,484
1:1:1 in microsynteny	18,595	47.4%	18,595	18,595	18,595	55,785
total in microsynteny	30,339	77.3%	27,240	27,063	28,005	82,308
1:1:1 in macrosynteny	19,701	50.2%	19,701	19,701	19,701	59,103
total in macrosynteny	32,591	83.1%	29,064	30,615	30,553	90,232
total in homeologous groups	**39,238**	**100.0%**	**37,761**	**38,680**	**37,212**	**113,653**
conserved sub-genome orphans			12,412	12,987	10,844	36,243

non-conserved sub-genome singletons	10,084	12,185	8,679	30,948
non-conserved sub-genome duplicated orphans	71	83	38	192
total (filtered)	60,328	63,935	56,773	181,036

Supplementary Materials for

Shifting the limits in wheat research and breeding using a fully annotated reference genome

The International Wheat Genome Sequencing Consortium (IWGSC)*

*Correspondence to: rudi.appels@unimelb.edu.au (Rudi Appels), eversole@eversoleassociates.com (Kellye Eversole), and stein@ipk-gatersleben.de (Nils Stein)

This PDF file includes:

Materials and Methods
Figs. S1 to S58
Tables S1 to S42
Captions for databases S1 to S6

Other Supplementary Materials for this manuscript includes the following:

Databases S1 to S6 as zipped archives:
Additional Database S1. Metadata of 850 RNAseq samples used in the study
Additional Database S2. SlimGO ubiquitous and Tissue-exclusive genes.
Additional Database S3. GO terms of the WGCNA850 analysis.
Additional Database S4. WGCNA Module Assignment.
Additional Database S5. Module 8 and 11 TF Arabidopsis and rice orthologs.
Additional Database S6. Gene family expansion and contraction in the genome of bread wheat cv. Chinese Spring.

Materials and Methods

Materials

Genome, transcriptome and other data resources

The IWGSC RefSeq v1.0 assembly, annotation data and related data are available in the IWGSC Data Repository hosted at URGI: https://wheat-urgi.versailles.inra.fr/Seq-Repository. The data can be downloaded but also analyzed using tools: BLAST (https://urgi.versailles.inra.fr/blast_iwgsc/blast.php), JBrowse (https://urgi.versailles.inra.fr/jbrowseiwgsc/gmod_jbrowse/?data=myData%2FIWGSC_RefSeq_v1.0) and Intermine (https://urgi.versailles.inra.fr/WheatMine). The data are linked to wheat genetic and phenomic data via the Wheat@URGI portal (*55*).

Chromosome-specific BAC libraries and physical maps

Individual clones and BAC libraries used to construct chromosome-specific physical maps can be obtained at https://cnrgv.toulouse.inra.fr/en/Library/Wheat. Physical maps are available at: https://urgi.versailles.inra.fr/download/iwgsc/Physical_maps/ and displayable at https://urgi.versailles.inra.fr/gb2/gbrowse/wheat_phys_pub/.

BAC sequence assemblies

Sequence assemblies of BAC clones representing complete or partial MTPs from 8 chromosomes and 2 chromosome arms are available at: https://urgi.versailles.inra.fr/download/iwgsc/BAC_Assemblies/.

Whole Genome Profiling (WGP™) tags of MTP BAC clones

WGP™ data generated from BAC clones representing the MTP of all 21 wheat chromosomes are available for download from IWGSC-BayerCropScience WGP™ tags: https://urgi.versailles.inra.fr/download/iwgsc/IWGSC_BayerCropScience_WGPTM_tags.

Bionano optical maps

Bionanogenomics optical maps for group 7 chromosomes are available at: https://urgi.versailles.inra.fr/download/iwgsc/IWGSC_RefSeq_Annotations/v1.0/iwgsc_refseqv1.0_optical_maps_group7.zip.

Radiation Hybrid (RH) maps

RH maps constructed to validate long-range order in physical maps and sequence assemblies for wheat chromosomes are available at: https://urgi.versailles.inra.fr/download/iwgsc/IWGSC_RefSeq_Annotations/v1.0/iwgsc_refseqv1.0_RH_map.zip.

Genetic maps

GBS-SNP marker coordinates and maps of genetic vs physical distances (SynOpDH88_ChineseSpring_v0.5.pdf) and (SynOpRIL993_ChineseSpring_v0.5.pdf) are available at: https://urgi.versailles.inra.fr/download/iwgsc/IWGSC_RefSeq_Annotations/v1.0/iwgsc_refseqv1.0_SynOpRIL993_GBS.zip. GBS data is available under SRA accession number SRP134280 for the submission SUB3762955.

Sequence reads used for whole genome assembly

The raw sequence data used for *de novo* whole genome assembly of genotype 'Chinese Spring' (CS) is available from the Sequence Read Archive under accession number SRP114784.

Sequence reads of unpublished RNAseq data

The raw sequence data from 321 unpublished RNAseq samples are available under SRA accession IDs PRJEB25639, PRJEB23056, PRJNA436817, PRJEB25640, SRP133837, PRJEB25593.

Chromosome conformation capture (Hi-C) sequencing data

Hi-C sequence data generated from four independent Hi-C libraries are available under accession number PRJEB25248.

ChIP sequence data of histone marks and methylome data

All ChIP seq data are available under SRA study PRJNA420988 (SRP126222) and can be accessed using SRA RunSelector: https://www.ncbi.nlm.nih.gov/Traces/study/?acc=SRP126222. The CS bisulfite sequencing data is available under project ID SRP133674 (SRR6792673-SRR6792689 for the independent runs).

Chromosome-scale sequence assemblies (pseudomolecules)

Assemblies of all 21 wheat chromosomes are available at: https://urgi.versailles.inra.fr/download/iwgsc/IWGSC_RefSeq_Assemblies/.

Assemblies of organellar genomes

Assemblies representing the CS organellar genomes were assembled from the raw sequencing data produced for the whole genome assembly. A 135,905 bp circular chloroplast genome sequence and a 452,256 bp circular mitochondrial genome sequence were deposited at NCBI Genbank (MH051715, MH051716).

Genome annotations

All annotation data are available at: https://urgi.versailles.inra.fr/download/iwgsc/IWGSC_RefSeq_Annotations/.

Gene annotations are available here: https://urgi.versailles.inra.fr/download/iwgsc/IWGSC_RefSeq_Annotations/v1.1/iwgsc_refseqv1.1_genes_2017July06.zip.

Pseudogene annotations are available here: : https://urgi.versailles.inra.fr/download/iwgsc/IWGSC_RefSeq_Annotations/v1.0/iwgsc_refseqv1.0_PGSB_annotation_files.zip.

Functional annotation data for all HC and LC protein-coding genes (wheatCS_IWGSC_FunctionalAnnotation_v1__HCgenes_v1.0.TAB, wheatCS_IWGSC_FunctionalAnnotation_v1__HCgenes_v1.0-repr.TEcleaned.TAB, wheatCS_IWGSC_FunctionalAnnotation_v1__LCgenes_v1.0.TAB) are available at: https://urgi.versailles.inra.fr/download/iwgsc/IWGSC_RefSeq_Annotations/v1.0/iwgsc_refseqv1.0_FunctionalAnnotation_v1.zip.

Gene families

Information on expanded and contracted bread wheat gene families is available at: https://doi.ipk-gatersleben.de/DOI/912ca35a-2fbb-4d59-9dab-a06edf7fef73/4391642c-3958-425b-989e-da0ec1a277b9/2/1847940088.

Methods

1. Whole genome sequencing and assembly

1.1. DNA isolation and sequencing

Genomic DNA was isolated from fresh leaf tissue (~10 g) of cultivar CS using a phenol/chloroform large scale nuclei extraction protocol (*56*). The DNA was used to construct five sized sequencing libraries covering the range of 450 bp to 10 kb using standard protocols by the University of Illinois Roy J. Carver Biotechnology Center. The libraries were sequenced on an Illumina HiSeq 2500 to generate 3.69 Tb of data (equivalent to 234x genomic coverage, based on an estimated genome size of 15.76 Gb) using (Table S1).

1.2 Whole Genome Assembly (WGA)

The genome was assembled using the software package DenovoMAGIC2TM (NRGene, Nes Ziona, Israel) and scaffolded (Table S2) by applying gap-closure and error correction in three steps as described for the wild emmer wheat genome (*56*):

1. Read pre-processing and error correction: PCR duplicates, Illumina adaptors, Nextera linkers (for the mate pair (MP) libraries) and paired-end (PE) reads found to contain likely sequencing errors (i.e. sub-sequences of $\geq$ 23 bp not found in at least one other independent read) were removed. From the PE libraries, only pairs with at least 10 bp sequence overlap were merged to create 'stitched reads' (SRs).

2. *De novo* assembly of contigs: the SRs were used to build an initial De Bruijn graph of contigs (kmer=191 bp). By exploring graph structure, the software identified non-repetitive contigs and used SR information to resolve repeats and extend non-repetitive sequences of the contigs where possible (Table S2).

3. *De novo* assembly of scaffolds: a directed graph containing contigs as nodes and edges based on the PE and MP links as vertices was used for scaffolding. Erroneous connections were identified and filtered out to generate unconnected sub-graphs that were ordered into scaffolds. PE reads were used to find reliable paths in the graph for additional repeat resolving. This was accomplished through searching the graph for a unique path of contigs connecting pairs of reads mapping to two different non-repetitive contigs. The scaffolds were then ordered and linked using the MP libraries, estimating gaps between the contigs from the distances between MP links. Scaffold links were only accepted when confirmed with at least three filtered MPs, or at least one filtered MP with supporting confirmation from two or more filter failed MPs where the Nextera adaptor was not found. Scaffolds shorter than 380bp were masked and links between non-repetitive contigs mapping to the same scaffolds were united, generating a directed scaffold graph. A significant number of erroneous MPs linking long non-branched components in the scaffold graph were discarded by the scaffolding procedure that identified the non-branched components in the scaffolds graph. After filtering out the rare connections between them topological sorting based ordering of the initial scaffolds produced the final scaffolds.

1.3 Estimation of sequence accuracy

To estimate the sequence accuracy of the genome assembly a comparison was made between a scaffold from IWGSC RefSeq_v1.0 (scaffold4849-2) and a set of overlapping "finished" BAC clones spanning 760070 bp without inconsistencies from chromosome 3B TaaCsp3BFhA_0053M17, TaaCsp3BFhA_0078G10, TaaCsp3BFhA_0011O13,

TaaCsp3BFhA_0149J15, TaaCsp3BFhA_0013G07, TaaCsp3BFhA_0061H24 (*57*). Alignment of the two sequences with BLAST2 identified 728782 bps aligned in high scoring pairs (HSPs) larger than 20 kb. The aligned sequences contained 16 mismatches and 3 indels representing an error rate of 0.0026% i.e. an accuracy of 99.9974%.

In addition, we compared 5283 HC genes from IWGSC RefSeq v1.0 7A pseudomolecule [only genes with no assembly gaps (Ns), aligning across 100% length] with the BAC-based sequence assembly of chromosome 7A [GYDLE 7A, (*58*)] and the 7B-7D pseudomolecules using a minimum HSP of 30 bp with a sensitivity of 25 and 1 mismatch (~97% identity). Over 97% of the genes were identical between both independent 7A assemblies whereas 97% and 95% of the genes were dissimilar to homeologs on the 7B and 7D pseudomolecules. We conclude that the assembly process was highly subgenome-specific with very little evidence of mis-assembly of homeologous sequences.

1.4 Assembly of organellar genome sequences and detection of NUPT/NUMT

A sample of 150 million filtered and trimmed reads (50 or more consecutive bases with quality scores 20 or higher) of the CS WGA sequencing data (30 million from each of the five types of libraries) was used for the assembly of complete plastid and mitocondrial genomes of CS. Initial mapping of reads to reference sequences (cpDNA: NC_002762, mtDNA: NC_036024) was followed by iterative resolution steps combining local realignment, consensus resolution, segmental reorganisation, gap filling, dynamic remapping of all reads, interactive edition and assembly visualization all performed with NUCLEAR version 3.2.16 (GYDLE Inc., Québec, Canada) and VISION version 2.6.22 (GYDLE Inc., Québec, Canada). Organelle annotation was done using alignments with features extracted and curated from the GenBank records of the reference sequences. The read mapping parameters used to recruit sequences into the organelle assembly were: -l 40 -s 38 -m 1 --min-pct-cov 80. This selected High-scoring Segment Pairs (HSP = gapless local alignment meeting the requested criteria) of 40 bases or more, containing 38 consecutive identities and contain at most 1 mismatch every 40 bases (97.5% local similarity) that were combined into alignments (combination of HSPs with possible gaps between them) covering at least 80% of the fragment's sequence. The resolving phases of the assembly used local realignments (HSP length >= 30, 16 consecutive identities, 90% local similarity, alignment covering 50 or more bases) prior to resolving the consensus sequence. The assembler always keeps track of the mapping score of each read (in particular which mapped reads are perfectly aligned and which are not), therefore regions consistently connected and covered by strongly aligned reads are not subject to misassembly influenced by additional divergent reads, such as those carrying sequencing errors or representing insertions into the nuclear genome (which in addition to being divergent and unconnected to the main assembly have also much lower coverage). The organelle assemblies were completed in two rounds of resolve when the resulting sequence had no gap and all its bases covered by perfectly-mapped reads at high coverage (chloroplast ~10,000X, mitochondria ~200X). An independent assembly using a different sample of 150 million reads resulted in exactly the same organelle sequences.

For NUPT/NUMT analysis, the organelle genome were compared to the pseudomolecule sequences using NUCLEAR alignment parameters: -l 40 -s 21 -m 4 --max-gap-size 200 --min-score-cov 100 -F 3 --hsp-extend-masked (HSP length >= 40, 21 consecutive identities, 90% local similarity, alignment length >= 100 bp, inter-HSP gap <= 200 bp, masking of low-complexity regions). Alignments with more relaxed parameters (HSP length >= 30, 16 consecutive identities, 90% local similarity) yielded similar NUPT/NUMT results (less than 15% more alignments).

2. Data resources integrated into IWGSC RefSeq v1.0

2.1 Chromosome conformation capture sequencing (Hi-C)

Three dimensional (3D) chromosome conformation capture sequencing data were generated for physical ordering and orienting of sequence super-scaffolds. Four Hi-C libraries were generated for bread wheat cv. CS using a plant-adapted TCC version (*59*) of the original Hi-C protocol (*60*) essentially as described previously (*61*). The libraries were sequenced on an Illumina HiSeq2500 instrument according to manufacturer's instructions. Hi-C data pre-preprocessing and reads were assigned to HindIII fragments (*61*) using the CS whole-genome assembly (WGA) as the reference sequence.

2.2 Physical map de novo contig assembly

BAC-based physical maps were assembled for the 21 bread wheat chromosomes between 2008 and 2016. With the exception of 3B (*62*) chromosome- or chromosome arm-specific BAC libraries were developed at the Institute of Experimental Botany, Olomouc, Czech Republic (*63*) (see http://olomouc.ueb.cas.cz/dna-libraries/cereals). BAC fingerprints generated using either High Information Content Fingerprinting (HICF) with SNaPShot technology (*64*) or Whole Genome Profiling (WGP^{TM})(*65*) were assembled with standard FingerPrinted Contig (FPC) (*66*) or Linear Topological Contig (LTC) software (*67*) (Table S3 and S4), which were also used to select minimal tiling path (MTP) for sequencing.

The quality of physical map contigs was checked and improved using the following approaches: 1) application of LTC in chromosome arms primarily assembled by FPC; 2) integration with deletion, genetic and radiation hybrid maps; 3) alignment with Bionano optical maps (7AS, 7AL, 7DS). Detailed information of procedures applied for particular chromosome arms is provided in Table S3 and publications cited therein.

2.3 BAC clone / MTP sequencing

BAC clones selected from physical maps to represent complete or partial MTPs from 8 chromosomes and 2 chromosome arms were shotgun sequenced using various sequencing technologies: (i) Roche-454 sequencing of pooled BACs (chromosome 3B) (*14*); (ii) Illumina paired end sequencing of pooled BACs (1B, 7A, 7DS) (*68*); (iii) Illumina paired end shotgun sequencing of individually tagged multiplexed BACs (1A, 3D, 4AL, 6B, 7B, 7DL); Ion Torrent paired end sequencing (5BS). Reads were assembled with assembly algorithms suited to the data type (Table S6) and in some cases initial assemblies were improved by manual assessment and targeted sequencing to fill gaps (3B,1B); or incorporation of BAC-based or whole chromosome mate-pair sequences (1A, 3DL, 6B, 7A, 7B, 7DL). The BAC sequence data used for pseudomolecule assembly are summarized in Table S6.

2.4 Whole Genome Profiling (WGP^{TM}) of MTP clones

In addition to the construction of physical maps for chromosomes 2B, 2D, 4B, 5BL, 5DL, 6A and 6B (see Table S4), WGP^{TM} was used, following the same procedures (*69, 70*), to profile minimal tile path BACs identified from wheat chromosome physical maps constructed previously by HICF from chromosome-specific BAC libraries (Table S5).

2.5 Bionano optical maps for Group 7 chromosomes

Bionano optical maps of chromosome arms 7AS, 7AL, 7BS, 7BL, 7DS and 7DL were constructed using the protocol described for chromosome 7DS (*68*). A total of 2.8 million arms for each chromosome, corresponding to 2.0 – 3.1 µg DNA per telosome, were purified by flow cytometric sorting from cv. Chinese Spring ditelosomic lines(*71*) with purities ranging from 80 to

87% (Table S7). The DNA from each chromosome arm was nicked with Nt.BspQI (GCTCTTC recognition site), the nick sites were labelled and the DNA was stained with IrysPrep® Reagent Kit and IrysPrep® DNA Stain, respectively. The labelled molecules were analyzed on the Irys platform (Bionano Genomics, San Diego, USA). A total of 78 to 248 Gb data in fragments greater than 150 kb were collected per chromosome arm (corresponding to 192 and 689 arm equivalents, respectively) (Table S7) and used to assemble optical maps *de novo* using pairwise comparison of all single molecules and graph building in IrysSolve software (Bionano Genomics). A p-value threshold of $1e^{-10}$ was used during the pairwise assembly, $1e^{-11}$ for extension and refinement steps, and $1e^{-15}$ for a final refinement.

2.6 Radiation Hybrid (RH) Maps

Using methods described previously (*72*) a CS-specific whole genome RH panel was produced from crosses between male cultivars of the reference hexaploid wheat line CS and the tetraploid cultivar Altar 84 (Triticum turgidum L. (2n = 4x = 28; AABB). The F1 (RH1) plants grown from seeds harvested from the pollinated tetraploid wheat spikes represented individual independent RH panel members with quasi-pentaploid (AABBD) genotypes. A whole genome RH panel of 500 RH1 plants was generated (240 from 10Gy and 260 from 15Gy gamma irradiation treatment).

RH lines were selected for high throughput genotyping by initial characterization of DNA isolated from 10-Gy and 15-Gy RH lines for retention of seven genome-specific SSR markers (one per chromosome), i.e. lines with the lowest marker retention and with at least one break per chromosome. The 228 lines identified were then genotyped together with three CS and three Altar controls and two F1 controls (CS x AL; non-irradiated cross) on the Axiom TaBW280K SNP array containing 280,226 genome-wide markers (*73*). SNPs were assigned to six categories according to cluster patterns produced by the Affymetrix software: Polymorphic High Resolution (PHR), Off-Target Variants (OTV), Monomorphic High Resolution (MHR), No Minor Homozygous (NMH), Call Rate Below Threshold (CRBT) and Others. For subsequent analyses, only OTVs were considered as these markers can be used to detect presence-absence variations (PAVs) and correspond to probes showing four clusters, including a null allele. After removal of markers representing poor genotyping data rather than true deletions, 20,677 SNP markers were retained for use in WGRH mapping of CS chromosomes. A consequence of using the tetraploid line Altar to create the RH panel was the D-genome contained the highest number of SNP markers, 9,472 SNPs compared to the A- and B-genomes, with 4,501 and 6,704 markers, respectively.

RH maps were constructed with the software package Carthagene (*74*). RH markers were grouped using minimum two-point LOD scores of 15.0 and a threshold distance of 0.3 to reduce the possibility of pseudo-linkage of markers on RH groups. Subsequently, individual RH groups were used to construct maps using LOD scores of 15.0 and a threshold distance of 0.3, applying Carthagene's map validation commands 'greedy', 'annealing', 'flip' and 'polish' with default settings to improve marker ordering. The maps for each chromosome/ arm were finalized using genetic maps to orient the order of markers on scaffolds. Due to the pentaploid nature of the WGRH panel (AABBD), D- genome specific markers were mapped on D- chromosomes without the need for marker polymorphism. The requirement for A- and B- genome chromosome markers to be polymorphic between CS and Altar, without any null allele in CS, significantly reduced the numbers of usable markers on A- and B- genome chromosomes. After critical filtering and application of very stringent grouping criteria for RH mapping, 8,521 markers were used to construct RH maps for the 21 CS chromosomes. (Table S8).

2.7 Genetic mapping

Two genetic maps for sequence scaffold anchoring and ordering were constructed by genotyping-by-sequencing (GBS) of two populations developed from crosses between the parental lines Synthetic W7984 (M6) and Opata M85 (*75*). GBS reads were generated from the populations SynOpDH88, comprising 88 double haploids and SynOpRIL993, comprising 993 Recombinant Inbred Lines, after treatment with restriction enzymes Psti-Msp1 and Psti-Hpa1, respectively, as previously described (*76*). After demultiplexing, sequence reads were assigned to samples using the barcode followed by the TCGA overhang sequence and then aligned with bwa-mem(v0.7.12) to the IWGSC RefSeqv1.0 assembly. SNPs were called with samtools mpileup with –uv –t DP parameters and bcftools call –c –v (bctools v1.2). Only high quality GBS-SNP markers were retained (quality score >40; <15% missing data; >10% heterozygous calls; minor allele frequency >20%) and the markers were given identifiers indicating the CS pseudomolecule designation and chromosomal position, e.g. chr1A_13829065. GBS-SNP markers that aligned to the "Unanchored" scaffolds (ChrUn) were removed for subsequent analysis. MSTMap on the R/ASMap package for R was used for genetic linkage analysis. 7,832 from a total of 12,492 GBS-SNP markers were incorporated into the genetic linkage map for the SynOpDH88 population and 4,745 from a total of 8,698 high quality GBS-SNP markers were incorporated into the genetic linkage map for the SynOpRIL993 population.

For the analysis of recombination rate distribution along chromosomes a third genetic map based on 430 Single Seed Descent (SSD) individuals derived from a cross between CS and Renan (CsRe) was generated from genotyping data produced using the TaBW280K SNP array (*14*, *73*). Polymorphic SNPs were filtered to discard markers that deviated significantly ($P \leq 0.01$) from the expected 1:1 ratio in a chi-square test, markers with missing or heterozygous data in parents and markers with more than 15% missing data. SNPs were divided into 21 sets corresponding to the 21 chromosomes, based on CSS-based in silico assignment (*6*) prior to constructing genetic maps using MSTMap (*77*) with the default parameters: population type: RIL6; distance function: Kosambi; cut-off: 1^{e-11}; map dist.: 15; map size: 2; missing threshold: 0.20; estimation before clustering: yes; detect bad data: yes; objective function: ML. Once robust framework maps were obtained for each chromosome, a whole-genome map was built using selected markers covering all chromosomes and genetic bins. This map was used to place additional markers comprising unassigned markers from previous chromosomal analyses, as well as markers that were excluded during the filtration phase. Recombination patterns along the chromosomes were evaluated using 10-Mb sliding windows (step 1 Mb) (Fig. S24).

2.8 Genome size estimation

The size of the bread wheat genome was estimated from flow cytometric measurements of the amount of nuclear DNA in hexaploid wheat (*Triticum aestivum* cv. Chinese Spring). The genotype that was sequenced was analyzed to prevent errors due to copy number variation and intraspecific differences in genome size. As flow cytometry measures relative fluorescence intensity of cell nuclei stained by a DNA fluorochrome, determination of absolute DNA amounts requires comparison with a standard of known genome size (*78*). *Pisum sativum* cv. Ctirad was used as the reference standard in this work and its genome size (4,225,354,542 bp) was determined using human male leukocyte DNA as primary reference standard and the size of the human genome assembly GRCh38.11 released by the Genome Reference Consortium on June 14, 2017 (https://www.ncbi.nlm.nih.gov/grc/human), which reports a total of 3,253,848,404 bases. This approach yielded a mean genome size of hexaploid wheat of 15,764,430,570 bp, or 15.76 Gbp, indicating 92% genome coverage by the current 14.5 Gbp IWGSC RefSeq v1.0 wheat genome assembly.

An independent genome size estimate was obtained on the basis of read coverage decomposition as described for *Eucalyptus globulus* and *E. grandis* genome size estimates (*79*). The IWGSC RefSeq v1.0 average insert coverage at 1-fold was estimated using a subset of well assembled scaffolds (N=346; manually checked). Scaffolds containing regions of deep read coverage were excluded and thus the estimate range can be considered conservative. The 1x coverage estimate gained in this way was also checked against estimates from all scaffolds of length > 1M bp and was found to be almost identical for the mean but much reduced in variation (due to the leverage of the under-represented regions). The mean coverage estimate was then used as a scaling factor enabling scaffold contributions to be calculated from the observed coverage. This was carried out for the mean and 95% confidence interval (CI) range estimates. The mean estimate is 15.4 Gbp (s.d. 0.2 Gbp) and 95% CI was between 14.85 and 15.82 Gbp.

3. Assembly of chromosome-like pseudomolecules

Pseudomolecules of the 21 wheat chromosomes were assembled by integrating chromosome-specific and genome-wide map and sequence-based resources with IWGSC WGAv0.2 in a highly iterative procedure summarized in Fig. S1.

3.1 Genetic anchoring of scaffolds

Contigs of the chromosome shotgun sequence (CSS) assembly of bread wheat cv. CS (*6*) were mapped to the WGA with BWA mem version 0.7.13 (*80*). Primary alignments with a mapping quality ≥ 30 were extracted with SAMtools (*81*) and imported into R for further analysis. Chromosome arm assignments from flow-sorted chromosome data (*6*) and POPSEQ chromosome assignments (*7*) were lifted from aligned CSS contigs to the whole-genome assembly using a majority rule. POPSEQ genetic positions (centiMorgan coordinates) of WGS scaffolds were obtained by calculating the arithmetic mean across all POPSEQ-anchored CSS contigs aligned to a WGA scaffold. Chromosome assignment by Hi-C of a WGA scaffold was determined by tabulating the POPSEQ chromosome assignments of all other scaffolds with Hi-C links to this scaffold and applying a majority rule. Aggregation of map information was done using functionalities of the R package 'data.table' (http://CRAN.R-project.org/package=data.table). The CS x Renan genetic map (*82*) provided confirmation for the order of scaffolds and super-scaffolds in IWGSC RefSeq v1.0.

3.2 Detecting scaffold misjoins

WGA scaffolds misjoining two or more unlinked sequences ("chimeras") were identified by inspecting genetic marker and Hi-C link information and the alignments of CSS contigs to the WGA scaffolds. Putative chimeras carried a higher than average number of at least two types of assigned sequences (POPSEQ, Hi-C, or CSS) to chromosomes other than the major one. Scaffold breakpoints were identified with the CE method as implemented in the R package "breakpoint" (https://cran.r-project.org/web/packages/breakpoint/index.html). Putative chimeric scaffolds and detected breakpoints were visually inspected and confirmed chimeras were split.

3.3 Ordering and orienting scaffolds by Hi-C

Scaffolds that (i) were assigned to chromosomes both by Hi-C and by POPSEQ, and (ii) harbored at least 50 *Hind*III fragments were used for Hi-C map construction. Scaffolds were ordered using a custom R implementation (*61*) of the algorithm described in (*83*), and considering only Hi-C links within a single chromosome. If both scaffolds were anchored to the POPSEQ genetic map, the genetic distance between them was required to be ≤ 20 cM. The accuracy of scaffold order and the completeness of the Hi-C map were confirmed by alignment to the POPSEQ genetic map. POPSEQ-confirmed scaffolds were oriented by Hi-C as described in (*61*) using a bin size of 1 Mb.

3.4 Superscaffolding

Superscaffolding proceeded in two steps. First, Whole Genome Profiling (WGP™) tags, BAC sequence assemblies and optical maps were aligned to WGA scaffolds and evaluated using automated scripts to find putative links between adjacent WGA scaffolds. In a second step, potential scaffold joins were manually inspected, and high-confidence joins were accepted.

3.5 Automated pipeline for superscaffolding using chromosome-specific resources

WGP™ tags: WGP™ tags were aligned to the WGA scaffolds with BWAmem version 0.7.13(*80*). Alignments with a mapping quality ≥ 30 were imported into R for further analysis. WGP™ tags were assigned to fingerprinted (FP) contigs based on the physical maps of wheat chromosomes or chromosome arms downloaded from URGI (https://urgi.versailles.inra.fr/download/iwgsc/Physical_maps/). WGP™ tags that aligned within 200 bp of each other were grouped together and considered as a single tag for further analyses. Alignments were aggregated at the level of FP contigs. FP contigs with at least five tags aligned to two different WGS scaffolds were considered as potential joins. Pair-wise orientations of adjacent WGA scaffolds were determined by calculating correlation coefficients between the positions of WGP™ tags in the physical maps and their alignments to WGA scaffolds. For subsequent manual inspection tags were organized at the BAC level so that a complete set of tags was available for each BAC. For each chromosome, the following procedure was followed: 1) Tags were aligned to the WGA scaffolds assigned to chromosome pseudomolecules, requiring perfect alignment; 2) Alignments were processed with a custom Python script that assigned BACs to locations based on tag positions; 3) The script produced a tiling of the scaffolds with BACs, and produced an output that included the physical contig and index of each BAC.

BAC sequences: BAC sequence contigs were split into 5 kb fragments with a step size of 1 kb and aligned to WGA scaffolds with BWA mem version 0.7.15 (*80*). The alignment results were converted into BED format with BEDTools (*84*) and imported into R. Only alignments with a length of at least 3 kb and a mapping quality ≥ 30 were considered. Aligned fragments were grouped (i) at the level of individual BAC sequence scaffolds or contigs, if multiple BACs were sequenced together in pools; or (ii) at the level of fingerprinted contigs if individually barcoded BACs were sequenced and assembled. BAC groups with at least five fragments aligned to two or more different scaffolds were considered as potential joins. Pair-wise orientations of adjacent WGA scaffolds were inferred by calculating correlation coefficients between positions of BACs in the physical maps and their alignment to WGA scaffolds, or by comparing the positions of 5 kb sequence fragments in the BAC assemblies and their alignments to the WGA scaffolds.

Optical maps: Contigs of the optical maps for 7AS, 7AL, 7BS, 7BL and 7DS were aligned to the WGA scaffolds with IrysView RefAligner (http://www.bionanogenomics.com) and mapping results were imported into R. Optical contigs with alignments to two different WGA scaffolds with a confidence score ≥ 20 were considered as potential joins. Pair-wise orientations of adjacent WGA scaffolds were inferred by comparing the orientations of the optical map alignments as provided by RefAligner.

Manual inspection

The final stage in the IWGSC RefSeq v1.0 assembly was manual inspection of scaffolds and superscaffold links using alignment with physical maps, optical maps, and genetic maps to confirm or identify additional superscaffold joins and to identify false joins. Chimeric joins and orientation errors were identified using genetic maps by mapping sequences of genetic markers to updated pseudomolecule positions for each chromosome and generating plots of genetic distance to physical distance. Any obvious long-range outlier markers were identified and, if contained in a super-scaffold defined by manual joins, the super-scaffold join was invalidated. Such chimeric joins can be caused by errors in the physical map or misassemblies in the WGA scaffolds. Incorrect orientations of large scaffolds that could be identified in the genetic/physical alignments

were corrected. If differences in the genetic and physical order were ambiguous and not supported by multiple genetic maps, no change was made. The results of the manual inspection stage have been documented in the AGP ("A Golden Path") files for the chromosomes.

3.6 Gap filling using assembled BAC sequences

Chromosome specific BAC sequence assemblies available for 16 chromosome arms (1AS-L, 1BS-L, 3DS-L, 4AL, 5BS, 6BS-L, 7AS-L, 7BS-L, 7DS-L) and 3B were used to fill inter-scaffold gaps between adjacent WGA scaffolds. The strategy used sets of ISBP markers (*10*) (Insertion Site Based Polymorphism) shared between two scaffolds to identify overlapping scaffolds from two different assemblies, i.e. WGA vs BAC-based sequence assembly, to avoid performing a computationally expensive all-against-all alignment. TE models were identified for all WGA scaffolds using ClariTE (*85*) and the PERL script junctionDesigner.pl used to extract 150 bp ISBP markers (75 bp on each side of the junction between a given TE and its insertion site). Mapping 5,031,032 ISBPs with BWA (*81*) and requiring a perfect match to the BAC-based scaffold assemblies found 1,876,163 ISBPs that were then used to identify potential scaffold overlaps based on pairs of scaffolds sharing three or more ISBPs and residing on the same chromosome. 1,251 groups (accounting for a total of 2,233 scaffolds) of potentially overlapping scaffolds were identified by the PERL script slalomer.pl developed to perform this step. The scaffolds sharing common ISBPs were mapped fully with Nucmer (*86*) (cutoff 99% nucleotide identity over at least 5 kb) and the alignments were all manually inspected to keep only scaffolds that truly overlap, i.e. share identical sequences encompassing their extremities. The order of scaffolds along the WGA-based pseudomolecules was used as a template to identify potential joins for superscaffolds and to fill gaps between neighbors. For gap filling, the exact coordinates of overlapping segments were retrieved from the Nucmer output using the PERL script gapfiller.pl whose purpose is to update the AGP file (describing the positions of scaffolds on pseudomolecules) based on the Nucmer alignments. Gaps were filled if they met the criteria: (i) shared at least 5 kb contiguous aligned sequences with at least 99% nucleotide identity; (ii) alignments must include scaffold ends (while allowing unaligned ends of 10 kb at maximum); (iii) the difference in length between two aligned sequences does not exceed 10% of the length of the larger one. Using these criteria, 183 gaps were filled in the WGA-based pseudomolecules with 181 scaffolds originating from BAC-based sequencing projects.

4. Genome annotation

4.1 Centromere positioning

Centromeres were identified and positioned using published ChIP-seq data for CENH3 (*15*). Raw reads were downloaded from EMBL ENA (SRR1686799). After adapter trimming with cutadapt (*87*), reads were mapped to the CS pseudomolecules and unassigned scaffolds ("chrUn") with BWA-MEM (arXiv:1303.3997). Alignments were converted to BAM format with SAMtools (*81*) and sorted with Novosort (http://www.novocraft.com). Uniquely mapped (MAPQ >= 20), non-duplicated reads were extracted with SAMtools and counted in non-overlapping 100 kb windows with BEDTools (*84*). The resultant count tables were imported into the R statistical environment for visualization. To define approximate centromere boundaries, read counts in regions closely to visually defined ChIP-seq peaks were manually inspected. An enriched region was called if at least three (two for chromosome 7B) consecutive 100 kb bins had more than three times the genomic average of ChIP-seq reads (320 reads per bin) mapped to them. The consecutiveness was not considered for bins of "chrUn". Disjoint CENH3-enriched regions separated by fewer than 500 kb were merged.

4.2 Annotation of repetitive DNA

Transposable elements (TEs) were modeled using CLARITE and a wheat TE reference library named ClariTeRep as previously described (*85*). Briefly, CLARITE provides an annotation of TEs by analyzing the raw similarity search results, applying a defragmentation step, and reconstructing the nested insertion patterns.

4.3 Gene annotation

A federated gene prediction strategy (Fig. S8) was developed for the automated gene calling on IWGSC RefSeq v1.0 based on established and proven gene prediction pipelines and protocols at INRA-GDEC Clermont Ferrand, France, Helmholtz Zentrum, Munich, Germany (PGSB) and the Earlham Institute, UK.

4.3.1 Gene modeling using the TriAnnot pipeline

TriAnnot, a modular, customizable, and parallelized pipeline for plant genome sequence annotation (*88*), originally developed for the Triticeae and used for the annotation of wheat chromosome 3B (*14*) was used to model protein-coding genes in the wheat genome sequence. TriAnnot gene annotation of IWGSC RefSeq v1.0 combined the parallel annotation of individual RefSeq_v1.0 scaffolds and BAC-derived sequences used to fill gaps. Annotated features were positioned subsequently on the pseudomolecules using a custom script. The annotation process comprised four main steps: (1) TE repeat masking. TEs annotated with CLARITE were masked using RepeatMasker (cross_match engine, cutoff 250 - (*89*)). (2) Similarity search against transcripts and related proteomes. A similarity search was performed on the TE-masked sequence using BLAST (*90*) with the following datasets: wheat cv. CS transcripts (*91*); PacBio full-length transcripts of cv. Xiaoyan 81 (*92*); all available Triticeae ESTs and full-length cDNAs (EMBL release 126; tritfldb at http://www.psc.riken.jp); non-redundant proteomes of rice (UniProt Release 2016_03 and (*12*)), maize (UniProt Release 2016_03 and phytozome v11), sorghum (UniProt Release 2016_03 and phytozome v11), barley (UniProt Release 2016_03 and High Confidence proteins (*93*)), *Aegilops tauschii* (UniProt Release 2016_03 and (*53*)) and *Triticum urartu* (UniProt Release 2016_03 and (*52*)). Spliced alignments of BLAST hits generated by EXONERATE (*94*) were used to check gene models predicted in step#3 and for display as individual tracks in a genome browser. (3) Gene modeling. *Ab-initio* gene models were predicted using two gene finders trained with a wheat-specific matrix: FGeneSH (SOFTBERRY, http://linux1.softberry.com/berry.phtml) and AUGUSTUS (*95*). Evidence-driven gene model prediction was also computed with two different modules implemented in TriAnnot. The first module is based on BLASTX-EXONERATE spliced alignments of protein sequences from rice (*12*), Brachypodium (phytozome v11), sorghum (phytozome v11), maize (phytozome v11) and barley (High Confidence proteins (*93*)) and incorporated iterative extension over a range of ca. 200 codons to identify an in-frame start and stop codon in case of missing start and/or stop codons in the derived CDS model. Models with no start and/or stop codons are flagged as pseudogenes. The second module (named SIMsearch, derived from FPGP pipeline (*96*)) focused on similarity with wheat transcripts (full-length cDNAs (tritfldb at http://www.psc.riken.jp/english/ and EMBL release 126) and RNA-Seq-derived transcripts (*91*)) to predict the CDS borders by comparison with known proteins from related Poaceae. (4) Selection of the best gene model at every locus. At each locus, the five gene models delivered by TriAnnot (derived from two *ab-initio* gene finders, BLASTX-EXONERATE, and two SIMsearch-derived models) were evaluated using a scoring system that considered the metrics of the alignment of each gene model against known proteins (taking into account percentage identity and coverage). The highest scoring models were retained and subjected to two further steps. First, models with a canonical structure but less than 70% similarity across the length of the best

BLAST hit were classified as pseudogenes (i.e. suggesting a large truncation). In the second step gene models that were ambiguous or doubtful were discarded based on comparisons between TriAnnot gene models, TGACv1 gene models (*8*), CSS gene models (*6*), and RNA-Seq derived transcripts (*91*) mapped on the RefSeq_v1.0 pseudomolecules with Gmap (*97*) made with cuffcompare (*98*) and InterProscan5. All gene models were removed that were not supported by evidence (i.e. *ab-initio* only; no similarity with proteins, transcripts or Interpro domain) and that do not correspond to a gene model from the CSS or TGACv1 datasets. The final Triannot output identified 180,270 gene models comprising 65,884 high confidence genes, 41,342 low confidence genes and 73,044 pseudogenes.

4.3.2 PGSB gene prediction pipeline

The annotation process of the PGSB pipeline comprised two main steps: (1) Mapping: The PGSB gene annotation pipeline combined information from mapping splice site-aware alignments with reference proteins, RNA-Seq based gene structure predictions, alignment of IsoSeq reads and alignments of full-length cDNAs (flcDNAs). First, publicly available RNA-Seq data sets were mapped with RNA-Seq read aligner Hisat2 (*99*) (version 2.0.4, arguments: --dta) to predict transcript structures on the wheat assembly (E-MTAB-2137, SRP045409, ERP004714/URGI, E-MTAB-1729, PRJEB15048 and PRJEB23081). Alignment files were sorted and converted into BAM files using Samtools (*81*) (version 1.3, arguments: sort -@ 8 -T). The BAM files from each data set were then combined into a single alignment file using Bamtools (*100*) (version 2.4.1, arguments: merge) and mapped reads were assembled into transcript sequences with StringTie (*101*) (version 1.2.3, arguments: -m 150 -t -f 0.3). StringTie was configured to include only isoforms expressed at levels at least as high as 30 % of the main isoform and to include only isoforms with a minimum length of 150 bp. Predicted protein sequences from five reference plant species (*A. thaliana, B. distachyon, O. sativa, S. bicolor* and *S. italica*), as well as all available complete Triticeae protein sequences (downloaded from Uniprot at 10/05/16) (*102*) were then aligned against the chromosome pseudomolecules using the splice-aware alignment software GenomeThreader (*103*) (version 1.6.6; parameters used: -startcodon - finalstopcodon -species rice -gcmincoverage 70 -prseedlength 7 -prhdist 4 -force). Mapping was performed for each chromosome separately to reduce running time and the resulting gene structure predictions were then combined using a custom python script. In addition, the GeMoMa tool (*104*) (version 1.4.2) was used with annotations of protein-coding genes from *A. thaliana* to generate high-quality homologous gene predictions using specifically the conservation of intron splice sites for protein detection. Full length cDNA sequences from wheat and barley (*105*), together with publicly available IsoSeq reads (*8*) were also included in the prediction pipeline. GMAP (*97*) (Version 2016-06-30; parameter: -f gff3_gene) was used to align sequences to the wheat assembly and the resulting transcript predictions were combined using a custom python script. (2) Prediction and selection of open-reading frames (ORFs). All predicted sequences from protein alignments, RNA-Seq mapping and long transcript sequence mapping were combined into a single structure file using Cuffcompare (*106*) (version 2.2.1). StringTie (version 1.2.3) was used to remove redundant transcript sequences and to merge fragments in the combined structure file. Using a script from Transdecoder suite (https://github.com/TransDecoder/TransDecoder/releases, version 3.0.0, cufflinks_gtf_genome_to_cdna_fasta.pl) transcript sequences were extracted and stored in a single fasta file. Similarly, Transdecoder longorfs (arguments: -p 0) was used to predict potential protein translations for each transcript sequence. Thereby, translations were forced to include the left-most methionine as a start codon if available. All potential protein sequences were then

mapped against a set of validated protein sequences from angiosperms (downloaded from Uniprot, 08/03/16) using protein BLAST (*90*) (version 2.3.0, -max_target_seqs 1 -evalue 1e-05) and scanned for the presence of protein domains using Hmmer3 (*107*) (version 3.1b2). A table with BLAST results and protein domain information was then used by Transdecoder predict to select a single best translation for each transcript sequence. Finally, gene predictions from Transdecoder were merged with gene predictions from protein alignments, removing protein sequences that were fully included in another protein sequence at each locus to produce a non-redundant set of predicted protein sequences.

4.3.3 Production of IWGSC RefSeq Annotation v1.0 by gene model consolidation and integration

The two independent gene prediction pipelines generated alternative gene models for many loci. To evaluate and select the "best" representative gene model for each locus a rule-based approach was developed to use a combination of supporting evidence (e.g. high quality transcriptome data, protein homology) and intrinsic gene characteristics (e.g. CDS length, proportion of canonical introns). To enable an unbiased assessment of the alternative gene predictions, an independent set of quality filtered PacBio transcripts, RNA-Seq and cross species protein alignments to the genome assembly was generated (Tables S13, S14 and S15). RNA-Seq reads were assembled using three alternative approaches (Cufflinks, CLASS2 and StringTie) and integrated into a single set of transcripts using Mikado (*108*) (Table S16). A set of high confidence splice junctions was identified from RNA-Seq alignments using Portcullis (*109*). The gene model selection approach used heuristics including splicing agreement with wheat transcripts and cross-species BLAST alignment coverage. To measure the congruence between a gene model and its supporting evidence an average F1 score was calculated (using nucleotide, junction and exon F1) from the aligned PacBio transcripts, Mikado transcript assemblies and proteins. Homology support was indicated by determining query and target coverage using BLAST alignment of gene models to a plant protein database. Mikado was used to cluster genes from the two pipelines into loci, assign an overall score to each gene model and select a representative (highest scoring) gene model for each locus. Scoring utilized the externally generated F1 and homology scores in conjunction with selected Mikado metrics (Table S17). Gene models located on the opposite strand or intronic to another gene with no supporting evidence in the quality filtered data were excluded, the majority (3520) being single exon models based on incorrectly aligned transcripts/proteins. Models with extremely long introns (>75 Kb) or exons (>30 kb) that represented alignment artefacts (233) were also removed.

Following selection of the representative gene model, Mikado evaluated overlapping transcripts to identify high quality alternative gene models (splice variants) based on defined criteria. Gene models that met the following requirements were retained:

- assigned to a single locus (to avoid selecting fusion transcripts)
- contain novel splicing (class codes j,J,G and h as determined by Mikado compare)
- cDNA overlap > 0.6 (relative to representative)
- CDS overlap > 0.6 (relative to representative)
- min score percentage > 0.5 (relative to representative)
- proportion of canonical introns = 1
- max exon length < 10,000 bp
- max intron length < 10,000 bp
- contain only verified introns (i.e. pass portcullis junction filter)
- do not contain any retained intron event, i.e. the CDS does not end within a CDS intron of another transcript in the locus

Gene models were refined by adding UTR features based on supporting cDNA, PacBio transcripts or RNA-Seq assemblies. PacBio transcripts and cDNAs were aligned to the genome with GMAP (Genome Mapping and Alignment Program). After filtering to reduce errors originating from alignment artefacts, chimeric transcripts and over-extended UTRs the Mikado transcript assemblies were assembled by PASA (The Program to Assemble Spliced Alignments) with the aligned cDNAs and PacBio transcripts. PASA takes existing annotations and compares them to the PASA assembly clusters to identify potential updates. UTR additions only (PASA status 13 and 14) were selected and the corresponding gene models updated ensuring CDS features remained unchanged. A second round of PASA UTR updates was performed using the Mikado PacBio assemblies. Following PASA additional checks were carried out and changes implemented to remove UTRs from models lacking start or stop codons, from models with greater than four 5' or 3' UTR features, or any model with UTR introns over 30kb (common alignment artefacts). UTR start and end positions were standardized across transcripts sharing UTR exons.

Comparison of the long transcripts generated by PacBio sequencing (ENA PRJEB15048) with the annotated gene models was used as a measure of testing annotation quality, noting that not all PacBio reads represent full length transcripts and the presence of retained introns and alignment errors can reduce the agreement between aligned data sets. Comparing TriAnnot, PGSB and RefSeq Annotation v1.1 gene models with PacBio transcripts aligned to the IWGSC RefSeq v1.0 sequence assembly showed that the integrated data in RefSeq Annotation v1.1 represents a higher proportion of more complete gene models than either of the outputs from the two automated pipelines alone. RefSeq Annotation v1.1 also provides more complete coverage of the bread wheat gene space than previous wheat genome annotations released in 2014 (IWGSC CSS, (*6*)) or 2017 (TGACv1, (*8*)), as judged by greater than 90% coverage of 1.5 million PacBio transcripts.

Over 80% of the genes defined as high confidence by either the TriAnnot or the PGSB pipelines overlapped a gene in the alternative annotation, with a substantial percentage of genes showing highly similar structures (67% TriAnnot, 48% PGSB). Less agreement was found between gene models classified as low confidence, in total combining low and high confidence genes 66,064 (37%) were specific to TriAnnot and 89,988 genes (44%) specific to PGSB. Differences between the two annotations reflect the challenge of annotating a transcriptionally complex polyploid species as well as differences in the evidence datasets utilized and individual characteristics of the annotation pipelines. The final RefSeq Annotation v1.1 (see Methods 4.3.5) incorporates 205,643 PGSB gene models (432,097 transcripts) and 180,270 TriAnnot gene models (180,270 transcripts) and removes aberrant transcripts that originate from incorrect alignments.

Overall 98% of RefSeq v1.1 genes aligned to the TGACv1 assembly and 78% to the IWGSC CSS using GMAP (version 20160923) with 95% identity and 80% coverage. Using BLAST alignment to assess the representation of previous wheat proteins in the RefSeq Annotation v1.1, a large proportion of high confidence genes identified in earlier studies (*6*) (*8*)were found (TGAC v1 87%, IWGSC CSS 74%, minimum of 95% identity, 75% coverage), with the majority also classified as high confidence (81% of TGAC v1.0, 68% of IWGSC CSS). A more detailed comparison of RefSeq Annotation v1.1 gene structures with the previous gene models aligned to the IWGSC RefSeq v1.0 assembly revealed greater agreement with the TGACv1 genes (Fig. S11), as expected given the greater contiguity of the TGACv1.0 assembly compared with the IWGSC CSS. Overall, high levels of similarity were found between high confidence genes annotated in RefSeq annotation v1.1 TGAC v1 (identical gene structures for >50% genes and highly similar structures for a further 33%). Little agreement was seen for low

confidence genes with either the TGACv1 or IWGSC CSS annotation. By definition, low confidence genes have reduced homology support to help guide annotation and contain gene fragments and pseudogenes that are likely to show greater variability in gene structure between alternative annotation pipelines. A more detailed classification of these genes and other intergenic transcribed sequences will be a key part of future wheat annotation releases.

4.3.4 Gene confidence assignment

The IWGSC RefSeq Annotation v1.0 gene models were classified into HC (High-Confidence) or LC (Low-Confidence) genes using predictions based on their sequence homology to gene products in public databases [**UniPoa**: Annotated *Poaceae* proteins (SwissProt & trEMBL); Sequences were downloaded from Uniprot (Feb 2017, https://www.ebi.ac.uk/uniprot) and further filtered for complete sequences with start and stop codons; **UniMag**: Validated Magnoliophyta proteins (SwissProt); Sequences were downloaded from UniProt (Feb 2017) and further filtered for complete sequences with start and stop codons] and/or known repetitive sequences in **TREP** [The database of hypothetical proteins ("PTREP") deduced from the non-redundant database of transposable elements (TE) within the TREP database (http://botserv2.uzh.ch/kelldata/trep-db/index.html)]. PTREP was useful for the identification of divergent TEs having no significant similarity at the DNA level. **HC genes** have complete gene models with very good sequence homology to experimentally verified plant proteins from SwissProt (HC1) or with very good sequence homology to annotated *Poaceae* proteins in SwissProt or trEMBL, and no good hits in the transposon database TREP (HC2). "Complete" gene models are defined as containing both start and stop codons (which do not necessarily represent the biologically "true" start and stop sites). **LC genes** have incomplete gene models with very good sequence homology to experimentally verified plant proteins from SwissProt (LC1), complete gene models with no significant homology to TREP, UniPoa or Unimag databases (see definition below) (LC2) or incomplete gene models with very good sequence homology to any annotated (also automatically) *Poaceae* protein in SwissProt or trEMBL but no good hits in the TREP database (LC1). Incomplete gene models with no significant homology to any of the three databases were classified as LC3. TREP genes have incomplete gene models with no significant homology to experimentally verified plant proteins from SwissProt, but good homology to TREP entries. For each transcript in the initial data set, sequence homology to each of the three databases was determined (BLASTP, e-value cutoff 10^{-10}) and classified according to the respective best hit: step 1: Alignment with maximal (and at least 90%) overlap between query and subject sequence for the two protein databases; alignment with maximal (and at least 90%) query coverage for TREP database; step 2: classification into distinct confidence groups and sub-groups according to the following rules:

```
# Primary confidence class
   unimag & complete <- "HC"
   !unimag & (!trep & unipoa) & complete <- "HC"
   (unimag | (!trep & unipoa)) & !complete <- "LC"
   !unimag & !trep & !unipoa & complete <- "LC"
   !(unimag & complete) & trep <- "TREP"
# Secondary confidence class
   unimag & complete <- "HC1"
   !unimag & (!trep & unipoa) & complete <- "HC2"
   (unimag | (!trep & unipoa)) & !complete <- "LC1"
   !unimag & !trep & !unipoa & complete <- "LC2"
   !unimag & !trep & !unipoa & !complete <- "LC3"
   !(unimag & complete) & trep <- "TREP"
```

The confidence group of each transcript is annotated in the respective GFF/GTF file. In cases where transcripts with different confidence classes are present at a single gene locus, the "best" confidence label of all transcripts present was assigned to the respective locus.

4.3.5 Annotation update and integration of manually curated genes

The automated annotation of eight gene families (CBF, NLR, WAK, RK, AATset9, Prolamin, and PPR) was updated to incorporate manual annotation. In addition, 3,318 HC genes were re-classified as LC-TE, following identification of TE elements from the functional annotation. The semi-automated process developed to integrate the manual curation data used a Python script based on common tools (GenomeTool, GFFCompare, pyBEDTools) to manage the integration process (Fig. S9). Gffcompare was used initially to check that the curated gene sets did not overlap each other and to identify the RefSeq Annotation v1.0 models to be updated. 5 types of modification were identified depending on the overlap between manually curated genes and the automated annotation (Fig. S9). The gene model updates included in RefSeq Annotation v1.1 are summarized in Table S12 and comprise 3,685 manually curated genes, of which 528 were not present in RefSeq Annotation v1.0 and 3,020 were replaced with a single manually annotated gene. The manually annotated genes have been designated HC3. In addition, 354 LC genes were removed from the LC gene set (161,537 genes) after gffcomp was used to identify LC genes overlapping the 3,685 manually curated genes. The final IWGSC Annotation v1.1 HC gene set (IWGSC_V1.1_HC.gff3) contains 107,891 genes including 528 genes not annotated in the v1.0 HC gene-set. The v1.1-LC gene set (IWGSC_V1.1_LC.gff3) contains 161,537 models, including 3,318 genes functionally designated TE that were re-classified. The characteristics of the predicted gene models are summarized in Table S18. To minimize the impact of artefacts arising from RNA-Seq alignment and assembly that can artificially inflate estimates of alternative splicing, a conservative approach was taken that excluded splice variants with non-canonical splicing, or with fragmented or truncated coding sequences. As a result, 133,745 distinct transcripts were associated with HC genes (average 1.24 transcripts per gene) with 16% of HC genes having an annotated splice variant.

4.4 Evaluation of the flanking / promoter regions of wheat genes

To assess the quality of the RefSeq v1.0 assembly in the immediate vicinity of genes, which is important for analysis of promotors and regulatory elements, the 5' upstream and 3' downstream flanking regions were compared in 269,428 HC and LC gene models of RefSeq v1.0, 217,907 HC and LC gene models from TGACv1.0 (*8*) and 99,386 HC gene models of the CSS assembly (*6*). The "bedtools flank" command (*84*) was used to extend gene coordinates from 1kb to 10kb upstream and downstream of the start/stop codon and corresponding nucleotide sequences were extracted using "bedtools getfasta". In subsequent steps, nucleotide sequences shorter than the predefined length or containing any "N" sequences were discarded. The proportions of retained 5' upstream and 3' downstream sequences are shown in (Fig. S12).

4.5 Pseudogenes

4.5.1 Pseudogene annotation

Two complementary approaches were used to identify pseudogenes in IWGSC RefSeq v1.0: (1) *De novo* genome-wide identification of pseudogenes derived from HC genes: a specialized pseudogene detection and analysis pipeline was employed to identify and classify pseudogenes in a genome-wide manner, independently from elements annotated in the gene prediction process. Using a homology-based approach, pseudogenes derived from HC genes were identified by determining internal stop codons and other structural features that disrupt the gene models. This genome-wide analysis identified 288,839 pseudogenes, including 10,440 predictions overlapping with pseudogene annotations in the LC gene set. (2) Identification of disrupted or truncated gene

models in the LC gene set: Pseudogenes in the LC gene set were identified by detecting internal stop codons in the LC gene 'open reading frames (ORF)'. 25,419 LC pseudogene predictions were identified of which 10,440 overlapped with the genome-wide pseudogene set. A significant overlap was defined as >96% coverage of the annotated pseudogene with the LC gene model, >15% coverage of the LC gene model with the annotated pseudogene and the presence of a premature stop codon (PTC) in the ORF of the LC gene model. Potential pseudogenes in the LC gene set were kept as LC genes in the v1.1 gene annotation, with a note indicating their potential pseudogene role.

4.5.2 Pseudogene classification

Intron sequences were used to classify pseudogenes as 'duplicated' or 'retroposed' where fragmentation did not disrupt splice sites. For the intron loss/retention criterion, six pseudogene classes were defined: (1) 'duplicated' pseudogenes still containing introns at each covered splice site; (2) 'retroposed' or 'processed' pseudogenes having lost all introns; (3) 'chimeric' pseudogenes having both retained and lost introns; (4) 'single-exon gene' pseudogenes are duplicates of genes with only one exon; (5) 'single-exon splice variant' pseudogenes are duplicates of isoforms with only one exon; (6) 'fragmented' pseudogenes are short gene fragments not sufficiently covering a gene splice site. A splice site was only considered covered if at least 10 base pairs of the exons on either side were present in the duplicate. The gap had to be at least 30 base pairs long to be considered a duplicated intron.

288,839 pseudogenes and gene fragments were identified in the bread wheat genome (Table S21, S22). 48,619 (16.8%) represent at least 80% of the CDS of a parent gene locus (high-coverage pseudogenes). Of these, 42.1% retained their exon-intron structure and are thus classified as "duplicated". The distribution of pseudogenes on the 21 chromosomes of bread wheat followed the distribution of genes (Fig. S10) and, whilst the three sub-genomes have similar pseudogene content, fewer and less degenerated pseudogenes were found on the D sub-genome compared to sub-genomes A and B (Table S22).

4.6 Annotation of miRNA and tRNA

A two-step homology-based *in silico* method was applied to each chromosome pseudomolecule separately for miRNA identification. Chromosome sequences were compared with all known plant mature miRNA sequences retrieved from miRBase (v21, June 2014) (*110*) allowing at most a single base mismatch between mature miRNA and chromosome sequences using the in-house script SUmirFind (https://github.com/hikmetbudak/miRNA-annotation/blob/master/ SUmirFind.pl) (*111*). Candidate precursors of mature miRNAs were extracted and assessed for their secondary structure formation features with UNAFold v3.8 (*112*) using the in-house script, SUmirFold (https://github.com/hikmetbudak/miRNA-annotation/blob/master/ SUmirFold.pl). Additional criteria were applied for the precursor sequences which satisfied the folding evaluation (*113*). Finally, false-positives were eliminated from the results of SUmirFold by using SUmirScreen (https://github.com/hikmetbudak/miRNA-annotation/blob/master/ SUmirScreen.py) and the genomic distribution of the final miRNA list was obtained with SUmirLocate python scripts (https://github.com/hikmetbudak/miRNA-annotation/blob/master/ SUmirLocate.py).

tRNA annotation was performed as described previously (*114*) with tRNAscan-SE software (version 1.3.1), which uses a series of algorithms to predict tRNA sequences from the genome and examine their secondary structure features (*115*).

4.7 Functional annotation of genes

4.7.1 Automated functional annotation

Functions were assigned to annotated genes with the AHRD tool (Automated Assignment of Human Readable Descriptions, https://github.com/groupschoof/AHRD, version 3.3.3) to generate more informative annotation than can be derived for the Triticeae where the UniProt databases contain large numbers of uncharacterized genes and a best BLAST hit approach alone would return about 30% of 'unknown' descriptions. BLAST hits against the following databases were used as AHRD input: Swiss-Prot (version 02-15-17), *Arabidopsis* Araport 11 (version 201606) and custom made TrEMBL (version 02-15-17) *Viridiplantae* subset. The AHRD parameters re provided with the AHRD output files. Gene ontology, Pfam and InterPro assignments were derived from InterProScan Runs (version 5.23-62.0). A postprocessing filter (disTEG: distinction between TEs and Genes) on the AHRD and domain descriptions tagged the genes as either G for canonical genes with a nonTE description, TE for obvious transposons, TE? for potential transposons or U for unknowns, without any description. The numbers of genes assigned to these four categories in RefSeq annotation v1.0 are shown in Table S19. The HC genes with TE tags were moved subsequently from the HC to the LC category in RefSeq annotation v1.1.

4.7.2 Orthology-based ontology annotation of wheat genes

In addition to automated functional annotation, inferred orthologous relationships determined by phylogenomics, as described below, were used to transfer automatic and experimentally validated annotations from orthologous genes to the respective genes in the bread wheat genome. Gene Ontology (GO; (*116*)), Plant Ontology (PO; (*117*)) and Plant Trait Ontology (TO; (*118*)) term annotations were obtained and pooled from Gene Ontology (http://geneontology.org/gene-associations), TAIR (https://www.arabidopsis.org/), and Gramene (ftp://ftp.gramene.org/pub/gramene/release52/data/ontology/) resources. Gene identifiers where mapped to public resources using the UniProtKB mapping table (ftp://ftp.uniprot.org/pub/databases/uniprot/current_release/knowledgebase/idmapping/). The pfam2GO mapping table available from the Gene Ontology resource (http://geneontology.org/external2go/pfam2go) was also employed to transfer GO terms based on the inferred domain architectures. The source evidence classes of the annotated, orthologous genes were translated into target evidence codes of wheat genes as follows: a) automatic annotations: IEA (Inferred by Electronic Annotation), b) experimental and reviewed computational analyses (for full list of evidence codes in these categories see http://www.geneontology.org/page/guide-go-evidence-codes): e.g. EXP (Inferred from Experiment) and e.g. RCA (Reviewed Computational Analysis), ISO (Inferred by Sequence Orthology) c) pfam2GO: ISM (Inferred from Sequence Model). The comprehensive ontology annotation including source term publication references and gene identifiers in GAF2 format comprising more than 5 million annotations is available from Table S20.

5. Transcriptome and gene co-expression network analysis

5.1 Expression analysis

The analysis used 529 previously published (described in Table S30) and 321 new RNAseq samples from six studies (Table S31) (*19*). Metadata was assigned as in (*119*) for tissue, age, variety and stress (Database S1). The tissues from where RNA was extracted for the RNA-Seq were defined as low level tissues. To facilitate analyses, we grouped these low level tissues based on their biological origin into a hierarchical structure with the highest hierarchy represented by the 4 high level tissues Roots, Leaves, Spike, Grain. Given the relatively large number of low level tissues (59), an intermediate level of tissues comprising 32 factors (median 12 replicates per factor) was defined and used for this study (Table S32). The 850 samples were mapped to the

RefSeqv1.0+UTR transcriptome (default parameters) with Kallisto v0.42.3 (*120*) and transcripts per million (tpm) were calculated per gene using tximport v1.2.0. To determine a minimum threshold required for a gene to be considered expressed, the 1% most highly expressed samples for each gene were examined. This criterion allowed tissue-specific expression to be accounted for, while still requiring at least eight samples to have a minimum expression abundance. This analysis identified a clustering of very low expressed genes between 0 and 0.5 tpm (corresponding to less than 10 reads/counts per gene, Fig. S30). Subsequent application of the criteria that over 1% of samples all required expression values over 0.5 tpm for a gene to be considered expressed across the 850 samples removed some of the expected low-level non-target homeolog mapping (which occurs when homeologs are identical across a long stretch of sequence), while retaining more lowly expressed genes. By applying this criterion to the 850 samples, expression was detected for 94,114 high confidence (HC) genes and 77,920 low confidence (LC) genes, corresponding to 84.95 % and 49.07 % of HC and LC genes, respectively. For the PCA analysis, tpm values for the 94,114 expressed HC genes were transformed (log2 (tpm+1)) and the PCA calculated using the prcomp function in R.

Distribution of gene expression: The number of HC and LC genes expressed in each intermediate tissue (Database S1) were defined as genes for which three samples had expression values over 0.5 tpm. The tpm abundance of each gene was then averaged across its expressed tissues to determine an average expression of the gene across the intermediate tissues. The average expression values were assigned to bins for visualization. The values for all HC and LC genes are presented in Fig. S31.

Expression breadth: The number of expressed genes was determined for each tissue using the same criteria as for the distribution of gene expression (three samples with expression values over 0.5 tpm). Using this criterion, 89,444 genes were found to be expressed in at least one intermediate tissue (Table S32). Each chromosome was segmented into bins corresponding to 1% of the physical size and genes were assigned to the bins based on their physical position to generate comparable scales across chromosomes. Using the genomic compartment breakpoints (Fig. S25, Table S29) to delimit the R1, R2a, C, R2b and R3 regions for each scaled chromosome, a representative artificial chromosome was produced with the average breakpoint positions to define each genomic compartment. The original bins were rescaled to the artificial chromosomes with the following formula:

$$scaledBin_i = \left[\left(\frac{originaBin_i - originalBinStart_p}{originalBinSize_p}\right) * averageBinSize_p\right] + averageBinStart_p$$

where i correspond to the 1% bin and i∈p, where p is the partition group. The average of each bin was calculated and further grouped into bins of 2% for display purposes (Fig. S36).

Tissue exclusivity: To determine if a gene was expressed within a given tissue, the average expression of each gene was calculated for each of the 32 intermediate tissues (Table S32). Tissue exclusivity was defined as those genes whose average expression was over 0.5 tpm in a single intermediate tissue, and therefore had average expression < 0.5 tpm for all other intermediate tissues.

5.2 Co-expression analysis (WGCNA)

The WGCNA R package (*121*) was used to build the co-expression network with HC genes expressed > 0.5 tpm in > 1 % of the 850 samples (94,114 genes). The expression count of each

gene was normalized using variance stabilizing transformation from DESeq2 (*122*) to eliminate differences in sequencing depth between studies. A soft power threshold of 6 was used because it was the first power to exceed a scale-free topology fit index of 0.9. A signed hybrid network was constructed blockwise in three blocks using the function blockwiseModules with a maximum block size of 46,000 genes and a biweight mid-correlation "bicor" with maxPOutliers = 0.05. The blockwiseModules function calculated the topographical overlap matrices (TOM) using TOMType = "unsigned" and the minimum module size was set to 30. Similar modules were merged by the parameter mergeCutHeight=0.15. Modules were tested for correlations to high level tissues using the cor() function. The significance of correlations were calculated using the function corPvalueStudent() and corrected for multiple testing using p.adjust() using the method of (*123*). The most central genes in modules were identified using the function signedKME() which calculates the correlation between the expression patterns of each gene and the module eigengene. The most highly correlated genes were considered central to the module.

6. Epigenomic analyses

6.1 Analysis of DNA methylation

Cytosine methylation was profiled in DNA extracted from two-week old CS leaf tissue in three different contexts: CpG dinucleotides, CHG and CHH (where H corresponds to A, T or C). 2.25 billion high quality whole genome bisulphite Illumina sequence (WGBS) reads were aligned with Bismark version 0.16.1 (*124*) to IWGSC RefSeq v1.0. Despite the complications of working with a highly repetitive complex polyploid species, unique bisulfite read alignment was found to be in excess of 60%. A total of 79,851,988,588 high confidence cytosine methylation calls representing 77.1% of the assembled genome with an average read depth of 16-fold and a minimum depth of 4-fold were used in subsequent analyses.

6.2 ChIP-seq analysis of histone marks

ChIP assays were performed with anti-H3K9ac (Millipore, ref. 07-352), anti-H3K27me3 (Millipore, ref. 07-449), anti-H3K4me3 (Millipore, ref. 07-473) and anti-H3K36me3 (Abcam, ab9050) antibodies, using a procedure adapted from (*125*). Briefly, after fixation of 10-day-old *in vitro* seedlings in 1% (v/v) formaldehyde, tissues were homogenized, nuclei isolated and lysed. Cross-linked chromatin was sonicated using Covaris S220. Protein/DNA complexes were immunoprecipitated with antibodies overnight at 4°C with gentle shaking and incubated for 1h at 4°C with 50 µL of Dynabeads Protein A (Invitrogen, Ref. 100-02D). The beads were washed 2 × 5 min in ChIP wash buffer 1 (0.1% SDS, 1% Triton X-100, 20 mM Tris-HCl pH 8.0, 2 mM EDTA pH 8.0, 150 mM NaCl), 2 × 5 min in ChIP Wash Buffer 2 (0.1% SDS, 1% Triton X-100, 20 mM Tris-HCl pH 8, 2 mM EDTA pH 8, 500 mM NaCl), 2 × 5 min in ChIP wash buffer 3 (0.25 M LiCl, 1% NP-40, 1% sodium deoxycholate, 10 mM Tris-HCl pH 8.0, 1 mM EDTA pH 8.0) and twice in TE (10 mM Tris-HCl pH 8.0, 1 mM EDTA pH 8.0). ChIPed DNA was eluted by two 15-min incubations at 65°C with 250µL elution buffer (1% SDS, 0.1 M NaHCO3). Chromatin was reverse-crosslinked by adding 20µL of 5M NaCl and incubating overnight at 65°C. Reverse-cross-linked DNA was treated with RNase and proteinase K, and extracted with phenol-chloroform. DNA was precipitated with ethanol in the presence of 20µg of glycogen and resuspended in 20µL of nuclease-free water (Ambion) in a DNA low-bind tube. 10 ng of immuno precipitate (IP) or input DNA were used for ChIP-Seq library construction using NEB-Next Ultra II DNA Library Prep Kit for Illumina (New England Biolabs) according to manufacturer's recommendations. For all libraries, ten cycles of PCR were used. The quality of the libraries was assessed with Agilent 2100 Bioanalyzer (Agilent), and the libraries were sequenced using 2x75bp pair-end reads on NextSeq 500 platform (Illumina). Raw FASTQ files were preprocessed with Trimmomatic v0.36 (*126*) to remove Illumina sequencing adapters, trim 5' and 3' ends with

quality score below 5 (Phred+33) and discard reads shorter than 20 bp after trimming. Paired-end reads were aligned against IWGSC RefSeq v1.0 using bowtie2 v2.3.3 with --very-sensitive settings (*127*). Alignments with MAPQ < 10 were discarded and duplicate reads removed with Picard MarkDuplicates (http://broadinstitute.github.io/picard/). Enrichment peaks were called with MACS2 v2.1.1 using the following settings: -f BAM -B --nomodel --to-large -q 0.05 --broad --bdg -g 17e9 --bw 300. ChIP-seq input data were used as a control. The peaks were annotated according to their position and overlap with HC genes (iwgsc_refseqv1.0_HighConf_2017Mar13.gff3). The distribution of histone marks along chromosomes was estimated as a function of the percentage of mark-associated genes in a sliding window of 10 Mb (step = 1 Mb).

7. Gene family analysis

7.1 Identification of gene families

Gene families were defined in an automated phylogenomics approach incorporating the predicted protein sequences from bread wheat (RefSeq Annotation v1.0), nine other grasses and four Viridiplantae genomes (Table S23; Fig. S13). Wheat sub-genomes were handled as independent taxa. Protein sequences were screened for known protein domains using HMMer3 hmmsearch (-cut_ga) against the PFAM 30.0 database and a set of custom HMMs representing gene families inferred previously (*128*). Protein sequences with domain matches from HMMs associated with TEs were classified as TE-related proteins. Domain matches were filtered and assembled into domain architectures using the DAMA software (*129*). Protein sequences were compared in all vs. all blastp searches using the NCBI blast+ toolkit as suggested in the OrthoFinder manual (*130*). Resulting blastp hits were filtered using the following criteria: A) both proteins have annotated domain architectures and the alignment covers the entire domain ranges of each protein; B) at least one of the proteins does not have annotated domains, but the alignment covers any contained domains and at least 60% of both proteins; C) the alignment covers at least 70% of the longer and 90% of the shorter protein. Links between TE-related proteins determined in the previous steps were discarded. The inferred domain architecture and protein alignment statistics were employed to discern the representative isoform for loci with multiple splice variants in any of the three bread wheat sub-genomes by choosing the best supported variant. The filtered protein matches were used as input for reconstruction of gene families in the form of orthologous groups using OrthoFinder (*130*). The resulting gene families and phylogenetic trees were analyzed to infer homologous relationships among gene family members (orthologs, homeologs, inparalogs and outparalogs) and definition of subfamilies by re-rooting the cladograms based on the ‘get farthest_oldest_node’ (or as a fallback the ‘get_midpoint’_outgroup) method. Subsequent species tree reconciliation using the Species Overlap algorithm (*131*) was implemented using the ETE3 toolkit (*132*). During this procedure, orthologs among the three bread wheat sub-genomes were classified as homoeologs. Fig. S14 provides an example of the inferred speciation and duplication events in the resulting gene trees. Internal nodes representing the origin of subtrees i.e. subfamilies, initiated by pre-speciation duplication events and speciation events, were placed into taxonomic context using the species tree (Fig. S13) and the NCBI taxonomy database. The resulting 14,275 subtrees containing only orthologs were used to infer a species tree with branch lengths using the coalescence approach implemented in ASTRAL (*133*). The species tree was rooted using the four non-grass taxa and cut to contain only the *Poaceae* taxa under study (Fig. S15). The phylogenomics workflow identified 30,597 gene families including 26,080 families with members from at least one of the three wheat sub-genomes. Overall, 63,523,422 homologous relationships, comprising 2,555,680

orthologous, 123,588 homeologous, 1,797,522 inparalogous and 59,046,632 outparalogous links, were inferred.

7.2 Expansion and contraction of gene families

Gene family expansions and contractions in either one of the wheat sub-genomes, the wheat A- or D-lineage or the wheat genome in general were inferred using a previously established phylogenomic approach (*134*) (Fig. S42). Log-transformed gene family sizes among the 10 grasses were compared using phylogenetic comparative one-way ANOVA (*135*), correcting for phylogenetic interdependency using a species tree (Fig. S13) that was computed by coalescence analysis (*133*) of 14,275 orthologue-only subfamily clades extracted from the gene family trees derived by OrthoFinder. To account for hexaploidy in the bread wheat genome, all three sub-genomes were treated as separate entities i.e. taxa. False-positives from remnant chimeric gene families were excluded from the analysis by only considering gene families where at least 51% of the members harbored consistent domain architecture. This filter excluded 18 families. Gene family sizes were log-scaled.

7.3 Functional annotation of expanded and contracted wheat gene families

Sets of expanded/contracted gene families at 90% confidence (FDR) were assessed for enriched biological processes (GO), molecular functions (GO), cellular components (GO), plant structure developmental stages (PO), plant anatomical entities (PO) or plant morphology traits (TO) using ontology term enrichment with the Parent-Child method implemented in the Ontologizer software (*136*). To further dissect overlap and unique features in sets of enriched terms among the expanded and contracted gene families, the FGNet Bioconductor R package (*137*) was used to construct a functional ontology term network with the overlapping and distinct enriched GO, PO and TO terms. The resulting graph was clustered into 7 related subnetworks with maximal overlap by GLAY community clustering (*138*) (Fig. S45-S51).

7.4 Validation of phylogenomic gene family annotation

The orthologous groups of gene families derived from the automated phylogenomic approach were evaluated against seven manually curated gene families: Aquaporins, C-Repeat Binding Factors (CBF), Dehydrins, Nucleotide-Binding Site – Leucine-Rich Repeat genes (NLR), Pentatricopeptide Repeat genes (PPR), Prolamins, and Cell Wall Associated Kinase genes (WAK) (Table S37). Each orthologous group (OG), was assessed for expansion or contraction in the Poaceae taxa. The FDR-corrected p-values indicated that between 15% (PPRs) and 75% (CBFs) of the subfamilies were either expanded in wheat, in one of its sub-genomes, or in one of the ancestral lineages. Only a small number of examples of contraction of orthologous groups (OGs) was found. The uncorrected p-values indicated expansion – from 30% of the OGs in PPRs to 100.00% in CBFs. A more detailed phylogenomic analysis was undertaken for the CBFs (124 sequences) and Dehydrins (158 sequences). The domain composition was determined from the manually curated candidate sequence lists: CBFs – AP2 domain (PF00847); Dehydrins – Dehydrin domain (PF00257) and all proteins with at least one of these domains was extracted from the evograph dataset. The amino acid sequences were then aligned using UPP (*139*) and trees were constructed with FastTree (*140*) and visualized with iTOL (*141*), rooting the trees at mid-point. In these gene families, 96.97% of the OG were monophyletic (100% if those with a bootstrap support <0.75 are removed). The same is true when only considering expanded OGs (Table S38; Fig. S55, S56).

7.5 Comparative analysis of homeologous genomes

Homeologous groups (*142*) were defined based on the homologous relationships inferred from gene trees, and initially constructed for an unfiltered set of 260,162 genes comprising HC and LC genes. This set was iteratively analyzed using the results from all relevant analyses (AHRD, HMMER3/PFAM-domains, TE-overlap, pseudogene analysis) described above to

identify potential pseudogenes and TE-related loci. This resulted in the final, filtered dataset comprising 181,036 genes (103,757 HC and 77,279 LC genes). As both HC and LC genes were included in the analysis, the resulting homeolog groups were classed as either 'HC-only', 'LC-only' or 'mixed'. In addition, TE-related loci among the homeologs are included but tagged with 'is_filtered=TRUE'. Homeologous groups harboring >=50% of these loci were considered as TE-related in their entirety. Each group of homeologous genes represents a clade of orthologous taxa in the gene tree of a family. Orthologs between sub-genomes were inferred as homeologs, allowing for sub-genome-specific inparalogs that emerged from post-hybridization duplication events. The homeologous groups were analyzed and annotated by comparing the chromosomal locations of group members and their orthologs in other species. In contrast to other methods used to define homeologs, e.g. best reciprocal BLAST hits, this definition of homeologs relies on the topology of a phylogenetic tree, resulting in less false-positive inferences due to a more stringent assessment of gene orthology beyond mere sequence similarity cut offs. The stringency, in turn, is limited by the scalability and performance of large-scale phylogenetic reconstruction, which is affected by the quality and completeness of the gene models in wheat and from the other species used in the phylogenomics approach. Thus, the total number of homeologs inferred by this approach should be considered a conservative estimate of the true number of homeologous loci in bread wheat.

Each homeologous group was assigned a theoretical and an absolute cardinality, based on the number of homeologs identified in each sub-genome. Table 3 shows an overview of the contributions of different homeolog cardinalities in the wheat genome.

7.6 Analysis of synteny

Microsynteny of the homeologs, i.e. the conservation and collinearity of local gene ordering between orthologous chromosomal regions, was analyzed using the MCScanX software (*143*) on the homeologous gene pairs. 1,256 blocks were analyzed with respect to their chromosomal region, size, orientation (positive or negative) and relative chromosomal location (see below). In addition, the macrosynteny of homeologs was described. i.e. the conservation of chromosome macrostructure accompanied by overall conservation of chromosomal location and identity of genetic markers like homeologs, but not excluding the occurrence of local inversions, insertions or deletions. This was assessed by analyzing the chromosomal position of the individual homeolog groups with respect to their relative chromosomal position and compared to the chromosomal location of their respective orthologs in barley (*144*), *Aegilops tauschii* (*53*) and *Triticum urartu* (*52*). For both macro- and micro-synteny any regional bias was avoided by using a relaxed block size requirement (>=3 genes per block). The chromosomal identity of the majority of orthologous genes for each homeologous group was considered to be the ancestral state of that group. To account for different sizes and possible reorganization of chromosomes, the relative chromosomal position was analyzed in relation to the predicted centromere positions: A) short arm: -(1-(gene_start/posCEN)) B) +(gene_start-posCEN)/(chr_length-posCEN+1). These CEN-relative positions were subsequently compared by their standard deviations to further assess macrosynteny. In addition, a situation where any of the homeologs is not located on the inferred ancestral chromosomal location of a homeolog group, the maximal standard deviation of CEN-relative positions of all microsyntenic 1:1:1 homeologs (0.1983149) was used as a lower limit to test if any of the homeologs in a group substantially deviated in their relative chromosomal position or whether they displayed a conserved relative position indicative of macrosynteny. Both criteria were used to decide whether a homeologous gene pair is in macrosynteny (both on ancestral chromosome or both on same chromosome with conserved relative position) or not.

7.7 Error assessment for homeologous groups with a potential gene loss in one subgenome

The error of prediction of gene loss was assessed using BLASTP searches to determine the number of genes classified as absent in homeologous groups with an absolute cardinality of 1:0:1 or 1:1:0 or 0:1:1 but present in unanchored contigs compiled in chrUn. Protein sequences of these groups were aligned against each other and against the protein sequences of genes located on chrUn. Hits on chrUn were considered as putative homeologs if both members of a homeologous group could be aligned to the same chrUn protein sequence with BLASTP scores and query coverages >= 100% of the average value of the reciprocal alignments. As the chromosomal origin of the additional copies could not be determined, they could either represent A) missing homeologs or B) additional subgenome inparalogs, or C) assembly artifacts. In order to correct for possible errors in our inference of gene losses, we assumed A) to be true for all cases (worst-case scenario) and removed all groups with additional copies from the set with potential gene losses and performed a chisq.test in R. Results are presented in Table S25.

7.8 Nucleotide divergence between homeologs in coding (CDS)/protein sequence

Divergence and synonymous (Ks) and non-synonymous substitution (Ka) rates were determined from pairwise comparisons of homoeologs in each orthologous group and tandemly repeated genes in each tandem cluster. Dialign2 (*145*) was applied to generate pairwise protein alignments which were transformed into codon based nucleotide alignments using a custom python script. Only aligned positions with quality ≥1 were scored. Protein and nucleotide similarities were reported as the percentage of mismatches relative to the lengths of aligned protein and coding sequences. Substitution rates were computed as model-averaged values of several substitution models (parameter-'MS') applying KaKs Calculator 2.0 (*146*) on the codon alignments.

Homeolog sequence similarities at protein and CDS levels were measured as the percentage sequence identity of pairwise member comparisons for each homeologous group. Three categories were analyzed separately: all ortholog clusters; strict 1:1 relationship, i.e. at most one homeologous copy is found in each sub-genome; and one-to-many relations for which, in at least one sub-genome, the copy number of the homeolog has been expanded. These categories were further subdivided into the three possible sub-genome permutations ('AB', 'AD', 'BD'). In addition, the one-to-many category sequence similarities were surveyed for the intra-sub-genome expanded homeologs, 'AA', 'BB' and 'DD'.

8.1 IWGSC RefSeq v1.0 guided dissection of the QTL *SSt1*

Markers that were previously reported to be associated with the peak of the *SSt1* QTL in the Lillian/Vesper genetic map were downloaded from (*49*), and their IWGSC RefSeq v1.0 anchored physical positions were extracted. Markers were also anchored to TGACv1 (*8*) and Triticum 3.1 (*9*) and the corresponding scaffolds/contigs were aligned to IWGSC RefSeq v1.0 by NUCmer (Fig. S57). Sequence size and gene content were compared between Ta3B and chromosome 3B from RefSeq v1.0 (Table S39, S40). All gene and marker mappings were performed using GMAP software with at least 80% coverage and 95% identity.

RNA-Seq was performed on wheat cultivars Lillian (solid-stemmed) and Vesper (hollow-stemmed), and durum wheat cultivars Langdon (LDN, hollow-stemmed) and LDN-GB-3B [solid-stemmed, chromosome 3B (from Golden Ball) substitution line of Langdon]. Tissue was extracted at Zadoks stage 32 (*147*) (entire lowermost node, extending approximately 0.5 cm up along the stem). Individually barcoded cDNA libraries were prepared using the Truseq v2 unstranded kit (Illumina) per the manufacturer's recommended protocol. Reads were aligned to the IWGSC RefSeq v1.0 reference sequence using STAR version 2.5 (*148*) with default

parameters, except the maximum mismatch rate (--outFilterMismatchNmax) was set to 6 (minimum 96% sequence identity) and the maximum intron length (--alignIntronMax) was set to 10 Kb. BAM files containing aligned reads were inputted into Stringtie (*149*) to count reads mapping to genes in IWGSC RefSeq v1.0 annotation v1.0 HC gene models. A matrix of raw read counts was analyzed by DESeq2 (*122*) for analysis of differential expression between hollow by solid-stemmed comparisons. Data were filtered for differentially expressed genes using an adjusted $p < 0.01$.

A single-strand conformation polymorphism (SSCP) marker was developed to assay the promotor of one of the differentially expressed genes, *TraesCS3B01G608800*, which carries a repeating AG(n) element 71 bp upstream of the transcriptional start site (Fig. S58). This repeating element was targeted using the following primers and the amplicon size quantified by capillary electrophoresis (Table S42): SSR_F: CAAATCGCCACAAGCTAGAGA, SSR_R: GTGTTCCAGCAGCTTGATGAG.

We also developed a quantitative PCR (qPCR) assay to test for possible copy number variation (CNV) of *TraesCS3B01G608800* (Fig. 5C). qPCR reactions were performed in 10 µl reactions in a 384 well microtiter plate and quantification was performed using SYBR green fluorescence measured in a BioRAD CFX384 cycler. The relative number of copies of *TraesCS3B01G608800* was determined using the ΔΔCT method (*150*) using the gene *TraesCS3B01G61220* as an endogenous control gene with a single copy. Primer sequences used were as follows: TraesCS3B01G61220_F1: CTCAACGAACGACAACGAT, *TraesCS3B01G61220*_F2: AGATCACCAGCTGCTCTACACCT, *TraesCS3B01G61220*_R1: ATGCGTAGGAGTCCATGAG, TraesCS3B01G61220_R2: GGCACTATCATAGACGGCG, *TraesCS3B01G608800*_F1: GTTCCTGCACGCCATGGAC, *TraesCS3B01G608800*_F2: GATGTCCGGGAATCCTCAAT, *TraesCS3B01G608800*_R1: TCCCCCATCGTCGCCATTA, *TraesCS3B01G608800*_R2: TAGTCCCTCTTGGCCGGCT.

A high-throughput and low-cost KASP marker was developed that can be used for MAS for SSt1 in breeding (Fig. 5C). The marker was developed near *TraesCS3B01G608800*, within the gene *TraesCS3B01G890300*LC.1 that uses the primers: usw204-HF: GGCAAAGAACAAAAGCGGTAGAC, usw204-FF: GGCAAAGAACAAAAGCGGTAGAG, usw204_R: GGAGGCTGCGCTAAGAAATTTC.

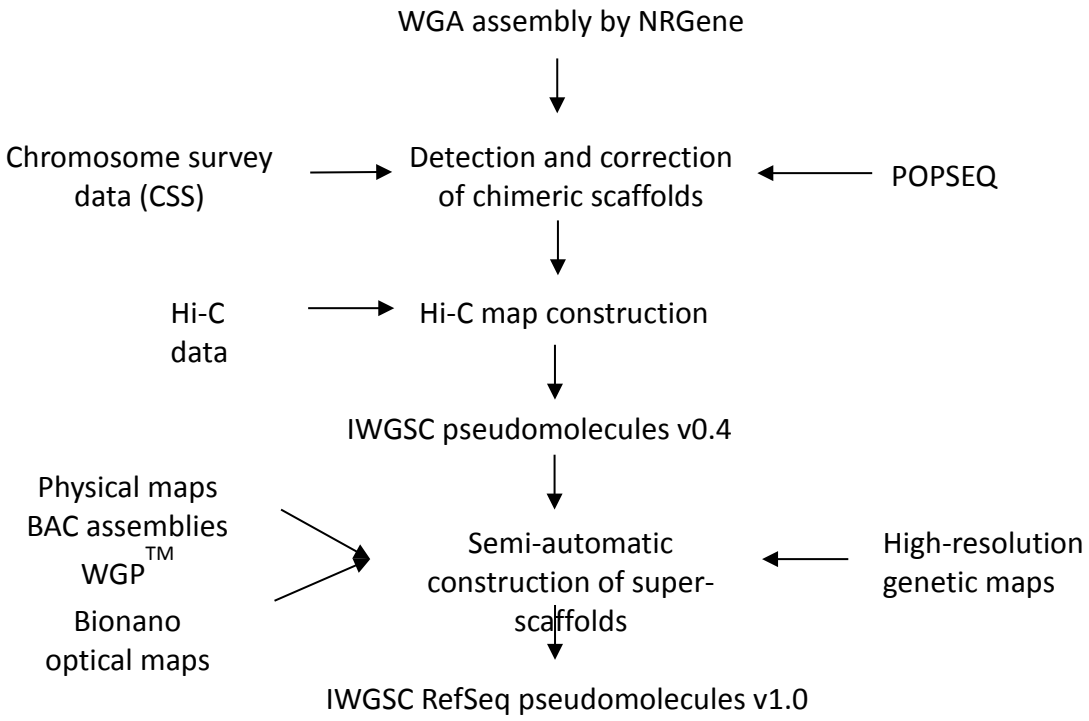

Fig. S1

Data integration pipeline for the assembly of IWGSC RefSeq v1.0. The whole genome assembly (WGA) used DNA from the cultivar CS.

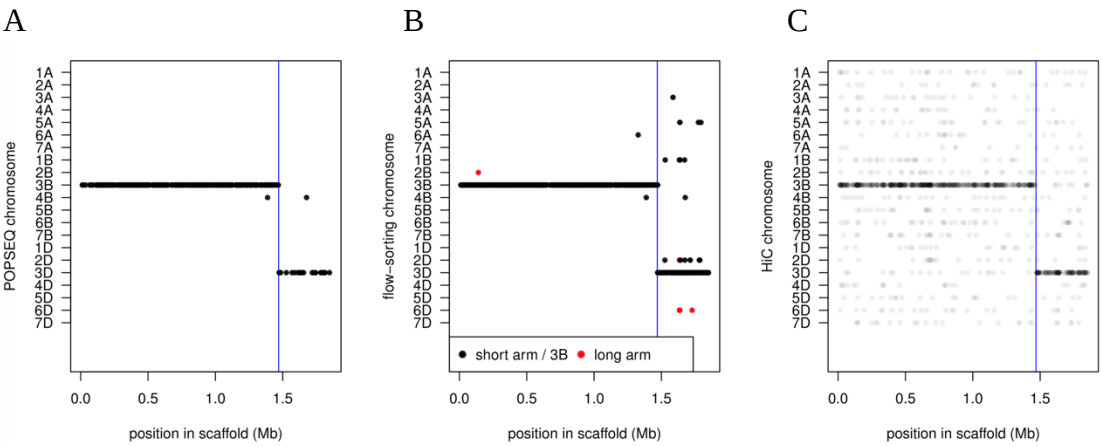

Fig. S2.

Example of a chimeric scaffold in the whole-genome assembly. The scaffold initially joined unlinked sequences from chromosomes 3B and 3D. The chimeric nature of the scaffold was detected A) by the POPSEQ genetic map, B) by the alignment of sequence contigs of the chromosome survey sequencing data (*6*), and C) by chromosome conformation capture data (Hi-C). The vertical blue lines indicates in all three panels the breakpoint at which the scaffold was split into two parts.

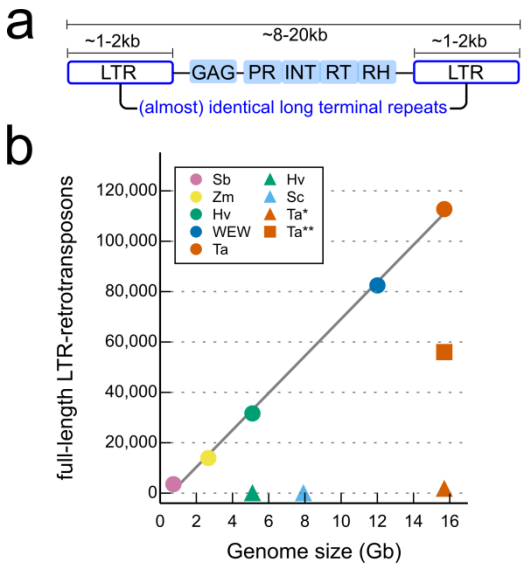

Fig. S3

Number of full length LTR-retrotransposons in different genome assemblies. (a) Schematic structure of a full length LTR-retrotransposon (fl-LTR). (b) fl-LTR content of different grass genome assemblies. The (almost) identical 1-2 kb long terminal repeats of fl-LTRs were often not correctly reconstructed in older contig assemblies (triangles). Circles denote more complete assemblies, triangles lower quality contig assemblies. Sb: *Sorghum bicolor* (*151*); Zm: *Zea mays* (*152*); Hv: *Hordeum vulgare*, triangle (*93*) circle (*144*); Sc: *Secale cereale* (*153*); WEW: wild emmer wheat (*56*); Ta: bread wheat, triangle IWGSC-2014 (*6*), square TGACv1 (*8*), circle IWGSC RefSeq v1.0.

All		84.7%
Class 1	Gypsy	46.7%
	Copia	16.7%
	Unclassified LTR-RTs	3.2%
	LINE	0.9%
	SINE	0.01%
Class 2	CACTA	15.5%
	Mutator	0.38%
	Mariner	0.16%
	Harbinger	0.16%
	hAT	0.01%
	Helitron	0.004%
	Unclassified Class 2	0.27%
Unknown	Unclassified repeats	0.68%

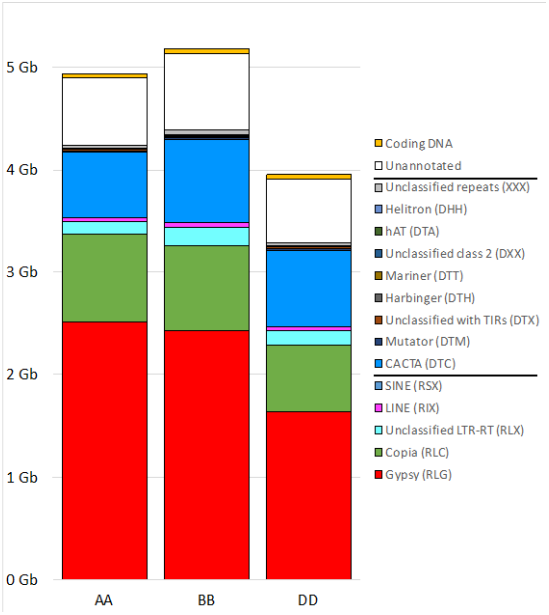

Fig. S4

Sub-genome distribution of the main TE classes in wheat. The right-hand side panel provides a summary of the relative TE distribution between the A, B and D sub-genomes of wheat.

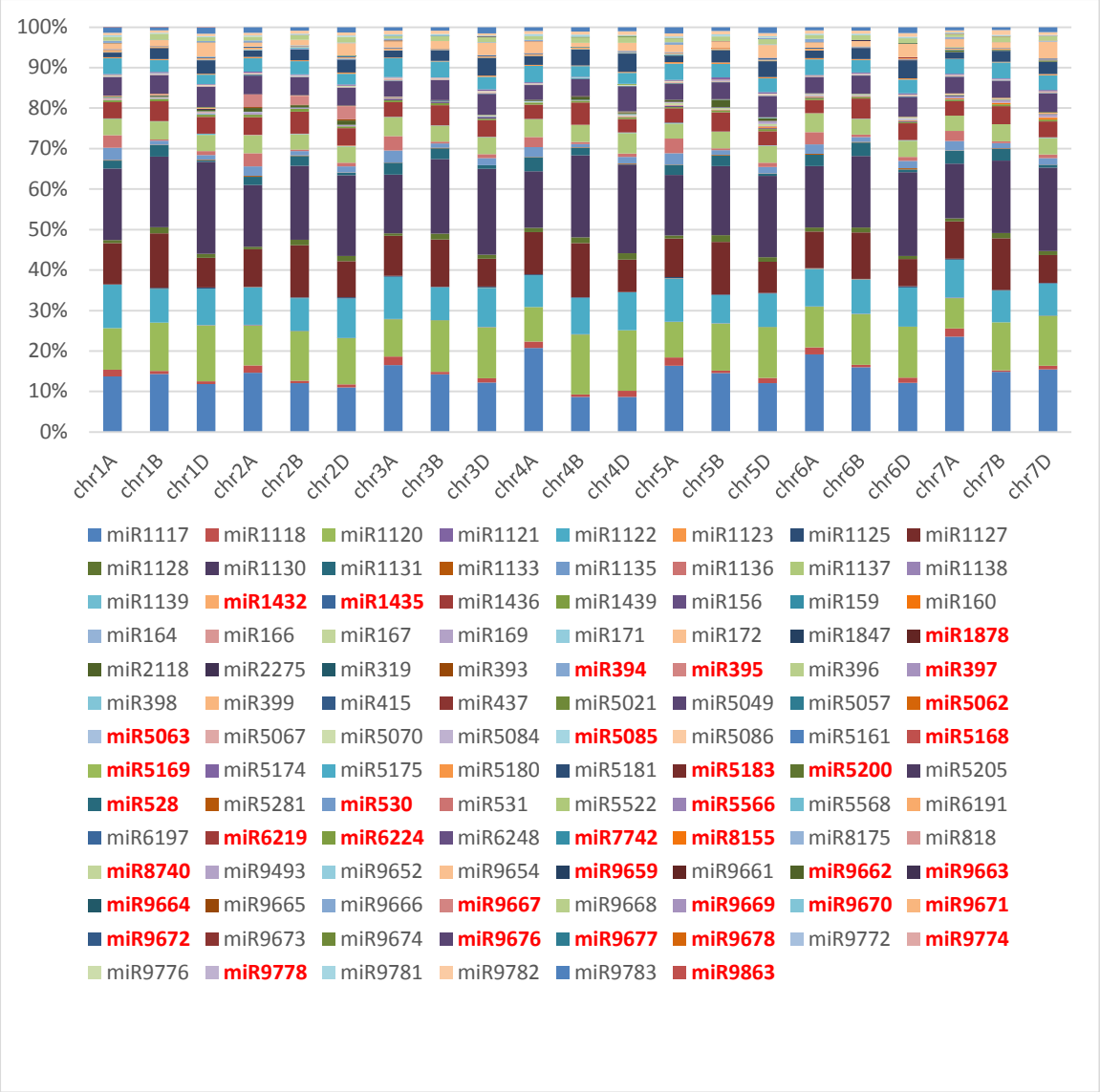

Fig. S5

Distribution of miRNA families in the 21 chromosomes of wheat. 36 miRNA families showed chromosome or homeolog specificity (highlighted in red): miR1432 (2ABD), miR1878 (5ABD), miR394 (6ABD), miR395 (2ABD), miR397 (6AB), miR5062 (5AB), miR5063 (3AB), miR5085 (4B), miR5168 (5ABD), miR5169 (4D), miR5183 (5A), miR5200 (7ABD), miR528 (5A), miR530 (2ABD), miR5566 (6D), miR6219 (6D), miR6224 (2D), miR7742 (4B), miR8155 (5B), miR8740 (7A), miR9659 (6B), miR9662 (6D), miR9663 (6B), miR9664 (1ABD), miR9667 (7ABD), miR9669 (3D), miR9670 (6ABD), miR9671 (7A), miR9672 (5D), miR9676 (3BD), miR9677 (3ABD), miR9678 (7ABD), miR9774 (2B), miR9778 (7ABD), miR9863 (1ABD). New miRNA families identified in the IWGSC RefSeq v1.0 (using all miRBase miRNAs): miR5021, miR5063, miR5067, miR5566, miR8155, miR8175, miR8740, miR9493.

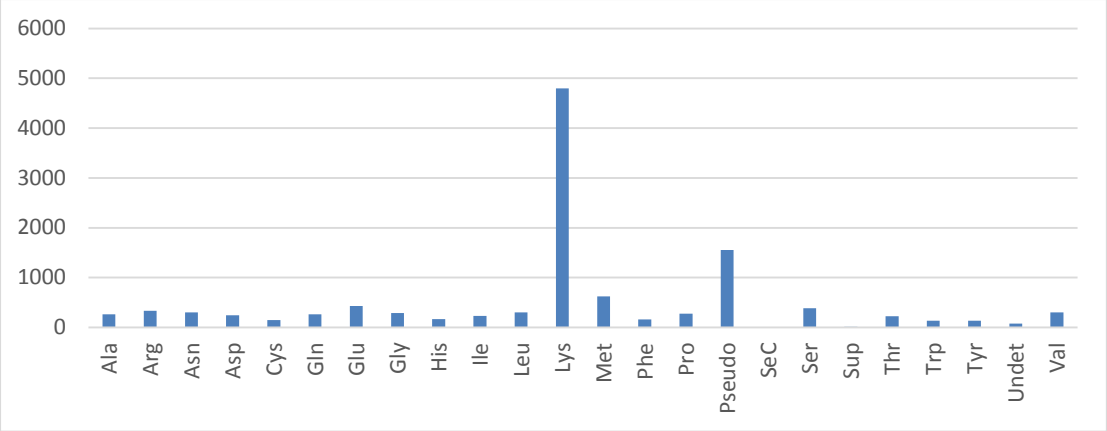

Fig. S6

tRNA gene frequency in IWGSC RefSeq v1.0. Numbers (Y axis) of tRNA coding genes for each amino acid (X axis). Pseudogenes and undet genes could not be assigned, and SeC (selenocysteine) and Sup (suppressor tRNAs) were detected in small amounts.

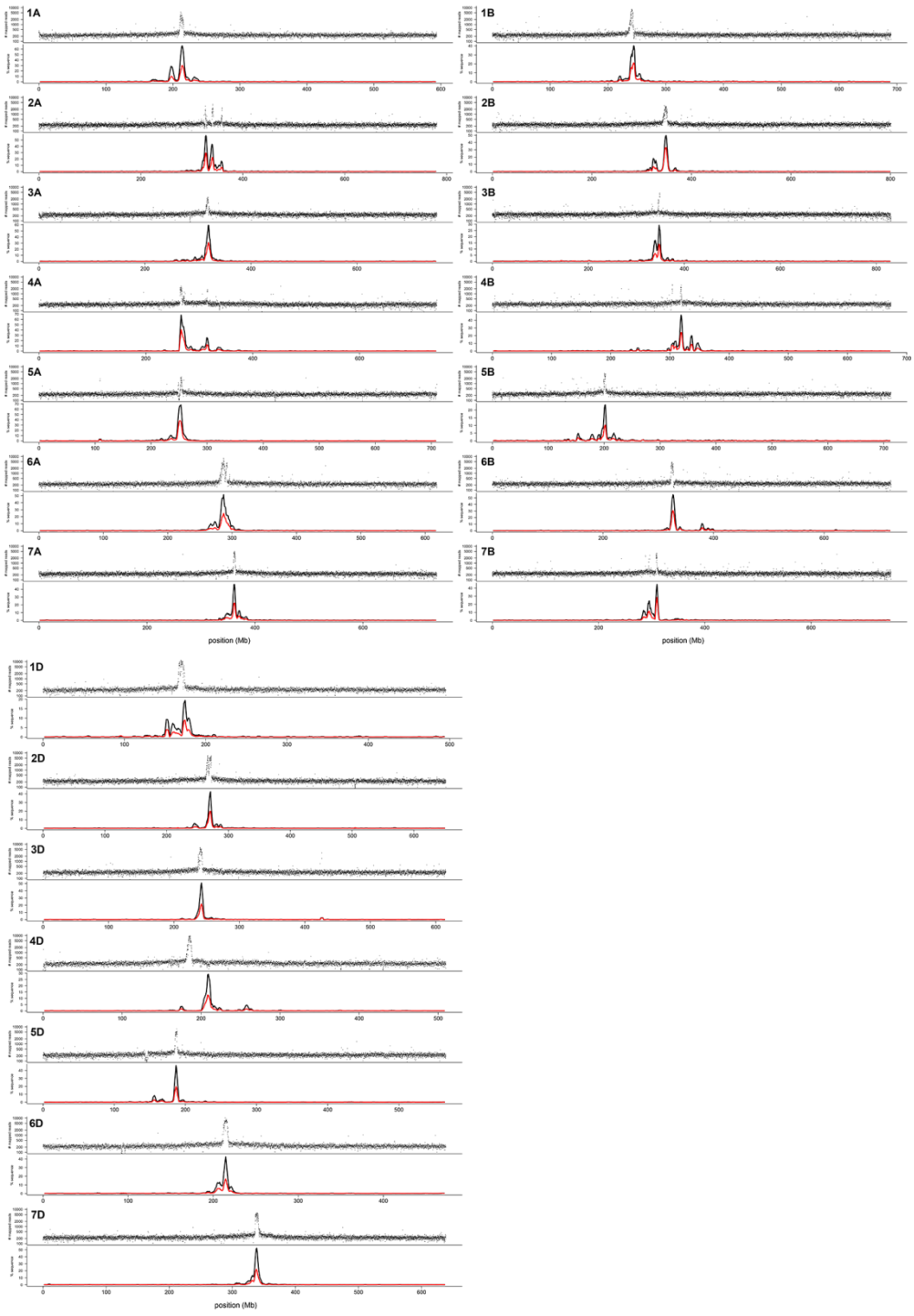

Fig. S7

Positioning of centromeres in wheat chromosome pseudomolecules. Distribution of CENH3 ChIP-Seq data across the 21 bread wheat chromosomes is shown in each upper panels. Lower panels show distribution and proportion of the total pseudomolecule sequence composed of TE of the Cereba (black)/Quinta (red) families. The most likely physical position of centromeres is at the peak of the CENH3 signal.

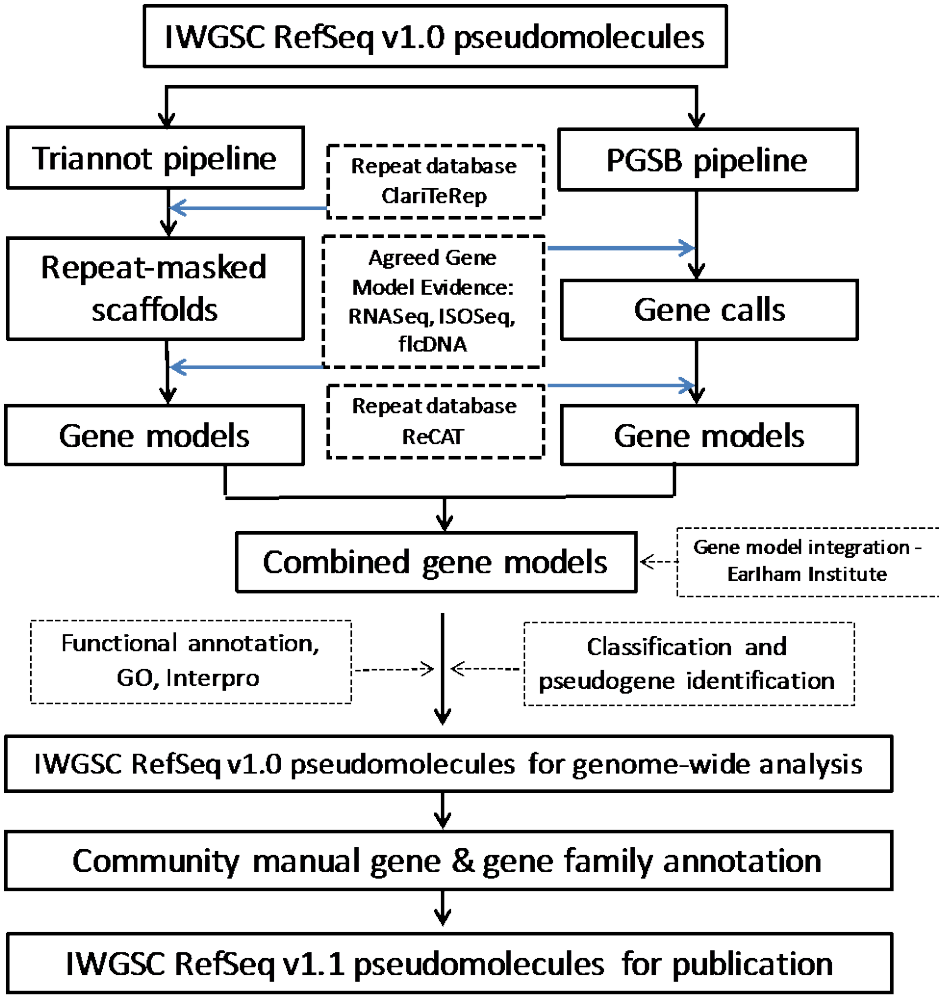

Fig. S8

IWGSC RefSeq v1.0 Genome annotation pipeline.

A

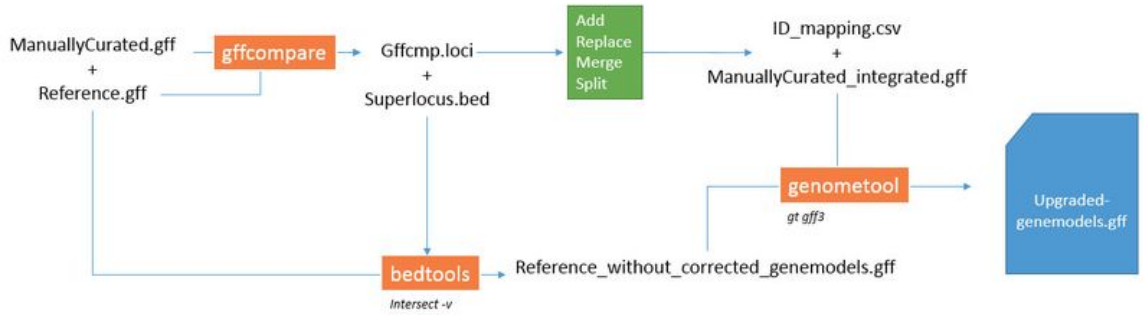

B

Fig. S9

Semi-automated pipeline for integration of manually curated gene models. (A) Pipeline implementation and gene model modifications resulting from integration of 5 types of manual curation: (1) Add: new gene not annotated in automated annotation is annotated and a new gene-ID generated that reflects the position of the gene relative to the 2 surrounding genes (based on 9 bin intervals between the 2 genes.). (2) Replacement: the manually-curated gene corresponds to an already annotated gene. The gene ID is updated to correspond to the TraesCSCCVVGNNNNNN template, incorporating a change in confidence class, if necessary. (3): Split: manual curation indicates an existing gene model should be split. The new gene structure is annotated and the gene IDs modified accordingly. (4) Merge: the manual curation indicates existing gene models should be merged. The new gene structure is annotated and the gene IDs modified accordingly. (5) Multilocus: a special case where multiple reference and manual genes overlap is treated as an extension of the Merge/Split case. The new gene structures are annotated and the gene IDs updated accordingly. (B) Consequences of manual curation for gene models.

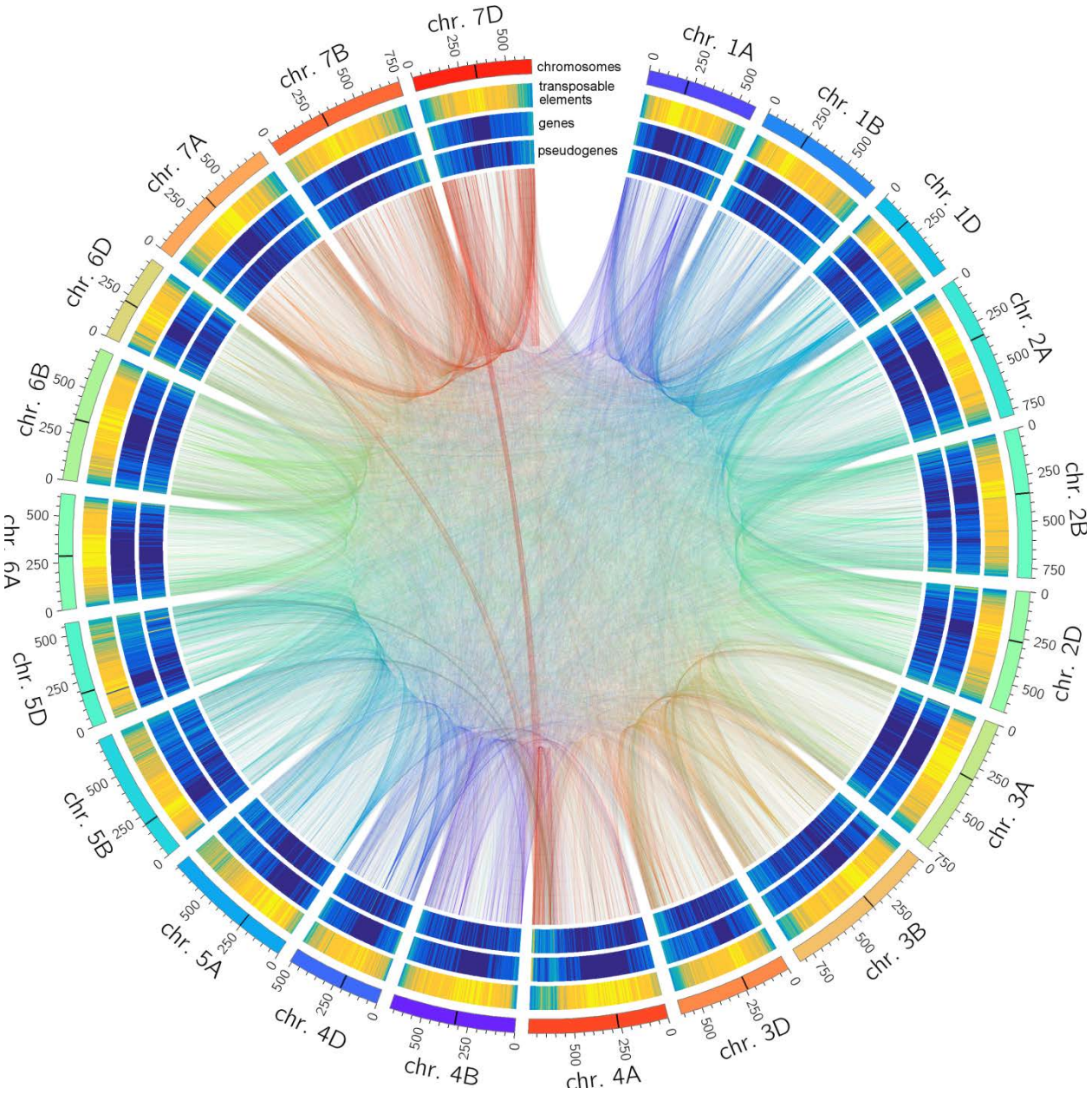

Fig. S10

Distribution of high-coverage pseudogenes (288,839; representing at least 80% of the CDS of a parent gene locus, see 4.5.2) in the IWGSC RefSeq v1.0 assembly. The four concentric circles visualize, from outside to inside, the 21 wheat chromosomes at physical scale, a heat map for the distribution of transposable elements, followed by the distribution of HC genes, and in the innermost circle the distribution of high-coverage pseudogenes. Lines in the center connect pseudogenes with their parent genes and are shown in the color of the chromosome harboring the parent gene.

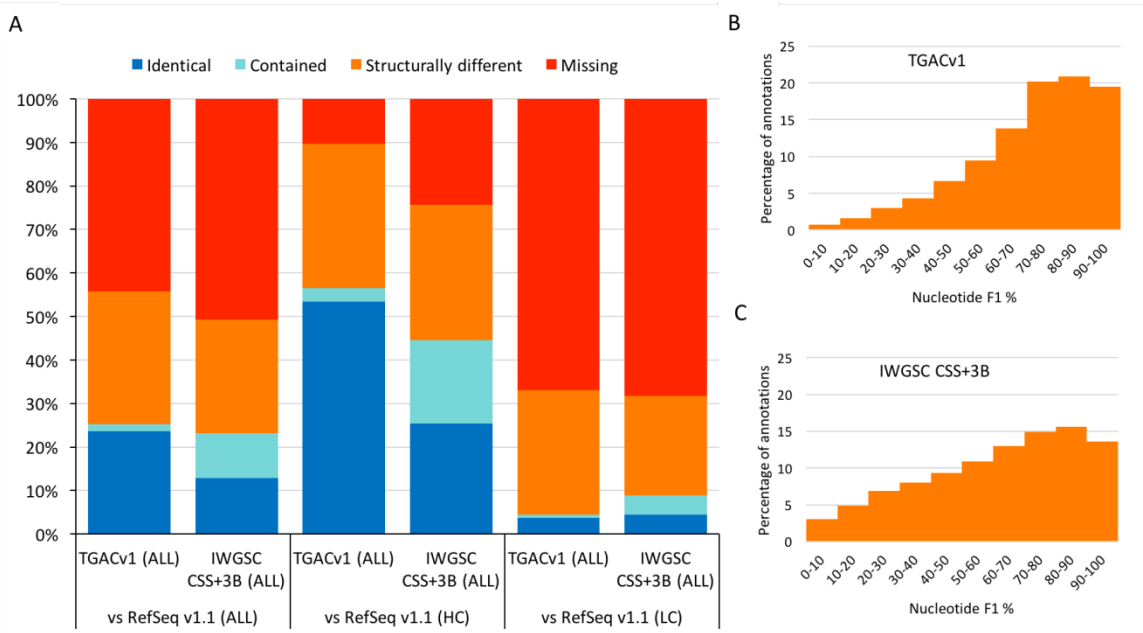

Fig. S11

Comparison of RefSeq annotation v1.1 to earlier wheat gene sets. (A) Identical indicates shared exon–intron structure; contained, exactly contained within the alternative gene; structurally different, alternative exon–intron structure; and missing, no overlap with the alternative gene. High confidence (HC), low confidence (LC) and the full set of RefSeq (ALL) gene models were compared to TGACv1 and earlier IWGSC gene sets aligned to the IWGSC v1.0 assembly. (B, C) Extent of nucleotide overlap (nF1) between RefSeq v1.1 and TGACv1 (B) or IWGSC CSS+3B (C) genes classified as structurally different.

Fig. S12

Analysis of gene model flanking region length in different wheat genome assemblies. The completeness of flanking regions length was analysed in IWGSC RefSeq v1.0 compared to previous wheat assemblies TGACv1 (*8*) and IWGSC 2014 (*6*). Plotted are percentages of full-length "N"-free flanking regions (A: 5'-upstream and 3'-downstream combined; B: 5'-upstream and 3'-downstream separated) with increasing length. 93% of the predicted HC/LC gene models in RefSeq v1.0 contain a "N"-free flanking region of 1000 nt, compared to 88% in the TGACv1 assembly and 56% in the IWGSC CSS models. With increased flanking length of up to 10kb, 61% of RefSeq v1.0 gene models still retain a contiguous nucleotide sequence upstream and downstream of predicted gene models, whereas this number decreases to 37% in TGACv1 and to 5% in IWGSC CSS models.

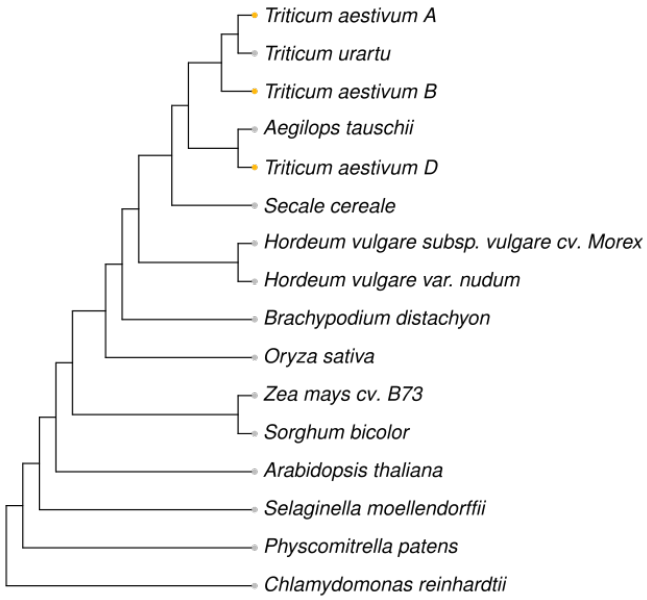

Fig. S13

Cladogram of the taxa used for phylogenomics.

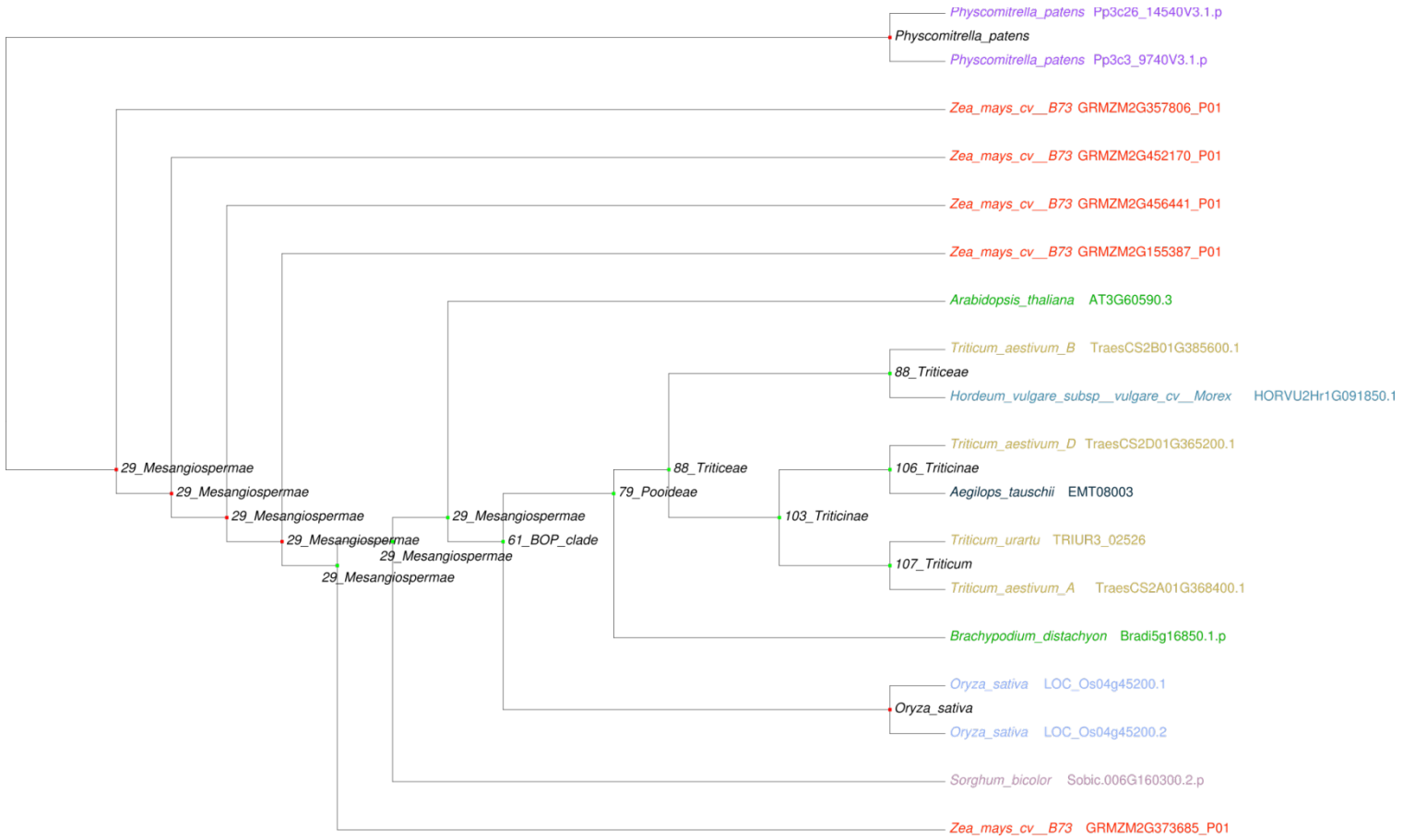

Fig. S14

Phylogenomic gene tree analysis of a yet uncharacterized plastid-localized cytochrome P450 subfamily. The family can be traced to the last common ancestor of land plants, showing the rooted, reconciled gene tree used for the inference of homolog relationships in the phylogenomics workflow. Where applicable, the originating data source for the selection of a representative isoform was used for phylogenetic inference. In this case the Phytozome database considered two splice variants in rice as two separate loci. Node colors encode the type of reconciled evolutionary event: green=speciation = orthologous relationships; red=duplication = inparalogous and outparalogous relationships. Inparalogs were called if descendant tips of a duplication node belong to the same taxon; Outparalogs derive from a node whose descendant tips harbor multiple taxa.

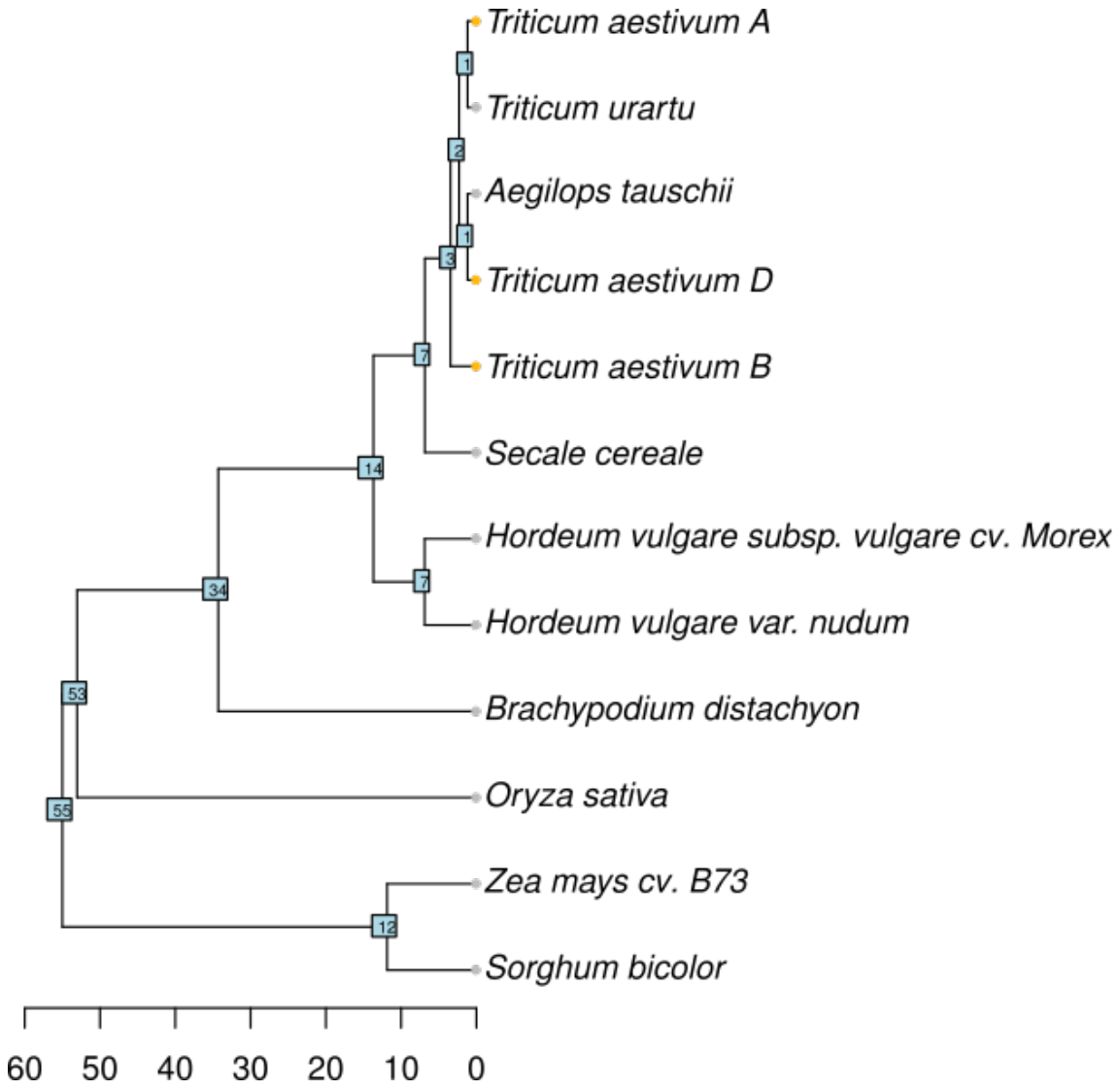

Fig. S15

Chronogram of the investigated Poaceae taxa. Divergence times were estimated using the penalized likelihood approach (*154*) and fixed calibration points inferred from a more comprehensive study on molecular dating of grasses (*155*)

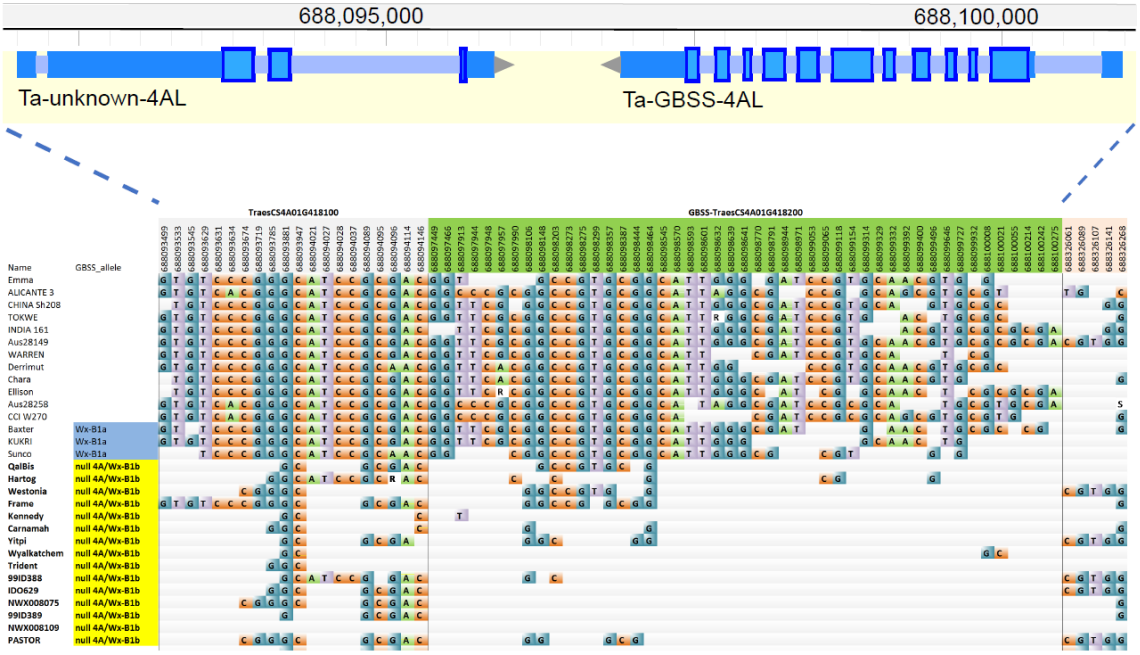

Fig. S16

Granule Bound Starch Synthase (GBSS; TraesCS4A01G418200) on chromosome 4A. The association of a null allele for GBSS-4AL (Wx-B1b, TraesCS4A01G418200) with udon noodle quality is well established (Zhao et al 1998). This gene model groups as an outparalog to a clade that is localized on chr 7 in *Triticeae*. The available data suggest the GBSS on chromosome 4A is a highly divergent translocated homeolog originally located in 7B. This gene shows an additional complexity in 3.9% (25) of a set of 644 (hexaploid) wheat varieties and landraces assessed using SNPs identified from snapshot exome sequence data (Jordan et al, 2015; a subset of 40 illustrated for wheat lines and accessions available from the Australian Germplasm Collection) where significant sections of TraesCS4A01G418200 within the green highlight target region to be deleted. Based on the distribution of missing SNP sequences, the lines highlighted in yellow that were independently confirmed GBSS-4AL/Wx-B1b null alleles, all carried deletions missing SNP sequences at positions 688098545-688099053 (6 exons at 3' end of gene) in chromosome 4A of the IWGSC RefSeq v1.0. A subset of deletions encompassed a larger region, 688098545-688099932 within 4A, but did not extend outside the gene model for TraesCS4A01G418200 and thus would not be expected to show any detrimental effects due deletion of the adjoining gene models (TraesCS4A01G418100, light grey highlight, and TraesCS4A01G418300, light orange highlight) and is consistent with varieties carrying the different forms of the deletion performing successfully at the agronomic level to satisfy the high value commercial udon noodle market. Lines that carried the Wx-B1a deletion did not show any missing SNP sequences in the GBSS-4L gene (TraesCS4A01G418200).

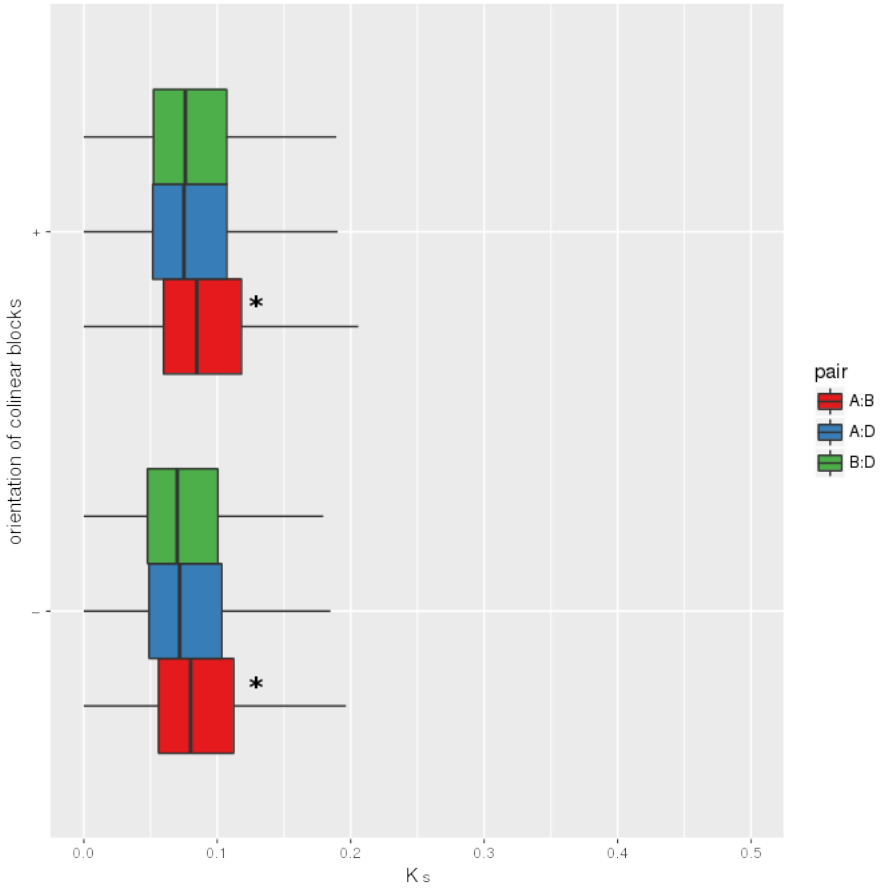

Fig. S17

Synonymous substitution rates (K_s) in homeologous gene pairs located in colinear blocks in the three wheat sub-genomes. The analysis of mutation rates within the protein-coding regions of homeologous gene pairs, reveals that the synonymous substitution rate is highest among homeologous A:B gene pairs (indicated by asterisks, significance: 99% confidence in Kruskal-Wallis rank sum test) as compared to A:D and B:D. This is consistent with the proposed sequence of polyploidization events in bread wheat, starting with hybridization of the A and B genome progenitors.

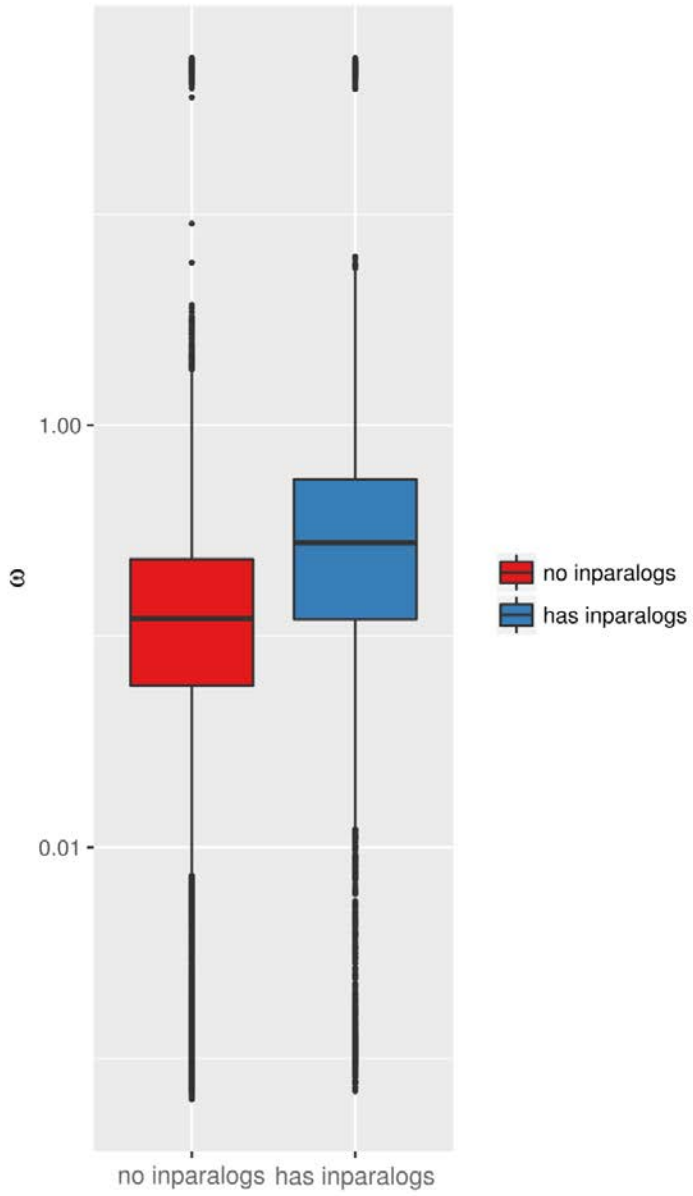

Fig. S18

Rate of non-synonymous to synonymous substitutions (K_a/K_s or ω) in homeologous gene pairs. Homeologs with sub-genome inparalogs (blue; gene duplications after hexaploidization) show higher levels of variation in ω along the chromosome and bear evidence of peaks of positive selection in contrast to homeologs without sub-genome inparalogs (red), which appear to be less variable and under purifying selection. Boxes represent lower (25%) and upper (75%) quartiles. The central line represents the median (50%) value. Outliers are plotted as individual dots.

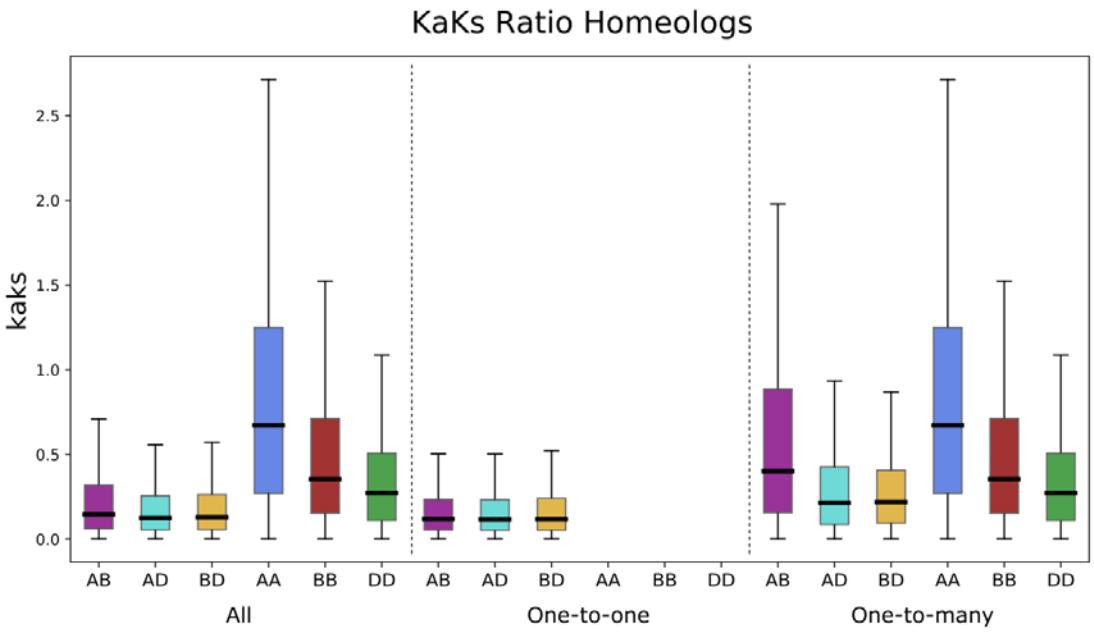

Fig. S19

Ka/Ks ratios of different homeolog categories and their subdivisions. Ka/Ks ratios are shown on the y-axis, median and spread (1st and 3rd quartile) for the three categories, ‘all’, ‘one-to-one’ and ‘one-to-many’ are illustrated as boxplots. Categories are further divided into pairwise sub-genome comparisons, AB, AD and BD, and intra-sub-genome comparisons if applicable. Boxes represent lower (25%) and upper (75%) quartiles. The central line within each colored box represents the median (50%) value. Lines represent the upper and lower whisker.

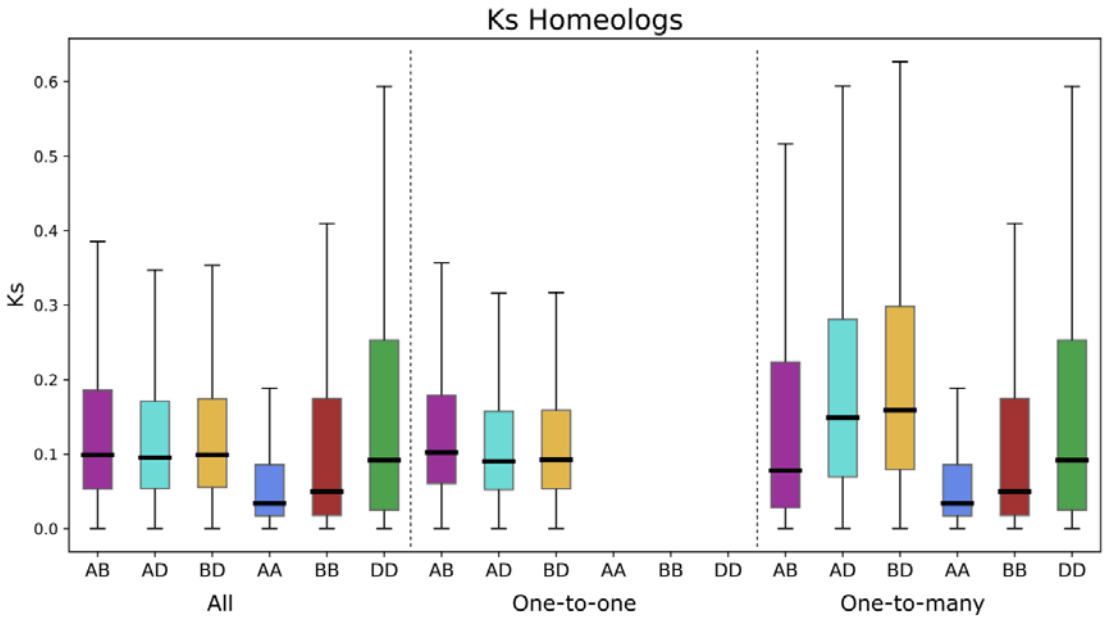

Fig. S20

Ks divergence in homeologous genes. Homeologous gene pairs with duplications in at least one of the sub-genomes (A:B, A:D, B:D) and the corresponding sub-genome inparalog pairs (A:A, B:B, D:D) bear evidence of elevated evolutionary rates. They showed higher ratios of non-synonymous to synonymous nucleotide substitutions (Ka/Ks or ω) than homeologous gene pairs from strict 1:1:1 or 1:1 groups. This phenomenon is particularly pronounced among sub-genome inparalogs, especially those found in the A or the B sub-genomes. The latter also have higher copy number than those in the D genome. Ks ratios are shown on the y-axis. Median and spread (1st and 3rd quartile) for the three categories, 'all', 'one-to-one' and 'one-to-many' are illustrated as boxplots. Categories are further divided into pairwise sub-genome comparisons, AB, AD and BD, and intra-sub-genome comparisons if applicable. Boxes represent lower (25%) and upper (75%) quartiles. The central line represents the median (50%) value. Lines represent the upper and lower whisker.

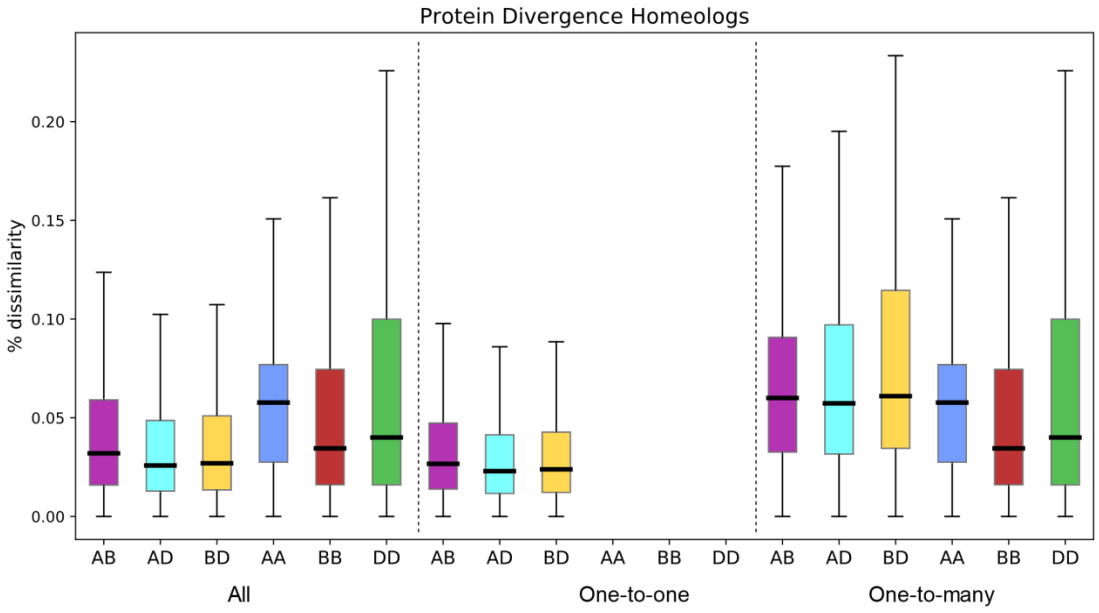

Fig. S21

Protein divergence in homeologous genes. Protein divergence in homeologous gene clusters is shown on the y-axis as percentage dissimilarity. Median values and spread (1st and 3rd quartile) for the three categories, 'all', 'one-to-one' and 'one-to-many' are illustrated as boxplots. Categories are further divided into pairwise sub-genome comparisons, AB, AD and BD, and intra-sub-genome comparisons if applicable. Median protein sequence identity was highest for the one-to-one homeologs: 96.05% (SE±2.23%), 96.38% (SE±2.21%) and 96.56% (SE±2.12%) for AB, BD and AD subdivisions, respectively. Lower protein sequence identities (90.9%- 92%) were generally observed in the one/many-to-many categories for 'AB', 'AD' and 'BD'. However, intra-sub-genomic homeologs of the one-to-many categories, i.e. tandem genes in 'AA', 'BB' and 'DD', showed higher similarities in all three subdivisions [92.2% ('DD'; SE±3.1%) to 93.8% ('BB'; SE±2.8%)]. Sequence identities at CDS levels exhibited a very similar trend (Fig. S22).

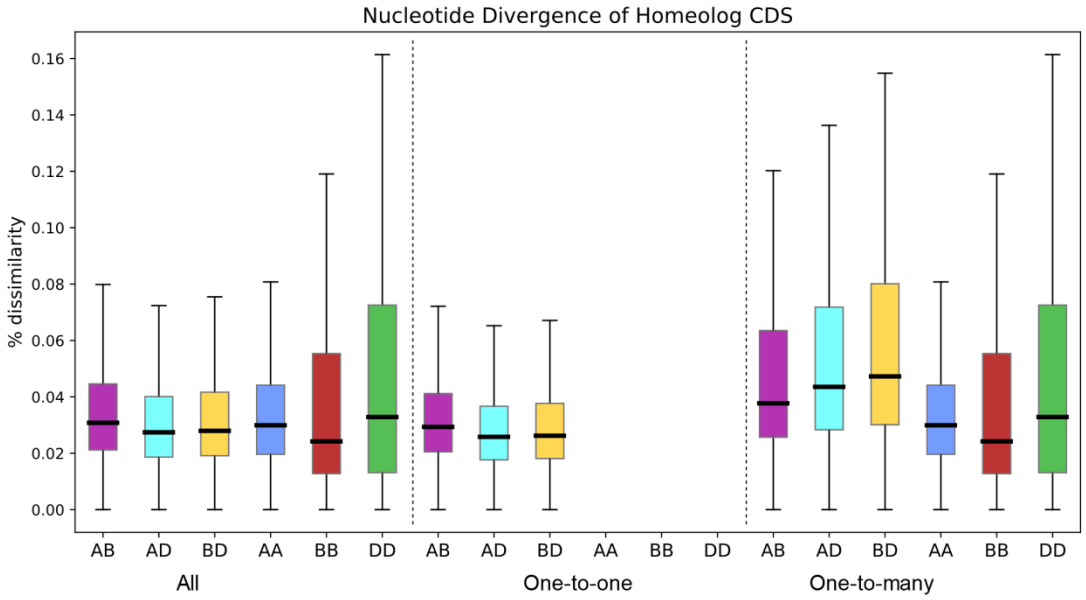

Fig. S22

CDS divergence of homeologous genes. CDS divergence is shown as percentage dissimilarity on the y-axis. Median values and spread (1st and 3rd quartile) for the three categories, 'all', 'one-to-one' and 'one-to-many' illustrated as boxplots. Categories are further divided into pairwise sub-genome comparisons, AB, AD and BD, and intra-sub-genome comparisons if applicable. One-to-one homeolog identities showed only small variation (96.3% ('AB'; SE±1.9%) - 96.8% ('AD'; SE±1.8%)), and were significantly higher than inter-sub-genomic one-to-many relations (92.8% (SE±2.8%)(BD), 93.3% (SE±2.7%)(AD) and 94.1% (SE±2.6%)(AB). Tandemly repeated homeologs were significantly more similar compared to the inter-sub-genomic gene pairs, with coding sequence identities ranging from 94.1% (SE±2.7%) for 'DD' to 95% (SE±2.7%) for 'AA' to 95.3% (SE±2.5%) for 'BB' subdivisions. In contrast to the protein divergence of the tandemly repeated homeologs in the one-to-many clusters which ranges between the one-to-one and one-to-many inter-sub-genome identities, nucleotide divergence of intra-sub-genome duplicated homeologs were comparable to the one-to-one relationships. These findings are supported by an increased level of non-synonymous substitutions and elevated KaKs ratios for tandem homeologs in comparison to the median ratios of homeologs between two sub-genomes in 1:N groups (Fig. S19). On the other hand, these latter subdivisions as well as 1:1 homeologs show higher Ks values compared to intra-sub-genomic homeologs of the one-to-many relations, indicating overall accelerated evolutionary rates and origins of tandem duplications occurring during the evolution of the hexaploid genome of bread wheat (Fig. S20).

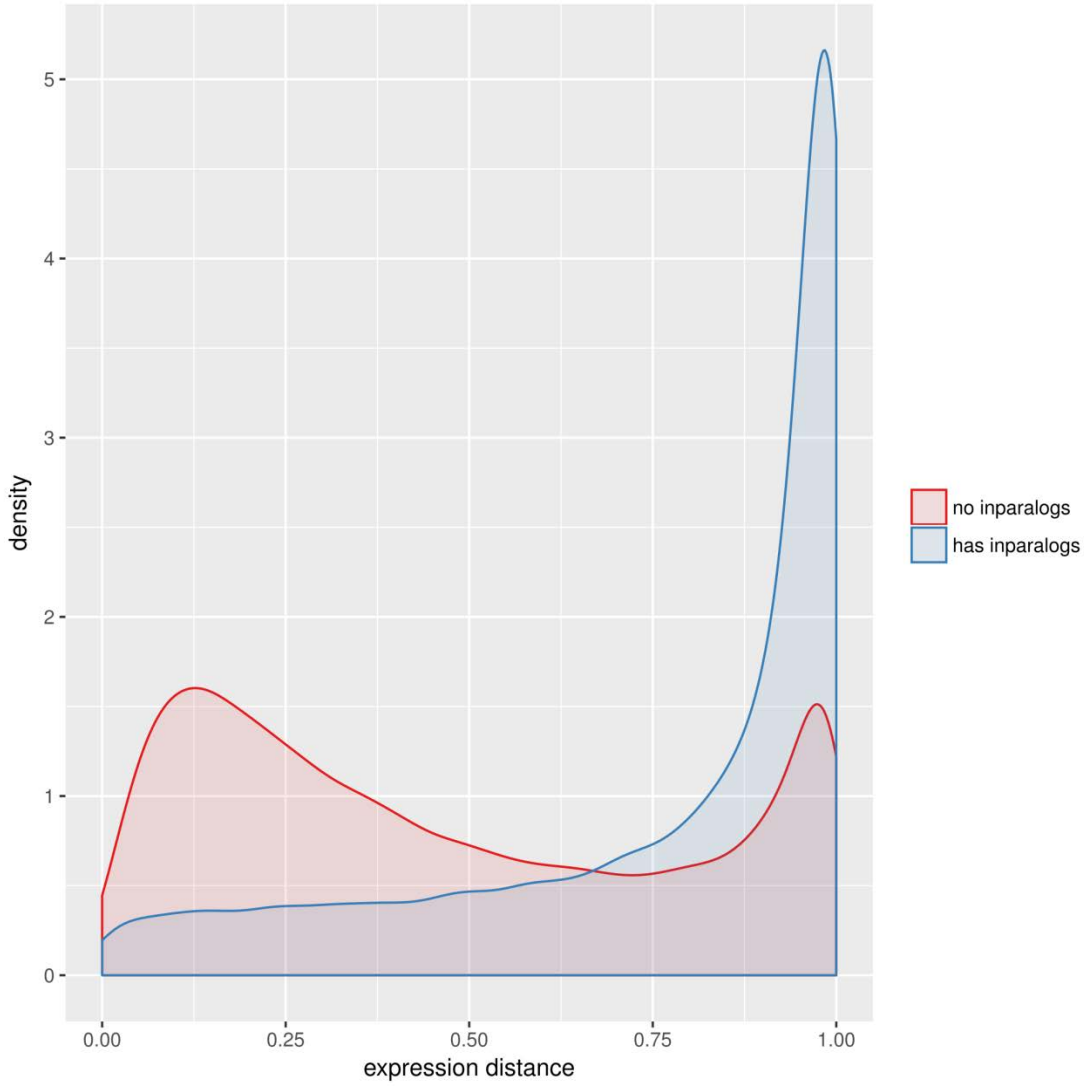

Fig. S23

Expression divergence of homeologous gene pairs with (blue) and without (red) sub-genome inparalogs (duplicates that arose after hexaploidization). Homeologous gene pairs with inparalogs exhibit a higher expression divergence. Shown is a density plot of the distribution of the expression divergence (x-axis) among homoeologs. Expression divergence is expressed as the inverse of the bi-weight mid-correlations (bicor) between the expression vectors across all samples among a pair of homeologous genes (1-bicor). Together with the patterns obtained for the mutation rates, these observations are consistent with gene duplication acting as an important motor of functional innovation enabling diversification of sub-genome inparalogs and resulting in sub- and neo-functionalization in addition to the dosage-effect provided by allohexaploidy.

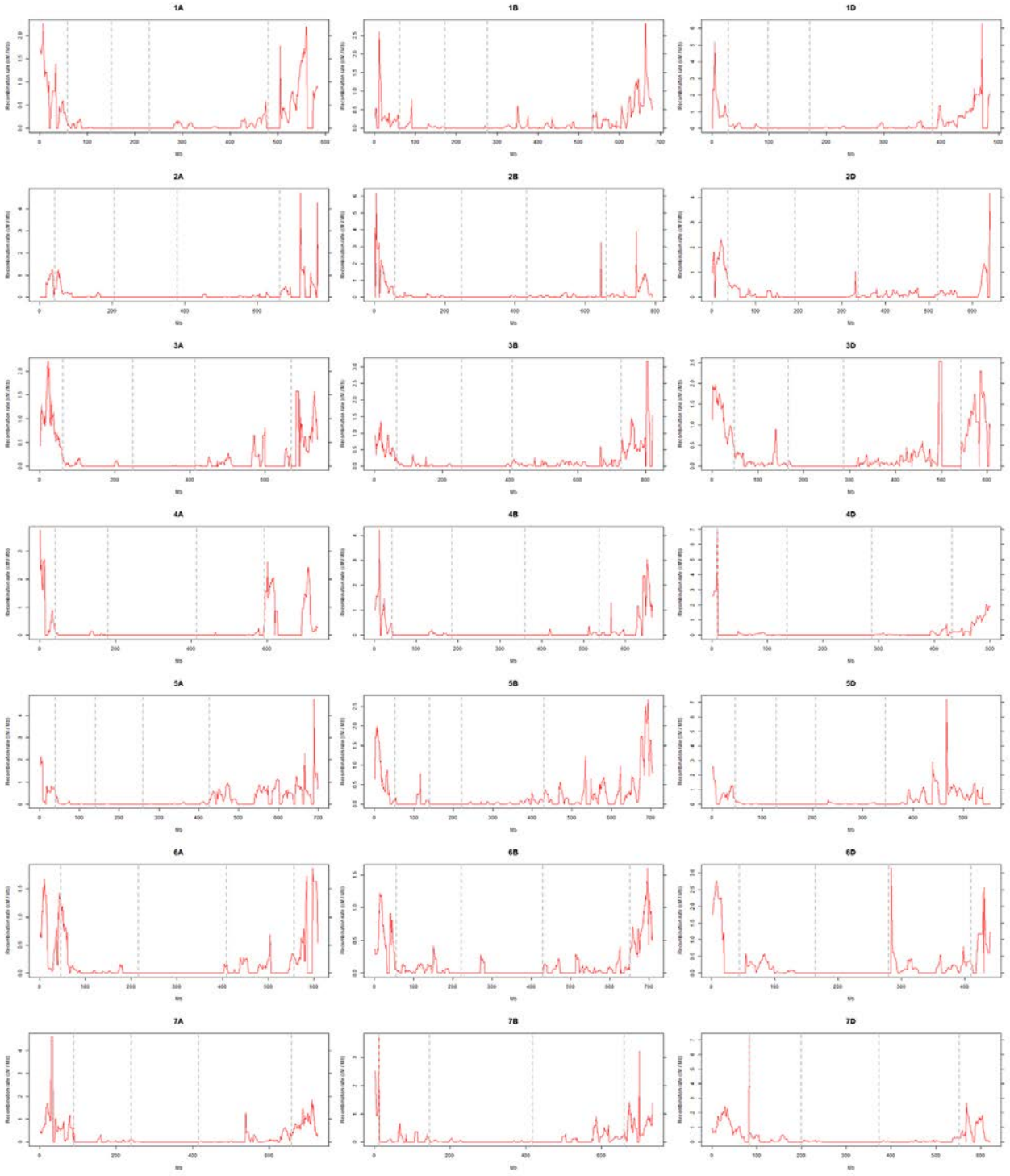

Fig. S24

Analysis of recombination rate distribution along wheat chromosomes. The CS x Renan (CsRe) map contained 146,602 SNPs genetically mapped in 21 linkage groups corresponding to the 21 chromosomes of bread wheat, with no unlinked markers. The D-genome contained the fewest mapped markers (18%), while the A- and B-genomes were similarly covered with 40 and 41% of mapped markers, respectively. Chromosome 3B has the most markers (10,638) and chromosome

4D (2,624) the least. The genetic map covers 3,592 cM with 25,385 unique genetic positions. The D-chromosomes had the longest genetic maps, with an average of 204 cM and a cumulative length of 1,427 cM, followed by the A-chromosomes (mean length = 164 cM; cumulative length = 1,146 cM) and the B-chromosomes (mean = 145 cM; cumulative = 1,018 cM). Average recombination rates (in red) were calculated in 10-Mb sliding windows (step 1 Mb) and estimated to be 0.26 cM/Mb for the whole genome (range 0.16 cM/Mb for chromosome 6B to 0.41 for chromosome 5D). The D-genome exhibited the highest recombination rate (0.36 cM/Mb) which reflects the low polymorphism level of this genome while A- and B-genomes had lower rates. Local rates varied between 0 and ~7 cM/Mb. Highest rates were observed for D chromosomes (1D, 4D, 5D, 7D) confirming that the D genome recombines more than the other two homeologous genomes. Cross-overs were found to occur mainly in the distal regions whereas most of the chromosomal proximal regions were recombination-poor. The X-axis represents the position on chromosomes (in Mb), the Y-axis the recombination rate (in cM / Mb).

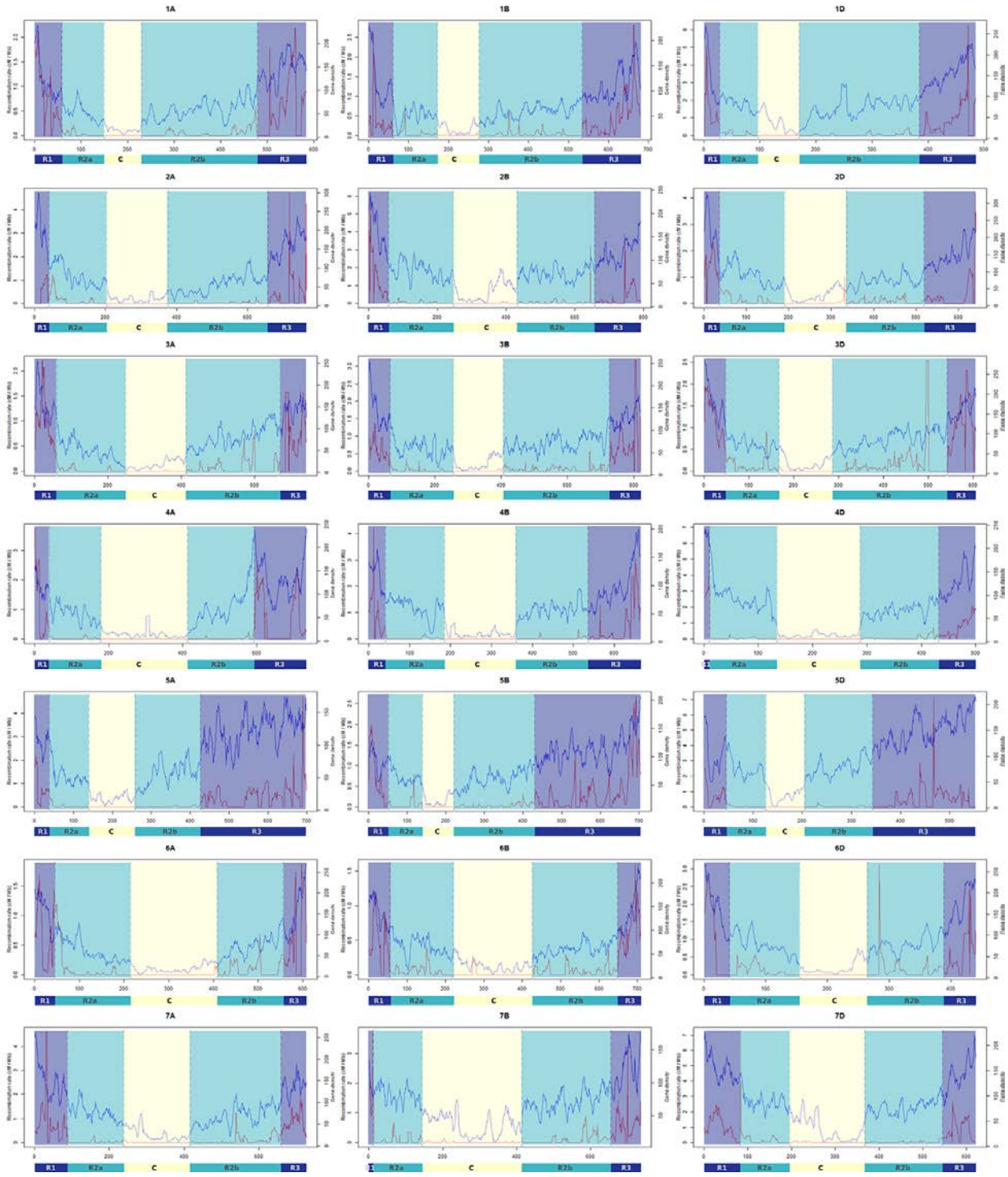

Fig. S25

Structural and functional partitioning of wheat chromosomes. The distribution of recombination rate (cM/Mb)(red line), gene density (genes/Mb)(blue line), together with TE density (%TE/Mb), expression breadth (number of conditions in which a gene is expressed) and proportions of genes associated with histone marks (% genes / Mb)(not shown) were determined using the R package changepointv2.2.2 with Binary Segmentation method and BIC penalty on the mean change in

these features. Sliding window size: 10 Mb, step: 1 Mb. The five main regions of wheat chromosomes are represented: R1 and R3 (dark blue), R2a and R2b (dark cyan); C (yellow).

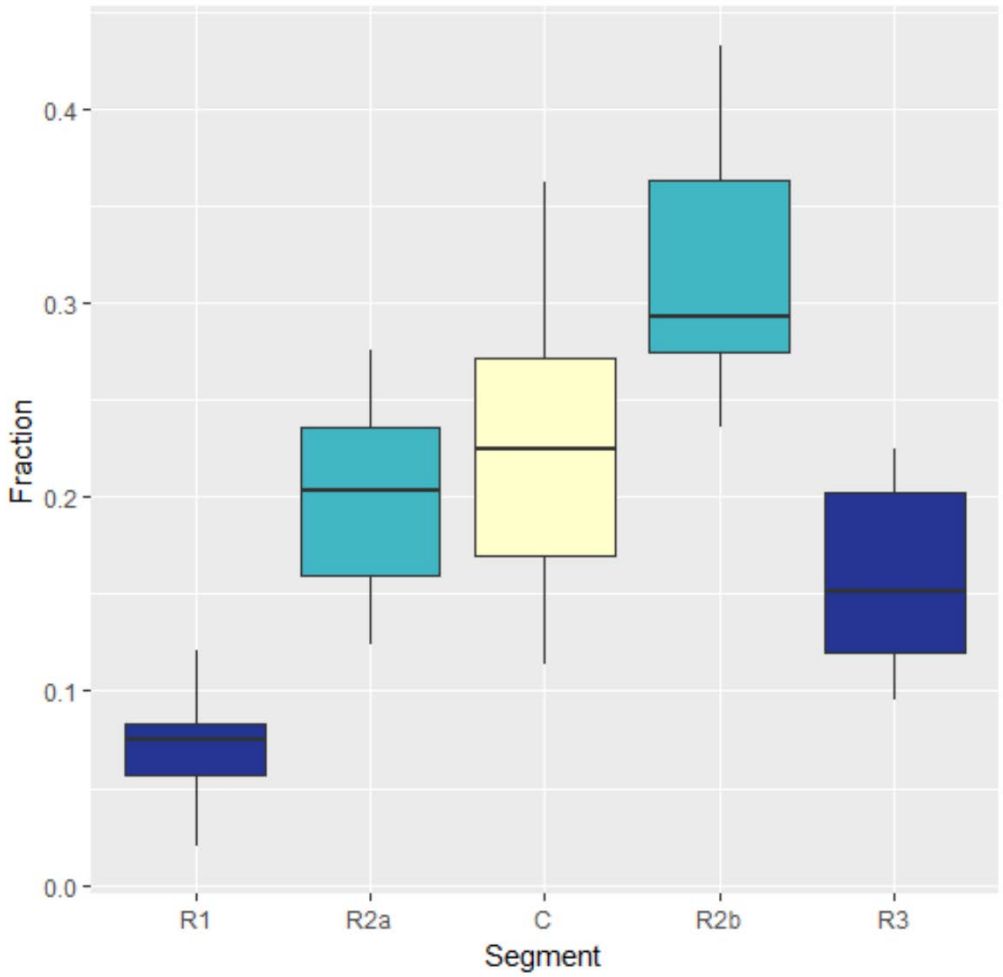

Fig. S26

Conservation of the genomic fractions covered by chromosomal segments R1 and R3 (dark blue), R2a and R2b (dark cyan) and C (yellow) across the genome.

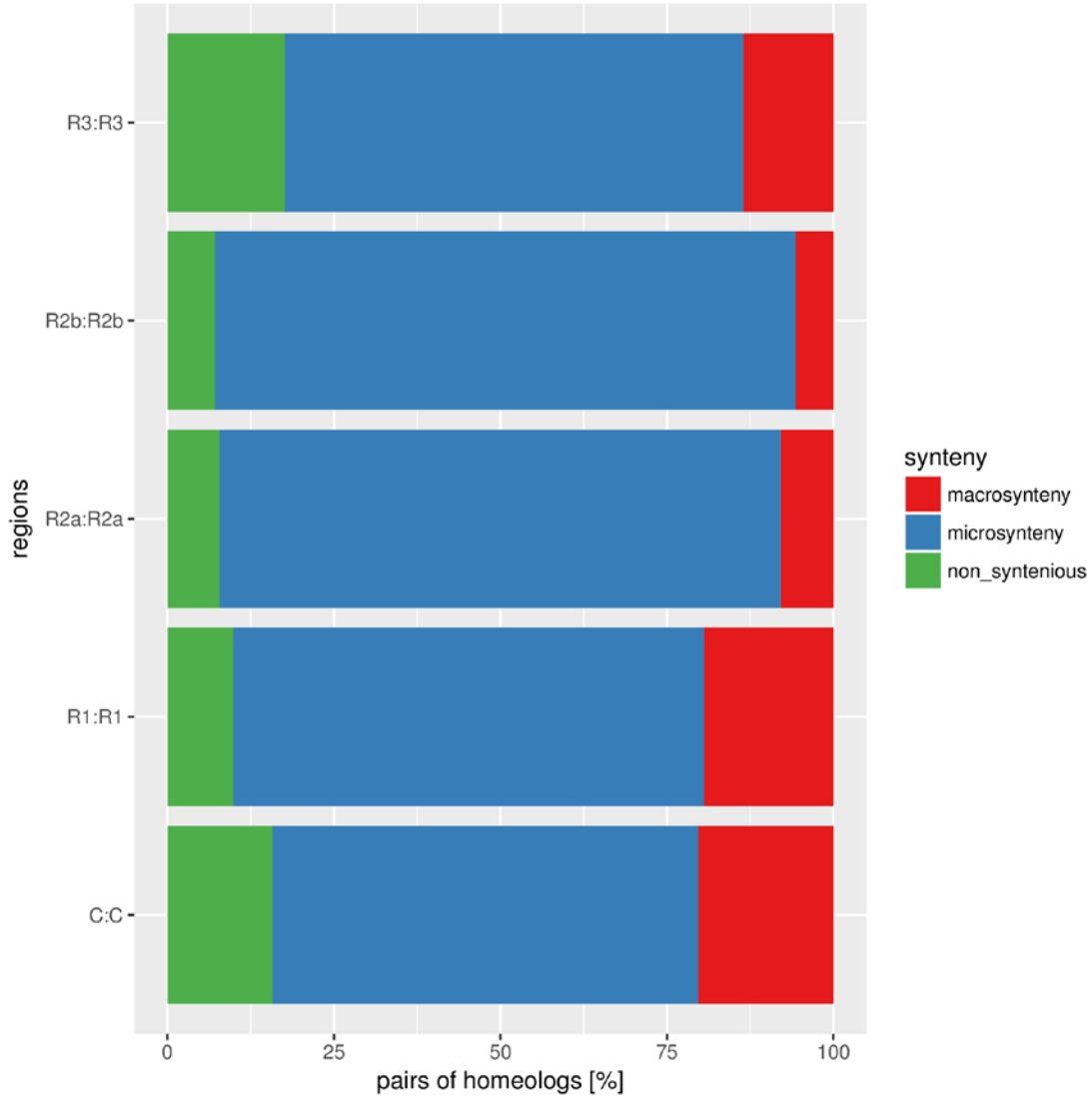

Fig. S27

Distribution of homeologous wheat genes in respect to chromosomal compartments. The evolution of homeologs in relation to their location in chromosomal compartments was assessed by comparing the percentage of genomic distribution of macrosyntenic (red), microsyntenic (blue) or non-syntenic (green) homeologous gene pairs in the distal R1 and R3 regions, the interstitial R2a and R2b regions and the proximal C region. Homeologous pairs located in the interstitial regions (R2a and R2b) showed higher levels of synteny compared to the distal (R1 and R3) and proximal regions (C). The comparison was limited to gene pairs located in the same compartment.

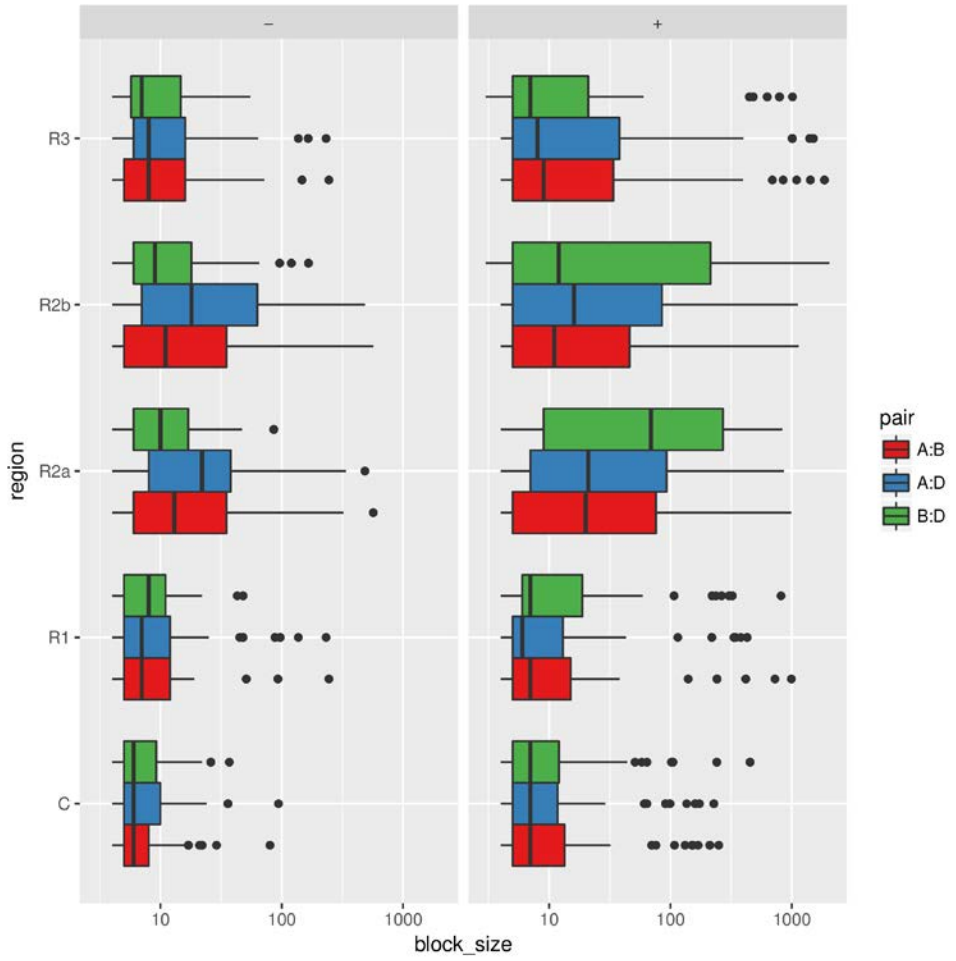

Fig. S28

Comparison of syntenic block sizes (number of syntenic genes) in same (+) or in inverse orientation (-) among the three wheat sub-genomes, separated for the chromosomal compartments (C, R1-R3). Box-whisker plots show the homoeolog block sizes. Boxes represent lower (25%) and upper (75%) quartiles. The central line represents the median (50%) value. Outliers are plotted as individual dots, lines represent the upper and lower whisker. R2a and R2b compartments harbor larger syntenic blocks, with more microsyntenic genes, than the highly recombinant, distal R1 and R3 regions, although the latter are more gene dense. The R1 and R3 regions show similar ratios of homeologs in macrosyntenic or non-syntenic context as compartment C. Interestingly, distal and proximal regions of the chromosome harbor quite antagonistic features (distal: high recombination rate, gene and DNA transposon density and low LTR retrotransposon content; proximal: low gene density, low recombination and high LTR retrotransposon content). Although the distinct diversifying forces acting on both compartments might be acting on different timescales, surprisingly similar consequences for genome reorganization are observed. Further investigation of the size of syntenic blocks reveals an asymmetry of blocks sizes among the different sub-genome pairs particularly in the interstitial zones (R2a, R2b), with the sizes of syntenic blocks between B:D in R2a being significantly larger than A:D and A:B.

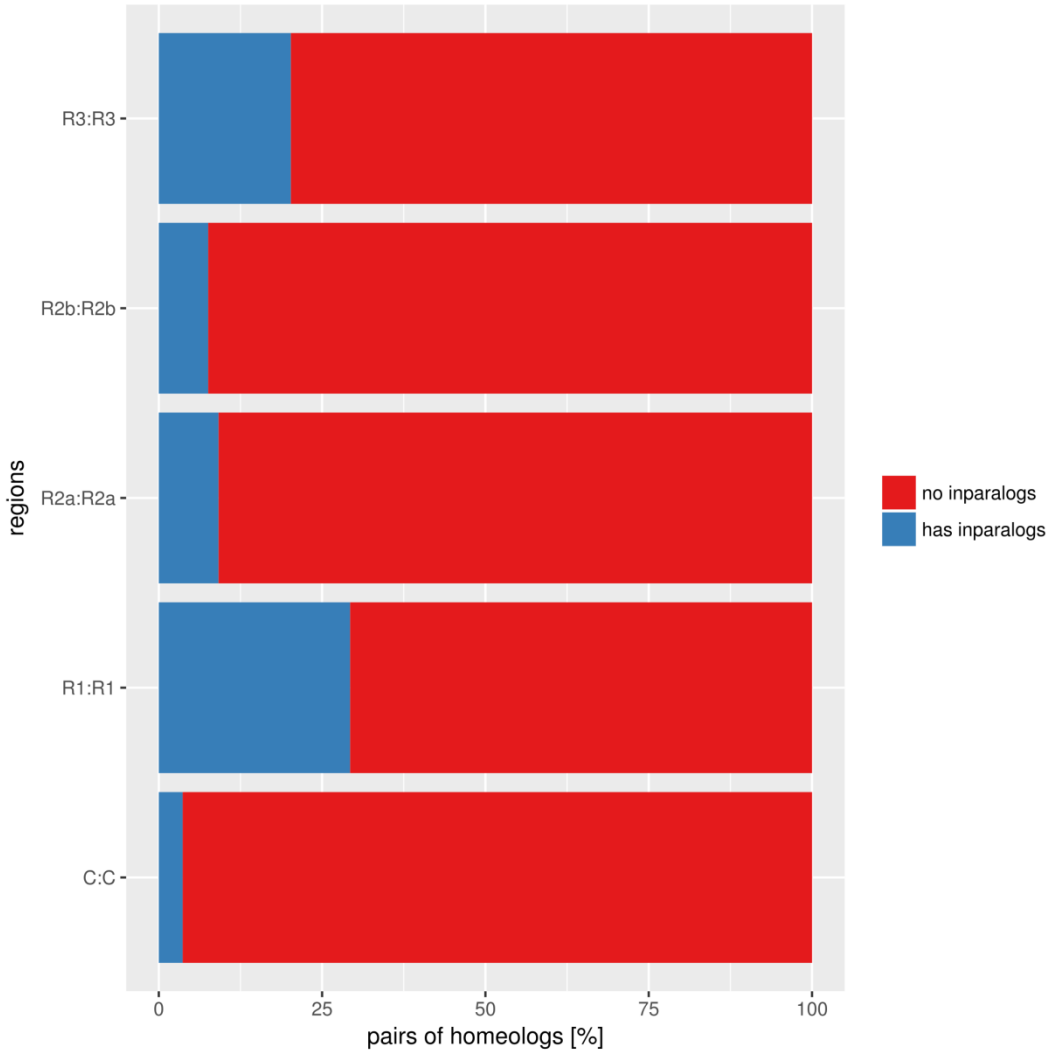

Fig. S29

Percentages of homeologous gene pairs with and without sub-genome inparalogs distributed to the different genomic compartments. Duplication of homeologs seems to occur at different rates in the different chromosomal compartments. Sub-genome inparalogs are much more frequent in the highly recombinant distal chromosomal regions R1 and R3.

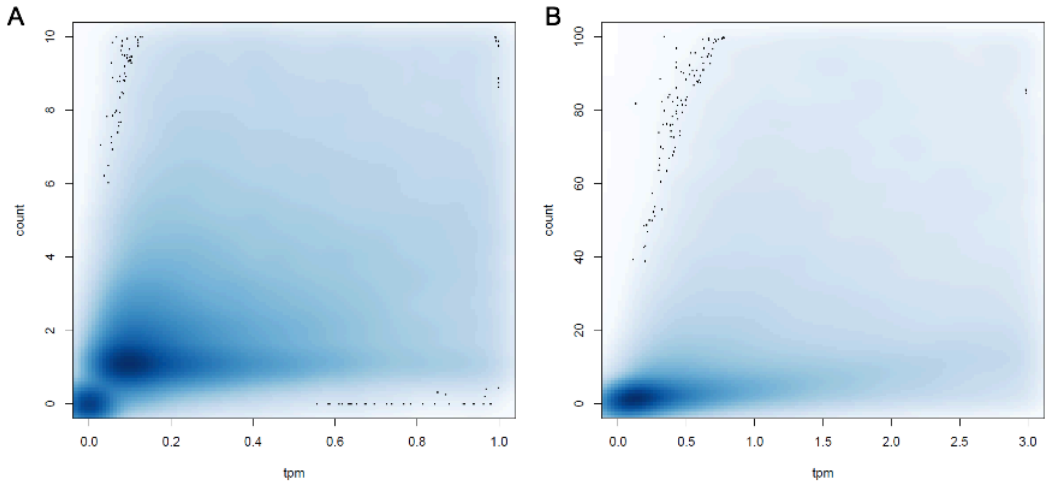

Fig. S30

Average expression abundance in transcript per million (tpm) and counts for the top 1% of samples from HC genes. (A) tpm values ranging from 0 to 1.0 are shown to illustrate clustering of non-expressed genes at the origin and the immediate vicinity. (B) tpm values ranging from 0 to 3.0 to show the wider context of very low expressed genes below the 0.5 tpm threshold used as the criterion for a gene to be considered expressed. Gene expression values are represented by the blue density plot, outliers (100 lowest density points) are indicated as black dots.

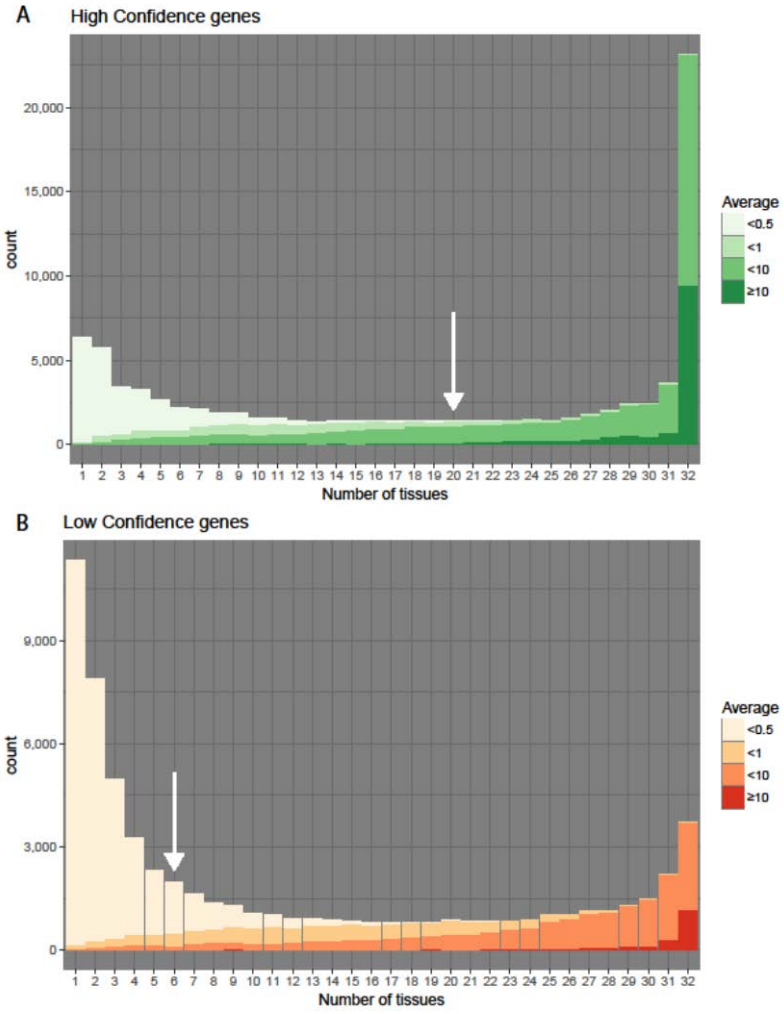

Fig. S31

Gene expression levels and number of intermediate tissues in which HC (A) and LC (B) genes are expressed. Arrows indicate the median number of tissues in which HC and LC genes are expressed.

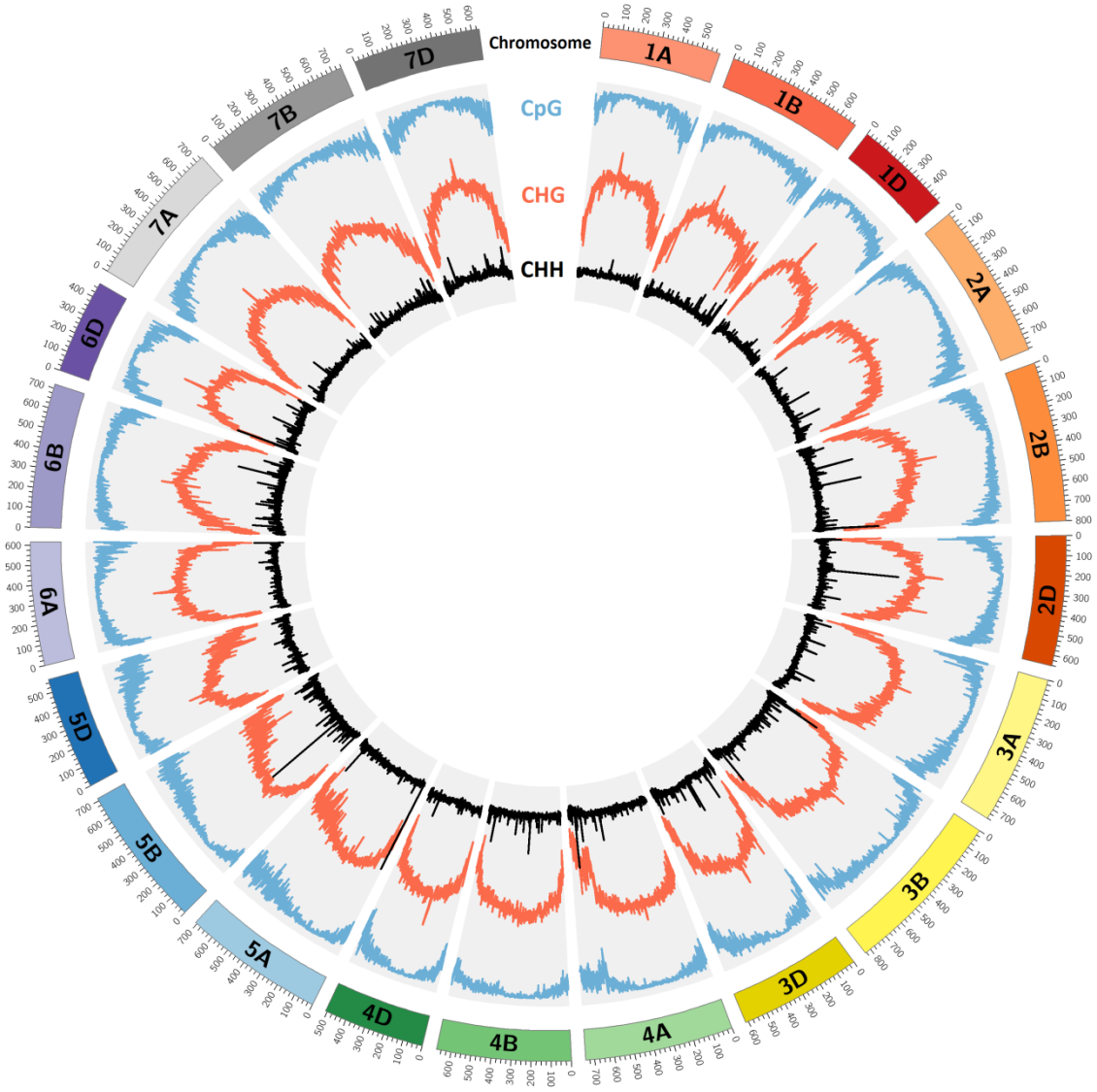

Fig. S32

DNA methylation distributions along wheat chromosomes. Wheat DNA methylation frequency of cytosines in the sequence contexts of CpG (average 92.7%, blue), CHG (average 51.3%, red) and CHH (average 2.7%, black) as revealed by whole genome bisulphite Illumina sequencing (WGBS) is shown from outside to inside in concentric circles of a Circos plot (*156*). The outermost circle is visualizing the 21 wheat chromosomes grouped according to homoeology. DNA methylation level frequencies are presented in 1 Mb windows. The observed levels of cytosine methylations are among the highest observed in angiosperms (*157*), likely reflecting the abundance of repetitive elements throughout the wheat genome. Methylation patterns in wheat largely follow those observed in other species, showing enrichment in CpG and CHG sequence contexts at pericentromeric regions (gene poor) and depletion toward the chromosome ends (gene rich).

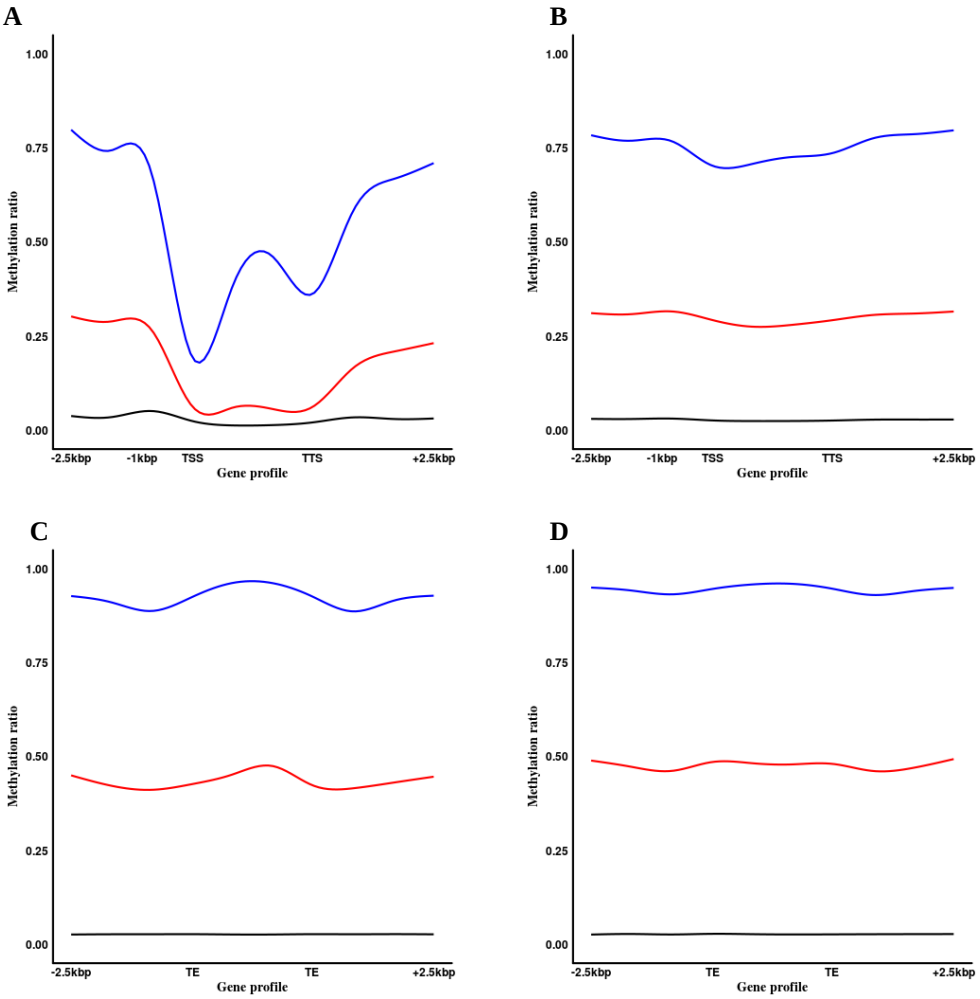

Fig. S33

Averaged DNA methylation profiles of annotated features in the wheat genome. Cytosine methylation in context of CpG (blue), CHG (red) and CHH (black) motifs is shown for A) high confidence (HC) genes (TSS = transcription start site; TTS = transcription termination site), B) low confidence (LC) genes, C) Copia (RLC) repeat elements (TE = transposable element start and stop sites), and D) Gypsy (RLG) repeat elements. High rates of DNA methylation likely serve to prevent transposition by restricting the expression of transposable elements. However, where repetitive elements are proximal to gene sequences, the enriched methylation can perform a regulatory function, predominantly silencing expression. The distinct and highly conserved methylation patterns observed in regions of HC genes and their regulatory regions showed higher levels of DNA methylation associated with the 5' regulatory regions in all contexts that diminished rapidly at the transcriptional start site (TSS). DNA methylation increased in the gene body where the CpG methylation formed a peak, whereas gene body methylation levels remained at extremely low levels at CHG and CHH sites. In the 3' regulatory region after the transcriptional termination site (TTS) methylation rapidly reverted to the levels in 5' sequences. This contrasted with the pattern observed for LC genes, where a near uniform level of methylation was observed in all sequence contexts. As a conclusion, many of the features

included in the LC annotation are either no genes, are truncated or have lost their function through mutation (i.e. pseudogenes).

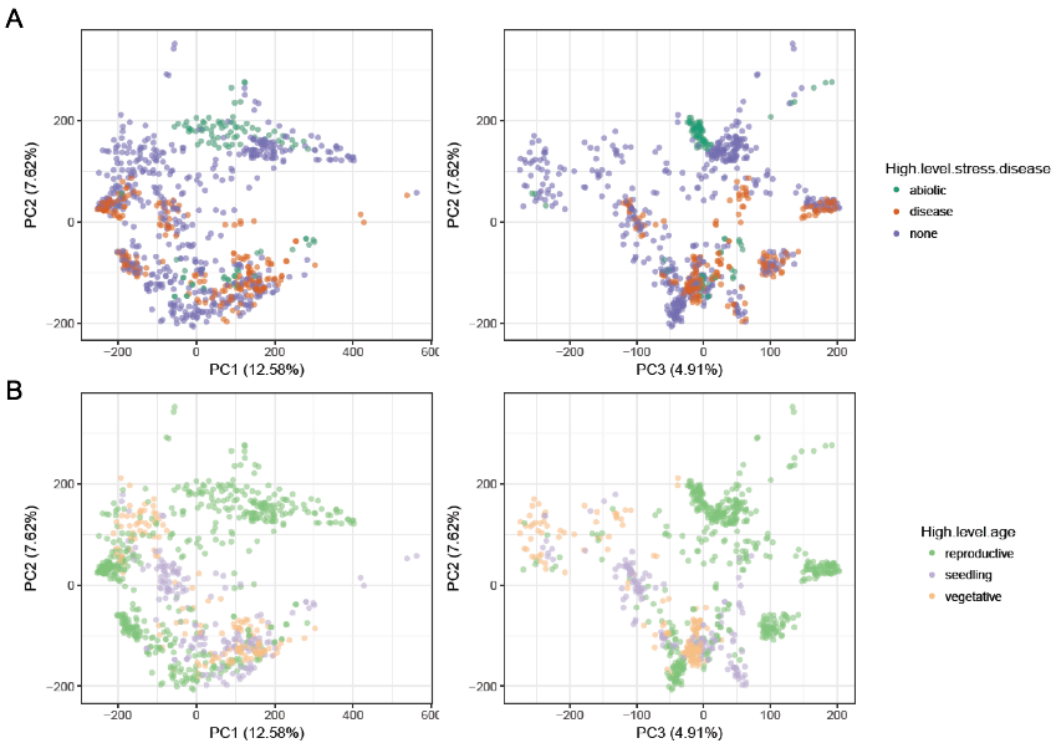

Fig. S34

Principal component analysis plots of the 850 RNA-Seq samples colored according to their high level stress/disease (A) or high level age (B).

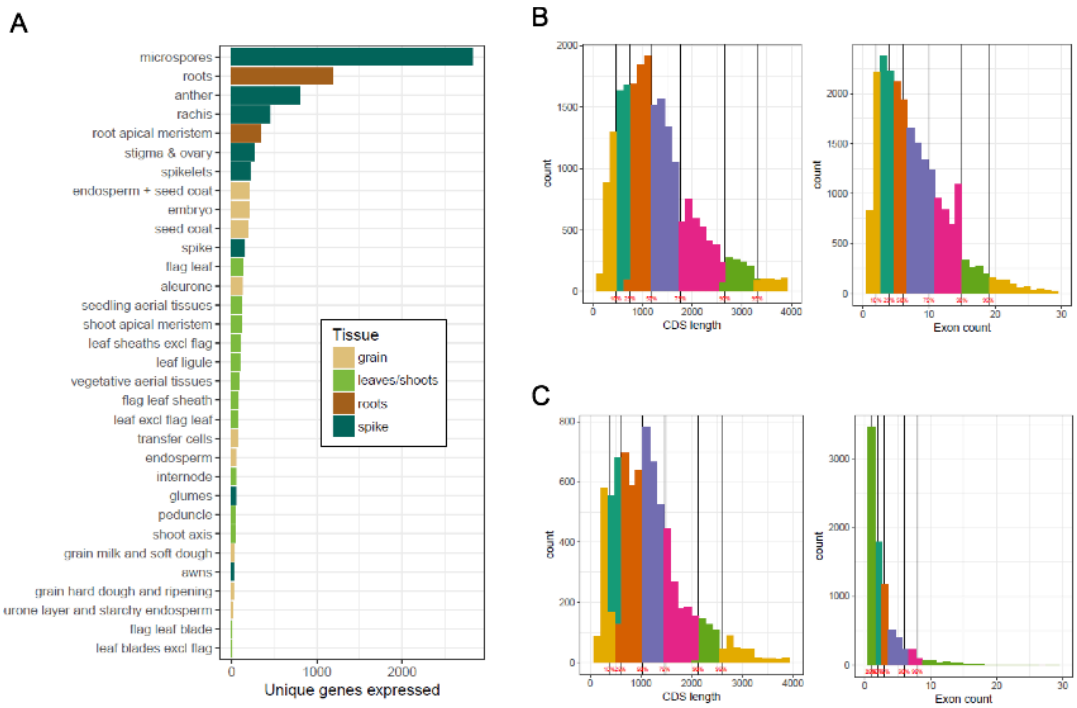

Fig. S35

Tissue specific gene expression in wheat. (A) Genes with tissue-exclusive expression across intermediate tissues. Comparison of coding sequence size and exon number between 23,146 ubiquitous (B) and 8,231 tissue-exclusive (C) genes. Bars are coloured according to quantiles which are defined by red percentages and solid vertical lines across each plot. From left to right quantiles are colored: 0-10% yellow, 10-25% green, 25-50% orange, 50-75% purple, 75-90% pink, 90-95% green, 95-100% yellow.

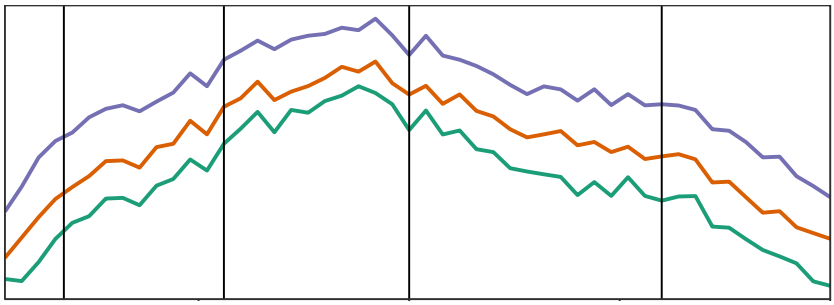

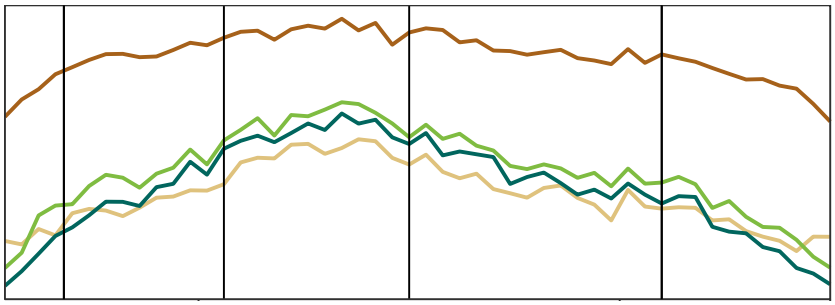

Fig. S36

Average percentage of conditions in which genes are expressed (expression breadth) based on physical position across wheat chromosomes. RNA-Seq samples were classified according to high level tissue (A), stress (B), and age (C) and the average expression across all 21 chromosomes was plotted based on their scale position within the corresponding genomic compartment.

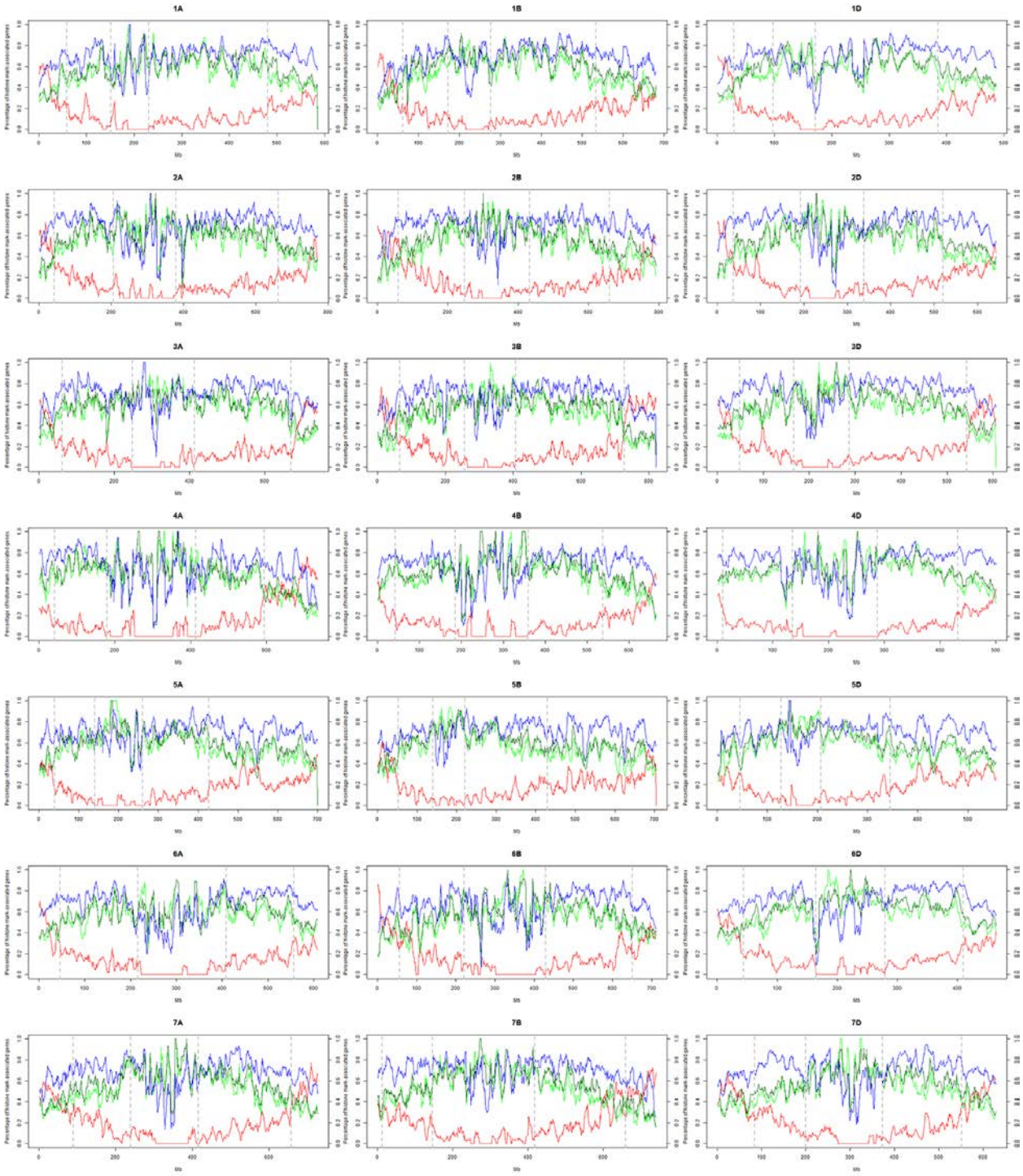

Fig. S37

Distribution of four histone marks along wheat chromosomes. Percentage of histone mark-associated genes are calculated in 10-Mb sliding windows (step 1 Mb). The distribution of histone marks along wheat chromosomes is following highly contrasting patterns. Whilst the repressive H3K27me3 mark (red) was enriched in the distal ends of the chromosomes with a pattern that is reminiscent to overall gene density, the active H3K36me3 (light green) and

H3K9ac marks (dark green) were more abundant within the proximal regions. In addition, the expression breadth pattern was correlated with the distribution of the repressive H3K27me3 (R= -0.76, P < 2.2E-16) and with the active H3K36me3 and H3K9ac (R= 0.9 and 0.83, respectively, P < 2.2E-16) histone marks. The modification H3K4me3 in shown in blue. The X-axis represents the physical position on chromosomes.

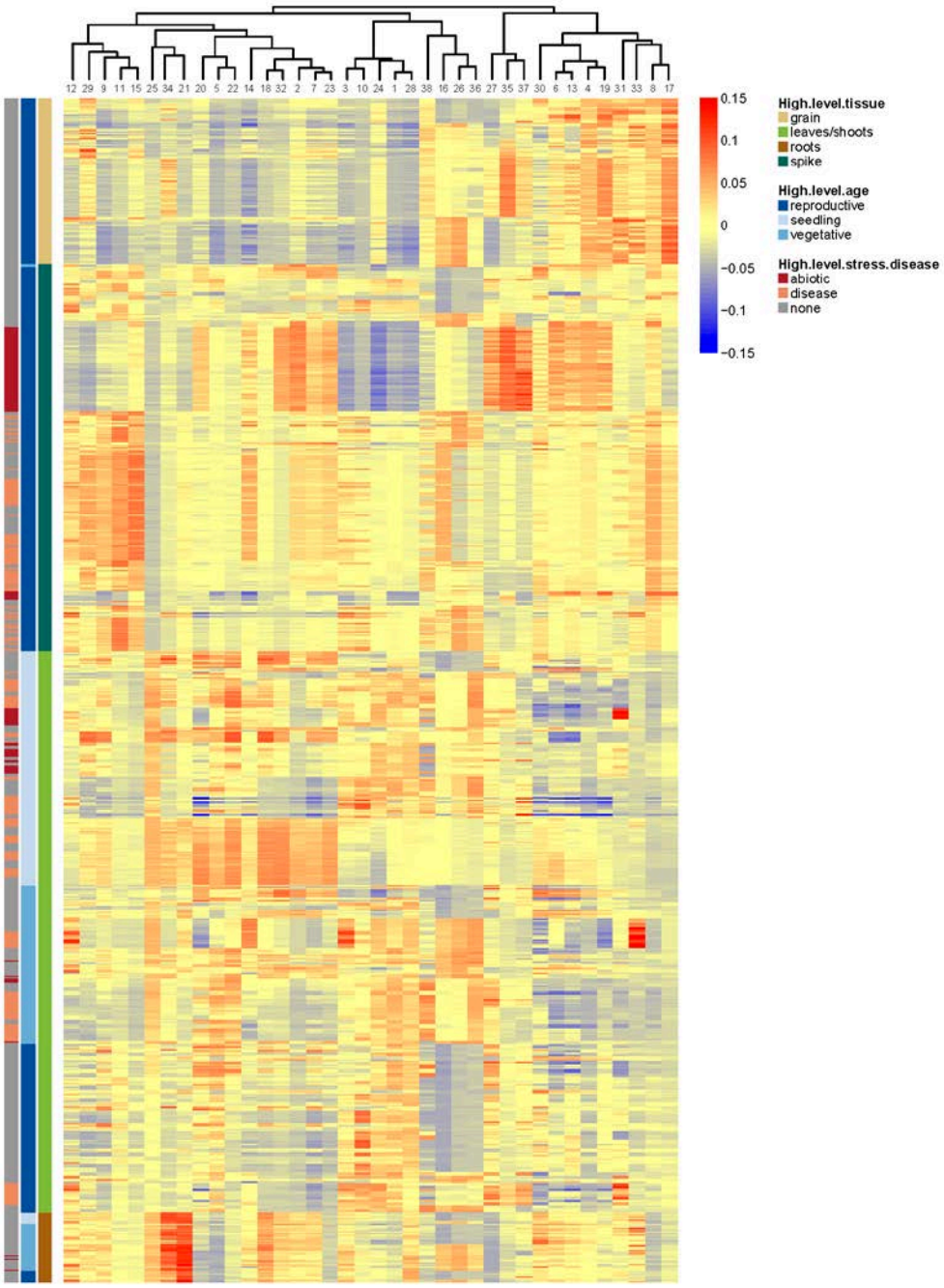

Fig. S38

Heatmap illustrating the expression of a representative gene (eigengene) per module. Modules are represented as columns, with the dendrogram illustrating eigengene relatedness. Each row represents one sample and the coloured bars beside the heatmap indicate the High Level Tissue, Age and Stress from which the sample originated. Expression levels were normalised by DESeq2 variance stabilising transformation. Values >0.15 or <-0.15 were capped at 0.15 or -0.15, respectively. This capped 16 out of 32,300 values (12 values >0.15 and 4 values <-0.15).

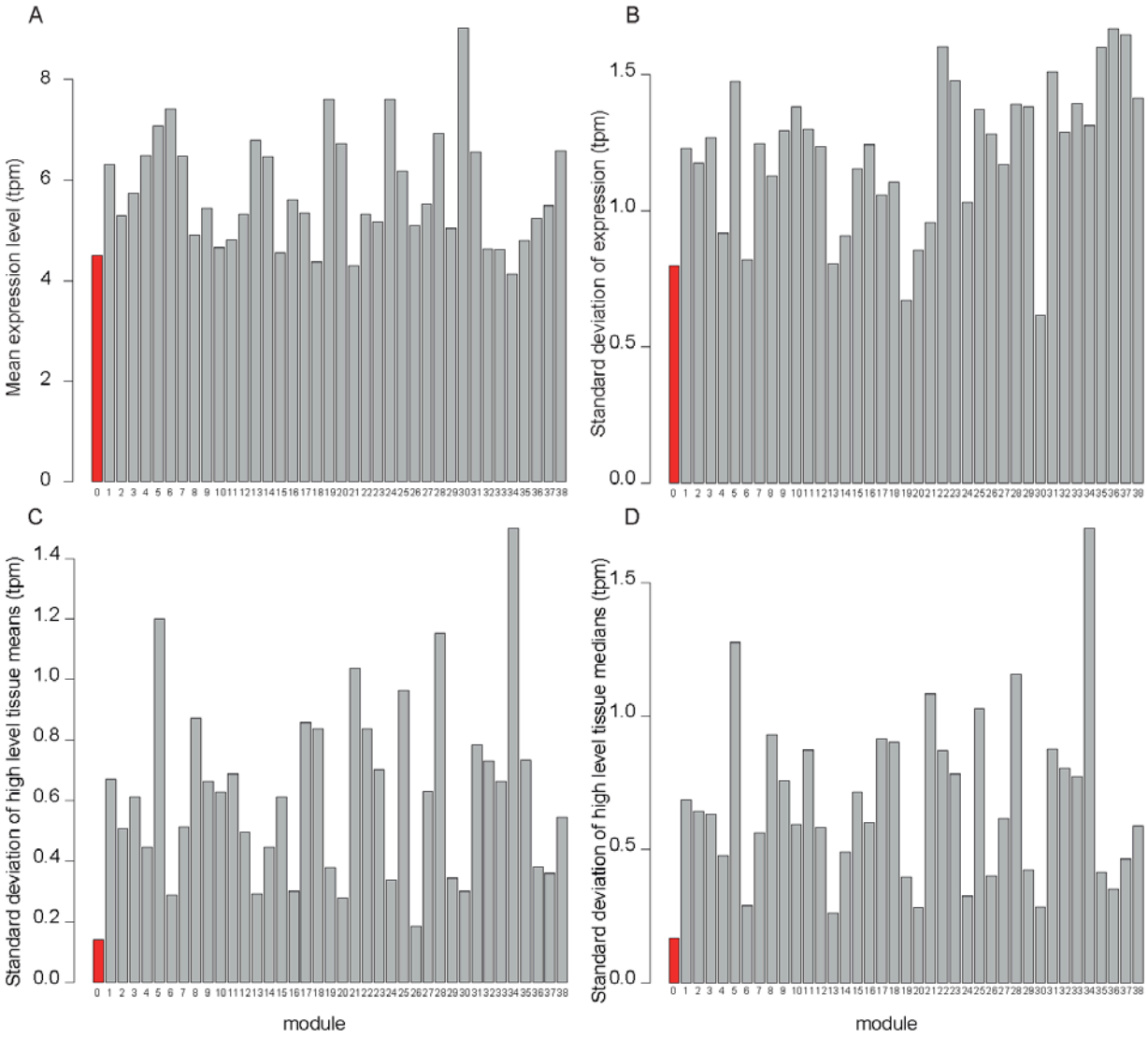

Fig. S39

Characteristics of genes assigned to WGCNA modules compared to unassigned genes (module 0, red). Mean expression level (tpm) (A) and standard deviation of expression (B) for all genes in each module. Standard deviation of the mean (C) and median (D) values calculated for each module for high level tissues. Unassigned genes (module 0) tend to be expressed at lower levels and have reduced variation in expression across high level tissues.

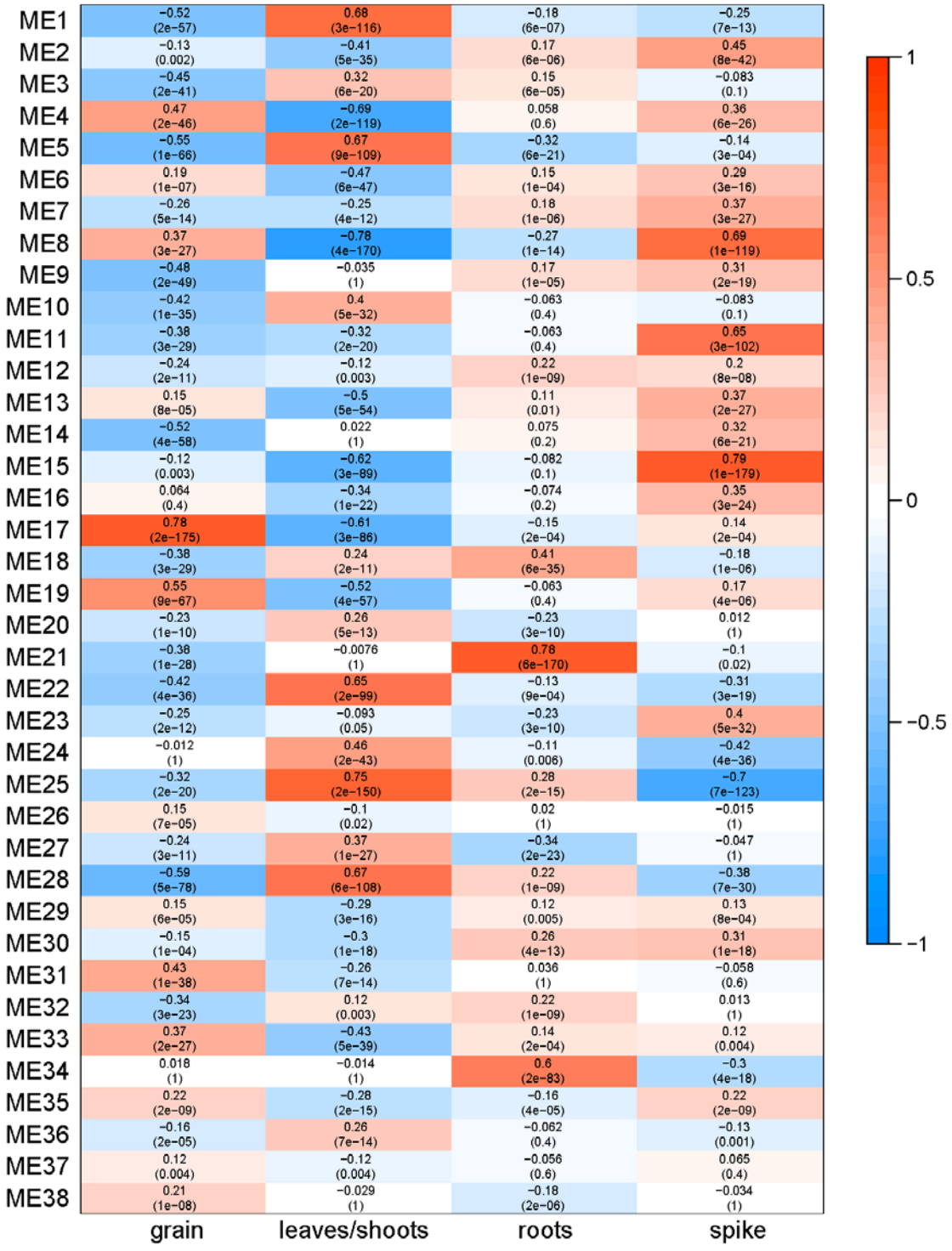

Fig. S40

Correlation between the module eigengene (kME; representative gene expression pattern) and the high level tissue for each module in the WGCNA co-expression network.

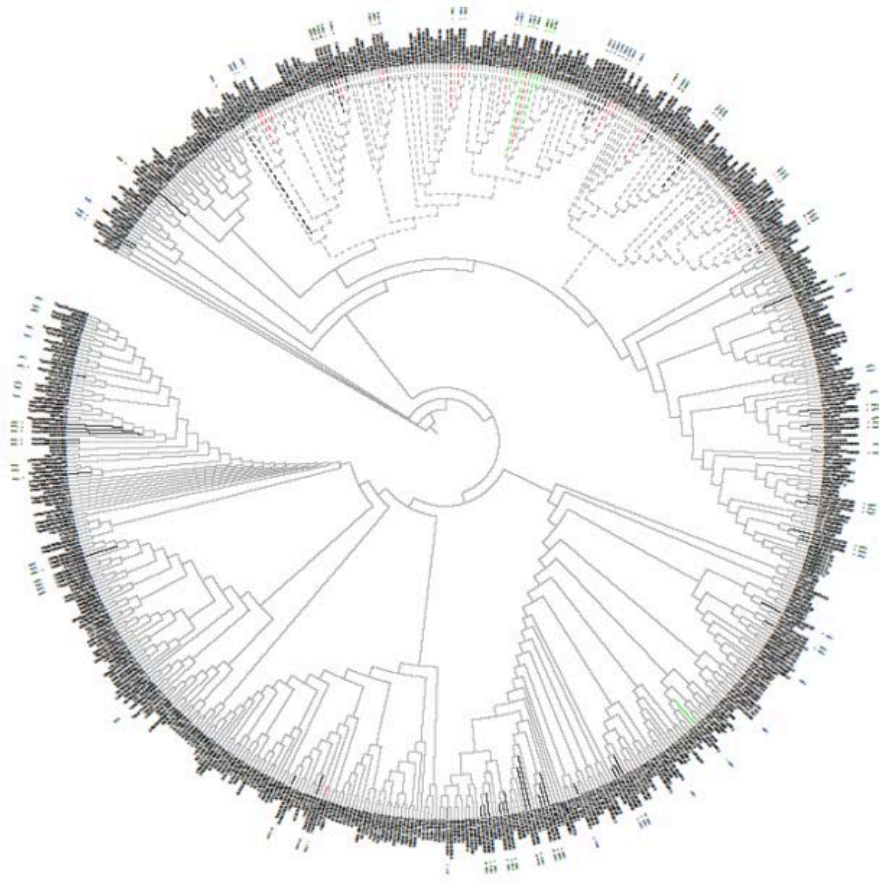

Fig. S41

Phylogenetic tree for MADS transcription factor gene family OG0000041. Red branches are genes within module 8, green branches are genes within module 11 and black branches are genes in other modules. Grey branches indicate non-wheat genes or wheat genes not allocated to a module in the WGCNA network. The dotted branches are the clades in which Arabidopsis and rice orthologues were found to be involved in flowering regulation. Numbers around the outside of the phylogenetic tree indicate the module to which the gene was allocated and the gene family is described in the outer ring. For a high resolution image see iTOL: http://itol.embl.de/shared/borrillp

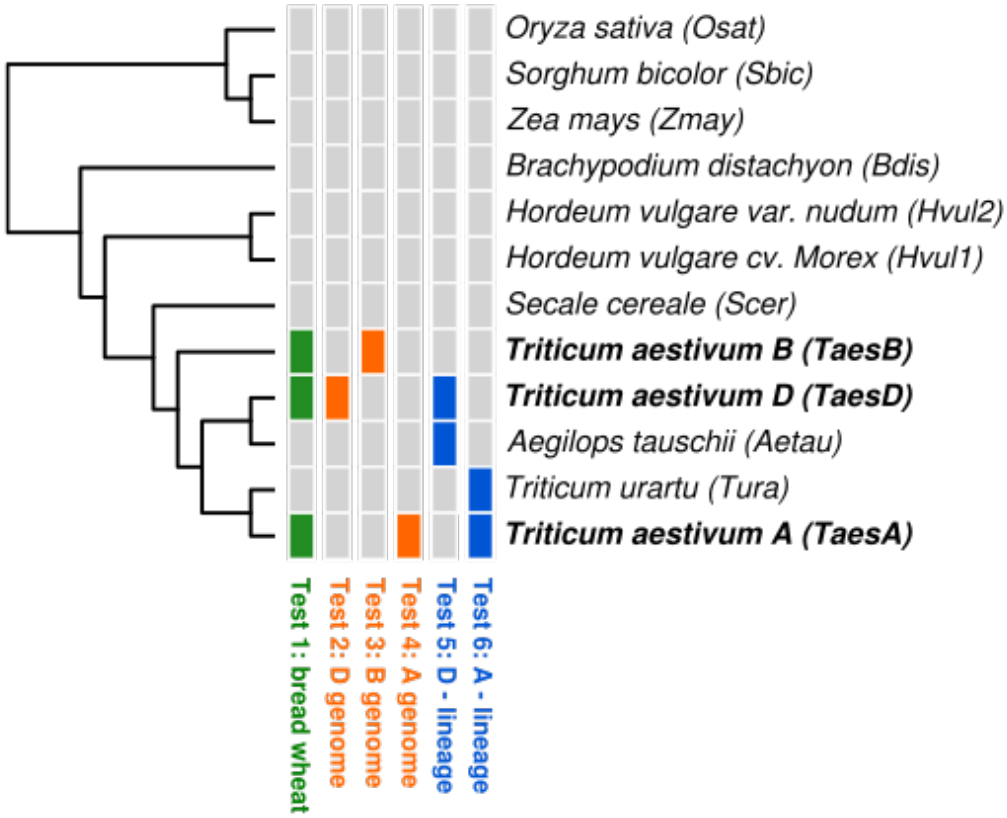

Fig. S42

Taxon sets compared in the phylogenetic comparative ANOVA (phyloANOVA) of gene family sizes. The cladogram on the left depicts the phylogenetic relationships of the 12 genomes under comparison (3 bread wheat sub-genomes and the genomes of 9 other grasses). The 6 columns in the colored matrix between the cladogram and the taxon labels depict each of the phyloANOVA tests used to infer significant expansions and contractions in the 26,080 gene families. Each set of colored cells (green, orange and blue) indicates the taxon set whose log-scaled gene family sizes were compared with the other grass taxa (grey cells). P-values of ANOVA test statistics were corrected for multiple testing by using the false-discovery rate (*158*). T-values of phyloANOVA tests with FDR<0.1 were subsequently used to infer expansion (t>0) and contraction (t<0) of gene families in the respective genome set (Tests 1-6).

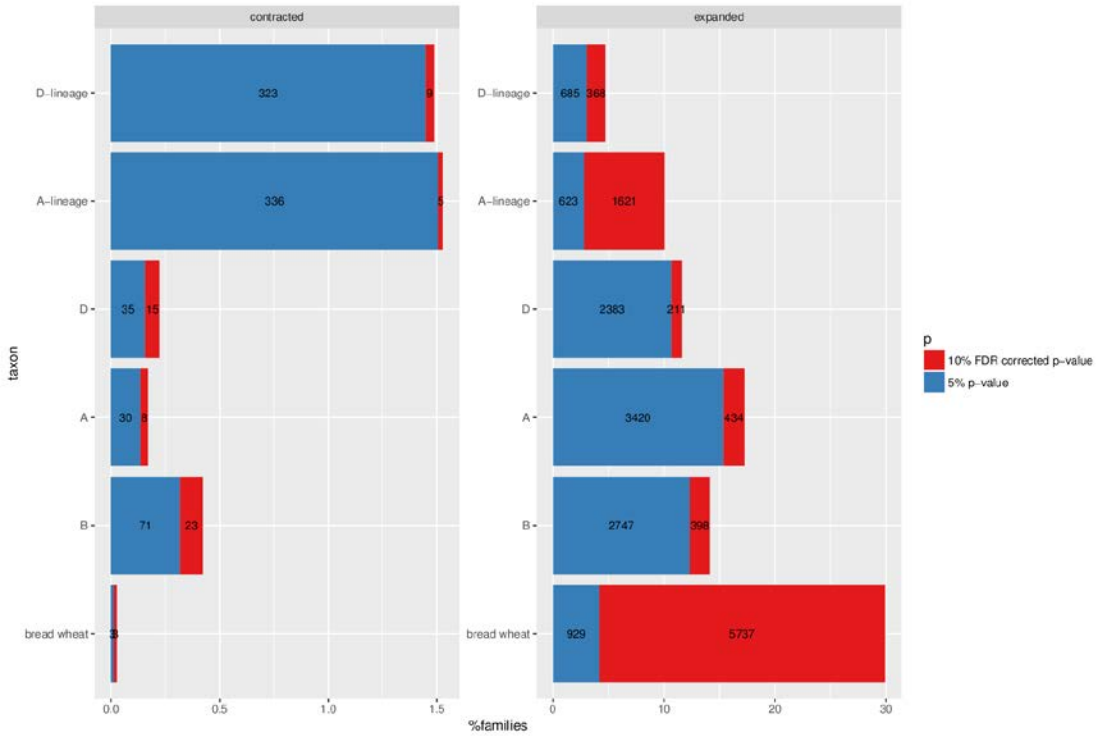

Fig. S43

Expansion and contraction of gene families in the bread wheat genome. Stacked barplot of the percentages of significantly contracted (left panel) or expanded (right panel) gene families [95% confidence level based on the uncorrected p-values (blue), 90% confidence based on the FDR-corrected p-values (red)]. Absolute numbers of gene families in each set are annotated as numbers in the bars. The values in each of the stacked columns are additive – families with a FDR-corrected p-value<0.1 also have a p-value <0.05. Only non-TE families and families with consistent domain architectures are shown. Gene families comprising only pseudogenes were excluded. Up to 25% of all gene families were equally expanded in all sub-genomes of bread wheat in comparison to the other grasses, while maximally 10-14% (D and A) of all gene families are expanded in one of the sub-genomes (using uncorrected p<0.05). Considering type I errors in (multiple) hypothesis testing and correcting for FDR, reduces these numbers to 21% and 1-2% (FDR<0.1). While the size changes that were only detectable using the uncorrected p<0.05 cutoff might still contain losses/gains of single loci representing size fluctuations without selective consequences, the FDR<0.1 should provide a more robust measure to pick up changes that go beyond these fluctuations, possibly reflecting selective processes and adaptive traits. All large-scale analyses reported in the main text rely on the sets defined at 10% FDR. The majority of recorded expansions affected the sub-genomes similarly (5,737 expanded non-TE, non-pseudogene families at FDR<0.1). The statistically significant differences between the sub-genomes in terms of sub-genome-specific expansions (χ2 82.206, p-value < 2.2e-16; A>B>D) and contractions (χ2 7.3478, p-value = 0.02538; B>D>A) are largely consistent with a scenario where the progenitors diverged 5-3 mya (Fig. S15); the A and B sub-genomes coexisted for a longer time period (1-0.5 my) before the tetraploid A:B progenitor hybridized with the D progenitor about 10,000 years ago. The A genome-lineage-specific expansions (1,621), were

greater than the number of expansions in the D genome and more losses and fewer gains were observed in B than in A, a possible consequence if the B progenitor was the maternal donor in the initial tetraploidization event. Employing the 10% FDR cutoff, there was no overlap between the sets of contracted and expanded gene families. By relaxing the criteria to $p<0.05$, a maximum overlap of 31 gene families was found expanded in A and contracted in B. All other set intersections between the sub-genomes were either zero or do not go beyond four families. This suggests that unbalanced translocations among sub-genomes did not play a major role in the sub-genome-specific expansions, but processes like trans-duplication were more likely to give rise to the gene family expansions observed in bread wheat.

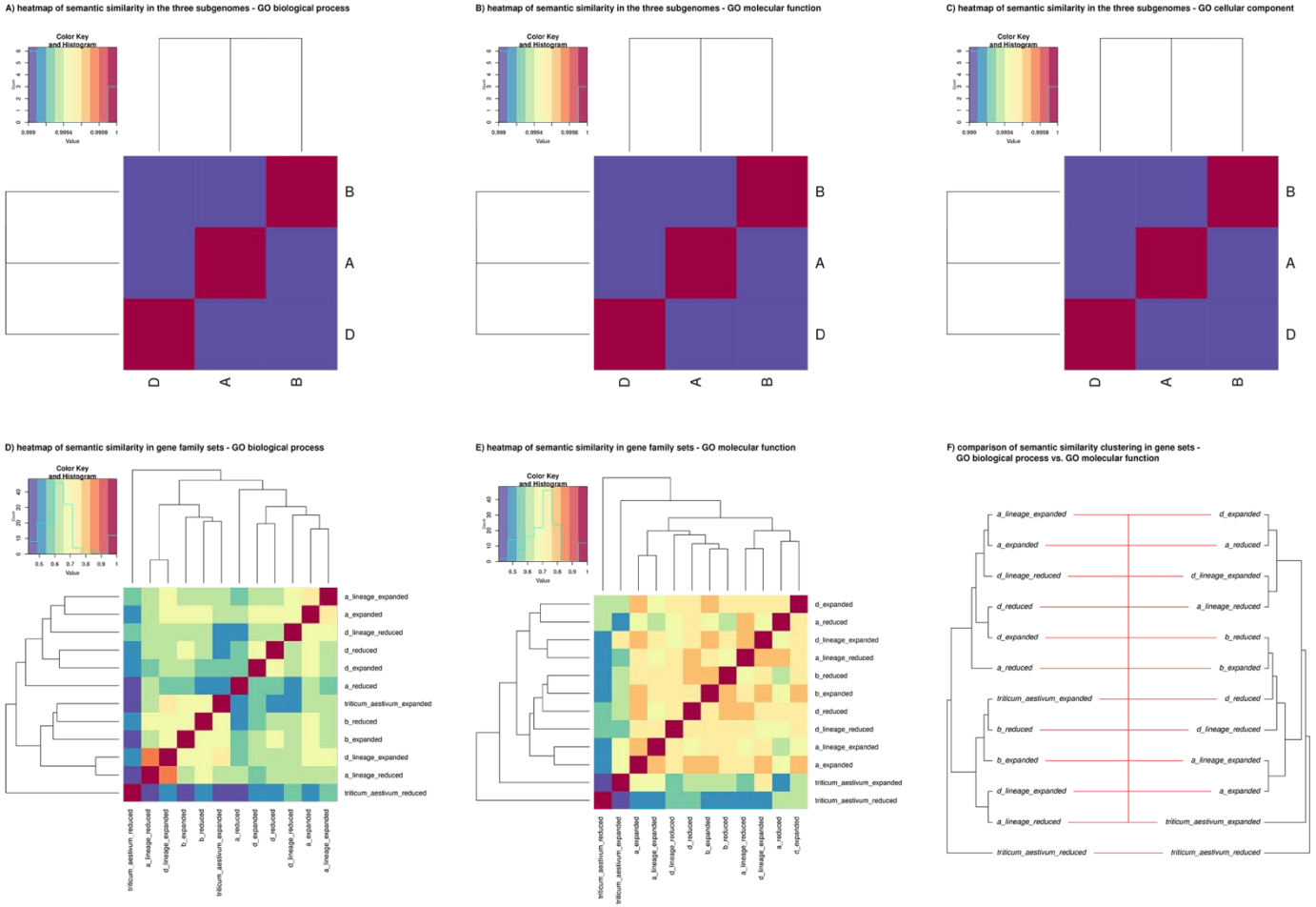

Fig. S44

Functional similarity of the three wheat sub-genomes (A-C) and the different sets of genes encoded by the expanded and contracted gene families (D-F) as measured by semantic similarity of Gene Ontology (GO) term annotations. Semantic similarity provides a quantitative measure for functional similarity of genes by measuring the distances of their assigned GO terms in the ontology graph.

Concepts that do not share any functional overlap have a semantic similarity of 0, highly related concepts show values close to 1 and the identical concept has a similarity of 1. Upper row: Heatmap matrices depicting the semantic similarity (*159*) of the three wheat sub-genomes for the GO biological process (BP; A), molecular function (MF; B) and cellular component (CC; C) category. Lower row (D-E): Heatmap matrices depicting the semantic similarity of the subsets of genes in significant expanded and contracted gene families (Fig. 4B) in the GO BP and MF category. F) Juxtaposition of the hierarchical clustering of semantic similarities of the gene family sets in the BP (left tree) and MF (right tree) GO category. The topology of the two trees often groups expansions in one sub-genome with contractions in another, indicating how losses in one are often balanced by gains in another sub-genome. Large numbers of significantly enriched Gene Ontology and Plant Ontology terms (1,169 distinct terms) were identified indicating that expanded families are involved in many aspects of wheat biology, morphology and development. Similarly, no distinct functional or morphological categories dominated the list of enriched GO and PO terms (272 distinct terms) for contracted gene families. But the assessment of functional overlap between the expanded and reduced gene family sets, as well as the overall gene complements of the sub-genomes indicated high overlap in terms of semantic similarity (0.999) for the sub-genomes and high semantic similarities between expansions in one genome and reductions in others, which overall suggests balancing of losses and gains potentially driven by gene transfer between the sub-genomes.

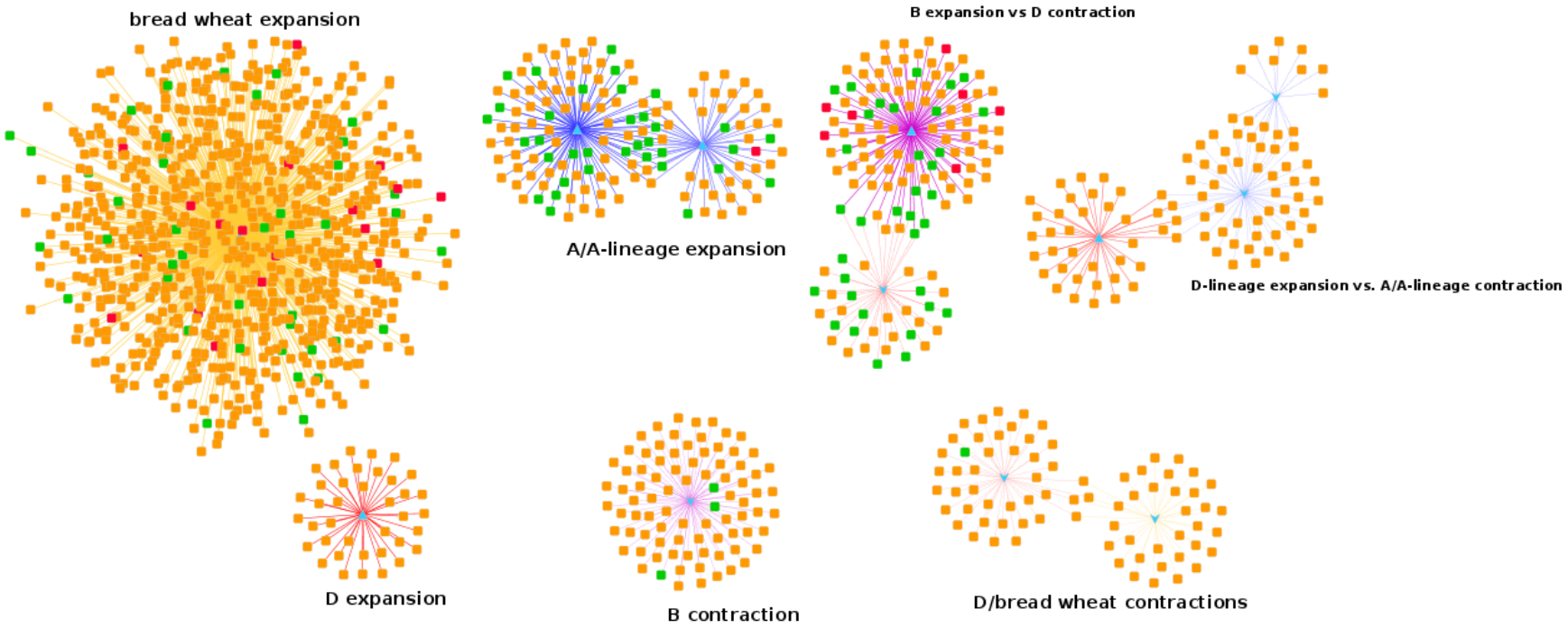

Fig. S45

Ontology term network for enriched terms among expanded and contracted wheat gene families. Each set is depicted as a blue, central node (upward facing triangles=expanded families; downward facing triangle=contracted families) linked to ontology terms [GO (orange nodes), PO (green nodes) and TO (red nodes)]. Overlapping enriched ontology terms were clustered using GLAY community clustering and the resulting subnetworks represent sets with significant conceptual overlap. Expanded views of the clusters are shown in Fig. S46-51. While the overall grouping of the community clustering reflects the results based on semantic similarity analysis of GO terms and is in line with overall balancing of losses and gains, some mild specialization can be inferred from the term composition of the sub-genome-specific expansion sets (D-genome and lineage: defense response, B-genome: plastid and housekeeping; A-genome and lineage: vegetative growth).

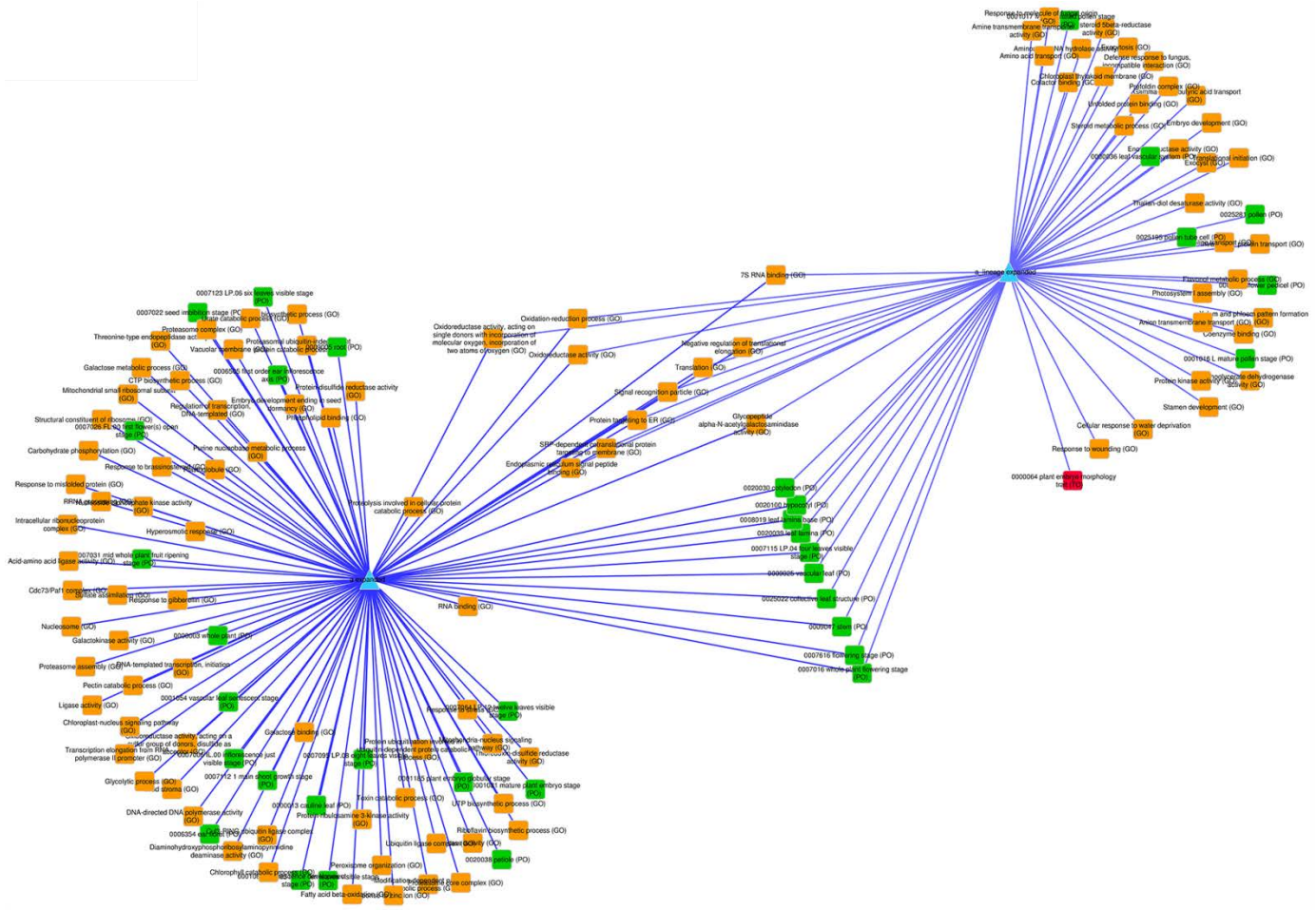

Fig. S46

Enriched ontology terms for the gene sets encoded by gene families expanded in the A genome and A-lineage. The two sets share 10 PO terms and 11 GO terms.

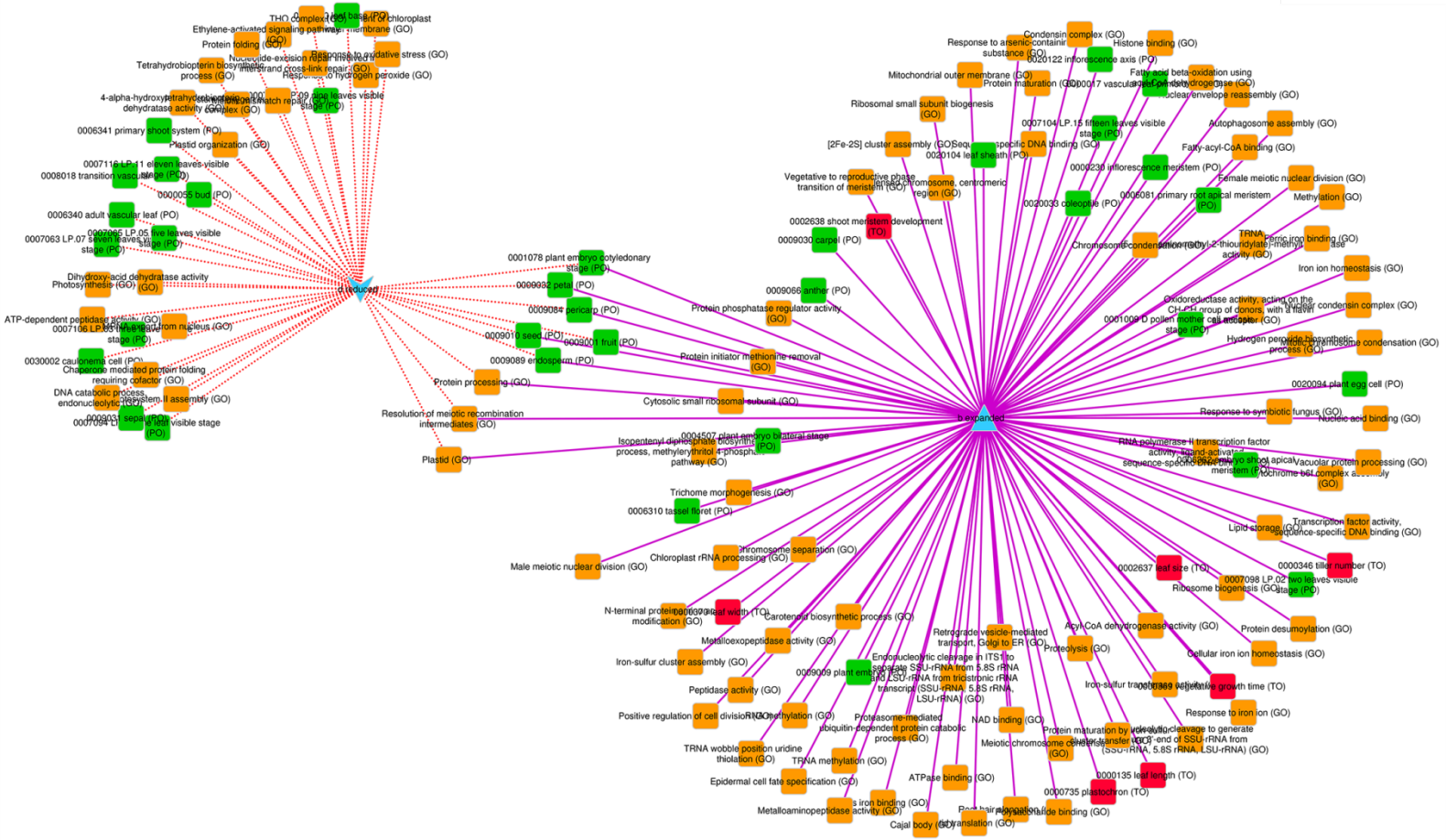

Fig. S47

Enriched ontology terms for the gene sets encoded by gene families contracted in the D genome and expanded in the B genome. The two sets share six PO terms and three GO terms.

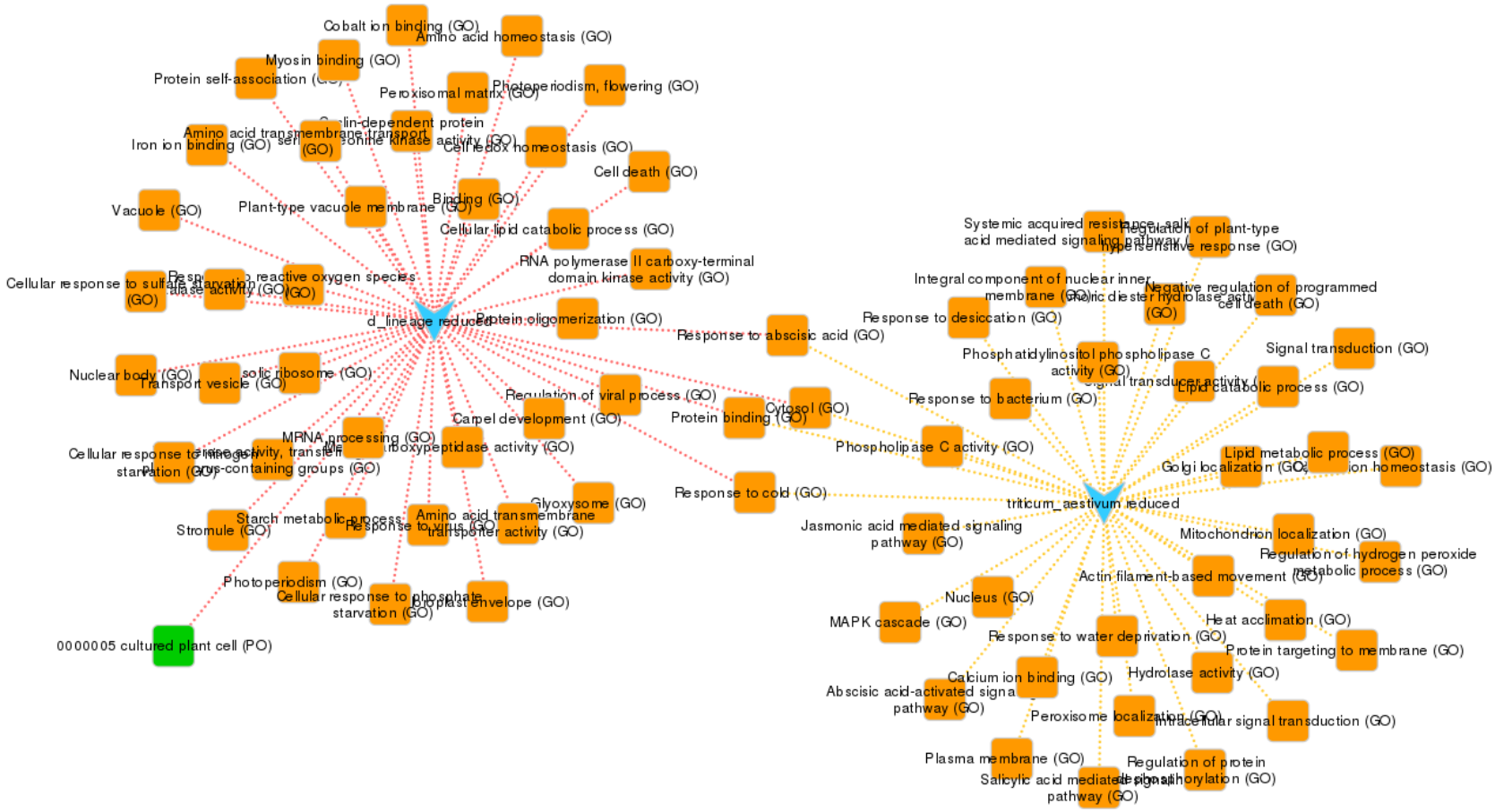

Fig. S48

Enriched ontology terms for the gene sets encoded by gene families contracted in the D-lineage and in bread wheat. The two sets share four enriched GO terms.

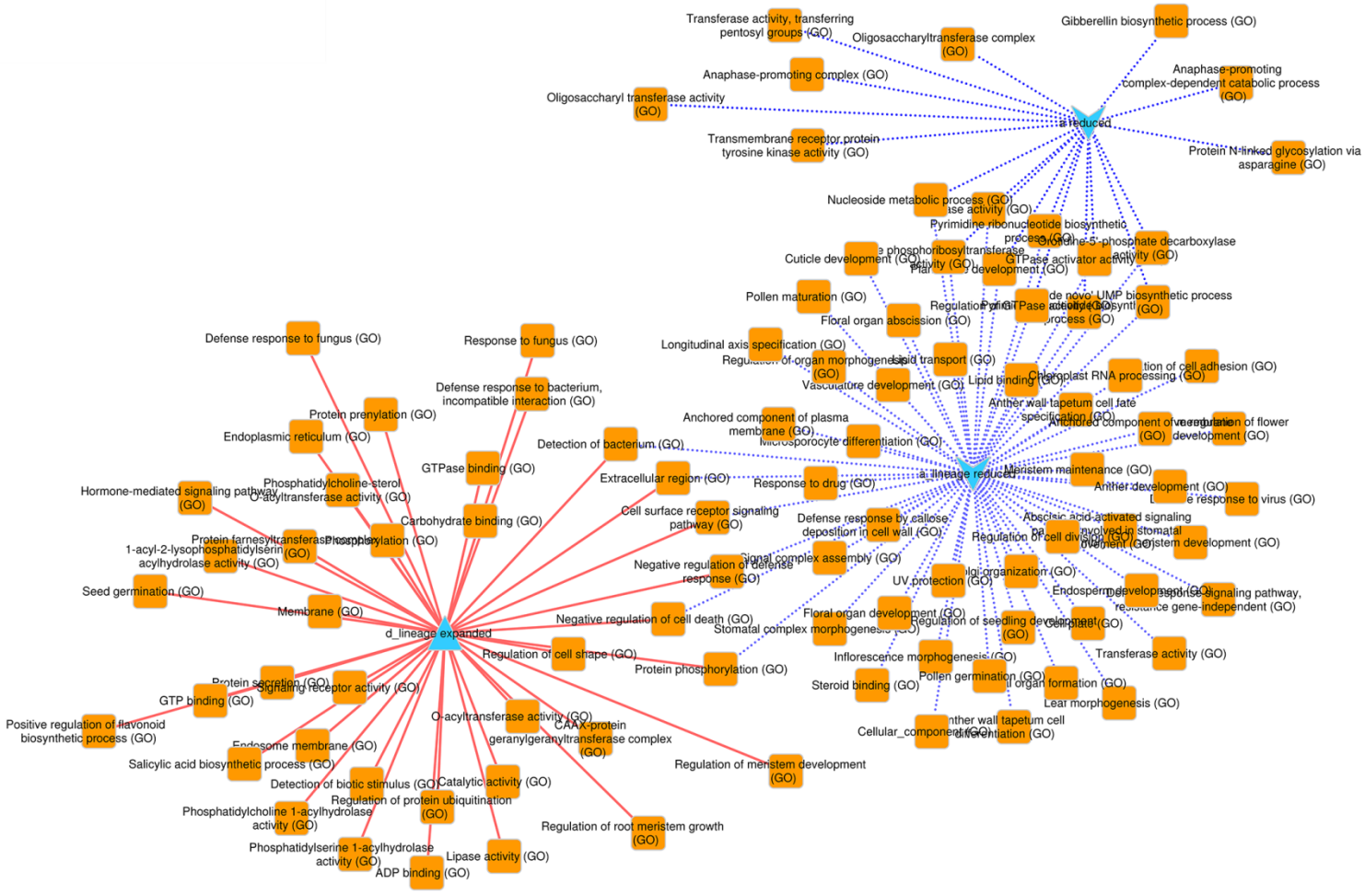

Fig. S49

Enriched ontology terms for the gene sets encoded by gene families contracted in the A genome and the A-lineage and expanded in the D-lineage.

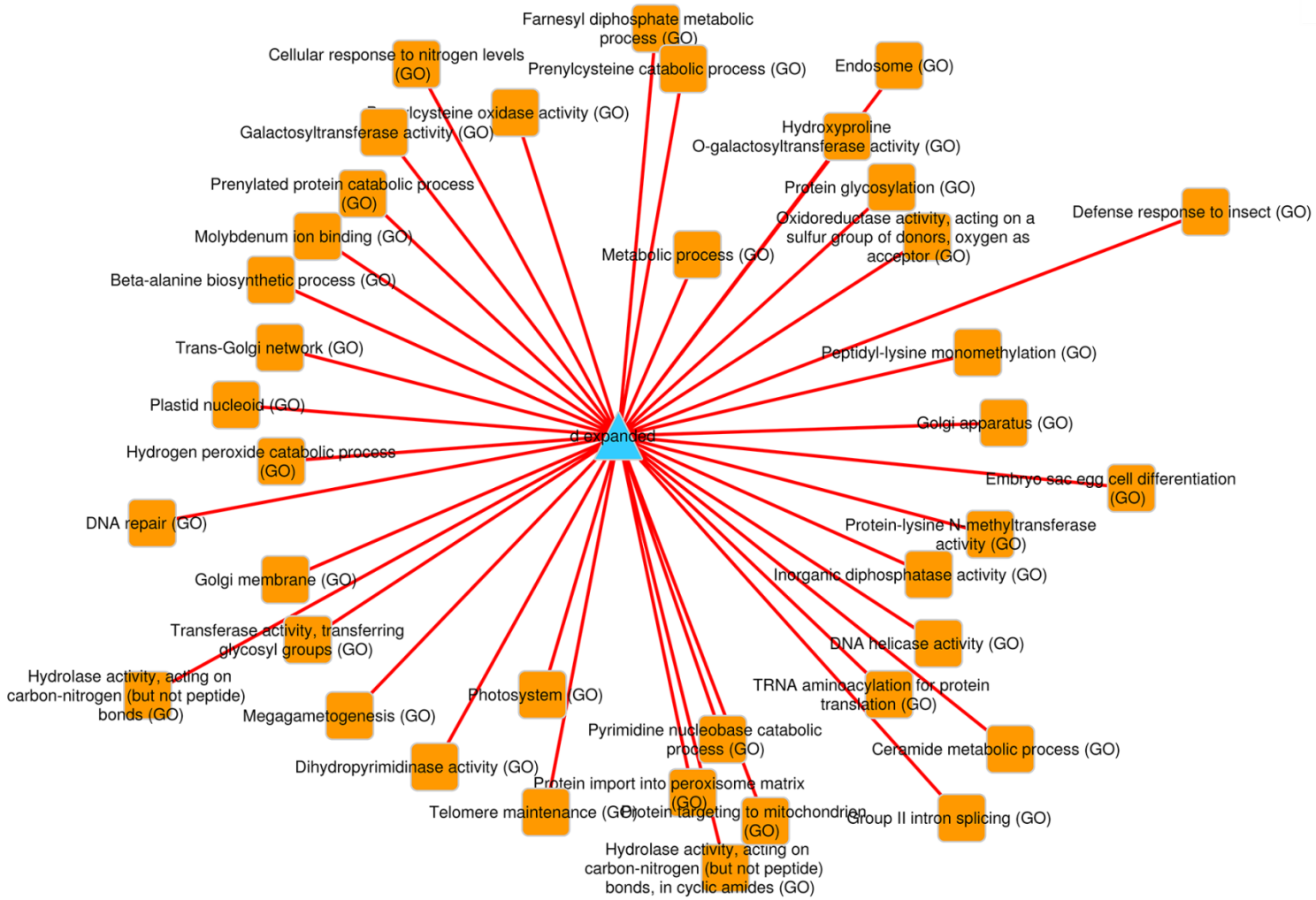

Fig. S50

Enriched ontology terms for the gene sets encoded by gene families expanded in the D genome.

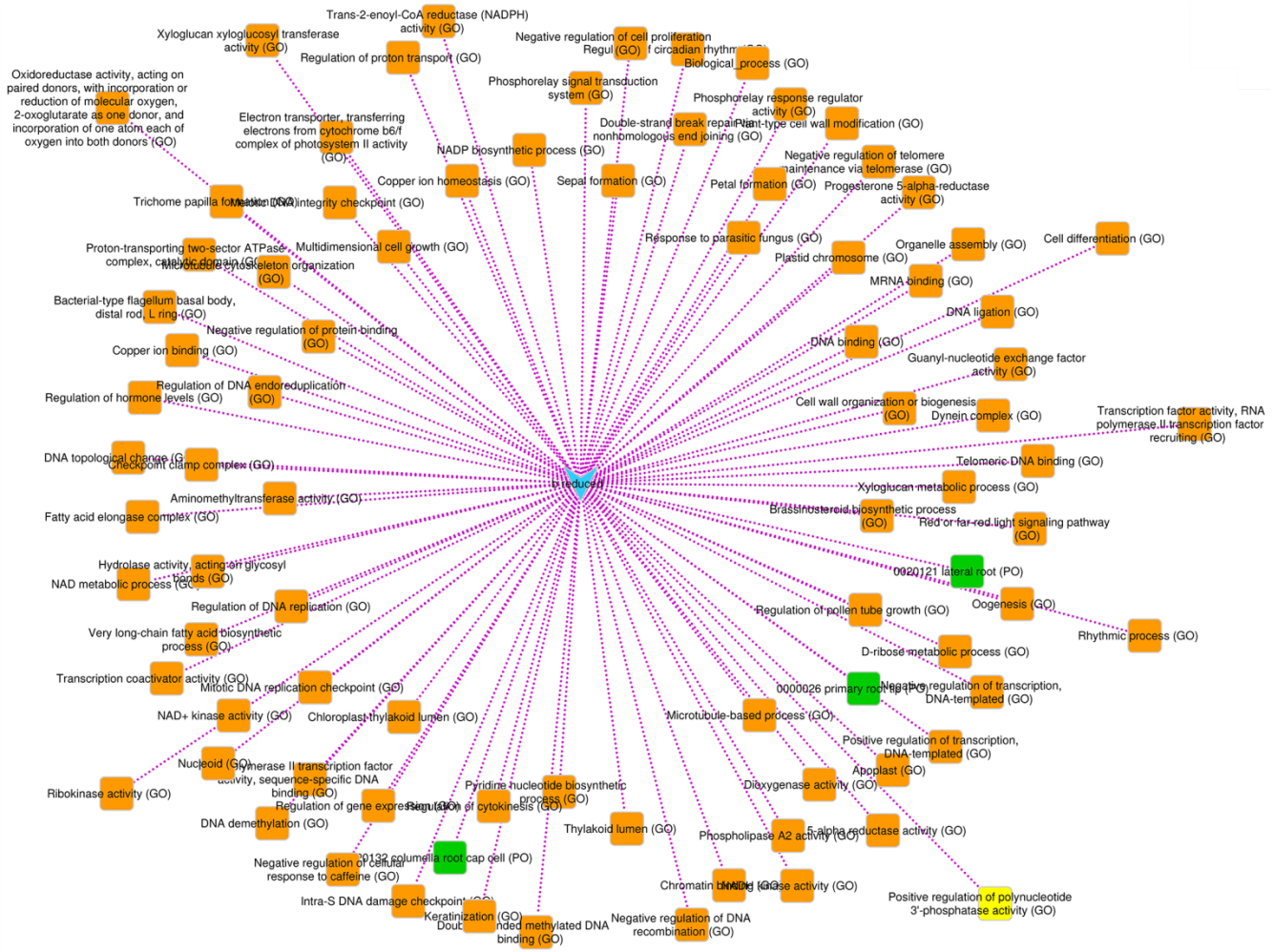

Fig. S51

Enriched ontology terms for the gene sets encoded by gene families contracted in the B genome.

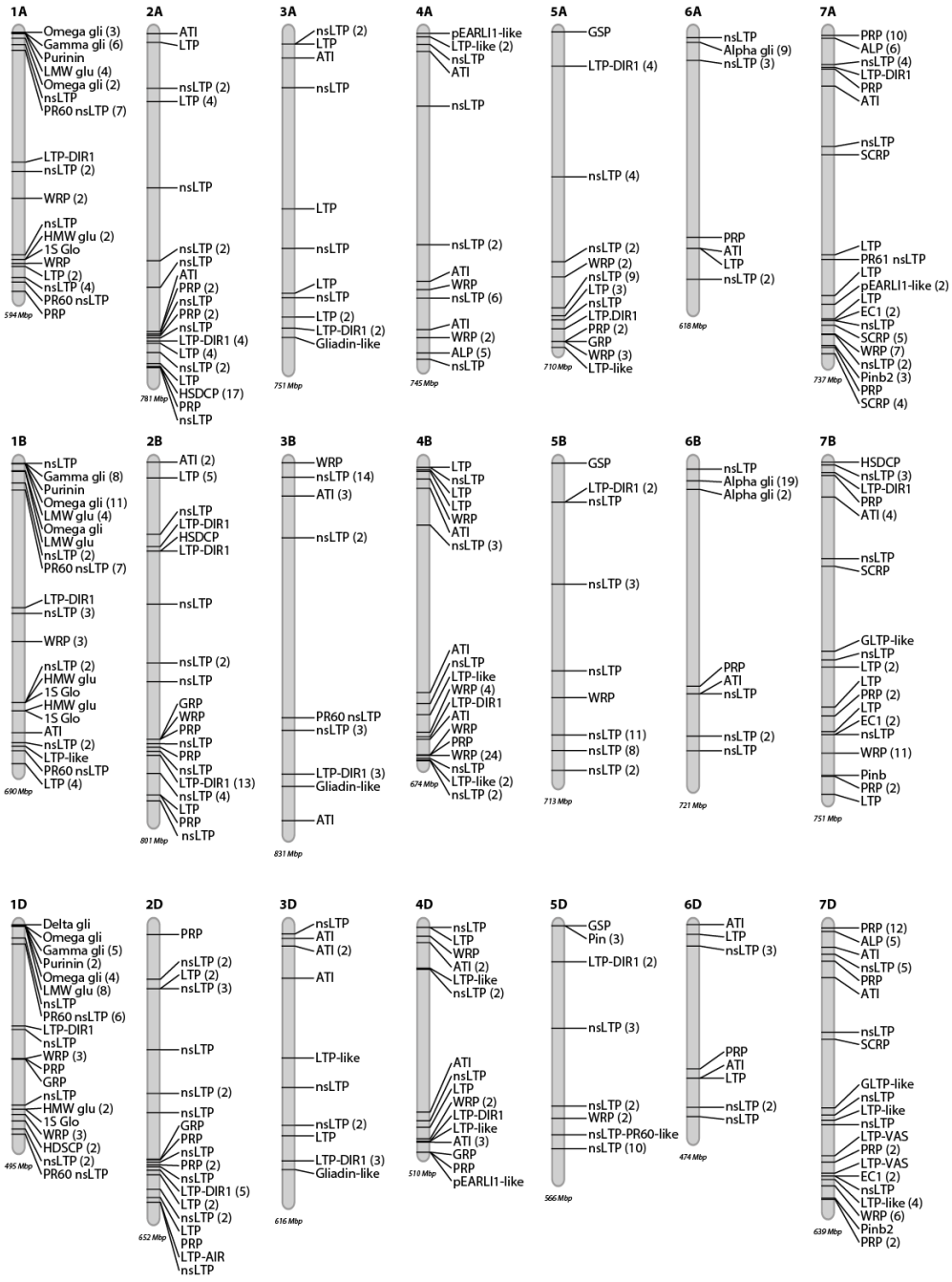

Fig. S52

Chromosomal distribution of the super-family of genes coding for the prolamin Pfam domain proteins in wheat. The gene families are generally monophyletic in phylogenomic studies and occur in clusters in the genome assembly. All gene models have been analysed with respect to content of epitopes associated with coeliac disease and allergies (*46*).

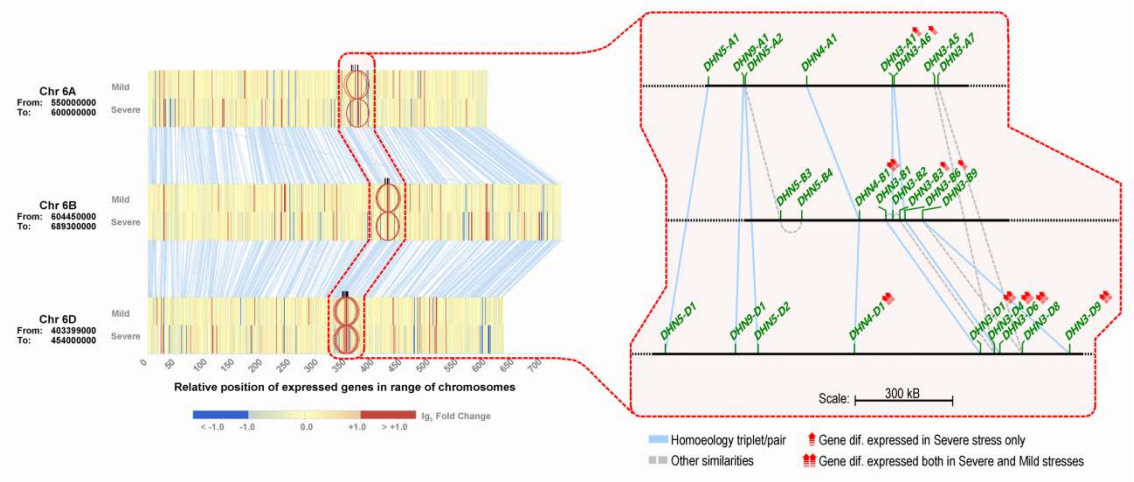

Fig. S53

Gene families and networks in drought tolerance. The left panel presents the differential expression of the dehydrins in a cluster on the long arms of chromosome 6 (full details in (*44*)). X axis provides gene positions in Mb. Each chromosome is represented by two bands of vertical lines: upper band is associated to Mild stress whereas the lower one is associated to Severe stress. Each vertical line corresponds to a sequential gene and its colour indicates differential expression (log Fold Change –lgFC; (*44*)). The cluster of dehydrins surrounded with a dotted red line are marked with short black lines on top of the Mild band in each chromosome. In addition, the dehydrins with a lgFCvalue > 1 are shown in the expanded right panel. The green names of the dehydrins are followed by red arrows when they are differentially expressed with a p-adjust value < 0.05. High levels of similarity are found between the dehydrin genes; a blue line connects homoeologous genes whereas a dotted grey line connects genes with an unassigned phylogenomic relationship. 6B dehydrin genes have the highest expression levels.

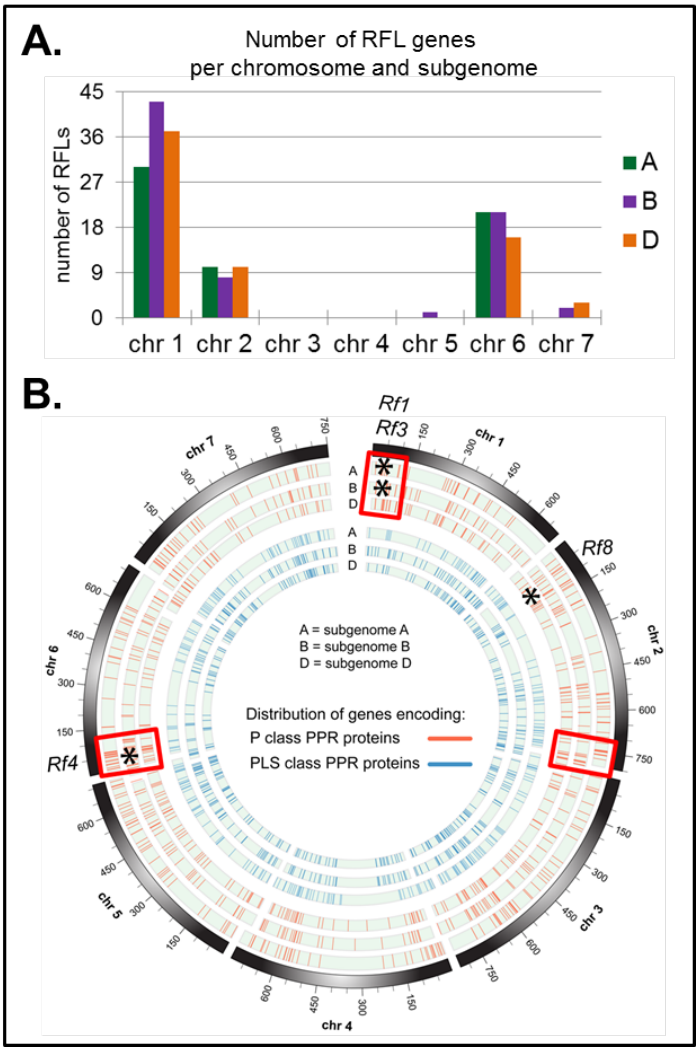

Fig. S54

Genome-wide distribution of RFL genes in IWGSC RefSeq v1.0. The RFL genes were identified by three methods: Orthofinder (*130*), OrthoMCL-DB (*160*) and phylogeny (*43*). In contrast to the ~500 PPR proteins encoded in flowering plant genomes (*161*), over 1600 PPR genes were found in wheat, a number nevertheless lower than expected from simply adding genes present in the progenitor diploid genomes (*161*). Evidence for gene inactivation and loss during polyploidization was found in truncated or frame-shifted gene fragments. Within the PPR gene family in IWGSC RefSeq v1.0 over 200 loci were identified as RFL genes that are organised in clusters on chromosomes 1, 2 and 6. The *Rf1* and *Rf3* restorer genes map to the largest cluster on chromosome 1 (*162*, *163*), whereas *Rf4* maps to a cluster on chromosome 6 (*162*). *Rf8* mapped to chromosome 2D (*164*). **A.** Number of RFL genes per chromosome and sub-genome. **B.** Co-localisation of RFL clusters with the mapped restorer loci in wheat. The approximate position of the mapped *Rf* genes is indicated (black asterisk). Genomic regions carrying clusters of RFL genes are boxed in red.

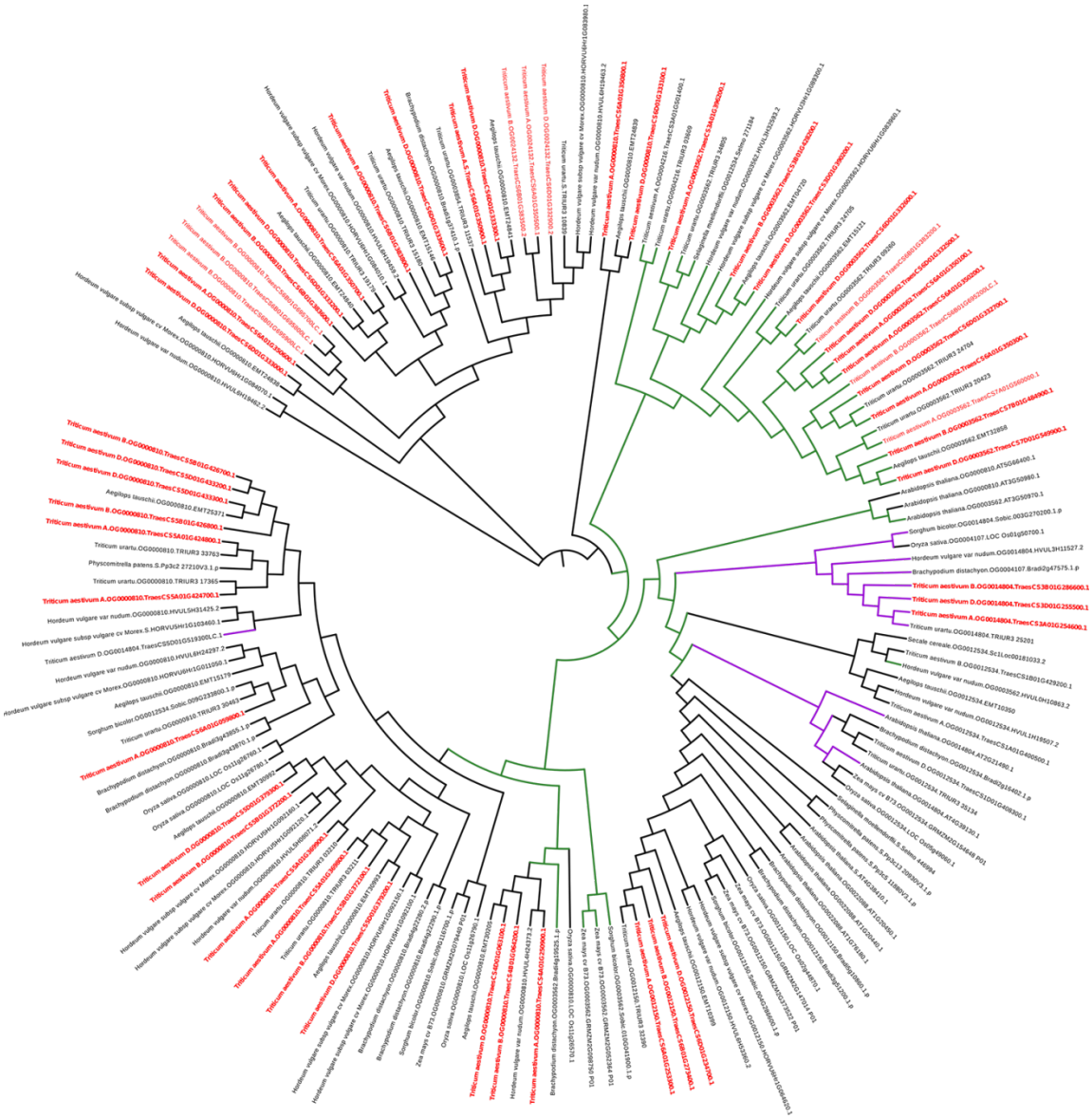

Fig. S55

Tree of expanded Dehydrin Orthologous Groups. The branches of the expanded orthologous groups are highlighted. OG0003562, green; OG0014804, purple. Wheat sequences are highlighted in red.

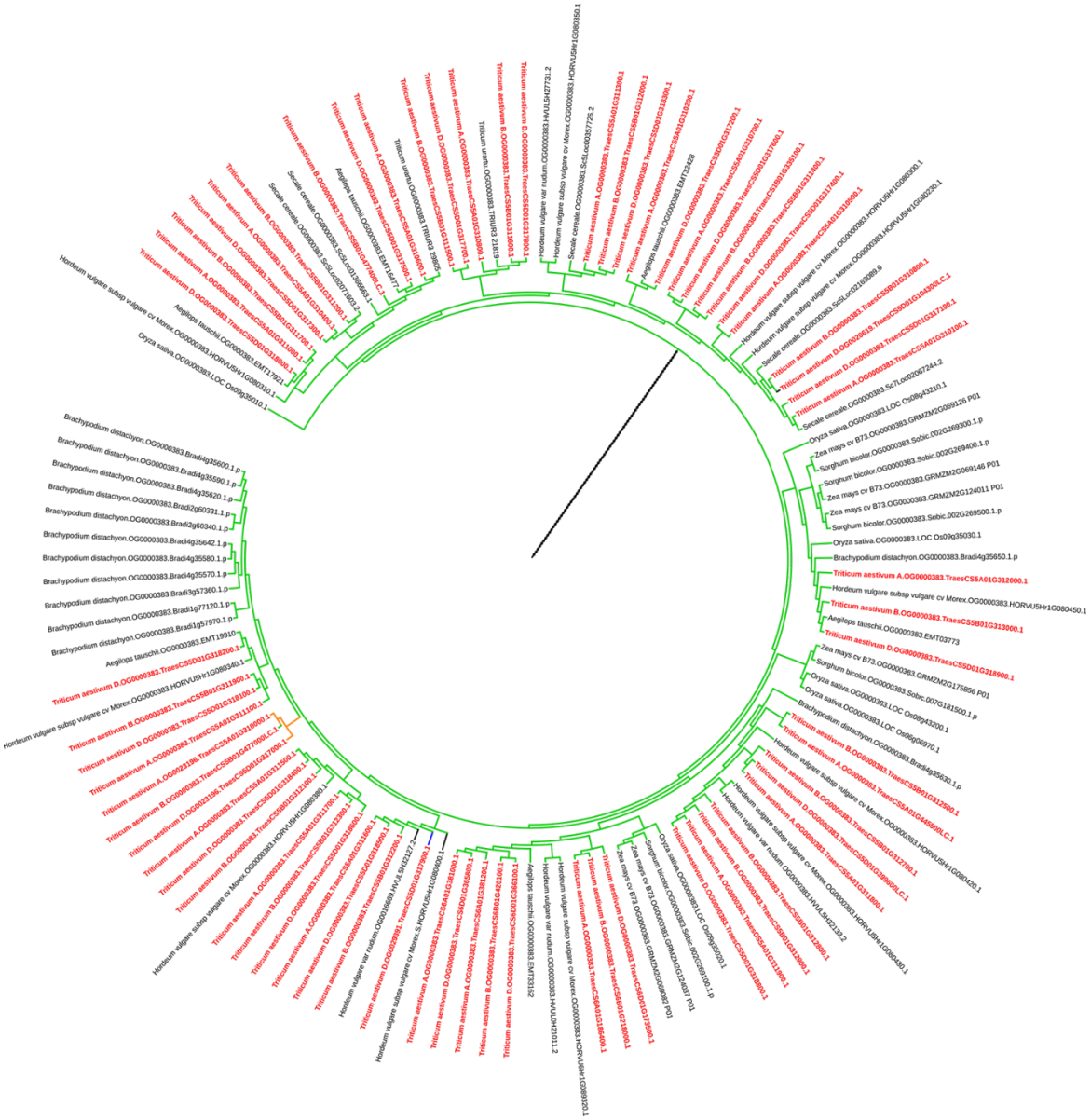

Fig. S56

The AP2 domain (Pfam: PF00847) was used to extract CBF orthologous groups from the bread wheat phylogenomics dataset (see Table S38) and to construct a tree. Sixty-one CBF genes were previously defined on group 5 chromosomes. Of those, 52 fall in OG0000383 (green clade). Seven sequences were not found in the AP2 tree and two fall into minor orthologous groups (OG0023196, orange branches; OG0029391, blue branch). OG0000383 is a monophyletic clade (bootstrap value = 1.00) consisting of 118 sequences of which 66 are from T. aestivum (highlighted in red). This orthologous group shows a highly significant expansion in T. aestivum ($p<0.001$). Manual curation confirmed that the 62 of the CBF genes in OG0000383 included 17 CBF genes from 5A, 19 CBF genes from 5B, and 18 CBF genes from 5D. It also includes genes from 6A (3), 6B (2), 6D (3). Eight of the sequences were either partial genes or pseudogenes.

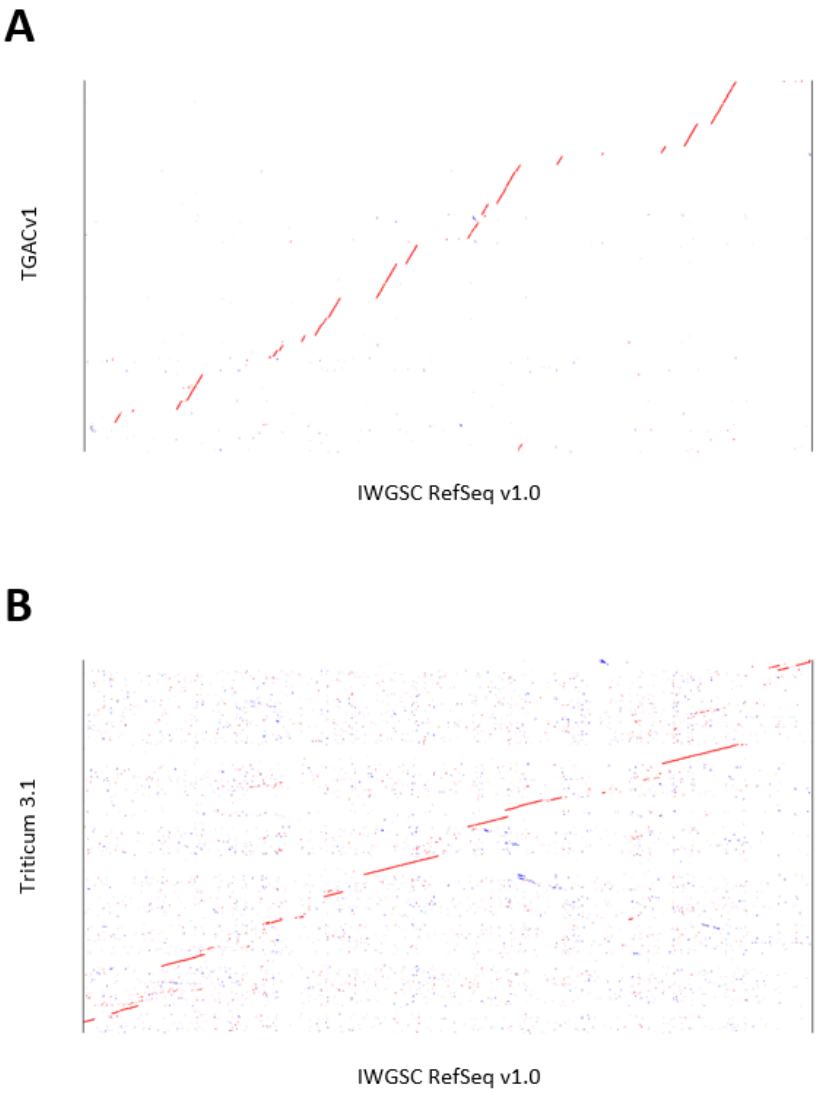

Fig. S57

NUCmer alignments of *SSt1* between IWGSC RefSeq v1.0 and available fragmented assemblies of CS. Scaffolds/contigs were retrieved from the fragmented assemblies using markers from the *SSt1* genetic map interval in Lillian/Vesper. A) Alignment of TGACv1 captures 39% of the interval, while B) alignment of Triticum 3.1 captures 61% of the interval. TGACv1 were prefiltered for placement in chromosome 3B, which was not possible for Triticum 3.1.

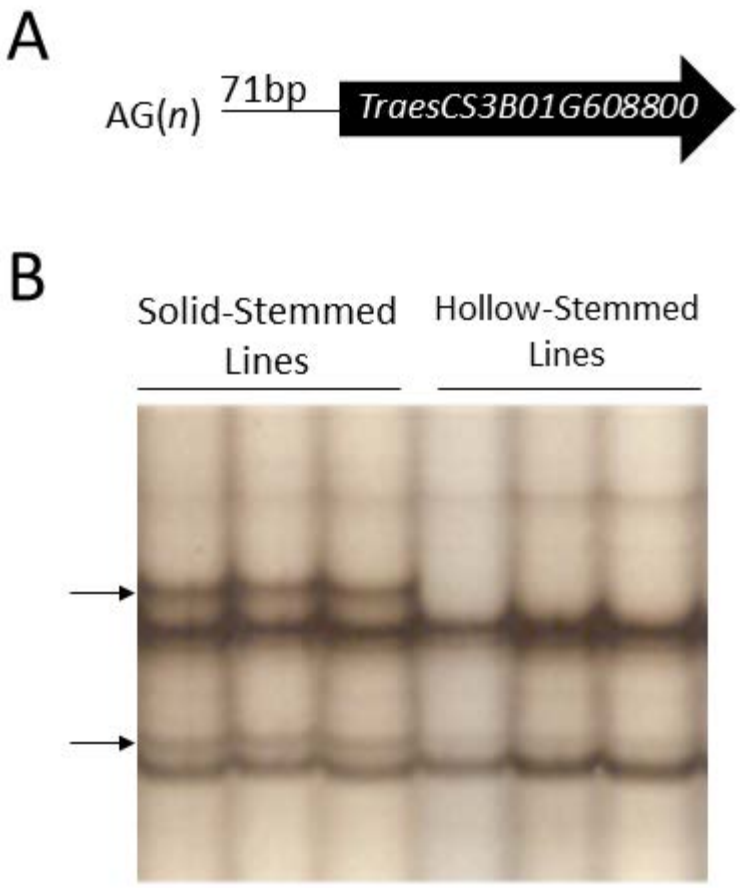

Fig. S58

Promoter variation in *TraesCS3B01G608800*. **A)** The gene *TraesCS3B01G608800* has a repeating AG(*n*) element 71 bp upstream of the transcription start site. **B)** Multiple variants of the AG(*n*) element are observed in solid-stemmed lines that are missing from hollow-stemmed lines (arrows), which were identified using single-strand conformation polymorphism (SSCP) gels.

Table S1.

Sequencing library data for bread wheat whole genome assembly

#	Library type	Insert size	Sequencing Instrument	Read length	Minimal Coverage
1	PCR-free PE library	450bp	HiSeq 2500	PE265bp	X76
2	PCR-free PE library	800bp	HiSeq 2500	PE160bp	X35
3	MP (Nextera MP Gel Plus)	2-4kbp	HiSeq 2500	PE160bp	X36
4	MP (Nextera MP Gel Plus)	5-7kbp	HiSeq 2500	PE160bp	X34
5	MP (Nextera MP Gel Plus)	8-10kbp	HiSeq 2500	PE160bp	X36

Table S2.

Results of IWGSC whole genome assemblies (WGA) with NRGene software package DenovoMAGIC2^{TM} before and after correction for scaffold mis-joins. A total of 227 putative chimeric scaffolds (166 detected by POPSEQ and 61 by the Hi-C data) were detected and broken in the second assembly version (IWGSC WGA v0.2).

	Initial WGA		**IWGSC WGAv0.2**	
	Contigs	**Scaffolds**	**Contigs**	**Scaffolds**
Total number of sequences	38,971,011	331,904	685,085	138,607
Assembly size (bp)	13,813,647,020	14,347,451,665	14,263,899,337	14,532,155,117
Gaps size (bp)	0	823,737,867	0	261,883,061
Gaps %	0	5.74%	0	1.80%
N_{50}-length (bp)	21,061	7,536,495	51,840	7,005,151
N_{90}-length (bp)	3,035	1,393,142	11,660	1,244,256
Maximal length (bp)	225,580	45,627,251	580,542	45,793,852

.

Table S3.

Summary of the IWGSC physical map data and associated publications.

Chromosome / chromosome arm	Project leader	Institution	BAC library size (clone number)	method	Assembly algorithm	Assembled contig length (Mb)	Contig N50 (kb)	Contig L50	MTP BACs	Reference
1AS	T. Wicker, B. Keller	U. Zurich, Switzerland	31104	HICF-SNaPShot	LTC	226	486	147	4155	(*165*)
1AL	H. Budak	Sabanci U., Turkey	92544	HICF-SNaPShot	LTC	461	1166	133	7470	(*166*)
1BS	T.Fahima, A. Korol	U. Haifa, Israel	55296	HICF-SNaPShot	LTC	261	2430	35	6447	(*167*)
1BL	E. Paux	INRA-GDEC, France	92160	HICF-SNaPShot	LTC	502	961	162	6023	(*168*)
1D,4D,6D	B. Gill	KSU, USA	286464	HICF-SNaPShot	LTC	1,690	1910	274	25650	
2AS	K.Singh	ICAR, Nat. Research Centre on Plant Biotechnology, New Delhi, India	55648	HICF-SNaPShot	LTC	496	2098	72	4442	
2AL			76800	HICF-SNaPShot	LTC	739	808	292	7708	
2BS	J. Jacobs	Bayer CropScience	67968	WGP™	LTC	385	3800	33	4805	
2BL			70656	WGP™	LTC	463	3900	34	6051	
2DS	J. Jacobs	Bayer CropScience	43008	WGP™	LTC	246	6600	14	3025	
2DL			58368	WGP™	LTC	359	4800	24	4840	
3AS	B. Gill	KSU, USA	110692	HICF-SNaPShot	FPC	432	674	144	5187	
3AL			78952	HICF-SNaPShot	FPC	515	986	136	5342	
3B	E. Paux	INRA Clermont Ferrand	150144	HICF-SNaPShot	FPC	811	857	390	9216	(*169*)

3DS	J. Bartoš, J. Doležel	IEB, Olomouc, Czech Republic	36864	HICF-SNaPShot	FPC	262	487	160	3823	(*170*)
3DL	J. Wright	Earlham Institute	64152	HICF-SNaPShot	FPC	637	897	138	6144	
4AS	M.Valarik, J. Doležel	IEB, Olomouc, Czech Republic	49152	HICF-SNaPShot	LTC	312	1359	60	4422	
4AL			92160	HICF-SNaPShot	LTC	479	480	273	8526	(*171*)
4BS	J. Jacobs	Bayer CropScience	58368	WGP™	LTC	348	4100	27	4870	
4BL			63744	WGP™	LTC	405	4300	30	5299	
5AS	D.Barabaschi, L. Cattavelli	CREA-GRC, Italy	46080	HICF-SNaPShot	LTC	330	820	128	4360	(*172*)
5AL			90240	HICF-SNaPShot	LTC	676	563	407	5528	
5BS	E. Salina	Inst.Cytology & Genetics, Novosibirsk, Russia	43776	HICF-SNaPShot	LTC	354	3078	34	3090	(*173*)
5BL	J. Jacobs	Bayer CropScience	76800	WGP™		567	4000	43	6166	
5DS	H. Budak	Sabanci U., Turkey	36864	HICF-SNaPShot	LTC	177	2173	27	2527	(*174*)
5DL	J. Jacobs	Bayer CropScience	72960	WGP™	LTC	352	4100	26	4753	
6AS	T.SchnurbuschN. Stein	IPK-Gatersleben, Germany	49152	WGP™	LTC	522	1090	1106	5139	(*69*)
6AL			55296	WGP™	LTC	543	945	921	5621	
6BS	H. Handa	NARO, Japan	57600	WGP™	FPC	492	1503	87	4983	(*70*)
6BL			76032	WGP™	FPC	495	2422	65	5981	
7AS	R. Appels	Murdoch U. Australia	58368	HICF-SNaPShot	FPC/LTC	353	1380	81	5280	(*58*)
7AL			61056	HICF-SNaPShot	FPC/LTC	402	1700	64	5832	
7BS	O-A. Olsen	NMBU, Ås, Norway	49152	HICF-SNaPShot	LTC	298	6367	14	3039	(*175*)

7BL			72960	HICF-SNaPShot	LTC	451	6820	22	5229	
7DS	H. Šimková, J. Doležel	IEB, Olomouc, Czech Republic	49152	HICF-SNaPShot	FPC	370	528	205	4608	(*176*)
7DL	S. Weining	Northwest A&F U., China	50304	HICF-SNaPShot	FPC	484	361	353	4457	

Table S4.

Summary of the Whole Genome Profiling Tags generated from chromosome-specific BAC libraries used for physical map construction.

Chromosome / chromosome arm	BAC library	Number of BACs with tags	Number of unique tags	Total number of tags (50bp)	Av. tags / BAC	Number of tags used for pseudomolecule assembly	Publication
2BS	TaaCsp2BShA	61,707	394,587	2,131,095	34.5	55947	
2BL	TaaCsp2BLhA	63,503	621,776	2,231,411	35.1	43084	
2DS	TaaCsp2DShA	37,634	136,792	1,129,020	30.0	19797	
2DL	TaaCsp2DLhA	50,586	212,681	1,410,847	27.9	28357	
4BS	TaaCsp4BShA	52,435	411,761	1,671,137	31.9	43957	
4BL	TaaCsp4BLhA	57,688	528,688	2,005,054	34.8	53669	
5BL	TaaCsp5BLhA	64,584	222,147	2,579,840	39.8	26666	
5DL	TaaCsp5DLhA	64,492	507,176	1,970,200	30.5	32153	
6AS	TaaCs6AShA	19,289	109,611	572,883	29.7	16634	(*69*)
6AL	TaaCsp6ALhA	18,660	108,811	533,676	28.6	16277	
6BS	TaaCsp6BShA	35,515	122,164	731609	20.6	17971	(*70*)
6BL	TaaCsp6BLhA	45,895	113,522	1,000,511	21.8	17933	

Table S5.

Summary of WGP™ tags derived from chromosome-specific BAC MTPs

		50 nucleotide tags				75 nucleotide tags				100 nucleotide tags				
Chromosome / chromosome arm	**MTP BAC library**	**Number of BACs with tags**	**Number of unique tags**	**Total number of tags**	**Av. tags / BAC**	**Number of BACs with tags**	**Number of unique tags**	**Total number of tags**	**Av. tags / BAC**	**Number of BACs with tags**	**Number of unique tags**	**Total number of tags**	**Av. tags / BAC**	**Number of tags used for pseudomolecule assembly**
1AS	TaaCsp1AShMTPv2	3959	75167	140619	35.5	3956	92424	166686	42.1	3950	102793	179461	45.4	24512
1AL	TaaCsp1ALhMTP	7336	148572	261979	35.7	7335	181130	304937	41.6	7336	197618	322605	44.0	45795
1BS	TaaCsp1BShMTP	6144	128429	257233	41.9	6150	359236	302783	49.2	6151	181504	328151	53.3	31302
1BL	TaaCsp1BLhMTPv1	8305	198096	366881	44.2	8312	241343	421272	50.7	8314	268405	448763	54.0	43746
1D,4D,6D	TaaCsp146eAMTP	6252	188623	256932	41.1	6270	237117	307074	49.0	6270	261970	328183	52.3	50220
1D,4D,6D	TaaCsp146eBMTP	13138	288739	448047	34.1	1315	368206	533811	40.6	13158	417627	574062	43.7	62094
1D,4D,6D	TaaCsp146eCMTP	5099	148154	186276	36.5	5101	184322	224430	43.6	5098	204719	239829	47	41698
2AS	TaaCsp2AShMTP	4533	113824	200290	44.2	4537	140903	236978	52.2	4539	155757	254287	56.0	39996
2AL	TaaCsp2ALhMTP	7735	146803	307254	39.7	7742	187907	369520	47.7	7741	216251	403114	52.1	43833
3AS	TaaCsp3AShMTP	5142	110043	198397	38.6	5143	132253	229330	44.6	5144	143548	242196	47.1	35360
3AL	TaaCsp3ALhMTP	5286	128787	194163	36.7	5286	154840	224254	42.4	5277	167608	237126	44.9	37824
3DS	TaaCsp13DShMTP	3780	92020	153511	40.6	3781	114850	184610	48.8	3782	130252	202109	53.4	27236
3DL	TaaCsp3DLhMTPv2	6081	117939	216120	35.5	6111	150115	261857	42.9	6130	172814	286789	46.8	37772
4AS	TaaCsp4AShMTP	4346	105516	192637	44.3	4346	122266	216065	49.7	4346	128183	223083	51.3	38543
4AL	TaaCsp4LShMTP	8240	176224	333128	40.4	8244	204680	368365	44.7	8244	215597	377772	45.8	43071
5AS	TaaCsp5AShMTPv2	5222	90394	191508	36.7	5228	104266	213930	40.9	5237	109488	220815	42.2	30741
5AL	TaaCsp5ALhMTPv2	8438	140730	300857	35.7	8438	167841	341026	40.4	8439	180282	356059	42.2	41496
5BS	TaaCsp5BShMTP	3117	77581	122607	39.3	3120	88001	135864	43.5	3118	92062	140336	45.0	20803
5DS	TaaCsp5DShMTP	2486	50401	95729	38.5	2489	60119	111671	44.9	2491	64947	118401	47.5	26666
7AS	TaaCsp7AShMTP	5712	151105	289804	50.7	5713	187408	341961	59.9	5716	208805	367791	64.3	40153
7AL	TaaCsp7ALhMTP	5706	138089	279147	48.9	5707	176141	337729	59.2	5707	203589	371525	65.1	38086
7BS	TaaCsp7BShMTP	3261	86318	150529	46.2	3263	100159	170956	52.4	3263	106773	179148	54.9	27729
7BL	TaaCsp7BLhMTP	5325	140869	253035	47.5	5322	165648	286549	53.8	5323	178900	301495	56.6	33144
7DS	TaaCsp7DShMTP	4545	107292	180326	39.7	4547	124412	202896	44.6	4547	130603	209492	46.1	33470
7DL	TaaCsp7DLhMTP	4358	117167	175779	40.3	4357	135725	197390	45.3	4358	142605	203679	46.7	32130

Table S6.

Chromosome-specific assembled BAC MTP sequences

Chromosome / chromosome arm	Project leader	Institution	Number of sequences	N50 (kb)	Total Length (Mb)	BAC format	Sequencing technology	Assembly algorithm	Publication
1A	C. Pozniak	U. Saskatchewan, Canada	45301	52	1218	single BACs	Illumina PE + MP	RAY, sspace	
1B	E. Paux	INRA-GDEC, France	13227	351	920	BAC pools	Illumina PE + 5kb MP	Newbler + sspace	
3B	C. Feuillet	INRA-GDEC, France	9158	167	1360	BAC pools	Roche-454 MP + finishing	Newbler	(*14*)
3DS	J. Bartoš,	IEB, Olomouc, Czech Republic	50760	49	498	single BACs	Illumina PE	RAY, CAP3	
3DL	M. Clark	Earlham Institute, UK	67447	28	728	single BACs	Illumina PE	ABySS / SOAPdenovo	(*177*)
4AL	M. Valarik, J. Doležel	IEB, Olomouc, Czech Republic	4470	43	46	single BACs	Illumina PE	CLC Bio genomic software	(*171*)
5BS	E. Salina	Inst.Cytology & Genetics, Novosobirsk, Russia.	17700	4	26	single BACs	Ion Torrent	MIRA	(*178*, *179*)
	N. Ravin	Research Center of Biotechnology RAS, Russia	12788	22	103	BAC pools	Roche-454	Newbler	
6B	H. Handa	NARO, Japan	24611	71	809	single BACs	Roche-454	GS assembler	
7A	R. Appels	Murdoch U., Australia	74190	28	878	BAC pools	Illumina PE	ABySS	(*58*)
7B	O-A. Olsen	NMBU, Ås, Norway	928529	26	1869	single BACs	Illumina PE	SOAPdenovo	
7DS	H. Šimková	IEB, Olomouc, Czech Republic	19455	72	562	BAC pools	Illumina PE	SASSY	
7DL	S. Weining	Northwest A&F U., China	7237	137	764	single BACs	Illumina PE + PacBio reads	SOAPdenovo	

Table S7.

Summary of the Group 7 chromosome Bionano optical map assemblies

Chromosome arm	7AS	7AL	7BS	7BL	7DS*	7DL
Arm size (Mb)	407	407	360	540	381	346
No, of arms sorted (million)	2.8	2.8	2.8	2.8	1.6	2.8
Purity of sorted arm (%)	80	86	83	87	84	83
DNA amount (µg)	2.3	2.3	2.1	3.1	1.2	2.0
Raw data > 150 kb (Gb)	78	97	248	131	69	118
Filtered molecules N50 (kb)	206	232	225	231	354	210
Arm coverage	192x	238x	689x	243x	181x	341x
No, of contigs	783	330	254	626	371	364
Assembly length (Mb)	447	413	355	512	350	316
Contig N50 (Mb)	1.6	2.1	2.0	1.5	1.3	1.3
Average contig length (Mb)	0.57	1.25	1.4	0.82	0.94	0.87

*** (*68*)**

Table S8.

Summary of marker distribution in the sub-genomes of Wheat Whole Genome Radiation Hybrid Maps

Genome	Number of markers per sub-genome	Total map length in centiRay(cR) (sub-genome level)	Average map resolution (Mb/cR)
D-chromosomes	4,584	5,245	0.8
B-chromosomes	2,206	5,550	1.02
A-chromosomes	1,731	5,694	0.93
Whole genome	**8,521**	**16,489**	**0.97**

Table S9.

Molecular markers assigned to IWGSC RefSeq v1.0.

Marker type[1]	Total markers mapped	Number of unique marker positions
SSR	595	504
SNP	875279	205807
DArt	4215	3025
EST	14508	6689
ISBP	4607897	4512979

[1]Details with respect to included markers and accessing GFF documents for the sequences can be found at https://wheat-urgi.versailles.inra.fr/Seq-Repository

Table S10.

Summary of miRNA content of wheat chromosomes

Chromosome	Number of unique pre-miRNA/mature miRNA pairs	Number of miRNA families	Highest abundance	Chromosome-specific miRNAs
1A	2342	46	miR1130	-
1B	4064	47	miR1130	-
1D	2532	47	miR1130	-
2A	3101	51	miR1130	-
2B	5199	52	miR1130	miR9774
2D	3364	51	miR1130	miR6224
3A	2899	47	miR1117	-
3B	5262	52	miR1130	-
3D	3042	50	miR1130	miR9669
4A	3210	45	miR1117	-
4B	3694	46	miR1130	miR5085, miR7742
4D	2070	47	miR1130	miR5169
5A	2862	55	miR1117	miR5183, miR528
5B	4831	56	miR1130	miR8155
5D	2792	56	miR1130	miR9672
6A	2331	45	miR1117	-
6B	4383	51	miR1130	miR9659, miR9663
6D	2221	51	miR1130	miR5566, miR6219, miR9662
7A	3341	55	miR1117	miR8740, miR9671
7B	4858	49	miR1130	-
7D	3352	52	miR1130	-

Table S11.

Delimiting centromeres based on CENH3 ChIP-seq.

Chromosome	**CENH3-enriched intervals**				
	Pseudomolecule positions (Mb)				Total length (Mb)
1A	210.2-215.8				5.7
1B	237.7-243.5				5.9
1D	166.2-173.8				7.7
2A	326.3-327.0	339.4-342.0	359.3-359.5		3.8
2B	344.4-351.3				7.0
2D	264.4-272.5				8.2
3A	316.9-319.9				3.1
3B	345.8-347.0	348.5-349.0			1.9
3D	237.1-243.2				5.5
4A	264.1-267.9	315.1-315.7			4.6
4B	303.9-304.4	317.8-319.6			2.5
4D	182.3-188.2				6.0
5A	108.9-109.1	248.7-249.0	252.5-255.1		3.4
5B	198.9-202.5				3.7
5D	185.6-188.7				3.2
6A	283.3-288.7	290.7-292.5			7.4
6B	323.0-327.5				4.6
6D	211.9-217.4				5.6
7A	360.2-363.8				3.7
7B	288.2-288.3	294.4-294.6	296.4-296.5	308-310.1	2.9
7D	336.3-341.7				5.5
Average					**4.9**
chrUn					39.8
Average incl, chrUn					**6.7**

chrUn - unassigned scaffolds

Table S12.

Summary of changes made to RefSeq Annotation v1.0 by integrating manually curated genes.

Integration status	IWGSC Annotation v1.0 HC genes	IWGSC Annotation v1.1 HC genes
No change	104,201	104,206
Add	-	528
Replace	3,020	3,020
Merge	224	94
Split	14	28
Multilocus	16	15
Total	107,475	107,891

Table S13.

Illumina RNA-Seq reads from the following datasets were used to support annotation integration: six different tissues described in (*8*) (PRJEB15048), grain-development samples from (*38*) (ERP004505), reads from (*6*) (ERP004714) collapsed into grain, leaf, root, spike and stem samples, seedling samples under normal condition and subjected to drought stress and heat stress (PRJNA257938) and reads from FHB challenged near isogenic wheat lines (PRJEB4202).

	PRJEB15048	ERP004505	ERP004714	PRJNA257938	PRJEB4202
Number of samples	6	7	5	7	20
Number of reads	731,931,657	873,550,049	1,412,029,174	921,578,806	1,827,362,091
Average no of reads per sample	121,988,610	124,792,864	282,405,835	131,654,115	91,368,105
Average overall alignment rate	95.93%	89.11%	93.84%	81.29%	87.12%

Table S14.

Pacific BioSciences trancript sequence (PacBio) reads (PRJEB15048) and alignments to IWGSC RefSeq v1.0 used to support annotation integration.

Stage	Leaf	Root	Seed	Seedling	Spike	Stem	Total
Total	199,119	315,137	219,965	209,923	277,704	287,474	1,509,322
Aligned	191,967	304,087	212,603	203,578	267,912	275,817	1,455,964
Aligned (%)	96.41%	96.49%	96.65%	96.98%	96.47%	95.95%	96.46%

Table S15.

Protein alignments used to support annotation integration, Protein sequences from 6 species were soft masked for low complexity (segmasker from NCBI BLAST+ 2,3,0) and aligned to the soft masked genome with exonerate v2.2.0 (*94*), Proteins were filtered at 50% identity and 80% coverage.

	A. thaliana	*B. distachyon*	*O. sativa*	*S. bicolor*	*S. italica*	*Z. mays*
Total Proteins	48,359	52,972	49,061	47,205	43,001	88,760
Proteins Aligned	15,683	36,710	27,359	27,335	27,146	44,252
Proteins Aligned (%)	32.43%	69.30%	55.77%	57.91%	63.13%	49.86%
Protein Alignments	82,321	181,573	141,023	137,605	138,783	224,775

Table S16.

Transcript assembly statistics.

Method	Loci	Transcripts	Average no of exons	Average cDNA size	Number of monoexonic transcripts
CLASS	342,738	5,821,796	5.61	1,335,32	628,375
Cufflinks	337,372	6,089,845	4.59	1,659,69	1,677,144
StringTie	499,560	5,999,887	4.73	1,683,71	1,682,569
Mikado PacBio	80,119	114,233	6.2	2,000,61	18,871
Mikado Illumina and PacBio	278,015	406,886	4	1,247,67	169,516

Table S17.

Metrics used for scoring transcripts.

Metric	Weighting	Metric type
Mean F1 across the base, exon and junction level vs. the best match among aligned PacBio transcripts	X 10	Evidence based
Mean F1 across the base, exon and junction level vs. the best match among Mikado RNA-Seq models	X 10	Evidence based
Mean F1 across the base, exon and junction level vs. the best match among aligned proteins (Table S14)	X 10	Evidence based
BLAST Query coverage of the best BLAST alignment across the protein databases (species described in Table S14 + uniprot Magnoliophyta)	X 10	Evidence based
BLAST Target coverage of the best BLAST alignment across the protein databases (species described in Table S14 + uniprot Magnoliophyta)	X 10	Evidence based
Proportion of Portcullis-verified introns assigned to the locus that can be found in the transcript	X 10	Evidence based
Proportion of introns that are canonical within the transcript	X 2	Intrinsic
Longest CDS	X 1	Intrinsic
Penalty on the number of introns greater than 50kbps	X -10	Intrinsic
Penalty for any transcript with introns over 10kbps	X -2	Intrinsic
Penalty on the presence of exons over 20kbps	X -10	Intrinsic

Table S18.

Characteristics of IWGSC RefSeq v1.1 wheat genes.

RefSeq V1.1	All	A	B	D	Unknown
Genes	269,428	86,930	94,002	79,047	9,449
Transcripts	298,775	96,383	103,931	88,631	9,830
Transcripts per gene	1.11	1.11	1.11	1.12	1.04
Transcript mean size cDNA (bp)	1,131,59	1,124,54	1,120,58	1,183,67	847,42
Exons per transcript	3.57	3.59	3.50	3.76	2.34
Exon mean size (bp)	317,32	313,52	320,00	315,22	362,32
Transcript mean size CDS (bp)	934,42	929,70	927,10	969,20	744,44
Single exon transcripts	131,105 (43.9%)	42,007 (43.58%)	46,387 (44.63%)	37,355 (42.15%)	5,356 (54.49%)
Genes with alternative splicing	19,762 (7.3%)	6,389(7.3%)	6,690(7.1%)	6,412(8.1%)	271(2.9%)
High Confidence (HC)	**All**	**A**	**B**	**D**	**Unknown**
Genes	107,891	35,345	35,643	34,212	2,691
Transcripts	133,745	43,697	44,221	42,828	2,999
Transcripts per gene	1.24	1.24	1.24	1.25	1.11
Transcript mean size cDNA (bp)	1,699,27	1,672,81	1,716,87	1,733,26	1,339,99
Exons per transcript	5.60	5.62	5.62	5.71	3.54
Exon mean size (bp)	303,34	297,65	305,70	303,38	378,69
Transcript mean size CDS (bp)	1,333,32	1,310,85	1,351,15	1,354,32	1,097,94
Single exon transcripts	26,973 (20.2%)	8,605 (19.69%)	8,872 (20.06%)	8,457 (19.75%)	1,039 (34.64%)
Genes with alternative splicing	16,961 (15.7%)	5,507(15.6%)	5,610(15.7%)	5,638(16.5%)	206(7.7%)
Low Confidence (LC)	**All**	**A**	**B**	**D**	**Unknown**
Genes	161,537	51,585	58,359	44,835	6,758
Transcripts	165,030	52,686	59,710	45,803	6,831
Transcripts per gene	1.02	1.02	1.02	1.02	1.01
Transcript mean size cDNA (bp)	671,52	669,85	678,96	669,78	631,16
Exons per transcript	1.92	1.90	1.94	1.92	1.81
Exon mean size (bp)	350,44	352,47	350,72	348,10	348,29
Transcript mean size CDS (bp)	611,15	613,52	613,10	609,15	934,42
Single exon transcripts	104,132 (63.1%)	33,402 (63.40%)	37,515 (62.83%)	28,898 (63.09%)	4,317 (63.20%)
Genes with alternative splicing	2,801 (1.7%)	882(1.7%)	1080(1.8%)	774(1.7%)	65(0.9%)

Table S19.

Automated Assignment of Human Readable Descriptions (AHRD) annotation of wheat gene models identified in RefSeq Annotation v1.0. Classification of HC genes by their functional description via disTEG (distinction between TEs and Genes). Note: for RefSeq Annotation v1.1 genes with obvious transposon descriptions (3318 HC genes) were re-classified as LC-TE.

	disTEG tag	**Wheat CS IWGSC HC genes v1.0**		**Wheat CS IWGSC LC genes v1.0**		
		Number	**%**	**Number**	**%**	
	G	99,118	89.5	81,552	51.4	canonical genes
	U	301	0.3	595	0.4	unknown
	TE?	8,083	7.3	15,099	9.5	potential transposons
	TE	3,288	3.0	61,526	38.8	obvious transposons
	sum	110,790	100	158,772	100	
Without TEs (G-TE)		**107,502**	97.0	97,246	61.2	
G-TE: with good scoring functional annotation		90,919	82.1			

Table S20.

Ontology term annotation statistics. 5,182,416 associations to 8,133 unique ontology terms describing biological processes, molecular functions, anatomical entities, developmental stages or genetically linked phenotypic traits of orthologous genes in well-characterized plant models like Arabidopsis, rice and maize were obtained for 117,595 wheat genes in 16,662 gene families. A) Summary of ontology term associations for each of the three source ontologies (Plant Ontology (PO), (*117*); Gene Ontology (GO), (*116*); Plant Trait Ontology (TO), https://bioportal.bioontology.org/ontologies/PTO). B) Summary of ontology term associations by evidence class (IEA-Inferred Electronic Annotation; EXP – Inferred from Experiment; ISM – Inferred from Sequence Model).

A) Ontology	**Number of associations**	**Number of families**	**Number of sequences**	**Number of terms**
PO	3,622,724	12,631	79,530	446
GO	1,560,102	15,983	113,815	7,408
TO	8,173	227	1,060	279
B) Evidence_code	**Count**			
ISO	4,989,419			
IEA	177,154			
ISM	155,326			

Table S21.

Genome-wide pseudogene analysis based on pseudogenes identified by *de novo* homology analysis of HC genes and disrupted or truncated gene models in the LC gene set: Sub-genome distribution and basic statistics for pseudogene set identified by *de novo* homology analysis.

Sub-genome	Genome-wide approach	LC-only	Total	%
Chr Un	13,062		13,062	
A	94,686	5,068	99,754	33%
B	103,353	5,744	109,097	36%
D	77,738	4,167	81,905	27%
All	288,839	14,979	303,818	100%

Table S22.

Genome-wide analysis based on pseudogenes identified by *de novo* homology analysis of HC genes and disrupted or truncated gene models in the LC gene set: Number and pseudogene types for all pseudogenes, subdivided by high and low coverage classes and sub-genome distribution. High coverage pseudogenes are represented by at least 80% of the CDS of a parent gene locus, low coverage below 80% (see also 4.5.2).

	number	%	mean length	mean coverage	mean identity	with ptc	% with ptc
all pseudogenes	**288,839**	**100.0**	**342.8**	**38.5**	**89.5**	**168,096**	**58.2**
-- duplicated	73,241	25.4	529.7	49.9	91.3	51,988	71.0
-- processed	7,199	2.5	347.8	42.2	89.8	5,062	70.3
-- single exon gene	85,754	29.7	348.1	52.2	88.6	47,040	54.9
-- single exon isoform	55	0.0	678.0	39.1	90.8	40	72.7
-- fragmented	118,587	41.1	213.1	20.8	88.9	60,471	51.0
-- chimeric	4,003	1.4	636.4	50.9	91.3	3,495	87.3
HighCov	**48,619**	**16.8**	**738.8**	**94.6**	**92.1**	**33,284**	**68.5**
-- duplicated	20,464	42.1	939.5	94.8	93.1	15,569	76.1
-- processed	1,372	2.8	623.5	94.1	92.0	1,029	75.0
-- single exon gene	23,589	48.5	564.1	94.7	91.3	14,217	60.3
-- single exon isoform	8	0.0	1,674.1	94.2	96.2	8	100.0
-- fragmented	1,974	4.1	708.5	91.6	91.6	1,363	69.1
-- chimeric	1,212	2.5	922.0	93.1	92.9	1,098	90.6
LowCov	**240,220**	**83.2**	**262.6**	**27.1**	**88.9**	**134,812**	**56.1**
-- duplicated	52,777	22.0	370.8	32.4	90.5	36,419	69.0
-- processed	5,827	2.4	282.9	29.9	89.3	4,033	69.2
-- single exon gene	62,165	25.9	266.1	36.1	87.5	32,823	52.8
-- single exon isoform	47	0.0	508.4	29.8	89.8	32	68.1
-- fragmented	116,613	48.5	204.7	19.6	88.9	59,108	50.7
-- chimeric	2,791	1.2	512.4	32.6	90.5	2,397	85.9
subgenome A	94,686	32.8	330.9	38.0	89.5	55,349	58.5
subgenome B	103,353	35.8	345.7	38.2	89.4	60,540	58.6
subgenome D	77,738	26.9	347.3	39.5	89.5	45,540	58.6
unknown	13,062	4.5	379.1	37.3	90.4	6,667	51.0
HighCov subgenome A	15,241	31.4	732.6	94.5	92.1	10,653	69.9
HighCov subgenome B	17,308	35.6	758.4	94.5	91.9	12,019	69.4
HighCov subgenome D	14,260	29.3	721.1	94.7	92.3	9,575	67.2
HighCov unknown	1,810	3.7	742.5	94.5	93.4	1,037	57.3

Table S23.

Species and genome annotation versions utilized for the phylogenomics analysis.

Taxon	NCBI taxonomy ID	Source	Original filename
Triticum aestivum A	4565	This study	Triticum_aestivum.IWGSC_V1.0_March_2017.all.proteins.subgenome_A.representative.fasta
Triticum urartu	4572	(*52*)	Triticum_urartu.ASM34745v1.pep.representative.fasta
Triticum aestivum B	4565	This study	Triticum_aestivum.IWGSC_V1.0_March_2017.all.proteins.subgenome_B.representative.fasta
Aegilops tauschii	37682	(*180*)	Aegilops_tauschii.ASM34733v1.pep.all.fa
Triticum aestivum D	4565	This study	Triticum_aestivum.IWGSC_V1.0_March_2017.all.proteins.subgenome_D.representative.fasta
Secale cereale	4550	(*153*)	RyeMIPSv3final_PROT_mar14.fa
Hordeum vulgare subsp, vulgare cv. Morex	112509	(*144*)	Hvulgare.IBSC_PGSB_r1.only_representative.proteins_HighConf.fa
Hordeum vulgare var. nudum	112509	(*181*)	Tibetan_Hulless_barley.pep.fa
Brachypodium distachyon	15368	Phytozome 12	Bdistachyon_314_v3.1.protein_primaryTranscriptOnly.fa
Oryza sativa	4530	Phytozome 12	Osativa_323_v7.0.protein_primaryTranscriptOnly.fa
Sorghum bicolor	4558	Phytozome 12	Sbicolor_313_v3.1.protein_primaryTranscriptOnly.fa
Zea mays cv. B73	4577	Phytozome 12	Zmays_284_Ensembl-18_2010-01-MaizeSequence.protein_primaryTranscriptOnly.fa
Arabidopsis thaliana	3702	Phytozome 12	Athaliana_447_Araport11.protein_primaryTranscriptOnly.fa
Selaginella moellendorffii	88036	Phytozome 12	Smoellendorffii_91_v1.0.protein_primaryTranscriptOnly.fa
Physcomitrella patens	3218	Phytozome 12	Ppatens_318_v3.3.protein_primaryTranscriptOnly.fa
Chlamydomonas reinhardtii	3055	Phytozome 12	Creinhardtii_281_v5.5.protein_primaryTranscriptOnly.fa

Table S24.

Groups of homeologous genes in the wheat genome. A homeologous gene group represents a group of shared genes among the A, B and/or D sub-genomes that were inferred as "sub-genome orthologs" by species tree reconciliation in the respective gene family. Unless otherwise stated numbers include both HC and LC genes filtered for TEs. * Sub-genome-specific genes are supported by at least one ortholog in the reference grass species.

homeologous group (A:B:D)	# in wheat genome	% of groups	# genes in A	# genes in B	# genes in D	# total genes	% genes A	% genes B	% genes D	%genes total
1:1:1	21,603	55.1%	21,603	21,603	21,603	64,809	35.8%	33.8%	38.1%	35.8%
1:1:n	644	1.6%	644	644	1,482	2,770	1.1%	1.0%	2.6%	1.5%
1:n:1	998	2.5%	998	2,396	998	4,392	1.7%	3.7%	1.8%	2.4%
n:1:1	761	1.9%	1,752	761	761	3,274	2.9%	1.2%	1.3%	1.8%
1:1:0	3,708	9.5%	3,708	3,708	0	7,416	6.1%	5.8%	0.0%	4.1%
1:0:1	4,057	10.3%	4,057	0	4,057	8,114	6.7%	0.0%	7.1%	4.5%
0:1:1	4,197	10.7%	0	4,197	4,197	8,394	0.0%	6.6%	7.4%	4.6%
other ratios	3,270	8.3%	4,999	5,371	4,114	14,484	8.3%	8.4%	7.2%	8.0%
1:1:1 in microsynteny	18,595	47.4%	18,595	18,595	18,595	55,785	30.8%	29.1%	32.8%	30.8%
total in microsynteny	30,339	77.3%	27,240	27,063	28,005	82,308	45.2%	42.3%	49.3%	45.5%
1:1:1 in macrosynteny	19,701	50.2%	19,701	19,701	19,701	59,103	32.7%	30.8%	34.7%	32.6%
total in macrosynteny	32,591	83.1%	29,064	30,615	30,553	90,232	48.2%	47.9%	53.8%	49.8%
HC-only	26,446	67.4%	24,753	24,922	25,047	74,722	41.0%	39.0%	44.1%	41.3%
total in homeologous groups	**39,238**	**100.0%**	**37,761**	**38,680**	**37,212**	**113,653**	**62.6%**	**60.5%**	**65.5%**	**62.8%**
conserved subgenome orphans*			12,412	12,987	10,844	36,243	20.6%	20.3%	19.1%	20.0%
non-conserved subgenome singletons			10,084	12,185	8,679	30,948	16.7%	19.1%	15.3%	17.1%
non-conserved subgenome duplicated orphans			71	83	38	192	0.1%	0.1%	0.1%	0.1%
total (filtered)			60,328	63,935	56,773	181,036	100.0%	100.0%	100.0%	100.0%

Table S25.

Error assessment for homeologous groups with a potential gene loss in one subgenome. The observed differences in potential gene losses still remain significant after worst-case adjustment.

homeologous group (A:B:D)	# groups on pseudomolecules	% groups on pseudomolecules	# groups with additional copy on chrUn	% groups with additional copy on chrUn	# worst-case adjusted groups total	% worst-case adjusted groups total	# expected groups on pseudomolecules	# expected worst-case adjusted groups total
1:1:0	3,694	9.4%	576	1.5%	3,118	8.0%	3,968	3,464
1:0:1	4,036	10.3%	452	1.2%	3,584	9.2%	3,968	3,464
0:1:1	4,174	10.7%	484	1.2%	3,690	9.4%	3,968	3,464
total these groups	11,904	30.4%	1,512	3.9%	10,392	26.6%	11,904	10,392
total all groups	39,099					**χ^2 test p-value**	2.07E-07	2.46E-12

Table S26.

Phylogenomic determination of the origin of ZIP4 (within Ph1 locus on chromosome 5B). Phylogenomic analysis indicates the ancestral locus of ZIP4 is a gene model on chr3B. This inparalog has homoeologs on 3A (TraesCS3A01G401700) and 3D (TraesCS3D01G396500) and its orthologs, Sc3Loc00242129.3, HORVU3Hr1G090150.1, HVUL3H17755,2, EMT19842 are all localized on chromosome 3. The inparalog on 3B is part of syntenic blocks A:B ID=255 and B:D ID=985 (all in compartment R2b). ZIP4 is located in compartment R3 in a non-syntenic location and, although TEs are not implicated, it may be a transduplication of the original 3B locus. The 3B gene model and its homoeologs are all in transcription expression module 2, the ancestral state of the family. In contrast, the translocated copy on 5B does not associate with any of the modules, consistent with evidence of expression divergence (correlation coefficient of 5B with 3D and 3B: (TraesCS5B01G255100 | TraesCS3D01G396500 = 0.482 compared to TraesCS3B01G434600 | TraesCS3D01G396500 = 0.786). The 5B locus also has higher Ka/Ks ratios compared with the 3A and 3D homoeologs or the inparalog on 3B. Recently, a single mutant of the *ZIP4* 5B locus was sufficient to increase homoeologous crossovers when crossed with wild relatives (*21*), providing functional evidence for the unique role of the 5B locus.

x locus	y locus	Ka/Ks
TraesCS3A01G401700	TraesCS3B01G434600	0.401
TraesCS3A01G401700	TraesCS5B01G255100	0.586
TraesCS3B01G434600	TraesCS3D01G396500	0.400
TraesCS3B01G434600	TraesCS5B01G255100	0.626
TraesCS5B01G255100	TraesCS3D01G396500	0.645

Table S27.

Tandemly repeated genes and clusters in five monocotyledonous species: bread wheat (ta, v1.0 annotation), barley (hv), *Brachypodium distachyon* (bd), rice (os) and sorghum (sbi). For bread wheat HC genes an all-against-all blastp similarity table was used to construct an undirected graph with nodes representing genes and edges between two nodes if the following criteria were met: (i) an e-value $\leq 1e^{-20}$, (ii) a maximal distance of 10 genes in the genome between the gene pair, and (iii) a minimal alignment coverage $\geq$ 70% of the shorter gene. Tandem genes and clusters were retrieved as connected components of this graph. The 9,616 clusters containing 29,737 high confidence genes detected in bread wheat were compared with other monocotyledonous species by repeating the approach with the proteomes of barley (Hv v1.0 (*144*)), rice (*182*), brachypodium and sorghum (v3.1 from https://phytozome.jgi.doe.gov/pz/portal.html). The percentages of tandem genes in column 5 are related to the total numbers (column 4) of genes located on pseudochromosomes of the respective species. For wheat, this excludes gene models located on chromosome "Unknown". The table also shows the distribution of tandem genes across the A(ta-A), B(ta-B) and D(ta-D) sub-genomes.

	Number of genes	Number of clusters	Total genes	% Tandem genes
ta	29,737	9,616	108,061	27.5
hv	7,499	2,888	37,577	20.0
bd	5,235	1,879	34,303	15.3
os	6,702	2,139	38,864	17.2
sbi	6,226	2,130	34,027	18.3
ta-A	9,462	3,102	36,302	26.1
ta-B	10,735	3,385	36,738	29.2
ta-D	9,540	3,129	35,021	27.2

Table S28.

Inversions between homeologous chromosomes across the wheat genome. The numbers of inversions between chromosome pairs were determined after filtering 'uncertain regions' of pseudomolecules, all scaffolds with unknown (?) orientations in the AGP and removing inversions that have more than 30% of the genes in an 'uncertain region'.

Chromosome pairs	Inversions with >=10 genes
1A_1B	9
1A_1D	9
1B_1D	9
2A_2B	8
2A_2D	11
2B_2D	6
3A_3B	10
3A_3D	10
3B_3D	9
4A_4B	9
4A_4D	10
4B_4D	6
5A_5B	10
5A_5D	8
5B_5D	8
6A_6B	11
6A_6D	12
6B_6D	7
7A_7B	12
7A_7D	9
7B_7D	5

Table S29.

Structural and functional partitioning of wheat chromosomes. The segmentation is based on the distribution of recombination rate, gene and transposable element density, gene expression breadth, percentage of H3K36me3-, H3K9ac-, and H3K27me3-associated genes.

		Boundary location (Mb)				Region length (Mb)					Chromosomal fraction				
Chromosome	Chromosome length (Mb)	R1/R2a	R2a/C	C/R2b	R2b/R3	R1	R2a	C	R2b	R3	R1	R2a	C	R2b	R3
chr1A	594	59	151	231	480	59	92	80	249	114	9.9%	15.5%	13.5%	41.9%	19.2%
chr1B	689	62	172	277	534	62	110	105	257	155	9.0%	16.0%	15.2%	37.3%	22.5%
chr1D	495	29	98	171	385	29	69	73	214	110	5.9%	13.9%	14.7%	43.2%	22.2%
chr2A	780	42	206	379	662	42	164	173	283	118	5.4%	21.0%	22.2%	36.3%	15.1%
chr2B	801	59	248	433	660	59	189	185	227	141	7.4%	23.6%	23.1%	28.3%	17.6%
chr2D	651	37	192	338	520	37	155	146	182	131	5.7%	23.8%	22.4%	28.0%	20.1%
chr3A	750	62	249	414	670	62	187	165	256	80	8.3%	24.9%	22.0%	34.1%	10.7%
chr3B	830	66	257	407	728	66	191	150	321	102	8.0%	23.0%	18.1%	38.7%	12.3%
chr3D	615	49	167	287	543	49	118	120	256	72	8.0%	19.2%	19.5%	41.6%	11.7%
chr4A	744	41	180	414	594	41	139	234	180	150	5.5%	18.7%	31.5%	24.2%	20.2%
chr4B	673	42	186	360	537	42	144	174	177	136	6.2%	21.4%	25.9%	26.3%	20.2%
chr4D	509	10	135	288	432	10	125	153	144	77	2.0%	24.6%	30.1%	28.3%	15.1%
chr5A	709	39	140	260	427	39	101	120	167	282	5.5%	14.2%	16.9%	23.6%	39.8%
chr5B	713	52	140	221	430	52	88	81	209	283	7.3%	12.3%	11.4%	29.3%	39.7%
chr5D	565	46	128	207	345	46	82	79	138	220	8.1%	14.5%	14.0%	24.4%	38.9%
chr6A	617	46	216	409	556	46	170	193	147	61	7.5%	27.6%	31.3%	23.8%	9.9%
chr6B	720	56	221	429	651	56	165	208	222	69	7.8%	22.9%	28.9%	30.8%	9.6%
chr6D	473	44	164	280	410	44	120	116	130	63	9.3%	25.4%	24.5%	27.5%	13.3%
chr7A	736	89	239	416	659	89	150	177	243	77	12.1%	20.4%	24.0%	33.0%	10.5%
chr7B	750	12	146	418	660	12	134	272	242	90	1.6%	17.9%	36.3%	32.3%	12.0%
chr7D	638	84	200	373	552	84	116	173	179	86	13.2%	18.2%	27.1%	28.1%	13.5%

Table S30.

Publicly available RNA-Seq samples used in this study.

SRA	Samples	Study details	Analysed expVIP	Total reads	Mapped reads	%
DRP000768	12	Phosphate starvation in roots and shoots	Y	118,053,746	100,948,404	85.51
ERP004505	30	Grain tissue-specific developmental timecourse	Y	873,709,556	718,254,718	82.21
ERP008767	9	Grain tissue-specific expression	Y	45,213,827	36,308,713	80.30
SRP004884	3	Flag leaf downregulation of *GPC*	Y	102,103,001	65,221,796	63.88
SRP013449	6	Grain tissue-specific developmental timecourse	Y	132,702,451	105,655,016	79.62
SRP017303	1	Seedling leaf	Y	33,361,836	15,232,257	45.66
SRP022869	4	Seedling leaf	Y	49,619,979	41,417,307	83.47
ERP003465	60	Fusarium graminearum infected spikelets	Y	1,827,362,091	1,568,753,997	85.85
SRP028357	4	Fifth leaf shoots/roots	Y	133,881,441	119,685,598	89.40
SRP029372	7	Grain tissue-specific developmental timecourse	Y	101,477,759	38,334,982	37.78
SRP038912	3	Stamen, pistil and pistilloidy stamen	Y	217,315,378	189,209,346	87.07
SRP041017	21	Powdery mildew and yellow rust infection timecourse	Y	395,463,786	327,718,364	82.87
SRP045409	14	Drought and heat stress time-course in seedlings	Y	921,578,806	688,753,403	74.74
SRP056412	42	Grain developmental timecourse (4A dormancy QTL)	Y	615,077,336	419,124,669	68.14
ERP004714	30	Developmental time-course of CS	Y	1,536,051,415	1,320,450,267	85.96
ERP016738	6	Developmental time-course of CS	N	824,241,135	663,188,969	80.46
ERP013829	72	Fusarium graminearum timecourse (rachis, palea, lemma)	N	2,061,182,960	1,649,533,020	80.03
SRP078208	8	Fusarium pseudograminearum infected coleoptile	N	161,807,328	137,267,473	84.83
ERP015130	16	Magnaporthe oryzae infected leaf	N	351,588,058	207,187,100	58.93
SRP068165	24	PEG timecourse leaves	N	1,054,250,452	944,502,318	89.59
SRP068156	14	Fusarium graminearum + hormone infected spikelets	N	561,431,175	476,370,730	84.85
SRP067916	5	Flag leaf timecourses	N	165,495,247	142,565,852	86.14
SRP064598	9	Microspores cold treatment	N	608,252,566	401,980,553	66.09
ERP009837	30	Zymoseptoria tritici leaf infection timecourse	N	1,081,355,610	905,111,026	83.70
SRP060670	6	Fusarium graminearum infected rachis	N	61,289,682	40,916,842	66.76
SRP048912	48	Fusarium graminearum infected shoots	N	769,083,359	651,917,469	84.77
SRP043554	6	Cold stress leaves	N	224,280,385	194,356,916	86.66
ERP013983	39	Yellow rust infection timecourse	N	866,322,161	687,543,489	79.36

Table S31.

Summary of unpublished RNA-Seq samples used in this study

Study details	Samples	SRA	Total reads	Mapped reads	%
Development time-course	209	PRJEB25639	8,269,498,786	6,603,975,140	79.86%
PAMP Triggered Immune Response	21	PRJEB23056	2,436,781,618	2,156,752,129	88.51%
CS Spike	10	PRJNA436817	429,796,610	333,383,697	77.57%
Developing spike	61	PRJEB25640	780,374,855	362,666,932	46.47%
CS tissues	13	SRP133837	544,053,283	467,082,558	85.85%
Aneuploidy controls	7	PRJEB25593	752,040,275	667,605,170	88.77%

Table S32.

Number of samples and tissue complexity of intermediate tissue represented in the 850 RNA-Seq samples. [1] Detailed description of wheat-specific terminology: **http://bio-gromit.bio.bris.ac.uk/cerealgenomics/WheatBP/glossary.htm**

Intermediate tissue [1]	Sample number	High-level tissue	Genes accounting for 50% tpm
Aleurone	12	Grain	803
Aleurone layer and starchy endosperm	4	Grain	47
Embryo	3	Grain	1,877
Endosperm	25	Grain	57
Endosperm + seed coat	3	Grain	247
Grain hard dough and ripening	22	Grain	289
Grain milk and soft dough	40	Grain	143
Seed coat	6	Grain	1,062
Transfer cells	4	Grain	46
Flag leaf	26	Leaves	891
Flag leaf blade	30	Leaves	1,646
Flag leaf sheath	12	Leaves	2,154
Internode	15	Leaves	3,909
Leaf blades excluding flag leaf	27	Leaves	1,345
Leaf excluding flag leaf	73	Leaves	1,576
Leaf ligule	3	Leaves	2,557
Leaf sheaths excluding flag leaf	12	Leaves	3,408
Peduncle	9	Leaves	2,194
Seedling aerial tissues	164	Leaves	2,321
Shoot apical meristem	6	Leaves	3,110
Shoot axis	12	Leaves	3,676
Vegetative aerial tissues	14	Leaves	1,473
Root apical meristem	6	Root	2,709
Roots	44	Root	4,569
Anther	5	Spike	3,182
Awns	6	Spike	1,985
Glumes	12	Spike	3,351
Microspores	9	Spike	1,042
Rachis	8	Spike	3,372
Spike	81	Spike	925
Spikelets	149	Spike	5,197
Stigma & ovary	8	Spike	3,652

Table S33.

Over- and under-represented GO slim terms based on chromosome compartment, Empty cells correspond to non-significant values.

			Over-represented			Under-represented		
Ontology	**GO_slim**	**Description**	**Distal**	**Interstitial**	**Proximal**	**Distal**	**Interstitial**	**Proximal**
BP	GO:0008219	cell death	1.4E-18				0.0E+00	
	GO:0009607	response to biotic stimulus	1.5E-16				0.0E+00	3.2E-03
	GO:0019748	secondary metabolic process	2.2E-13				0.0E+00	3.3E-03
	GO:0009605	response to external stimulus	9.0E-10				0.0E+00	
	GO:0006950	response to stress	4.8E-09				4.8E-09	2.3E-02
	GO:0009719	response to endogenous stimulus	5.8E-08				5.3E-07	3.4E-06
	GO:0007154	cell communication	3.1E-07				3.0E-06	
	GO:0009875	pollen-pistil interaction	2.1E-05				5.5E-05	
	GO:0009991	response to extracellular stimulus	2.7E-02				2.7E-02	
	GO:0006139	nucleobase-containing compound metabolic process		1.5E-47	1.4E-11	0.0E+00		
	GO:0016043	cellular component organization		3.1E-27	3.0E-10	0.0E+00		
	GO:0009987	cellular process		2.4E-24	7.4E-12	0.0E+00		
	GO:0008152	metabolic process		3.5E-22	5.7E-04	0.0E+00		
	GO:0009058	biosynthetic process		3.3E-20	2.0E-03	0.0E+00		
	GO:0006259	DNA metabolic process		5.6E-20	5.7E-07	0.0E+00		
	GO:0008150	biological_process		5.8E-18	9.4E-07	0.0E+00		
	GO:0006091	generation of precursor metabolites and energy		6.9E-15	7.7E-12	0.0E+00		
	GO:0005975	carbohydrate metabolic process		9.4E-13		0.0E+00		
	GO:0007049	cell cycle		7.7E-10	1.2E-07	0.0E+00		
	GO:0030154	cell differentiation		2.8E-09	2.3E-02	8.9E-09		
	GO:0006810	transport		4.3E-09	1.2E-07	2.8E-08		
	GO:0007275	multicellular organism development		3.8E-08	1.8E-03	4.0E-07		
	GO:0006412	translation		1.3E-07	3.9E-08	5.1E-07		
	GO:0040029	regulation of gene expression, epigenetic		5.7E-07	8.6E-08	2.3E-06		
	GO:0009628	response to abiotic stimulus		5.4E-06		1.0E-05		
	GO:0000003	reproduction		3.0E-05	1.2E-02	3.4E-05		
	GO:0009606	tropism		6.9E-05	7.5E-03	8.6E-05		
	GO:0009791	post-embryonic development		5.5E-03		5.5E-03		
	GO:0015979	photosynthesis		7.8E-03	1.0E-12	7.9E-03		
	GO:0009653	anatomical structure morphogenesis		9.3E-03		9.2E-03		
	GO:0016049	cell growth		2.0E-02		2.0E-02		
	GO:0019538	protein metabolic process			1.2E-07			

	GO:0006464	cellular protein modification process			1.2E-03			
CC	GO:0030312	external encapsulating structure	4.2E-11				0.0E+00	1.5E-02
	GO:0005618	cell wall	3.1E-07				2.0E-06	2.0E-03
	GO:0005575	cellular component		2.9E-246	3.9E-57	0.0E+00		
	GO:0005623	cell		1.6E-225	6.5E-64	0.0E+00		
	GO:0005622	intracellular		1.4E-207	7.8E-60	0.0E+00		
	GO:0005737	cytoplasm		2.6E-104	9.8E-33	0.0E+00		
	GO:0009536	plastid		1.7E-22	3.8E-17	0.0E+00		
	GO:0016020	membrane		4.5E-19	1.3E-13	0.0E+00		
	GO:0005739	mitochondrion		1.7E-16	2.6E-08	0.0E+00		
	GO:0005634	nucleus		1.4E-14	2.4E-08	0.0E+00		
	GO:0005856	cytoskeleton		2.1E-14	3.9E-04	0.0E+00		
	GO:0005794	Golgi apparatus		4.6E-12	4.4E-04	0.0E+00		
	GO:0005654	nucleoplasm		1.2E-10	1.0E-04	0.0E+00		
	GO:0005635	nuclear envelope		1.3E-05		3.1E-05		
	GO:0005773	vacuole		4.6E-03		4.5E-03		
	GO:0005777	peroxisome		1.0E-02		1.0E-02		
	GO:0005840	ribosome			4.7E-08			
	GO:0009579	thylakoid			4.1E-07			
	GO:0005829	cytosol			2.3E-03			
MF	GO:0000166	nucleotide binding	1.6E-39				0.0E+00	
	GO:0030246	carbohydrate binding	6.8E-36				0.0E+00	3.2E-03
	GO:0016301	kinase activity	1.8E-19				0.0E+00	
	GO:0016740	transferase activity	1.2E-13				0.0E+00	8.7E-08
	GO:0003674	molecular function	9.6E-06				2.3E-05	
	GO:0004871	signal transducer activity	4.0E-04				4.2E-04	
	GO:0004872	receptor activity	7.9E-03				7.9E-03	
	GO:0030234	enzyme regulator activity	1.8E-02				1.8E-02	
	GO:0005488	binding	3.4E-02				3.4E-02	
	GO:0003676	nucleic acid binding		5.2E-23	5.6E-08	0.0E+00		
	GO:0016787	hydrolase activity		9.3E-23	1.7E-04	0.0E+00		
	GO:0005215	transporter activity		2.3E-17	4.4E-04	0.0E+00		
	GO:0003723	RNA binding		5.6E-14	6.7E-20	0.0E+00		
	GO:0004518	nuclease activity		5.9E-10	4.3E-04	0.0E+00		
	GO:0005198	structural molecule activity		3.7E-09	9.6E-10	1.0E-08		
	GO:0003700	transcription factor activity, sequence-specific DNA binding		1.4E-04		1.4E-04		
	GO:0008135	translation factor activity, RNA binding		2.3E-04	1.6E-03	2.4E-04		
	GO:0003774	motor activity		3.2E-03		3.2E-03		
	GO:0003677	DNA binding		4.9E-02		4.9E-02		

GO:0005515	protein binding		1.3E-03	
GO:0003682	chromatin binding		1.2E-02	

Table S34.

Module assignment of homeologs for syntenic and non-syntenic triads and duplets. [1] Triads/duplets with all homeologs assigned to a module, [2] Triads/duplets with two (or three) homeologs further away than 50 % of the median distance to the furthest eigengene,[3] Percentage based on total triads/duplets.

Type (A:B:D)	Synteny	Triad/ Duplet[1]	Homoeolog assignment		Divergent expression[2]	Homoeologs in same module (%)	Homoeologs in different modules (%)	Divergent expression (%)[3]
			Same module	Different modules				
1:1:1	syntenic	8,617	4,997	3,620	1,393 (78)	58.0	42.0	16.2
0:1:1	syntenic	591	342	249	99	57.9	42.1	16.8
1:0:1	syntenic	684	415	269	124	60.7	39.3	18.1
1:1:0	syntenic	435	245	190	91	56.3	43.7	20.9
1:1:1	non-syntenic	392	191	201	83 (4)	48.7	51.3	21.2
0:1:1	non-syntenic	72	37	35	17	51.4	48.6	23.6
1:0:1	non-syntenic	80	45	35	20	56.3	43.8	25.0
1:1:0	non-syntenic	71	36	35	18	50.7	49.3	25.4
Triads (1:1:1)	syntenic + non-syntenic	9,009	5,188	3,821	1,476 (82)	57.6	42.4	16.4
Duplets	syntenic + non-syntenic	1,933	1,120	813	369	57.9	42.1	19.1
Total		10,942	6,308	4,634	1,845 (1,927)	57.6	42.4	16.9

Table S35.

Top 10 hub genes ranked by correlation to the module eigengene (kME) in WGCNA co-expression modules 8 and 11 (enriched for floral organ identity GO:0010093).

Module	Gene	kME correlation	kME pvalue	Human Readable annotation
8	TraesCS2A01G017100	0.95	0	NADH-quinone oxidoreductase subunit F
8	TraesCS2A01G545900	0.93	0	RING/U-box superfamily protein
8	TraesCS2D01G122200	0.93	0	Photosystem II reaction center protein M
8	TraesCS2D01G122300	0.92	0	Delta(24(24(1)))-sterol reductase
8	TraesCS4D01G247000	0.93	0	Chorismate synthase; RING/FYVE/PHD zinc finger superfamily protein
8	TraesCS5D01G514200	0.93	0	Threonine--tRNA ligase
8	TraesCS6B01G083400	0.93	0	F-box family protein-like protein
8	TraesCS6D01G058000	0.93	0	F-box family protein
8	TraesCS7D01G070800	0.93	0	F-box family protein
8	TraesCSU01G225400	0.94	0	Ribulokinase
11	TraesCS1A01G439000	0.91	0	3-ketoacyl-CoA synthase
11	TraesCS2A01G467200	0.92	0	Homeodomain-like protein
11	TraesCS2D01G468300	0.90	0	Aminodeoxychorismate synthase
11	TraesCS3B01G030300	0.92	0	Cytochrome P450
11	TraesCS3B01G030400	0.94	0	Dirigent protein
11	TraesCS4D01G247200	0.90	0	Cytochrome P450
11	TraesCS5D01G234100	0.92	0	Sugar transporter, putative
11	TraesCS5D01G293100	0.90	0	Auxin efflux carrier component
11	TraesCS7D01G020900	0.90	0	Benzyl alcohol O-benzoyltransferase
11	TraesCS7D01G220700	0.91	0	Protein kinase-like protein

Table S36.

Gene families in the wheat genome. Overview of gene families identified in bread wheat in comparison to 13 organisms belonging to the green lineage. Unless stated otherwise, numbers are based on TE-filtered gene sets comprising both HC and LC loci, Family percentages are relative to the number of families with at least one gene from one of the wheat sub-genomes (first row). Contracted gene families do comprise also families with no genes in either sub-genome.

	# total	% of gene families	# genes in A	# genes in B	# genes in D	# total genes	% genes A	% genes B	% genes D	%genes total
wheat gene families	26,080	100.0%	53,527	55,726	51,183	160,436	88.7%	87.2%	90.2%	88.6%
wheat families conserved in other species	21,751	83.4%	49,559	51,372	47,756	148,687	82.1%	80.4%	84.1%	82.1%
wheat families conserved outside Triticeae	16,526	63.4%	44,737	47,919	44,177	136,833	74.2%	74.9%	77.8%	75.6%
wheat families with pseudogenes	12,265	47.0%	40,289	42,877	38,817	121,983	66.8%	67.1%	68.4%	67.4%
wheat families with pseudogenes conserved in other species	11,461	43.9%	39,310	41,727	38,006	119,043	65.2%	65.3%	66.9%	65.8%
wheat families with pseudogenes conserved outside Triticeae	8,725	33.5%	35,036	38,093	34,731	107,860	58.1%	59.6%	61.2%	59.6%
wheat pseudogene-only families	505	1.9%	251	247	253	751	0.4%	0.4%	0.4%	0.4%
wheat pseudogene-only families conserved in other species	424	1.6%	189	164	197	550	0.3%	0.3%	0.3%	0.3%

wheat pseudogene-only families conserved outside Triticeae	122	0.5%	64	60	51	175	0.1%	0.1%	0.1%	0.1%
expanded wheat gene families (FDR<0.1)	8,592	32.9%	22,962	24,492	20,974	68,428	38.1%	38.3%	36.9%	37.8%
expanded wheat gene families with pseudogenes (FDR<0.1)	3,547	13.6%	18,516	20,569	17,377	56,462	30.7%	32.2%	30.6%	31.2%
contracted wheat gene families (FDR<0.1)	78	0.3%	83	67	65	215	0.1%	0.1%	0.1%	0.1%
wheat gene families similarly expanded in all subgenomes (FDR<0.1)	6,216	23.8%	20,456	23,651	19,970	64,077	33.9%	37.0%	35.2%	35.4%
wheat gene families expanded in one subgenome (FDR<0.1)	1,109	4.3%	1,718	1,655	1,016	4,389	2.8%	2.6%	1.8%	2.4%
wheat gene families expanded in one subgenome with pseudogenes (FDR<0.1)	387	1.5%	720	576	384	1,680	1.2%	0.9%	0.7%	0.9%
wheat gene families expanded in one subgenome lineage (FDR<0.1)	2,102	8.1%	2,305	319	792	3,416	3.8%	0.5%	1.4%	1.9%
wheat gene families	986	3.8%	1,294	228	375	1,897	2.1%	0.4%	0.7%	1.0%

expanded in one subgenome lineage with pseudogenes (FDR<0.1)										
HC+LC subgenome orphan (non-pseudogenic/non-TE)			9,333	11,075	8,001	28,409	18.6%	21.3%	16.7%	18.9%
HC (non-pseudogenic/non-TE)			35,251	35,545	34,208	105,004	70.2%	68.5%	71.3%	70.0%
HC+LC (non-pseudogenic/non-TE)			50,224	51,888	47,993	150,105	83.3%	81.2%	84.5%	82.9%
total genes (non-TE)			60,328	63,935	56,773	181,036	100.0%	100.0%	100.0%	100.0%

Table S37.

Overlap of manually annotated gene families and gene families identified using the automated phylogenomic approach. 85.24-100.00% of the manually annotated gene models were found in the respective family using the automated approach. Those that were not discovered using the automated approach did not fall in orthologous groups (i.e. were singletons), had no conserved domain structure or were only added, or significantly changed within the gene curation efforts for annotation version 1.1 (as this automated analysis was based on v1.0 gene models)

Gene Family	**Total number of genes manually assigned to gene family**	**Number of genes identified by automated approach in common with expert curation**	**% of genes identified by automated approach in common with expert curation**
Aquaporins	158	146	92.41
CBFs	61	54	88.52
Dehydrins	49	49	100.00
NLRs	2,052	1,811	88.26
PPRs	147	130	88.44
Prolamins	828	706	85.27
WAKs	555	555	100.00

Table S38.

Summary of the detailed analysis of tree topologies for the orthologous groups (OGs) of the Aquaporins, CBFs and DHN candidate gene families.

Gene Family	Orthologous Group	Topology	Bootstrap Value	% of mono-phyletic OGs	% of monophyletic OGs low BS values removed	% of monophyletic expanded OGs
Aquaporins	OG0000154	split at root	NA	90.91	100.00	100.00
	OG0000427	split at root	NA			
	OG0001355	monophyletic	0.886			
	OG0002982	monophyletic	1.000			
	OG0003682	monophyletic	0.444			
	OG0007810	polyphyletic	0.444			
	OG0010867	monophyletic	0.884			
	OG0011484	split at root	NA			
	OG0011556	monophyletic	1.000			
	OG0011644	monophyletic	0.606			
	OG0012131	monophyletic	1.000			
	OG0014331	monophyletic	1.000			
	OG0021232	monophyletic	0.762			
	OG0027911	monophyletic	0.864			
CBFs	OG0000383	monophyletic	1.000	100.00	100.00	100.00
	OG0023196	monophyletic	0.999			
	OG0029391	(one sequence)	NA			
Dehydrins	OG0000810	monophyletic	0.938	100.00	100.00	100.00
	OG0003562	split at root	NA			
	OG0012150	monophyletic	1.000			
	OG0014804	monophyletic	0.968			

Table S39.

Comparison of gene models to Ta3B and IWGSC RefSeq v1.0 Chr.3B.

Gene Models	Ta3B[a]	RefSeq v1.0	Difference
MIPS 2.2 Annotations	86%	93.7%	+9.0%
RefSeq 1.0 Annotations	88%	100%	+11.7%
Ta3B Annotations	100%	98.9%	-0.6%
Pseudomolecule size	774 Mbp	831 Mbp	57 Mbp

[a] Analysis was restricted to the pseudomolecule assembly of Ta3B (*14*).

Table S40.

IWGSC RefSeq v1.0 genes from *SSt1* absent in Ta3B.

Gene	Functional Annotation	Position
TraesCS3B01G598900	Ankyrin repeat-containing protein	820,286,268
TraesCS3B01G599000	F-box domain containing protein, expressed	820,333,146
TraesCS3B01G600100	Beta-adaptin-like protein	820,789,324
TraesCS3B01G600200	Dual-specificity RNA methyltransferase RlmN	820,893,665
TraesCS3B01G600300	Protein kinase	820,902,164
TraesCS3B01G605300	ubiquitin carboxyl-terminal hydrolase-like protein, putative (DUF627 and DUF629)	823,761,895
TraesCS3B01G605400	Divalent ion symporter	823,894,387
TraesCS3B01G606600	.	825,644,346
TraesCS3B01G606700	Disease resistance protein (TIR-NBS-LRR class) family	825,710,109
TraesCS3B01G606800	rRNA N-glycosidase	825,771,506
TraesCS3B01G606900	Epoxide hydrolase 2	825,849,367
TraesCS3B01G607000	Aspartic proteinase nepenthesin-1	825,868,243
TraesCS3B01G607100	Aspartic proteinase nepenthesin-1	825,886,089
TraesCS3B01G607200	SNARE-interacting protein KEULE	825,950,185
TraesCS3B01G607300	Pectinesterase inhibitor	825,970,605
TraesCS3B01G607400	Plant/T31B5-30 protein	825,992,065
TraesCS3B01G608200	Vacuolar fusion protein MON1	826,645,944
TraesCS3B01G608800	Dof zinc finger protein	828,110,909
TraesCS3B01G609000	Dof zinc finger protein	828,292,221
TraesCS3B01G612300	Transcription factor, MADS-box	829,742,374
TraesCS3B01G612500	Transcription factor, MADS-box	829,935,275
TraesCS3B01G612600	Transcription factor, MADS-box	830,055,777
TraesCS3B01G612800	Transcription factor, MADS-box	830,320,830
TraesCS3B01G612900	Transcription factor, MADS-box	830,610,856

Table S41

RNA-Seq based expression analysis of high confidence genes within *SSt1* interval on Chromosome 3B.

			Log_2 Fold Change		Adjusted p-value	
Transcript ID	Functional Annotation	CSV1,0 Position	LGB3B_vs_LDN	Lillian_vs_Vesper	LGB3B_vs_LDN	Lillian_vs_Vesper
TraesCS3B01G596700	2 Receptor-like protein kinase	819,502,902	-1.5	-1.1	0.0	0.0
TraesCS3B01G596800	Cytochrome P450	819,522,398	-2.1	-0.7	0.0	0.1
TraesCS3B01G596900	Receptor-like protein kinase	819,629,205	-1.8	0.0	0.0	1.0
TraesCS3B01G597000	Cytochrome P450	819,650,047	-2.4	-1.7	0.0	0.0
TraesCS3B01G597100	Phosphoenolpyruvate carboxykinase (ATP)	819,704,491	.	.	.	.
TraesCS3B01G597200	Cytochrome P450	819,740,077	.	.	.	.
TraesCS3B01G597300	Ae3	819,750,522	.	.	.	.
TraesCS3B01G597400	Pentatricopeptide repeat-containing protein	819,785,500	-0.2	0.3	0.9	0.8
TraesCS3B01G597500	Telomere-binding family protein	819,788,128	0.0	-0.3	1.0	0.5
TraesCS3B01G597600	Rab5-interacting family protein	819,809,430	0.1	-0.3	0.9	0.5
TraesCS3B01G597700	Haloacid dehalogenase-like hydrolase	819,854,349	0.1	-2.7	0.9	0.0
TraesCS3B01G597800	Vacuolar-processing enzyme	819,896,710	0.9	0.4	1.0	1.0
TraesCS3B01G597900	Vacuolar-processing enzyme	819,930,084	0.8	1.2	0.4	0.2
TraesCS3B01G598000	F-box family protein	819,948,218	.	-0.7	.	1.0
TraesCS3B01G598100	Pectinesterase	819,955,611	.	.	.	.
TraesCS3B01G598200	Glycosyltransferase	819,990,507	0.0	7.1	1.0	0.0
TraesCS3B01G598300	F-box family protein	820,074,306	-0.1	0.7	1.0	1.0
TraesCS3B01G598400	Glycosyltransferase	820,114,465	.	1.4	.	0.2
TraesCS3B01G598500	Glycosyltransferase	820,123,501	.	.	.	.
TraesCS3B01G598600	Ankyrin repeat-containing protein	820,130,589	-0.6	-1.7	0.8	0.2
TraesCS3B01G598700	Ankyrin repeat-containing protein	820,143,235	.	.	.	.
TraesCS3B01G598800	Ankyrin repeat-containing protein	820,163,917	-0.4	-1.0	0.8	1.0
TraesCS3B01G598900	Ankyrin repeat-containing protein	820,286,268	.	.	.	.
TraesCS3B01G599000	F-box domain containing	820,333,146	0.3	1.3	0.9	1.0
TraesCS3B01G599100	Ankyrin repeat-containing protein	820,397,835	.	.	.	.
TraesCS3B01G599200	Ankyrin repeat-containing protein	820,426,304	.	.	.	.
TraesCS3B01G599300	Ankyrin repeat-containing protein	820,446,972	0.3	1.8	0.9	0.1
TraesCS3B01G599400	Ankyrin repeat-containing protein	820,457,464	.	.	.	.
TraesCS3B01G599500	Kinetochore protein spc25	820,463,589	-0.3	0.5	0.8	0.6
TraesCS3B01G599600	Beta-adaptin-like protein	820,498,086	0.0	-1.9	1.0	0.0
TraesCS3B01G599700	NAC domain-containing protein	820,506,142	.	.	.	.
TraesCS3B01G599800	AP complex subunit	820,672,721	-0.4	-0.1	0.7	0.9
TraesCS3B01G599900	NAC domain-containing protein	820,761,513	.	.	.	.
TraesCS3B01G600000	NAC domain-containing protein	820,772,091	.	.	.	.
TraesCS3B01G600100	Beta-adaptin-like protein	820,789,324	0.0	1.6	1.0	0.1
TraesCS3B01G600200	Dual-specificity RNA methyltransferase	820,893,665	-0.2	0.1	0.9	0.9
TraesCS3B01G600300	Protein kinase	820,902,164	0.2	0.9	0.9	0.2
TraesCS3B01G600400	.	821,081,510	0.3	0.1	0.9	1.0
TraesCS3B01G600500	.	821,213,195	.	.	.	.
TraesCS3B01G600600	Calmodulin-binding protein, putative	821,215,369	-0.1	2.0	1.0	0.1
TraesCS3B01G600700	Calmodulin-binding protein, putative	821,276,027	.	.	.	.
TraesCS3B01G600800	Zinc finger family	821,554,671	.	5.6	.	0.0
TraesCS3B01G600900	Plant-specific domain TIGR01615	821,693,457	-0.4	0.2	0.6	0.6
TraesCS3B01G601000	Werner Syndrome-like exonuclease	821,804,687	.	.	.	.
TraesCS3B01G601100	Metallothionein	821,836,472	0.6	0.3	0.7	0.7
TraesCS3B01G601200	Vacuolar protein sorting	821,848,566	-0.3	-0.9	0.9	0.5

TraesCS3B01G601300	11S globulin seed	821,856,251	.	.	.	.
TraesCS3B01G601400	Sn1-specific diacylglycerol lipase	821,884,273	.	.	.	.
TraesCS3B01G601500	11S globulin seed	821,978,328	.	.	.	.
TraesCS3B01G601600	Metallothionein	822,039,201	0.7	-0.2	0.2	0.9
TraesCS3B01G601700	Metallothionein	822,067,205	0.8	1.0	0.3	0.1
TraesCS3B01G601800	Metallothionein	822,094,677	0.8	0.3	0.3	0.8
TraesCS3B01G601900	Plant invertase/pectin methylesterase	822,101,995	.	.	.	.
TraesCS3B01G602000	30S ribosomal protein	822,103,561	0.1	-0.6	1.0	0.3
TraesCS3B01G602100	30S ribosomal protein	822,114,565	-0.1	-0.7	1.0	0.0
TraesCS3B01G602200	SANT domain-containing protein	822,189,827	-0.1	-0.4	0.8	0.2
TraesCS3B01G602300	Mitochondrial ATP synthase	822,216,860	.	.	.	.
TraesCS3B01G602400	PR5-like receptor kinase	822,535,369	0.7	6.4	0.6	0.0
TraesCS3B01G602500	Lipoxygenase	822,548,132	-0.4	6.4	0.8	0.0
TraesCS3B01G602600	Extra-large guanine nucleotide	822,668,181	.	.	.	.
TraesCS3B01G602700	Protein kinase-like protein	822,676,261	2.5	1.6	0.0	0.0
TraesCS3B01G602800	Plant cadmium resistance	822,808,188	-1.8	-0.6	0.0	1.0
TraesCS3B01G602900	Dirigent protein	822,816,997	.	.	.	.
TraesCS3B01G603000	Gibberellin 2-beta-dioxygenase	822,819,355	-0.4	-4.3	0.8	0.0
TraesCS3B01G603100	Chaperone protein dnaJ	822,824,640	0.3	-7.0	0.7	0.0
TraesCS3B01G603200	SKP1-like protein	822,835,413	.	.	.	.
TraesCS3B01G603300	Kinase family protein	822,879,781	0.7	1.3	1.0	0.2
TraesCS3B01G603400	3 E3 SUMO-protein ligase	822,882,640	-0.1	0.2	0.9	0.6
TraesCS3B01G603500	Protein IQ-DOMAIN 1	822,903,506	0.0	-1.0	1.0	0.0
TraesCS3B01G603600	Serine/threonine-protein kinase ATM	822,968,033	.	.	.	.
TraesCS3B01G603700	Serine/threonine-protein kinase ATM	822,972,695	0.6	1.5	0.1	0.0
TraesCS3B01G603800	Kinase-like protein	822,977,716	0.7	-0.7	0.0	0.3
TraesCS3B01G603900	GATA transcription factor	822,984,216	2.5	2.7	0.0	0.0
TraesCS3B01G604000	Protein phosphatase 2C	823,028,880	0.5	0.4	0.5	0.5
TraesCS3B01G604100	NBS-LRR disease resistance	823,072,667	5.3	8.5	0.0	0.0
TraesCS3B01G604200	Ubiquitin carboxyl-terminal hydrolase	823,087,419	0.2	2.1	1.0	0.1
TraesCS3B01G604300	rRNA N-glycosidase	823,181,174	.	.	.	.
TraesCS3B01G604400	rRNA N-glycosidase	823,193,985	.	.	.	.
TraesCS3B01G604500	NBS-LRR resistance-like protein	823,290,293	0.1	0.7	1.0	1.0
TraesCS3B01G604600	2 Disease resistance protein	823,294,611	0.1	.	1.0	.
TraesCS3B01G604700	External alternative NAD(P)H-ubiquinone	823,328,283	-0.5	0.6	0.7	0.7
TraesCS3B01G604800	NBS-LRR-like resistance protein	823,425,742	6.7	7.2	0.0	0.0
TraesCS3B01G604900	Disease resistance protein	823,430,745	6.2	8.4	0.0	0.0
TraesCS3B01G605000	transmembrane protein, putative	823,551,897	-0.3	-0.8	1.0	1.0
TraesCS3B01G605100	Kinase interacting (KIP1-like)	823,573,764	0.2	1.0	0.9	0.0
TraesCS3B01G605200	Transmembrane protein, putative	823,592,606	.	.	.	.
TraesCS3B01G605300	ubiquitin carboxyl-terminal hydrolase-like	823,761,895	.	.	.	.
TraesCS3B01G605400	Divalent ion symporter	823,894,387	.	.	.	.
TraesCS3B01G605500	Cortactin-binding protein 2	823,984,063	0.2	1.5	0.9	1.0
TraesCS3B01G605600	AGAP002737-PA	824,006,142	0.4	1.2	0.9	1.0
TraesCS3B01G605700	Lipoxygenase	824,258,372	0.2	1.5	0.9	0.3
TraesCS3B01G605800	plant/protein	824,379,570	.	.	.	.
TraesCS3B01G605900	F-box protein	824,391,739	.	0.8	.	1.0
TraesCS3B01G606000	F-box protein	825,289,551	.	.	.	.
TraesCS3B01G606100	AGAP002737-PA	825,314,966	0.1	-2.1	1.0	0.1
TraesCS3B01G606200	AGAP002737-PA	825,492,715	0.2	-2.2	0.9	0.1
TraesCS3B01G606300	CAP-gly domain linker	825,495,597	-0.1	-1.8	1.0	0.2
TraesCS3B01G606400	Aspartic proteinase nepenthesin-1	825,539,090	.	.	.	.
TraesCS3B01G606500	plant/protein	825,571,873	1.1	0.6	0.1	0.7
TraesCS3B01G606600	.	825,644,346	.	.	.	.
TraesCS3B01G606700	Disease resistance protein	825,710,109	0.1	3.5	1.0	1.0
TraesCS3B01G606800	rRNA N-glycosidase	825,771,506	.	0.8	.	1.0
TraesCS3B01G606900	Epoxide hydrolase 2	825,849,367	0.1	0.6	1.0	1.0
TraesCS3B01G607000	Aspartic proteinase nepenthesin-1	825,868,243	.	.	.	.
TraesCS3B01G607100	Aspartic proteinase nepenthesin-1	825,886,089	.	.	.	.
TraesCS3B01G607200	SNARE-interacting protein KEULE	825,950,185	.	.	.	.
TraesCS3B01G607300	Pectinesterase inhibitor	825,970,605	.	.	.	.
TraesCS3B01G607400	Plant/T31B5-30 protein	825,992,065	.	0.8	.	1.0
TraesCS3B01G607500	Chaperone protein dnaJ	826,082,197	0.0	0.0	1.0	1.0
TraesCS3B01G607600	ABC transporter B	826,086,442	-0.2	-0.7	0.8	0.0

TraesCS3B01G607700	Disease resistance protein	826,101,725	.	.	.	.
TraesCS3B01G607800	ubiquinone biosynthesis protein	826,261,223	.	.	.	.
TraesCS3B01G607900	Dirigent protein	826,321,283	.	-1.4	.	0.3
TraesCS3B01G608000	Pro-apoptotic serine protease	826,363,262	.	.	.	.
TraesCS3B01G608100	Leucine-rich repeat (LRR)	826,484,373	.	.	.	.
TraesCS3B01G608200	Vacuolar fusion protein	826,645,944	-0.2	-0.9	0.8	0.0
TraesCS3B01G608300	Monopolar spindle protein	826,651,868	0.1	-1.0	1.0	0.5
TraesCS3B01G608400	GDSL esterase/lipase	826,711,412	0.2	-2.0	1.0	0.1
TraesCS3B01G608500	Aquaporin	826,725,085	0.9	1.6	0.2	0.0
TraesCS3B01G608600	MADS-box transcription factor	826,918,889	-0.6	-1.3	0.6	1.0
TraesCS3B01G608700	Agamous-like MADS-box protein	827,515,120	.	.	.	.
TraesCS3B01G608800	Dof zinc finger	828,110,909	-1.7	-2.3	0.0	0.0
TraesCS3B01G608900	Dof zinc finger	828,253,029	.	.	.	.
TraesCS3B01G609000	Dof zinc finger	828,292,221	.	.	.	.
TraesCS3B01G609100	Dof zinc finger	828,331,215	.	0.7	.	1.0
TraesCS3B01G609200	transmembrane protein	828,413,608	-0.2	-0.8	0.9	0.4
TraesCS3B01G609300	F-box protein-like protein	828,417,014	.	.	.	.
TraesCS3B01G609400	Cytochrome P450	828,420,001	-0.2	-0.7	1.0	0.7
TraesCS3B01G609500	Ankyrin repeat family	828,546,437	0.1	0.9	0.9	0.2
TraesCS3B01G609600	Cytochrome P450	828,763,303	-0.1	0.3	1.0	1.0
TraesCS3B01G609700	Nodulin MtN2/EamA-like	828,766,993	.	.	.	.
TraesCS3B01G609800	3-oxo-5-alpha-steroid 4-dehydrogenase family	828,770,429	-0.1	0.6	1.0	0.6
TraesCS3B01G609900	Pre-mRNA-splicing factor ISY1-like	828,781,704	.	.	.	.
TraesCS3B01G610000	2 Protein CHUP1, chloroplastic	828,825,898	.	.	.	.
TraesCS3B01G610100	2 Pectin acetylesterase	828,917,506	-0.2	2.5	0.9	0.0
TraesCS3B01G610200	Pectin acetylesterase	828,949,097	-1.1	-2.9	0.1	0.0
TraesCS3B01G610300	Pectin acetylesterase	828,991,506	.	0.8	.	1.0
TraesCS3B01G610400	2 Pectin acetylesterase	829,013,144	0.2	-0.4	0.9	0.3
TraesCS3B01G610500	91A protein	829,016,168	0.4	0.2	0.5	0.5
TraesCS3B01G610600	Pectin acetylesterase	829,037,444	0.6	1.2	1.0	0.2
TraesCS3B01G610700	B3 domain-containing protein	829,054,314	.	.	.	.
TraesCS3B01G610800	Histone H2A	829,113,007	-0.1	-0.8	0.9	0.3
TraesCS3B01G610900	RNA-binding protein	829,114,036	0.0	.	1.0	.
TraesCS3B01G611000	.	829,117,291	0.0	-2.3	1.0	0.0
TraesCS3B01G611100	Receptor-like protein kinase	829,203,567	0.2	-2.6	0.9	0.0
TraesCS3B01G611200	DNA topoisomerase 3	829,223,901	.	.	.	.
TraesCS3B01G611300	Histone H2A	829,244,086	.	.	.	.
TraesCS3B01G611400	Outer-membrane lipoprotein LolB	829,246,632	-0.1	4.2	0.9	0.0
TraesCS3B01G611500	transmembrane protein, putative	829,252,291	0.5	-1.9	0.8	0.2
TraesCS3B01G611600	Soluble inorganic pyrophosphatase	829,273,469	-0.1	-0.3	0.9	0.6
TraesCS3B01G611700	Kelch repeat-containing F-box	829,283,466	-0.1	0.6	0.9	0.1
TraesCS3B01G611800	Soluble inorganic pyrophosphatase	829,288,040	1.0	1.1	0.0	0.1
TraesCS3B01G611900	Ubiquitin family protein	829,349,677	.	.	.	.
TraesCS3B01G612000	O-methyltransferase	829,391,763	0.9	2.6	1.0	0.0
TraesCS3B01G612100	Protein	829,508,771	-0.7	-1.0	0.6	0.3
TraesCS3B01G612200	2 MYB transcription factor	829,541,507	0.6	1.5	0.5	0.0
TraesCS3B01G612300	Transcription factor, MADS-box	829,742,374	.	.	.	.
TraesCS3B01G612400	Transcription factor, MADS-box	829,817,279	0.1	.	1.0	.
TraesCS3B01G612500	Transcription factor, MADS-box	829,935,275	.	.	.	.
TraesCS3B01G612600	Transcription factor, MADS-box	830,055,777	.	.	.	.
TraesCS3B01G612700	Transcription factor, MADS-box	830,112,178	.	.	.	.
TraesCS3B01G612800	Transcription factor, MADS-box	830,320,830	.	0.7	.	1.0
TraesCS3B01G612900	Transcription factor, MADS-box	830,610,856	.	.	.	.

Table S42.

Copy number variation analysis of the gene *TraesCS3B01G608800* in 96 diverse hexaploid cultivars

Sample	Solidness	*TraesCS3B01G608800* Copy Number (qPCR)	SEM	*TraesCS3B01G608800* SSR - Band Sizes (bp) 396	408	410	416	418	420	422
Choteau	4.3	9.9	0.5			410		418		422
Fortuna	3.0	10.4	0.2			410		418		422
Lancer	3.0	10.3	0.4			410		418		422
AAC Bailey	2.5	9.6	0.9			410		418		422
AC Eatonia	2.5	8.5	0.5			410		418		422
Frontana	2.5	2.3	0.3				416	418		
G9608B1-L12J11BF02	2.5	6.0	0.2							
Janz	2.5	1.4	0.1	396			416			
Leader	2.5	3.7	0.2					418		
Lillian	2.5	10.1	0.7			410		418		422
LJP1091P	2.5	7.7	0.4	396	408			418		422
Mott	2.5	10.3	1.1	396		410		418		422
Rescue	2.5	6.2	0.1			410		418		422
S615	2.5	10.8	0.3			410		418		422
AC Abbey	1.9	6.4	0.4			410		418		422
CDC Landmark	1.9	7.7	0.4			409		418		422
Glencross	1.8	5.9	0.4						420	422
McKenzie	1.8	8.9	0.4							
CDC Rama	1.7	3.5	0.2						420	422
Unity	1.7	11.1	0.7			410		418		422
Glenlea	1.5	3.8	0.2						420	422
CDC Teal	1.3	2.7	0.1					418		
AC Crystal	1.2	2.9	0.2							422
AC Vista	1.2	3.1	0.2							422
Alvena	1.2	4.4	0.2							422
Burnside	1.2	6.0	0.2						420	422
AC Andrew	1.1	2.4	0.1				416	418		
AC Splendor	1.1	3.3	0.1					418		
AC Taber	1.1	2.6	0.1							422
CDC Bison	1.1	5.1	0.2						420	422
CDC Stanley	1.1	1.8	0.1							
CDC Walrus	1.1	2.4	0.0				416	418		
Kane	1.1	4.6	0.2					418		
Katepwa	1.1	2.8	0.1					418		
Laser	1.1	4.1	0.1					418	420	
5500HR	1.0	2.8	0.1						420	
5600HR	1.0	3.0	0.4					418		
5601HR	1.0	3.0	0.1					418		
5602HR	1.0	3.7	0.1				416	418	420	
5603HR	1.0	3.4	0.2				416		420	
5700PR	1.0	2.4	0.2							422
5701PR	1.0	2.7	0.1					418		
5702PR	1.0	2.1	0.2				416			
AC Barrie	1.0	2.9	0.1							
AC Cadillac	1.0	3.5	0.3							
AC Domain	1.0	3.1	0.2					418		
AC Elsa	1.0	3.0	0.2							422
AC Foremost	1.0	2.5	0.1							422
AC Intrepid	1.0	3.2	0.2							
AC Karma	1.0	2.5	0.2							422

Alikat	1.0	2.2	0.2			418		
Carberry	1.0	3.2	0.1			418		
CDC Abound	1.0	3.9	0.3			418		
CDC Alsask	1.0	2.8	0.2			418		
CDC Bounty	1.0	3.0	0.2			418		
CDC Go	1.0	3.1	0.1			418		
CDC Imagine	1.0	4.1	0.5					
CDC Kernen	1.0	2.1	0.2			418		
CDC Merlin	1.0	2.8	0.1			418		
CDC Osler	1.0	3.0	0.2			418		
CDC Thrive	1.0	2.5	0.1			418		
CDC Utmost	1.0	2.0	0.3			418	420	
Chinese Spring	1.0	1.4	0.0					
Cutler	1.0	4.1	0.3					422
Glenn	1.0	4.0	0.4		416	418		
Goodeve VB	1.0	4.2	0.2			418		
GP069	1.0	2.7	0.1					422
Harvest	1.0	4.6	1.0					
Helios	1.0	4.8	0.3			418		
Infinity	1.0	3.8	0.2		416	418		
Journey	1.0	3.0	0.1			418		
Laura	1.0	3.2	0.2			418		
Lovitt	1.0	3.2	0.1			418		
Minnedosa	1.0	3.4	0.3					422
Muchmore	1.0	3.8	0.3			418		
Neepawa	1.0	4.2	0.3			418		
Park	1.0	2.4	0.2				420	
Peace	1.0	4.6	0.6				420	
Prodigy	1.0	4.1	0.3					
PT559	1.0	2.7	0.1			418		
Red Fife	1.0	2.6	0.1		416			
RL4137	1.0	0.8	0.1			418		
Roblin	1.0	3.1	0.1			418		
Sadash	1.0	3.2	0.1		416	418		
Selkirk	1.0	3.6	0.3				420	
Snowbird	1.0	2.4	0.2			418		
Snowstar	1.0	3.7	0.2			418		
Somerset	1.0	4.5	0.3			418		
Stanley	1.0	3.6	0.3			418		
Stettler	1.0	3.7	0.2			418		
Sumai 3	1.0	3.2	0.1		416		420	
Superb	1.0	3.1	0.1			418		
SY985	1.0	2.9	0.2					422
Vesper	1.0	2.9	0.2			418	420	
Waskada	1.0	3.3	0.3			418		

Additional Database S1 (separate .xls file)
Metadata of 850 RNAseq samples used in the study

Additional Database S2 (separate .xls file)
SlimGO ubiquitous and Tissue-exclusive genes.

Additional Database S3 (separate .xls file)
GO terms of the WGCNA850 analysis.

Additional Database S4 (separate .xls file)
WGCNA Module Assignment.

Additional Database S5 (separate .xls file)
Module 8 and 11 TF Arabidopsis and rice orthologs.

Additional Database S6 (https://doi.ipk-gatersleben.de/DOI/912ca35a-2fbb-4d59-9dab-a06edf7fef73/4391642c-3958-425b-989e-da0ec1a277b9/2/1847940088**)**
Gene family expansion and contraction in the genome of bread wheat cv. Chinese Spring.